



UNIVERSITY OF TRENTO

International PhD Program in Biomolecular Sciences

**Department of Cellular, Computational
and Integrative Biology – CIBIO**

31st Cycle

**IDENTIFICATION AND CHARACTERIZATION
OF SMALL MOLECULES INHIBITING
THE RNA BINDING PROTEIN HUR**

Tutor: Dr. **ALESSANDRO PROVENZANI**

Advisor: Dr. **VITO GIUSEPPE D'AGOSTINO**

Department of Cellular, Computational
and Integrative Biology – CIBIO

Laboratory of Genomic Screening

Ph.D. Thesis of

ISABELLE BONOMO

Department of Cellular, Computational
and Integrative Biology – CIBIO

Laboratory of Genomic Screening

Academic Year 2017-2018

Original authorship

Declaration:

I, Isabelle Bonomo, confirm that this is my own work and the use of all material from other sources has been properly and fully acknowledged.

Trento, 16/10/19

Isabelle Bonomo

ABSTRACT

Post-transcriptional control of gene expression in Eukaryotes plays a pivotal role in determining intricate networks defining physiological and pathological conditions among each organism. RNA Binding Proteins (RBPs), by exploiting RNA-protein and protein-protein interactions, have been recognized as the main actors in modulating these processes. As a consequence, RBPs aberrant expression, modulation or mis-localization, leads to the insurgence of complex phenotypes and diseases. Therefore, targeting and modulating the activity of RBPs found associated to different pathologies represents a new promising therapeutic strategy. During my PhD I aimed at identify, characterize and refine inhibitors targeting the RNA binding protein HuR. HuR belongs to the ELAVL protein family, it is ubiquitously expressed in the cells and among tissues and highly conserved throughout mammalian evolution. By binding AU/U rich elements (ARE) in the 3'UTRs of mRNAs, HuR mainly stabilizes its target transcripts, enhancing their translation. ARE sequences are found in 7% of the human mRNAs, coding for protein involved in key cellular processes as: immune response and inflammation, cell division and proliferation, angiogenesis, senescence and apoptosis. Hence, dysregulation in HuR expression and in its subcellular localization have been associated with the insurgence of several pathologies, mostly cancers and inflammation diseases. Notably, malignant transformations and poor prognosis in patients have been found characterized by highly nuclear or cytosolic HuR expression in a significant number of human cancers. Indeed, the majority of HuR regulated transcripts encode for protein responsible for the appearance of several cancerogenic traits. In particular, critical crosstalk established between cancer cells and inflammation processes play a pivotal role in worsening and compromising cancers development and onset. Moreover, considering that 90% of mRNAs coding for cytokines and chemokines contains repeated AREs sites in the 3'UTR, HuR plays a strong regulatory role in immune system (innate and adaptive) development and homeostasis as well as in pathogenic mechanisms. The searching for HuR inhibitors represents a challenging area, in the drug discovery field, due to its pleiotropic functions and its intrinsic structural complexity, which presents unfolded regions and sequences prone to aggregation. HuR disruptors have been reported in the literature, but without systematic studies, thus the identification of a new class of small molecules is still at the beginning. Among the molecules discovered so far, in 2015 our group identified through a High-throughput Screening a natural compound, DHTS, as a *bona fide* HuR inhibitor. Following that finding, we, me included, ascribed to the molecule a well-defined mechanism of action, identifying the specific binding sites on which HuR:DHTS interaction is based, defining that upon the mRNA binding DHTS interplays with HuR maintaining the protein in a closed conformation, thus inhibiting its function. Furthermore, we demonstrated DHTS anti-cancer activity *in vitro*, in cellular context and *in vivo*, in an HuR-dependent manner. In this way, DHTS represented the molecular scaffold, for the generation of a new class of highly potent HuR inhibitors, called Tanshinone Mimics (TMs). A functional oriented approach was

applied for the synthesis of new molecules harboring only DHTS chemical elements responsible for HuR targeting, leading to a completely new molecular scaffold, not previously described in the literature, with respect to the ancestor molecule. I have characterized and identified more potent molecules, describing their anticancer properties, through the evaluation of their capabilities of downregulating the total expression level of well-known HuR targets, coding for proteins involved in tumor insurgence and progression, as VEGF, ERBB2 and CTNNB1, and reducing cancer cell migration, cell cycle progression in a minor extent. On the other end, I have explored TMs anti-inflammatory properties, counteracting the inflammatory response mediated by macrophages, directly impairing the binding between HuR and its pro-inflammatory targets, diminishing their expression and related protein secretion, resulting in impairing macrophages M1 pro-inflammatory polarization. Moreover, I have put evidences on TMs activity *in vivo* in reducing cytokines secretion level in the sera of acute inflammation mouse models. Lastly, I have evaluated TMs activity in affecting T-cells proliferation, on which HuR it is known to play a regulatory role, showing TMs to enhance T cells migratory properties in neuroinflammation disorders.

In conclusion, we identified TMs with Structure-Activity Relationships (SARs) towards HuR inhibition and its biological implications, aimed at ameliorating their specificity and bioavailability suitable for *in vivo* therapeutic strategies.

Table of Contents

ABSTRACT

| | |
|---|-----------|
| 1. Background..... | 1 |
| 1.1 RNA Binding Proteins: structure and roles..... | 1 |
| 1.2 Targeting RNA Binding Proteins as a new promising therapeutic strategy..... | 4 |
| 2. Introduction..... | 5 |
| 2.1 The RNA Binding Protein HuR..... | 5 |
| 2.2 HuR regulation, functions and association with diseases..... | 8 |
| 2.3 HuR in cancer..... | 9 |
| 2.4 HuR in inflammation..... | 11 |
| 2.5 Targeting HuR with small molecules..... | 13 |
| 2.6 Identification and characterization of Dihydratanshinone-1 (DHTS) and Tanshinone Mimics (TMs)..... | 16 |
| 3. Hypothesis and Aim..... | 17 |
| 4. Results and Comments..... | 19 |
| 4.1 Insights on DHTS mechanism of action towards HuR inhibition..... | 19 |
| 4.2 Characterization of DHTS mechanism of inhibition for the generation of a more potent family of HuR inhibitors..... | 20 |
| 4.3 Tanshinone Mimics (TMs): identification and evaluation of a new class of HuR inhibitors..... | 23 |
| 4.4 TMs affect viability and migration of cancer cells by modulating HuR post transcriptional activity, without changing its subcellular localization..... | 26 |
| 4.5 Characterization of TMs-II and 7n, leading compound with a biochemical and biological activity in cancer cell lines..... | 33 |
| 4.6 Evidences on TMs anti-inflammatory properties: TMs show toxicity in macrophages cell lines, as well as reduction in cytokines expression..... | 37 |
| 4.7 TMs affect HuR post-transcriptional function by downregulating cytokines production and release in RAW 264.7..... | 40 |
| 4.8 Upon LPS response, TMs do not affect Nf-Kb localization in the cells, but directly impair HuR-mRNA binding..... | 45 |

| | |
|---|-----------|
| 4.9 Evaluation of TMs effects in primary murine macrophages derived from bone marrow (BMDMs), with <i>in vivo</i> evidences. | 50 |
| 4.10 Ongoing work: TMs activity in adaptive immunity..... | 55 |
| 5. Discussion and Future Aims..... | 60 |
| 6. Conclusion | 70 |
| 7. Materials and Methods | 72 |
| 7.1 AlphaScreen and RNA-Electrophoretic Mobility Shift Assays (REMSAs)..... | 72 |
| 7.2 NMR, DMR, Molecular modelling and Computational Dynamics..... | 72 |
| 7.3. RNA Immunoprecipitation (RIP) assays..... | 72 |
| 7.4 RIP-Chip protocol. | 73 |
| 7.5 Analysis of enriched mRNAs | 74 |
| 7.6 Total RNA extraction and qRT-PCR | 74 |
| 7.7 Biotinylated RNA Pull Down assay | 75 |
| 7.8 Immunoblotting analysis | 75 |
| 7.9 Immunofluorescence and OPP Click-IT assay..... | 76 |
| 7.10 Polysome profiling assays | 76 |
| 7.11 Flow cytometry and Enzyme-linked immunosorbent assay (ELISA)..... | 77 |
| 7.12 Cell lines and primary cell cultures..... | 77 |
| 7.13 Primary murine naïve, M1 macrophages, Th1/Th17 T-cells in vitro differentiation and reagents used for cell treatments..... | 78 |
| 7.14 NO and Caspase 3/7 detection assays..... | 78 |
| 7.15 Cell viability assays | 78 |
| 7.16 Cell cycle, proliferation and migration assays. | 79 |
| 7.17 Animal inflammation models and sera collection..... | 79 |
| 7.18 Statistical analysis | 80 |
| References | 81 |
| APPENDIX | 94 |

ABBREVIATIONS and ACRONYMS

| | |
|----------------|--|
| HuR | Hu human antigen R |
| RBP | RNA Binding Protein |
| mRNA | messenger Ribonucleid Acid |
| RNP | Ribo-Nucleo Protein |
| PTM | Post-Translational Modifications |
| RIP | RNA Immunoprecipitation |
| RBD | RNA Bindind Domain |
| RRM | RNA Recognition Motif |
| ARE | AU/U Rich Elements |
| UTR | UnTranslated Regions |
| ELAV | Embryonic Lethal Abnormal Vision |
| NF- κ B | Nuclear Factor kappa-light-chain-enhancer of activated B cells |
| ATP | Adenosine Tri-Phosphate |
| VEGF | Vascular Endothelial Growth Factor |
| TNF α | Tumor Necrosis Facotr Alpha |
| CTNNB1 | β -catenin |
| ERBB2/HER2 | human epidermal growth factor receptor 2) |
| PABPC1 | Poly(A) Binding Protein Cytoplasmic 1 |
| YTHDF1 | YTH N6-Methyladenosine RNA Binding Protein 1 |
| BRIP1 | BRCA1 Interacting Protein C-Terminal Helicase 1 |
| TTP | Tristetraprolin |
| TIA-1 | T-cell restricted Intracellular Antigen -1 |
| LPS | Lipopolysaccharides |
| TRL4 | Toll-Like Receptor-4 |
| CXCL2 | chemokine (C-X-C motif) ligand 2 |
| CXCL10 | chemokine (C-X-C motif) ligand 10 |
| CCR6 | C-C chemokine receptor type 6 |
| CCL20 | Chemokine (C-C motif) ligand 20 |
| CD4 | Cluster of Differentiation 4 |
| IFN γ | Interferon gamma |
| ROR γ T | RAR-related orphan receptor gamma |
| IL- | Interleukin- |
| DHTS | Dihydrotanshinone |
| TM | Tanshinone Mimics |
| TM-I | Tanshinone Mimics 1st geberation |
| TM-II | Tanshinone Mimincs 2nd generation |
| Act-D | Actinomycin-D |
| DMSO | Dimethyl sulfoxide |
| CHX | Cycloheximide |
| OPP | O-propargyl-puromycin |
| PMA | Phorbol 12-Myristate 13-Acetate |
| PHA | Phytohaemagglutinin |
| Iono | Ionomycin |

| | |
|-----------|---|
| BMDMS | Bone Marrow Derived Macrophages |
| PEMS | Peritoneal Exudate Macrophages |
| TAMS | Tumor Associated Macrophages |
| NO | Nitric Oxide |
| IC50 | Inhibitory Concentration 50 |
| Bi-TNF | Biotinylated TNF |
| Bi-AU | Biotinylated AU |
| Bi-neg | Biotinylated negative |
| NMR | Nuclear Magnetic Resonance |
| DMR | Dynamic Mass Redistribution |
| MD | Molecular Dynamics |
| CD | Circular Dichroism |
| siRNA | Silencing RNA |
| ASO | Antisense Oligonucleotides |
| CLIP | UV Crosslinking and Immunoprecipitation |
| SARs | Structure Activity Relationships |
| PAR-iCLIP | Photoactivatable ribonucleoside-enhanced Crosslinking and Immunoprecipitation |
| qRT-PCR | Real-time reverse transcription-PCR |
| BSA | Bovine Serum Albumin |

1. Background

1.1 RNA Binding Proteins: structure and roles.

Post-transcriptional regulation is a crucial step of gene expression in defining the protein synthesis, abundance, turnover and homeostasis in eukaryotic cells. It involves all the mRNA metabolism from its transcription, maturation/processing, post-transcription, translation and proteolysis (Moore, 2005). In this context, RNA-binding proteins (RBPs) play pivotal roles, starting from controlling the elongation and termination of a RNA transcript, its alternative splicing, export and localization, stability and corresponding protein translation (Glisovic *et al.*, 2008; Turner and Díaz-Muñoz, 2018).

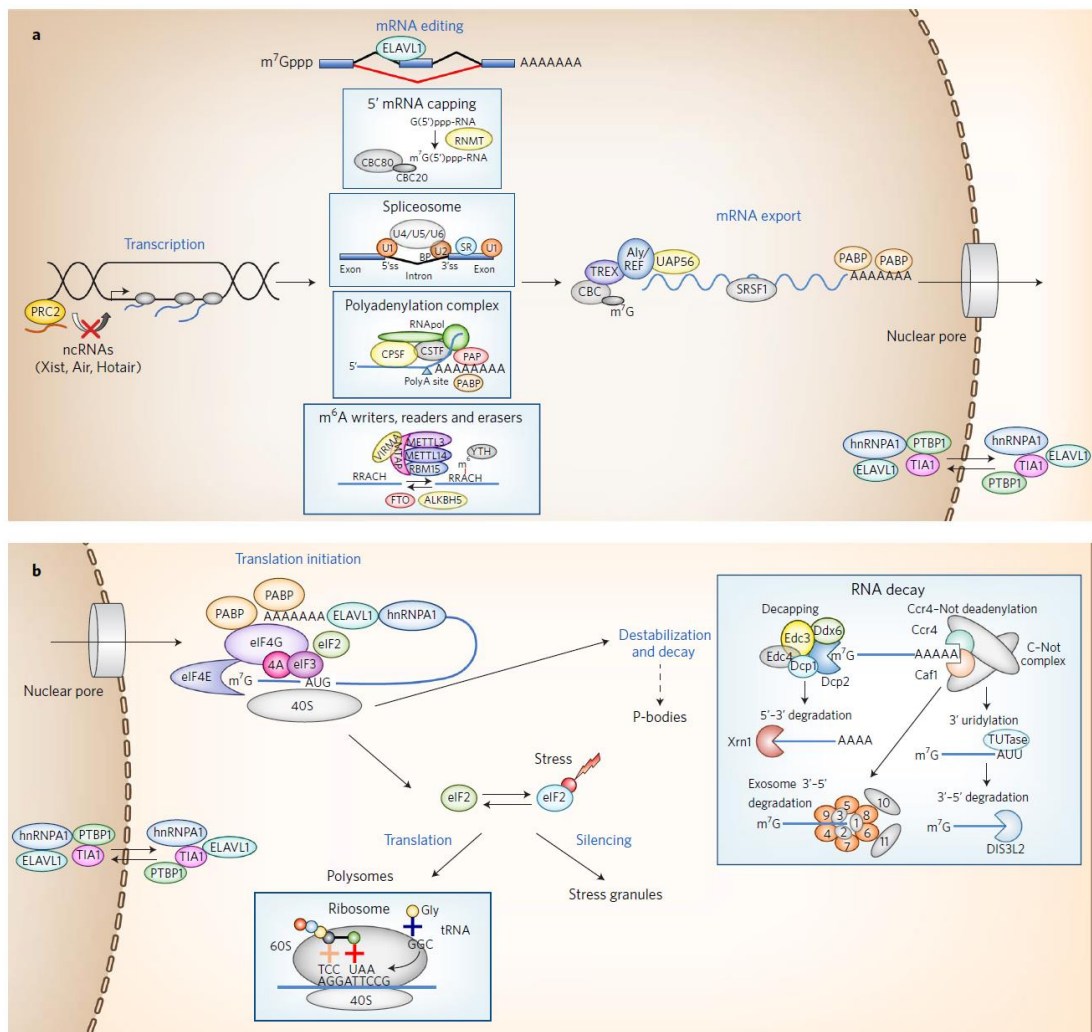


Figure 1. Overview of RBPs importance during mRNA lifespan (adopted from Turner *et al.*, 2018). RBPs control gene transcription, 5' RNA capping, splicing, polyadenylation and methylation, mRNA export, translation initiation, mRNA translational silencing, mRNA destabilization, and mRNA decay. The shuttling from the nucleus to the cytoplasm is a key event that helps RBPs in playing different roles.

In particular, in (a) there are represented RBPs, as PRC2, that are responsible for the modulation of epigenetic processes by binding of ncRNAs, or the transcription-export complex 1 (TREX-1), which includes Aly/REF and UAP56 proteins involved in mRNA export by binding the cap-binding complex (CBC). The eIF4 complex, that initiates the CAP-dependent translation by recruiting the 40S ribosomal subunit, and the following interaction with polyA-binding proteins (PABP) protects mRNA from degradation. During stress stimuli, eIF2 α blocks mRNA translation. Other RBPs presented are the ones involved in mRNA destabilization and decay and degradation by exonucleases, such as Xrn1 and DIS3L2. On the other end, in (b) the ribosome, the decapping complex, the CCR4–NOT deadenylation complex, and mRNA decay mechanisms are represented.

Usually, RBPs bind coding and non coding RNA sequences through the recognition of thousands of different, but specific for each protein, sites (Baltz *et al.*, 2012; Freeberg *et al.*, 2013), thus forming ribonucleoprotein (RNP) complexes. RNP complexes regulate multiple processes among the cells, tissues and organisms, during the development in both physiological and disease state (Dreyfuss, Kim and Kataoka, 2002). RNA binding proteins are found ubiquitously expressed among all the tissue and evolutionary conserved, suggesting their predominant function at the basis of the cellular processes and involvement in the etiology of different diseases, from cancer to neurological disorders (Lukong *et al.*, 2008; Nussbacher *et al.*, 2015). Although the regulation of protein-synthesis directly or indirectly involves the vast majority of the RBPs, it has been reported that one of the third of them has unrevealed roles (D'Agostino *et al.*, 2019) .

The recent development of solids large-scale quantitative approaches allowed the genome-wide identification of RNA binding proteins and their targets. Improvements in next-generation sequencing, RIP- and CLIP based in vivo, RNA secondary structure profiling, small and long RNA-seq, 3'-end sequencing methods and mass spectrometry have been pivotal for the identification of binding properties of RBPs, demonstrating that the majority of RBPs are capable bind to a vast number of transcripts in cells at defined binding sites, therefore a collection of 1.542 RNA Binding proteins interacting with the all known forms of RNA has been proposed (Gerstberger, Hafner and Tuschl, 2014). The interaction between *cis-element* present in the RNA sequence and the RNA Binding Domains (RBDs) of the protein is at the basis of the mechanism mediated by the RNA binding protein (Cléry, Blatter and Allain, 2008), however the diversity of functions, the structures responsible for RNA recognition are built from few analogous RNA-binding modules. The principle at the basis of the RNA recognition is given by two main factors: first, the interaction between the entire folded protein, involving the hydrogen bonds with the backbone atoms and secondly specific interaction between amino acid chain and nucleotides (Auweter, Oberstrass and Allain, 2006). Typically, RBDs are composed of 35-90 amino acids and contact few nucleotides (3-5 nt), and the combinations of RBDs within the same structure is responsible for the increasing of affinity and specificity. These different RNA recognition structures are grouped in RNA Binding Domains (Table 1) (Lunde, Moore and Varani, 2007). The most common are shown in Figure 2, and are: RNA recognition motifs (RRMs) (Cléry, Blatter and Allain, 2008), the most abundant domains in the eukaryotes, the heterogeneous nuclear RNP (hnRNP) K domains (KH) (Valverde, Edwards and Regan, 2008), DEAD box helicase domains, double-stranded RNA-binding motifs (DSRMs)(Linder and Jankowsky, 2011) and zinc-finger domains (Hamosh *et al.*, 2005).

Table1 Table showing a detailed list of the common RNA Binding domains and their features. (Lunde *et al.*, 2007)

| Domain | Topology | RNA-recognition surface | Protein–RNA interactions | Representative structures (PDB ID) |
|-------------------------|------------------------------------|--|--|--|
| RRM | $\alpha\beta$ | Surface of β -sheet | Interacts with about four nucleotides of ssRNA through stacking, electrostatics and hydrogen bonding | U1A N-terminal RRM ¹⁸ (1URN) |
| KH (type I and type II) | $\alpha\beta$ | Hydrophobic cleft formed by variable loop between $\beta 2$, $\beta 3$ and GXXG loop. Type II: same as type I, except variable loop is between $\alpha 2$ and $\beta 2$ | Recognizes about four nucleotides of ssRNA through hydrophobic interactions between non-aromatic residues and the bases; sugar-phosphate backbone contacts from the GXXG loop, and hydrogen bonding to bases | Nova-1 KH3 (type I) ⁴¹ (1EC6), NusA (type II) ³⁷ (2ASB) |
| dsRBD | $\alpha\beta$ | Helix $\alpha 1$, N-terminal portion of helix $\alpha 2$, and loop between $\beta 1$ and $\beta 2$ | Shape-specific recognition of the minor–major groove pattern of dsRNA through contacts to the sugar-phosphate backbone; specific contacts from the N-terminal α -helix to RNA in some proteins | dsRBD3 from Staufen ⁵¹ (1EKZ) |
| ZnF-CCHH | $\alpha\beta$ | Primarily residues in α -helices | Protein side chain contacts to bulged bases in loops and through electrostatic interactions between side chains and the RNA backbone | Fingers 4–6 of TFIIIA ⁴⁶ (1UN6) |
| ZnF-CCCH | Little regular secondary structure | Aromatic side chains form hydrophobic binding pockets for bases that make direct hydrogen bonds to protein backbone | Stacking interactions between aromatic residues and bases create a kink in RNA that allows for the direct recognition of Watson–Crick edges of the bases by the protein backbone | Fingers 1 and 2 of TIS11d ³⁷ (1RGO) |
| S1 | β | Core formed by two β -strands with contributions from surrounding loops | Stacking interactions between bases and aromatic residues and hydrogen bonding to the bases | Ribonuclease II ²¹ (2IX1), exosome ⁹⁹ (2NN6) |
| PAZ | $\alpha\beta$ | Hydrophobic pocket formed by OB-like β -barrel and small $\alpha\beta$ motif | Recognizes single-stranded 3' overhangs of siRNA through stacking interactions and hydrogen bonds | PAZ ⁷³ (1SI3), Argonaute ⁷⁶ (1U04), Dicer ⁷² (2FFL) |
| PIWI | $\alpha\beta$ | Highly conserved pocket, including a metal ion that is bound to the exposed C-terminal carboxylate | Recognizes the defining 5' phosphate group in the siRNA guide strand with a highly conserved binding pocket that includes a metal ion | PIWI ⁷⁵ (1YTU), Argonaute (1U04) ⁷⁶ |
| TRAP | β | Edges of β -sheets between each of the 11 subunits that form the entire protein structure | Recognizes the GAG triplet through stacking interactions and hydrogen bonding to bases; limited contacts to the backbone | TRAP ¹²² (1C9S) |
| Pumilio | α | Two repeats combine to form binding pocket for individual bases; helix $\alpha 2$ provides specificity-determining residues | Binding pockets for bases provided by stacking interactions; specificity dictated by hydrogen bonds to the Watson–Crick face of a base by two amino acids in helix $\alpha 2$ | Pumilio ⁸⁴ (1M8Y) |
| SAM | α | Hydrophobic cavity between three helices surrounded by an electropositive region | Shape-dependent recognition of RNA stem–loop, mainly through interactions with the sugar-phosphate backbone and a single base in the loop | Vts1 ¹²³ (2ESE) |

dsRBD, double-stranded RNA-binding domain; KH, K-homology; OB-like, oligonucleotide/oligosaccharide binding-like; PDB ID, Protein Data Bank identification; RRM, RNA-recognition motif; siRNA, small interfering RNA; ssRNA, single-stranded RNA; ZnF, zinc finger.

However, recent studies have revealed the presence of complex interaction between protein and RNA that requires non-canonical RBDs, thus suggesting the existence of new types of interaction modes and binding modules that still remain to be deeply exploited (Hentze *et al.*, 2018).

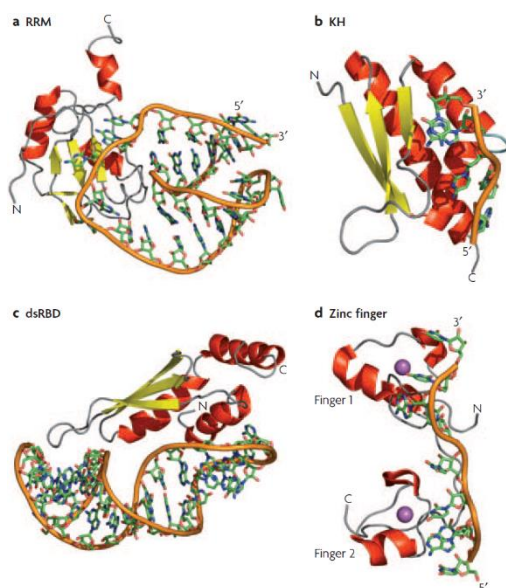


Figure 2. Representation of the RNA binding modules and their interaction with RNA molecule, adopted from Lunde *et al.*, 2007. A) RRM of human U1A binding single stranded RNA by the protein β -sheet protein and through two loops. B) Illustration of Nova-2 KH domain. The conserved exposed loop indicated in light blue interacts with RNA or DNA single strand, at the level of the short consensus sequence: 5'-AUCAC-3'. C) Rnt1 dsRBD is presented. A conserved protein loop is bound to RNA. D) Representation of TIS11d Zinc-fingers domain binding AU-rich element forming hydrogen bonds between the backbone of the protein and RNA nucleotides. The α -helices and the β -sheets composing the zinc finger are coordinated by a zinc atom.

1.2 Targeting RNA Binding Proteins as a new promising therapeutic strategy.

The network made of RNA-protein or protein-protein interactions controlled and created by the RBPs, define the RNA metabolism. Therefore, alterations in the modulation of their RNA-binding function rely on different genes and pathways, leading to complex and controversial phenotypes (Lukong *et al.*, 2008). In particular, aberrant expression of RBPs due to genomic, epigenetic processes or post-translational modifications (PTMs) alterations, forms incorrect post-transcriptional events driving the insurgence of pathological conditions (Hong, 2018). The most widely described diseases, caused by defects in RBPs, are the neurodegenerative ones. This is due to the high expression of RBPs in the brain and the predominant level of alternative splicing, one of the major event regulated by RBPs (Gabut, Chaudhry and Blencowe, 2008; Lukong *et al.*, 2008; Hong, 2018). Moreover, the loss of certain RBPs causes the insurgence of neurological disorders, including Fragile X-syndrome, Spinal Muscular Atrophy and many others (Keene, 2007; Lukong *et al.*, 2008; Hong, 2018). Genome-wide analysis and proteomic data identified many RBPs as pivotal players determining the insurgence, development and progression, not only of neurological and neuromuscular diseases, but also of other pathologies, such as cancers. In cancer, alteration of RBPs expression leads to a dramatic change in cell growth and proliferation dysregulating the expression and function of oncoproteins and tumor-suppressor proteins. It has been shown that, deregulation of specific RBPs is supportive in every step of cancer development, from sustained cell proliferation to evasion of apoptosis and immune surveillance, angiogenesis induction and metastasis stimulation (Pereira, Billaud and Almeida, 2017; Hong, 2018). A panorama showing association of RBPs with human diseases, has been established by using system biology approaches starting from protein interactomes (Lukong *et al.*, 2008) as shown in Table 2 (Keene, 2007).

Table 2 Table showing a detailed list of diseases in which RBPs aberrations are implied. (Keene *et al.*, 2007)

| | | |
|--|---|------------------------|
| Neurodegenerative diseases; POMA paraneoplastic neuropathies | hnRNP-P2; ELAV/HuB,C,D; NOVA1,2 | 49,113,120,124 |
| Fragile X mental retardation | FMRP | 78,81,90,125 |
| Turner syndrome | Ribosomal proteins (RP) | 125 |
| Mitochondrial and metabolic disorders | mitRP; IRP1,2; PCBP1,2 | 113,126 |
| Oculopharyngeal muscular dystrophy | PolyA-binding protein 2 | 127 |
| Spinal muscular atrophy | SMN1,2 | 128 |
| Myotonic dystrophy | CUG-BP/EDEN; CELF3,4,5, | 129 |
| α - and β -thalassaemia; cardiovascular disease | BRUNO; ELAV/Hu; hnRNP-L1; α CP1,2; ETR3 | 113,130 |
| Cancer and genotoxic responses; congenital dyskeratosis | ELAV/Hu; EIF4E; CUG-BP; IMP1-3; RP; musashi; telomerase | 98,103,121,126,131,132 |
| Immunoregulatory disorders | TTP; TIA, TIAR, HuR | 48,55,102,112,118 |

α CP, alpha-C-rich pyrimidine RBP; EIF4E, eukayotic translation initiation factor 4E; ELAV, embryonic lethal, abnormal vision homologue; BRUNO, CELF, ETR and CUG-BP constitute an ELAV-related RBP subfamily that bind to UA or UG-rich sequences including CUG triplet expanded repeats; FMRP, fragile X mental retardation protein; hnRNP, heterogeneous ribonucleoprotein; IMP, insulin-like growth factor mRNA-binding protein; IRP, iron response protein; mitRP, mitochondrial ribosomal protein; NOVA, neurooncological ventral antigen; PCBP, poly(rC)-binding protein; POMA, paraneoplastic opsoclonus-myoclonus ataxia; SMN, survival of motor neuron protein; TIA, T-cell-restricted intracellular antigen RBP; TIAR, TIA-related RBP; TTP, tristetraproline.

Because of these evidences, targeting altered RBPs and their RNA interactors is currently being considered as a new challenging, but promising, therapeutic strategy. For what concerns this field, different methods have been developed aimed in blocking RBPs activity in different contexts. The approaches applied so far are mainly two, one is based on RNA interference, such as the development of antisense oligonucleotides (ASO) against different RBPs. In cancer therapy, the application of ASO against eIF4E for example, is currently facing the clinical trials phase, or the using of small RNA interfering (siRNA) against the RNA Binding protein ELAVL1/HuR delivered with nanocarriers has been shown to compromise cell viability, migration and invasion in lung cancer (Hong, 2018). The second approach, is based on the identification and development of small molecules inhibiting RBPs activity, since recently the concept of considering RBPs as “druggable” targets is spreading, evolving and collecting more evidences (D’Agostino *et al.*, 2019). Through several high-throughput screening assays and further biochemical validation approaches, it has been possible to select compounds showing inhibitory activity towards different RBPs. Musashi, LIN28, KHSPR and the splicing factor SF3b are some examples of proteins whose mis-regulation has been associated with different diseases, such as cancer and neurodegeneration and towards them, different inhibitory compounds have been identified and validated as bioactive molecules (D’Agostino *et al.*, 2019)

In this open field, one of the most widely reported RBPs, is ELAVL1/HuR, that is, indeed the focus of this thesis. HuR is found associated with a variety of diseases and for this reason, the searching for inhibitory drugs still remain controversial and vast.

2. Introduction

2.1 The RNA Binding Protein HuR

HuR, also known as HuA or ELAVL1, belongs to the family of the embryonic lethal abnormal vision (ELAV) of RNA-binding proteins (Ma *et al.*, 1996; Good, 2006), was originally identified in *Drosophila melanogaster* as essential for neural development (Jiménez and Campos-Ortega, 1987; de Silanes *et al.*, 2008). In the human genome, HuR gene is located on the chromosome 19p13.2., the corresponding protein is made of 326 amino acid with a molecular weight of 36 kDa (Ma and Furneaux, 1997). Unlike the other ELAV protein members, whose expression is predominantly in neural tissue, HuR is ubiquitously expressed among cells and tissues and evolutionary conserved among mammals (Zucal, D’Agostino, Loffredo, Mantelli, Thongon, *et al.*, 2015). HuR localization inside the cells is mainly nuclear, but upon certain stimuli, such as stress, hypoxia or DNA damage, it shuttles to the cytoplasm (Abdelmohsen *et al.*, 2008) HuR binding sequence contains AU/UU-rich elements (AREs) located primarily at the level of the 3’ untranslated region (UTR), rarely HuR binds also 5’ UTR of certain number of transcripts (de Silanes *et al.*, 2004; Meng *et al.*, 2005). In this way, HuR generally regulates the fate of thousands of coding and noncoding RNAs from splicing, stability,

to translation (Brennan and Steitz, 2001). In particular, inside the nucleus, HuR is found co-transcriptionally bound to the nascent pre-mRNA, promoting its processing at the level of its splicing and alternative polyadenylation (Izquierdo, 2008; Keene *et al.*, 2011; Lebedeva *et al.*, 2011; Dutertre *et al.*, 2014; Bakheet *et al.*, 2018). Afterwards, HuR is involved in helping the export of its mature mRNA targets to the cytoplasm, where it performs mRNA-stabilizing function, mostly favoring than repressing translation and mediating the storage in the stress granules (Srikantan and Gorospe, 2011). A summary scheme of the whole roles exerted by HuR in the cells is shown in Figure 3.

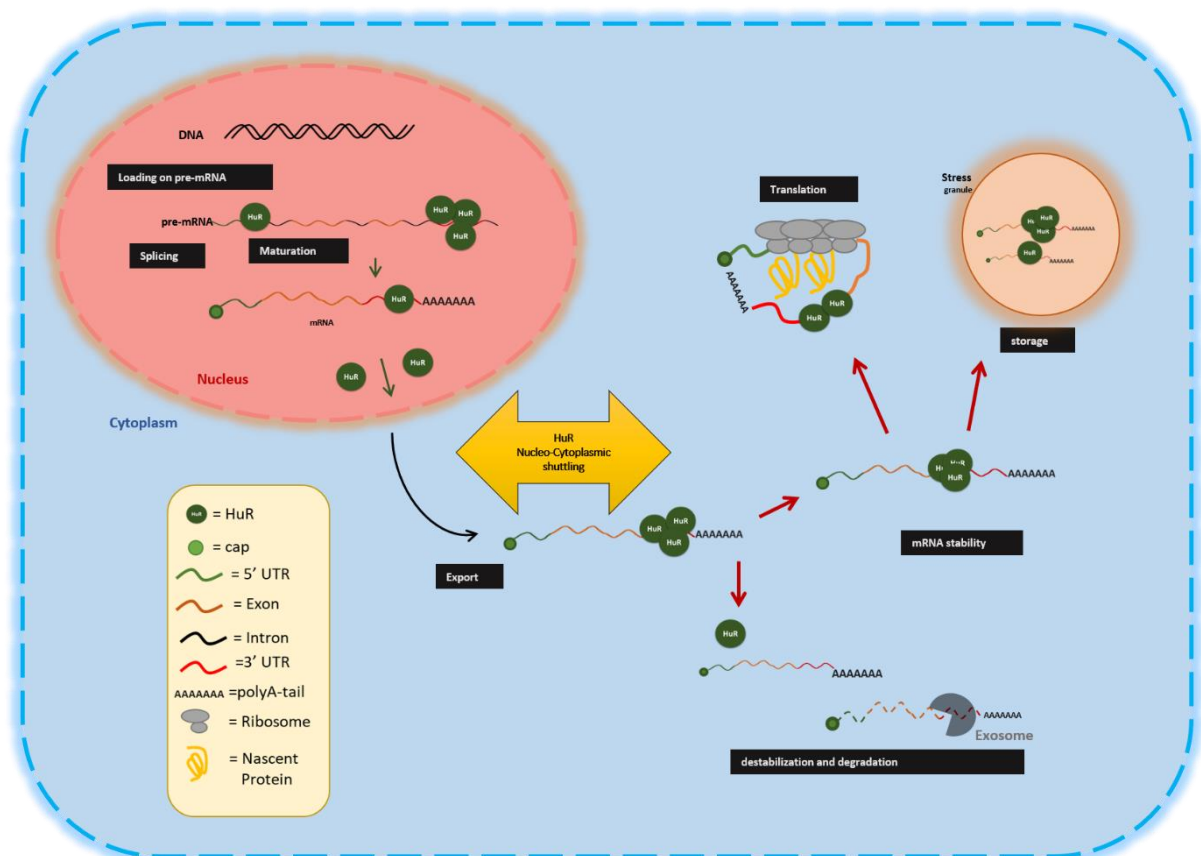


Figure 3. HuR roles inside the cell. (Modified from Subramanya Srikantan and Myriam Gorospe 2011). Inside the nucleus, HuR (green dots) binds pre-mRNA introns (thin green lines) and untranslated regions (red lines) promoting splicing and nuclear processing events. Thanks to the shuttling from the nucleus to the cytoplasm, HuR drives the export of the mature mRNA out of the nucleus, and in the cytoplasm it stabilizes mRNAs, helping mRNA storage (as in stress granules), and modulates target translation.

Hu/ELAV proteins share an akin structure, that is composed of three RNA-recognition motifs (RRMs): RRM1, RRM2, and RRM3. The firsts two RRM, RRM1 and RRM2 are organized in tandem, separated by the third RRM (RRM3) via a less conserved, flexible hinge region (Samson, 2008; Soller, Li and Haussmann, 2010). HuR protein structure is organized as previously described and represented in Figure 4A. As shown in the previous paragraph, RRM domains are made of four β -sheet two α -helices, with the following topology: $\beta 1-\alpha 1-\beta 2-\beta 3-\alpha 2-\beta 4$, in which the sheets are packed against the helices (Figure 2) (Cléry, Blatter and Allain, 2008).

At the N-terminus of HuR, RRM1 and RRM2 motifs are placed in tandem: RRM1 is primarily responsible for RNA binding, but the presence of the second RRM and the inter-domain linker significantly increases the RNA binding affinity of the two RRMs. According to the crystal structure of these two domains, that has been solved by Wang *et al* in 2013, in RNA free condition, RRM1 and 2 are organized in an open structure (Figure 4B). On the other end, in presence of RNA, they undergo conformational changes, assuming a closed shape and forming a positively charged cleft responsible for the binding of the RNA (Figure 4C) (H. Wang *et al.*, 2013). In the hinge region, that is a long loop made of 60 amino acids, between RRM1-2 and RRM3, is placed the domain responsible for HuR nucleo-cytoplasmic shuttling (HNS) and protein-protein interactions (Fan and Joan A Steitz, 1998; Guttinger *et al.*, 2004). If the first two RRMs and the hinge region have been clearly described, the roles of the RRM3 remain controversial. RRM3 is known to bind mRNA polyA tail and promote the protein oligomerization, but recently the crystal structure of this domain has been solved (Figure 4D) and new functions have been ascribed to it. Through high-resolution structural analysis and *in vitro* binding studies, it has been suggested that RRM3 participates in the RNA binding, according to the canonical properties of this domain (Pabis *et al.*, 2019). Putting all these observations together a new model of interaction and RNA binding has been proposed, in which all the three RRMs are bound together in a closed and multimeric conformation, but upon RNA interaction HuR acquires a rigid and aligned shape, pivotal for the exploiting of its function (H. Wang *et al.*, 2013; Pabis *et al.*, 2019).

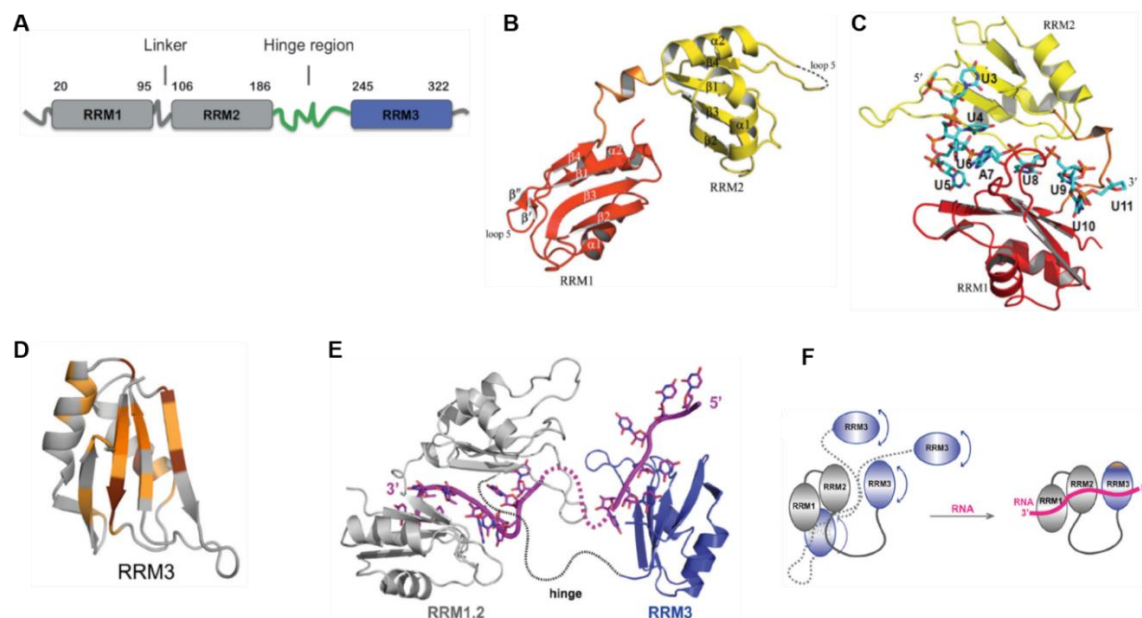


Figure 4 HuR global structure (modified from Wang *et al.*, 2013 and Pabis *et al.*, 2019).

A) Schematic representation of HuR protein structure and domains asset. B) Crystal structure of RRM1 and RRM2 without RNA bound. C) RRM1,2 crystal structure highlighting the conformational changes of RRM1 and RRM2 in presence of RNA. D) RRM3 crystal structure. E) Recent structure proposed of the three domains (RRM1,2 and 3) co-participating in the RNA binding. F) Schematic picture showing HuR and its domains, oligomerizing and interacting in absence of RNA and changing shape after RNA binding.

2.2 HuR regulation, functions and association with diseases

Considering its fundamental role inside the cells, HuR expression is finely regulated at different levels. From the transcriptional point of view, the mechanism of its regulation is still unclear.

It has been shown that the transcription factors NF- κ B (Kang *et al.*, 2008) and the Smad family proteins (Jeyaraj *et al.*, 2010) are responsible for the modulation of HuR expression. A further step of regulation is given by HuR itself, that is able to bind and stabilize its own mRNA (Pullmann *et al.*, 2007). At the level of the structure, *HuR* mRNA harbors different alternative polyadenylation variants, that are responsible for the transcript protection from degradation and decay and nucleo-cytoplasmic export promotion (Al-Ahmadi *et al.*, 2009; Chang *et al.*, 2010).

HuR translation instead, is negatively regulated mainly by different microRNAs, such as miR-519 and miR-125a (Guo, Wu and Hartley, 2009; Marasa *et al.*, 2010) and by post-translational modification. In particular, HuR is phosphorylated at different level by a variety of kinases, such as serin/threonine-kinase ChK2, the mitogen-activated protein kinase (MAPK) p38 and protein kinase C delta (Abdelmohsen *et al.*, 2007; Yu *et al.*, 2011; Schulz *et al.*, 2013; Akaike *et al.*, 2014). HuR is found also methylated by CARM1 (Pang *et al.*, 2013) and neddylated (Fernández-Ramos and Martínez-Chantar, 2015). These PTMs can occur either at the level of RRM1 or HNS site, affecting HuR affinity to targets or its localization. Furthermore, HuR is degraded after ubiquitination (Abdelmohsen *et al.*, 2009) by the proteasome machinery, or cleaved by caspases during apoptosis (Mazroui *et al.*, 2008).

Modulation of HuR expression, such as over-expression and depletion with small-interfering RNAs, clearly demonstrated that its ablation is related with impairment in the proper differentiation of different cellular lineages, including spermatocytes, myocytes, and adipocytes (Cuadrado *et al.*, 2003; Levadoux-Martin *et al.*, 2003; Van Der Giessen *et al.*, 2003; Cherry *et al.*, 2008)

Moreover, HuR deletion in mice affects the proper development of embryonic and extraembryonic structures, thus leading to embryo-lethality (Katsanou *et al.*, 2009), suggesting that vast impact generated by HuR loss, is related to its functions. Indeed, it specifically binds and regulates the fate of ARE containing mRNAs, estimated to represent the 7% of the human protein-coding gene transcripts. These mRNAs encode for protein involved in key processes as: immune response and inflammation (Atasoy *et al.*, 1998; Katsanou *et al.*, 2005; Yiakouvaki *et al.*, 2012; Kafasla, Skliris and Kontoyiannis, 2014), cell division (Wang *et al.*, 2000) angiogenesis (Levy *et al.*, 1998; Tang, Breen and Wagner, 2015), senescence (Wang *et al.*, 2002) and apoptosis (Abdelmohsen *et al.*, 2007)

In particular, *p21*, *c-FOS*, the vascular endothelial growth factor (*VEGF*), *SIRT1*, *TNF α* , *Bcl-2*, *Mcl-1*, *COX-2*, *p53*, numerous growth factors, cyclins, cyclin inhibitors, chemokines and cytokines are part of the vast panorama of transcripts bound and regulated by HuR (Figure 5) (Zucal *et al.*, 2015). For this reason, HuR is considered one of the major regulators of gene expression, being pivotal for cells and tissue homeostasis and physiology. As a consequence, HuR de-regulation leads to the appearance of different disorders, such as cardiovascular diseases (Gu *et al.*, 2017; Zhou *et al.*,

2018) nephropathies (Yu *et al.*, 2015; Shang and Zhao, 2017), retinal diseases (Amadio *et al.*, 2010; Khera, Dick and Nicholson, 2010; Viiri *et al.*, 2013), muscular disorders (Di Marco *et al.*, 2005; Nakano *et al.*, 2005; Wu *et al.*, 2017) and neurological diseases (Skloris *et al.*, 2015). However, among these pathologies, HuR has been found deeply involved in the development of a variety of cancers and inflammation diseases.

2.3 HuR in cancer

The transition from a normal cell to a cancer one implies the dysregulation of specific physiological processes, leading to the acquisition of the following phenotypes: enhanced proliferation, avoiding of apoptosis, sustained angiogenesis, migration, metastatic potential (Figure 5) and resistance to chemo- and radio-therapies (Riaz *et al.*, 2016)(Hanahan and Weinberg, 2011). As described above, a vast number of HuR-regulated mRNAs containing AU rich elements in their 3'UTRs, is known to be responsible for the appearance of these oncogenic traits (Kotb Abdelmohsen, 2013) (Figure 5).

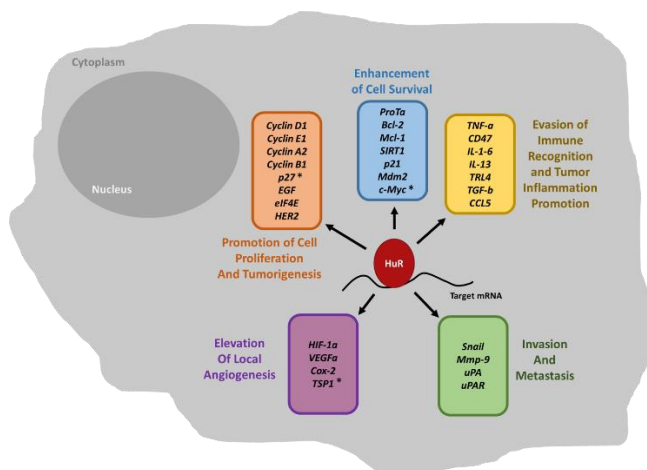


Figure 5. HuR targets mRNAs implicated in the insurgence of cancer traits (modified from Gorospe 2010 and Wang 2013). List of the most relevant HuR target mRNAs involved in five major aspects characterizing cancer.

* indicates transcripts with a decrease expression, due to the presence of HuR, since HuR represses them at the translational level (c-Myc, p27), or because its association with HuR is lower in the context of cancer (TSP1).

Dramatic HuR overexpression and high nuclear, or cytoplasmic localization have been associated with malignant transformation and related with patients prognosis in a significant number of human cancers, including breast, colon, ovarian, prostate, pancreatic, oral cancer, urinary, skin and many others (Kotta-Loizou, Giaginis and Theocharis, 2014).

Dixon and Nabors through studies pursued in brain and colon cancers have found an elevated HuR expression related with subsequent increasing in the expression of a number of its targets as COX-2, VEGF, TGF-β, IL-8 was observed (Dixon *et al.*, 2001; Nabors *et al.*, 2001).

Cyclooxygenase-2 (COX-2), being an inducible enzyme in the synthesis of prostaglandins, has been reported to be a relevant prognostic factor. Prostaglandins are recognized as HuR targets, as it regulates their aberrant expression, especially in cancer and colorectal cancer. In these studies, COX2 and HuR expression has been found elevated in normal epithelium, high-grade prostatic intraepithelial neoplasia, prostate (Barbisan *et al.*, 2009) and ovarian carcinomas (Lu *et al.*, 2006).

On the other end, angiogenesis is a pivotal mechanism eliciting tumor progression and HuR has been shown, as mentioned above, to control the faith of *Vascular endothelial growth factor-A (VEGF-A)*, *interleukin-8 (IL-8)*, *hypoxia-inducible factor- α (HIF- α)*, and *COX-2*, that are involved in this processes (Yoo *et al.*, 2006; Zucal *et al.*, 2015). Many studies based on the analyses of histological, clinical samples, demonstrated the existence of a positive correlation between cytoplasmic HuR accumulation and *VEGFA*, *VEGFC*, *COX2* and *IL-8* in human tumor samples. HuR was also found to be related with high-density of blood microvessels and furthermore its presence inside the cytoplasm has been associated with large size of human different tumors (J. Wang *et al.*, 2013).

For what concerns cell migration and metastasis, HuR stabilizes different transcripts, such as *Snail*, that regulates epithelial-mesenchymal transition, *MMP-9*, *uPA* and its receptor, known to be invasive factors (Tran, Maurer and Nagamine, 2003; Dong *et al.*, 2007; Yuan *et al.*, 2011). In fact, HuR knockdown strongly inhibited *MMP-9* expression and HuR depletion in breast epithelial immortalized cell line is correlated with a reduction in anchorage growth, cell invasion and high level of programmed cell death, due to HuR binding to *CTGF* and *RAB31* transcripts (Heinonen *et al.*, 2011).

As depicted in the Figure 5, many are the HuR related transcripts discovered so far and until now, more putative targets have been found and added to the list, demonstrating that HuR mainly acts as a positive agent determining the insurgence and progression of cancers. Indeed, in breast cancer, cytoplasmic HuR accumulation is associated with high-grade invasive ductal breast carcinoma, with poor outcome and poor survival. It has been shown, that HuR is able to bind and increase the expression of cyclin E1, estrogen receptor (ER), BRCA1, Cylclin D1 (Yuan *et al.*, 2011; Kotb Abdelmohsen, 2013). Not only, in human breast cancer cell lines, it has been shown that, via a regulatory network, an increased HuR expression driven by the factor HSF1, is related to an increased expression of *CTNNB1* mRNA (*β -catenin*), responsible for stimulating stem cell renewal and cell adhesion, critical for carcinogenesis (Chou *et al.*, 2015). HuR knockdown with shRNA in different breast cancer cell lines, as MCF7 and MDA-MB-231, reduces cells viability, tumor growth due to an induction of apoptosis (Saunus *et al.*, 2008; Zhang *et al.*, 2017). An increased uncontrolled HuR expression has been related with chemotherapy resistance. In fact, recently, in breast cancer therapy, it has been shown, by RNP immunoprecipitation and pulldown assays, that pharmacoresistance to tamoxifen was implied to an overproduction of *ERBB2* mRNA promoted by HuR (Tan *et al.*, 2017; Manzoni *et al.*, 2018a). Through similar experiments, in the context of chemo and radioresistance, in colon cancer cell lines, such as DLD-1 and HCT-15, it has been observed that HuR downregulates the production of caspase-2 mRNAs, by binding its 5'UTRs, decreasing apoptosis, thus increasing the resistance to therapeutic ionizing radiations. This effect indeed has been reverted by HuR depletion in these cell lines (Badawi *et al.*, 2017). Furthermore, overexpression of HuR increased the growth of colon and breast cancer cells in nude mouse xenograft model. On the other end, HuR silencing or complete knockout with CRISPR/cas9 in different pancreatic and colon cancer cell lines, inhibited tumor growth and development in xenograft model (Lal *et al.*, 2017).

In conclusion, all these evidences suggested that HuR exerts a critical role in vast majority of human cancers, thus can be considered as a valid target for therapeutic purpose.

2.4 HuR in inflammation

Evasion of the immune response and promotion of inflammation are two different mechanisms recognized as pivotal for the progression and evolution of cancer processes (Figure 5). HuR, plays an important role in innate, adaptive immunity and inflammatory pathways, in physiological and pathological condition. In fact, 90% of mRNAs coding for cytokines and chemokines contains repeated AREs sites in the 3'UTR, making these transcripts unstable and tightly regulated by stabilizer or de-stabilizer trans-factors like RBPs, as HuR, Tristetraprolin (TTP) and TIA1. This gives rise to a rapid degradation and turnover of these mRNAs in response to changes in cells/tissues environments (Fan and Joan A. Steitz, 1998; Fan *et al.*, 2005; Seko *et al.*, 2006).

First, HuR has been suggested to be involved in determining the insurgence of pro-inflammatory response to agents as lipopolisaccharide (LPS), since it prevents the degradation of *toll-like receptor 4 (TRL4)* mRNA, giving rise to an up-regulation of the inflammation processes in model of vascular inflammation and atherogenesis (Lin *et al.*, 2006).

Afterwards, HuR has been associated with diverse arrays of events consisting in the stabilization of the following inducible transcripts: *interferon- γ* , *TNF α* , *IL-6*; *IL-8*, *IL-3*, *IL-1 β* and the *urokinase-type plasminogen activator*, that are key mediators of the inflammatory and immune response (Anderson, 2010). Interferon- γ , TNF α represent the major pro-inflammatory agents secreted and found inside monocytes/macrophages infiltration. In particular, Interferon- γ is highly produced by Natural killer cells (NKs) and activated T lymphocytes (CD4+ Th1 cells), while high level of TNF α is associated with macrophages (Shang and Zhao, 2017).

A study revealed that CX3CL1/fractalkine, that is a chemokine specific to monocytes and NK cells, contains ARE sequence in 3'UTR of the transcript, that can be regulated by HuR in a post-transcriptional manner. In this way HuR has been suggested to modulate the cytokines and chemokines releasement by binding to the respective mRNAs but indirectly also affecting the maturation of the major players of the innate immunity (Matsumiya *et al.*, 2010). It has been suggested also, that HuR regulates angiogenesis and inflammation in macrophages (Zhang *et al.*, 2012). HuR roles in macrophages, have been strengthened recently when a transcriptome profiling analysis have been performed in bone-marrow derived macrophages (BMDMs) wild type and knockout for *ELAVL1* expression. PAR-CLIP-seq experiments have shown that the expression of macrophage-related genes involved in vascular development and angiogenesis, is tightly regulated at the post-transcriptional level by an intricaded interplay generated by HuR and different micro-RNAs (Lu *et al.*, 2014). Furthermore, in 2016, Sedlyarov *et al.* performed similar PAR-iCLIP experiments in primary macrophages upon inflammatory stimuli with LPS, proving the existence of a complicated

post-transcriptional regulation landscape balanced by the presence of a de-stabilizing activity of TTP and a stabilizing one given by HuR. In fact, authors were able to identify two groups of transcripts bound and modulated exclusively by either TTP or HuR and a third one, represented by mRNAs, as *TNF α* or *CXCL2* that can be bound simultaneously by both TTP and HuR,

This highlights the existence of a tight competition between these two proteins, that reflects in the insurgence of a vulnerable balance in the maintenance of the proper post-transcriptional pattern regulated by TTP and HuR at the same time (Sedlyarov *et al.*, 2016; Tiedje *et al.*, 2016).

Recently, during LPS response in macrophage cell lines, another mechanism has been described for HuR-mediated increasing in the stabilization and binding of different cytokines and chemokines' transcripts, such as *CXCL2*. It consists in a PTMs inferred by PARP1 to HuR, known as PAR-ylation. This modification of HuR influences its shuttling to the cytoplasm and increase its ability in binding different pro-inflammatory mRNAs (Ke *et al.*, 2017).

On the other end, it has been shown through the generation of an inducible *ELAVL1* knockout mouse model, that HuR seems to be essential for the maintenance of hematopoietic stem cells during hematopoiesis (Ghosh *et al.*, 2009).

Moreover, HuR has been proposed to be pivotal for the B cell development and function, as well for the maintenance of a homeostatic balance between T and B cells (de Graaf *et al.*, 2008; Diaz-Muñoz *et al.*, 2015). In addition, Papadaki *et al.*, (2009), demonstrated, by using Cre-LoxP system, that HuR deletion in thymocyte development reflects in a loss of the peripheral T cells, highlighting HuR importance in controlling thymocytes maturation and trafficking (Papadaki *et al.*, 2009). In T cells, HuR plays a role in modulating the maturation and polarization of Th2 and Th17 T-cell lineages, by positively binding and stabilizing the 3'UTRs of IL-2 and IL-17 transcripts (Chen *et al.*, 2013; Techasintana *et al.*, 2017). It has been reported also, that HuR deletion in distal lung epithelium decreases neutrophilia and pulmonary inflammation level induced by IL-17, increasing the mRNA decay of different chemokines (*CXCL1* and *CXCL5*) (Herjan *et al.*, 2013). Th17 cells, thanks to their ability to migrate, are the major mediators of the generation of inflammatory infiltrations in Central Nervous System (CNS) in the context of neuroinflammation. Functional studies and generation of *ELAVL1* conditional knockout in mice of CD4+ T cell lineage, clarified that In Experimental Autoimmune Encephalomyelitis (EAE), HuR binds directly the 3'UTR of *CCR6*. *CCR6* is a C-C chemokine receptor 6, sited in the surface of the Th17 cells and responsive to migration stimuli exerted by the releasement of *CCL20* or chemokine ligand 20, which is constitutively secreted by choroid-plexus epithelial cells in the site of inflammation. A complete ablation of HuR, significantly decreases the production of *CCR6*, thus lowering the portion of migrating Th17 cells, ameliorating the pathogenic neuroinflammation processes in the CNS and the EAE outcome in mice (Chen *et al.*, 2017). Although these evidences described HuR as pro-inflammatory agent, its role in inflammation remain still controversial.

Indeed, it has been demonstrated that in macrophages derived from mice lacking HuR in the myeloid-lineage cells, HuR deficiency has been linked with an increasing of pro-inflammatory cytokines. The HuR KO cells presented an increased CCR2-mediated chemotaxis and an enhancements in the use of inflammatory mRNAs (including *Tnf*, *Tgfb*, *Il10*, *Ccr2*, and *Ccl2*), due to mis-regulation in the translational and stability levels. This causes an increase susceptibility of these mice to develop colitis associated cancer (Yiakouvaki *et al.*, 2012).

Another example concerning HuR contradictory role, came out from experiments performed in a co-culture model of primary human macrophages and MC7 breast cancer cell line. Authors were able to demonstrate that HuR suppresses the production of CCL5, leukocyte attracting chemokine, reducing the infiltration of the pathogenic macrophages in the tumor site, preventing the exacerbation of the inflammation processes (Brauß *et al.*, 2017).

In conclusion, the role of HuR remains controversial in controlling the immune response and inflammation processes, and probably it is strictly related to the context.

However, despite of these minor, but existing evidences, it is clear that HuR is pivotal for maturation, migration, cytokine and chemokine secretion of cells belonging to the both innate and adaptive immunity response. The inhibition of HuR via small-interfering RNAs or chemicals it is emerging to be a valid approach to first better understand the role of HuR towards these processes and secondly from a therapeutic point of view, targeting HuR seems to be an effective strategy to ameliorate diseases outcome in which there is an uncontrolled inflammation processes ongoing.

2.5 Targeting HuR with small molecules

A number of small compounds interfering with HuR activity has been identified so far and they can be divided in two different groups: the first includes molecules known to indirectly act on HuR by affecting its localization inside the cell, and the second one, made of those showing to directly impair the interaction between HuR and its RNA target.

MPT0B098, a 7-aryl-indoline-1-benzene-sulfonamide compound showed toxicity in human cancer cell lines and has been described as a potent microtubule inhibitor, accelerating the degradation of hypoxia inducible factor α (HIF- α) at the level of its mRNA, whose stability and translation is enhanced by HuR. Indeed, MPT0B098 impedes the translocation of HuR from the nucleus to the cytoplasm, thus destabilizing its target mRNAs, such as HIF- α (Cheng *et al.*, 2013).

Hepatocellular carcinoma, Hep3B cells, that are highly metastatic underwent death if treated with N-Benzylcantharidinamide. This agent, blocks HuR translocation into the cytoplasm increasing the degradation of MMP9, a metastatic factor, whose mRNA is bound HuR that promotes its stability (Lee *et al.*, 2014). Similar mechanisms have been ascribed to Triptolide, an oxygenated diterpene inhibiting HuR shuttling, suppressing *TNF α* and *COX-2* in lung cancer cells (Sun *et al.*, 2011).

On the other end, several drugs stimulate HuR accumulation in the cytoplasm, as reported for

Actinomycin-D (Fan and Joan A Steitz, 1998)

In 2014, it has been shown that Doxorubicin reduces the association of HuR to certain polyA stretches inside different mRNAs in MCF7 cells, impairing the alternative splicing processes of transcripts coding for protein isoforms with cancer-related functions. A direct interaction between Doxorubicin and HuR with biochemical assays, has not been described yet. Thus, no functional mechanism has been proposed for this event, a possible explanation could be that different protein kinases implied in DNA damage signalling, are responsible for HuR phosphorylation causing its localization in the cytoplasm. Therefore, Doxo induces DNA damage in the cells and subsequent HuR translocation out of the nucleus, preventing its binding to exons and splicing promotion. On the other end, another hypothesis could be that Doxo being a topoisomerase inhibitor, prevented conformational changes on the chromatin, leading to the formation of not-accessible structure, impairing HuR pre-mRNA binding and related splicing, but no evidences regarding these events have been collected so far (Dutertre *et al.*, 2014).

Many others drugs similar to the ones described above have been identified, the limitation of their actions regards their specificity and mechanism of inhibition. Thus, the searching for compounds directly inhibiting HuR-RNA complex is still at its infancy. In 2007, Meisner *et al.*, performed a screening of 50,000 compounds and identified the first small HuR-inhibitors. In order to perform the screening assay, they used fluorescent distribution analysis (FIDA) by using a HuR shortened recombinant protein. From this screening, the most potent hits coming out were respectively dehydromutactin, MS-444 and okicenone. By using mathematical and experimental analysis, a mechanism of action for these compounds has been proposed. Indeed, it has been shown that by binding the HuR first two RRMs, they act preventing HuR homo-dimerization. This reflects in a global inhibition of HuR nucleus-cytoplasm shuttling, reduction in cytokine expression and primary T-cell line activation (Meisner *et al.*, 2007).

Quercetin, b-40 and b-41 are three compounds emerged from a screening of 179 compounds performed in 2009. In particular, authors identified these putative HuR inhibitors able to disrupt the interaction between HuR and the ARE sequence of *TNF α* , through electrophoretic mobility shift assays for RNA-protein complexes (RNA-EMSA) and filter binding biochemical approaches. In particular, they generated TTP and HuR recombinant S-transferase (GST) fusion proteins and tested *in vitro* their capability of binding the radiolabeled ARE sequence derived from *TNF α* in RNA-EMSA. Further experiments were performed in murine macrophage cell line RAW264.7, after stimulation with LPS, Quercetin and b-40 treatments caused a decrease in the stability of *TNF α* mRNA and a reduction in the secretion of the protein (Chae *et al.*, 2009).

A novel biochemical assay, suitable for HTS investigations, to study the *in vitro* HuR protein-RNA complex formation has been proposed in 2013 by our group. This assay is based on AlphaScreen technology, through which has been possible to quantify the binding efficacy between a purified HuR protein and a probe containing ARE sequences belonging to *TNF α* . This method has been extremely

useful for the quantification of binding parameters, such as the dissociation constant (K_D) between HuR and the target RNA quantified in the low nanomolar range. Using this assay, authors screened 2000 small molecules that have been further validated with RNA-EMSA and mitoxantrone have been selected as a modulator of HuR binding activity (D'Agostino, Adami and Provenzani, 2013). Moreover, in 2015, our group, exploiting this technique, identified the natural compound dihydrotanshinone-I (DHTS), as a highly promising hit showing a potent inhibition activity towards HuR and a clear mechanism of action for DHTS has been described so far. Recently, DHTS structure has been considered the leading molecular scaffold for the chemical synthesis of ameliorating molecules called Tanshinone Mimics (TM), and these compounds have been tested at different level. However, the discovery of DHTS and characterization of Tanshinone Mimics will be elucidated in details in the next paragraph. Apart from this, between 2015 and 2017, other HuR inhibitors have been proposed and identified. In particular, Wang et al., using a fluorescence based high-throughput screening, tested a library of 1597 compounds, and validated several hits with Nuclear Magnetic Resonance (NMR) and saturation transfer difference (STD) assay, furthermore they were able to ascribe a mechanism of action based in the disruption of HuR oligomerization, blocking the mRNA binding (Wang, Bhattacharya and Ivanov, 2015). In 2015, around 6000 compounds were screened via polarized fluorescence (FP) assay and authors identified molecules that were further validated with different methods as AlphaLISA, Surface Plasmon Resonance (SPR), RNP immunoprecipitation (IP) assays, luciferase reporter experiments and demonstrated their inhibitory activity ranging at the nanomolar concentration, preventing HuR function by competitive binding with HuR (Wu *et al.*, 2015). In 2017, with a similar screening approach, Kuer et al. isolated the compound azaphilone-9 (AZA-9) deriving from the fungal natural product asperbenzaldehy. AZA-9 is able to bind HuR and thus inhibiting HuR-ARE interaction and further validations performed with SPR revealed the direct binding between the compound and HuR. Through NMR studies and computational docking, it has been possible to identify residues inside the protein cleft involved in the binding with AZA-9 (Kaur *et al.*, 2017).

Most of the inhibitors presented so far have been identified as potent *in vitro* disruptors, but they lack of *in vivo* and biological activity proofs and considering the structural diversity of these compounds, and the different mechanism of inhibition proposed, the searching for highly potent and bio-active molecules considered HuR inhibitors still remain a challenge.

In Table3 the list of HuR inhibitors discovered until now is presented and the HTS assays used for the screening and further validation are mentioned.

Table 3. List of screening assays performed to identify HuR-RNA disruptors (Adjusted from D'Agostino et al., 2019).

| Target | Reference | Year | Screening Assay | Throughput | Validated Compounds |
|----------------------|-----------|------|---|------------|-----------------------|
| HuR-IL2 ARE | 72 | 2007 | Confocal fluctuation spectroscopic (anisotropy) | 50,000 | MS-444, okicenone |
| HuR-TNF α ARE | 103 | 2009 | RNA EMSA and filter binding assays | 179 | Quercetin, b-40, b-41 |
| HuR-TNF α ARE | 104 | 2013 | AlphaScreen | 2000 | Mitoxantrone |
| HuR-TNF α ARE | 105 | 2015 | AlphaScreen | 107 | Dihydrotanshinone-I |
| HuR-MSII ARE | 109 | 2015 | FP | 6000 | CMLD 1-6, NCI-3 |
| HuR-C-Fos ARE | 108 | 2015 | FP | 1597 | C10 |
| HuR-MSII ARE | 110 | 2017 | FP | 2000 | Azaphilone-9 (AZA-9) |

2.6 Identification and characterization of Dihydrotanshinone-1 (DHTS) and Tanshinone Mimics (TMs).

As mentioned above, D'Agostino et al., in 2015 performed an High-throughput screening (HTS) based on Alpha Screen technology: Amplified Luminescent Proximity Homogenous Assay. The method has been based on the application of a recombinant protein HuR (rHuR) tagged with the 6XHis sequence able to bind nickel conjugated acceptor beads. On the other side a biotinylated single strand AU-rich RNA probe (Bi-AU) is linked with streptavidin-coated donor beads. The binding between rHuR and the Bi-AU brings the beads in closed proximity and a fluorescent signal is detected. If there is an interference between this binding the signal evaluated is lower (D'Agostino, Adami and Provenzani, 2013). Dihydrotanshinone-I (DHTS) emerged as an HuR inhibitors in a secondary screening using a small library of anti-inflammatory compounds (D'Agostino *et al.*, 2015). DHTS (Figure 6A) is a natural compound extracted from the plant *Salvia miltiorrhiza* and well known in Chinese traditional medicine practice mainly to cure cardiovascular diseases (Chang, HM et al., 1990). The effectiveness in interfering with the binding between HuR and mRNA was further validated with complementary assays as Alpha screen and RNA-EMSA (Figure 6B). Through NMR titration and molecular dynamics simulation, it has been demonstrated that DHTS interacts with HuR at the level of the cleft formed by RRM1 and RRM2, stabilizing them in a closed conformation, thus preventing the binding with the target RNA (Figure 6C) (D'Agostino *et al.*, 2015; Lal *et al.*, 2017). DHTS anticancer activity has been shown in different cell lines, in which treatment with DHTS sub-toxic doses disrupt HuR interaction with known HuR oncogenic targets, such as *TNF α* , *CTNNB1* and *ERBB2* (Manzoni *et al.*, 2018). RNP Immunoprecipitation (RIP) experiments demonstrated that upon DHTS treatment a reduction in the association with *TNF α* mRNA was detected in MCF7 cell line stimulated with LPS (Figure 6D) and through polysome profiling approaches a reduction of the translation of *TNF α* was demonstrated (D'Agostino *et al.*, 2015). Moreover, DHTS has been demonstrated to inhibits *in vivo* xenograft tumor growth in a HuR dependent manner without systemic toxicity (Figure 6E/F) (Lal *et al.*, 2017).

Details will be presented in the *Results* section.

Starting from DHTS molecular scaffold, more potent analogs have been synthesized and described so far (Manzoni *et al.*, 2018) These optimized molecules show higher specificity for HuR than DHTS and improvements concerning their solubility for *in vivo* experimental approach.

My PhD project has been based in characterize and describe DHTS anticancer activity phenotypically and at the genome-wide level, in order to a better understanding for a rational design of DHTS analogs. On the other end, I have characterized the new class of analogs called Tanshinone Mimics (TMs) assigning to them anticancer and anti-inflammatory properties in which *in vivo* evidences have been collected.

The aim of my work is entirely present in the Hypothesis and Aims section

3. Hypothesis and Aim

Dysregulation of HuR, such as its overexpression or aberrant mis-localization in the cell, has been associated with several pathologies, like nephropathies, retinal, cardiovascular, muscular and neurological disorders, a variety of cancers and inflammation diseases. For example, HuR overexpression or cytoplasmic expression have been associated with malignant transformation and with poor prognosis in a significant number of human cancers, including breast, colon, ovarian, prostate, pancreatic, oral, urinary, skin and many others (Loizou *et al.*, 2014). This may be due to the fact that HuR regulates mRNAs coding for oncogenic proteins (e.g. *TNF α* , *VEGF*, *ERBB2* and *CTNNB1*). Moreover, critical for tumor progression, is the aberrant crosstalk established between cancer cells and uncontrolled inflammatory processes and HuR plays a strong regulatory role in immune system development and homeostasis either in the innate immunity and in the adaptive one, considering that 90% of mRNAs coding for cytokines and chemokines contains repeated AREs sites in the 3'UTR. In particular, it mediates macrophages inflammatory response and recently HuR has been found associated as a promoter of the neuro-inflammation processes in a mouse model of Multiple Sclerosis disease.

Therefore, HuR has been suggested as a drug target. However, due to its controversial role, several doubts remain concerning the opportunity of its pharmacological exploitation: considering the importance of HuR in supporting physiological processes in all the cells within the organism, it remains an open question whether blocking its activity by using small molecules could induce a general unspecific toxicity. Furthermore, regarding biochemical approaches applied so far, HuR represents a hard-to-study protein, showing several limitations, considering its tendency to precipitate when used for *in vitro* applications and the presence of unfolded regions in its structure which limit its utilization with canonical tools of drug discovery. Despite these, HuR still remains a promising target for therapeutics purposes. Reducing or controlling HuR functions could have a

significant impact in a large number of applications, mainly because its context-dependent activation orchestrates a gene expression reorganization proper to selected disease. Therefore, through HuR modulation, a vast number of coding and non-coding RNAs, mis-regulated in the specific disease, determining its insurgence and onset, would be affected, amplifying the therapeutic benefit of the treatments.

Until now, a variety of studies have been explored regarding the possibility of using small molecules impairing HuR functions. Among the small molecules identified as HuR inhibitors, in 2015 our group discovered the natural compounds DHTS as an HuR:mRNA complex disruptor *in vitro* and in cellular context. Our group ascribed a mechanism of action for DHTS, starting from describing HuR binding residues affected by DHTS activity until proving its anti-cancer properties, that is also reducing tumor growth in xenograft mouse model in a HuR dependent manner. DHTS has been used as the scaffold molecule from which our group, by applying a functional oriented synthesis, produced two generations of new chemical analogs called Tanshinone Mimics (TMs-I and TMs-II). Hence, we described Structure-Activity-Relationships (SARs) towards HuR binding, aiming at ameliorating the molecules towards a better HuR targeting specificity and bioavailability.

Specifically, my study has been focused on:

- Investigating deeply DHTS biological activity at genome-wide level, towards HuR inhibition, providing a full description of its mechanism of action pivotal for the rational synthesis of TMs
- Characterizing TMs biological anti-cancer activities in different cancer cell lines, identifying the most potent compounds and describing their mechanism of action in affecting HuR activity concerning selected targets involved in cancer, finally proving that TMs are suitable for *in vivo* applications
- Evaluating TMs anti-inflammatory properties: I have investigated their activity towards sustained inflammatory processes, promoted by LPS stimuli in cellular context (e.g. RAW264.7 and murine primary macrophages) and by collecting *in vivo* evidences in LPS-induced peritonitis mouse model.

Furthermore, I have investigated on TMs effects on adaptive immunity, in murine primary T-cells, differentiated respectively in Th1, Th17 lineages.

Summing up, during my PhD project I have contributed to characterize and identify HuR inhibitors from a biochemical and biological point of view, testing their suitability for *in vivo* models laying the groundwork for therapeutic purpose towards cancer disease and inflammatory disorders that arise from aberrant HuR functions.

4. Results and Comments

4.1 Insights on DHTS mechanism of action towards HuR inhibition.

As already mentioned in the Introduction, our group, in 2015, performed a high-throughput screening (HTS), aiming at the identification of HuR inhibitors. The assay was based in testing a library of anti-inflammatory compounds made of 107 molecules in their capability of disrupting the interaction between a recombinant version of human HuR (rHuR) and an RNA probe. The approach used to perform this assay was via Alpha screen technology suitable for HTS purposes. From this screening, dihydrotanshinone I (DHTS) came out and was further validated with biochemical methods as RNA-EMSA and dose response Alpha Screen assay. DHTS, has been revealed to impair HuR binding in nanomolar range concentration (D'Agostino *et al.*, 2015) (Figure 6B). Furthermore, through NMR and molecular modeling studies as docking calculations and molecular dynamics (MD) simulations, we have been able to characterize the binding between DHTS and HuR (Figure 6C). Indeed, the molecule prevents the binding between HuR and the target RNA by binding and stabilizing it in a closed conformation not accessible for the RNA. More precisely, we identified the β -platform region inside the RRM1 domain of HuR, to be responsible for DHTS and HuR binding. By mutagenesis, we generated HuR point-mutated recombinant proteins, in that region and thanks to this approach we individuated the aminoacidic residues responsible for DHTS binding (Lal *et al.*, 2017).

Afterwards, we evaluated DHTS biological activity, focusing mainly on DHTS anticancer properties in a HuR dependent manner. In particular, we first checked toxicity in a variety of cancer cell lines (MCF7, MDA-MB 231, HCT116, PANC-1) and the capacity of DHTS to disrupt the interaction between HuR and *TNF α* , a well characterized HuR target. We have demonstrated that DHTS downregulates *TNF α* at the transcription and translation levels in MCF7. In the same cell line, by performing RNA immunoprecipitation (RIP) experiments we showed that DHTS interferes with binding between HuR and *TNF α* (Lal *et al.*, 2017) (Figure 6D).

Furthermore, we investigated on DHTS activity *in vivo*. In collaboration with Dixon's group, in the university of Kansas, we proved that HuR dysregulation has been related with strong anti-cancer activity *in vivo*, in xenograft model of colon cancer (HCT116 cells). Specifically, when HuR expression was depleted in these cell line through CRISPR/cas9 technology a reduction in the tumor growth in xenograft mouse model was observed, comparable to what obtained in WT cells treated with DHTS. Re-introducing HuR in the KO cells provoked the rescue of the cellular growth (Figure 6E/F).

Moreover, we demonstrated the absence of systemic toxicity in treated animals encouraging the idea that general inhibition of HuR with small molecules can be useful for therapeutic efforts (Lal *et al.*, 2017).

My personal work starts in this context, in evaluating the activity of DHTS at the genome wide level.

The data I have generated have been of pivotal importance, because they are the first proof of concept of the effects of the general disruption of mRNA-HuR interactions inferred by DHTS.

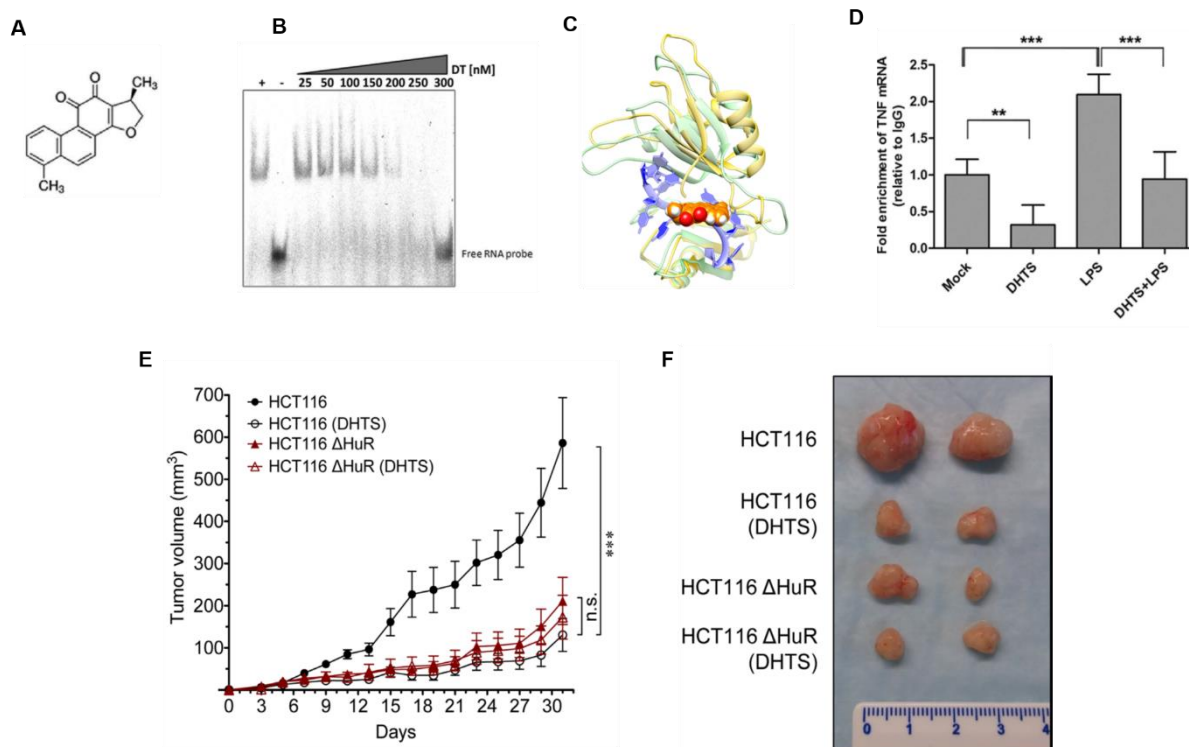


Figure 6. DHTS interferes with HuR-RNA binding *in vitro* and *in vivo* (Mod. from Lal *et al.*, 2017). A) DHTS' chemical structure B) DHTS inhibitory activity showed by a representative RNA-HuR recombinant protein electrophoretic mobility shift assays (RNA-EMSA). By increasing DHTS concentration the binding between the rHuR and the labeled ARE sequence is impaired. C) Global view of the HuR (green cartoons)-DHTS (orange spheres) complex. Note how the insertion of DHTS (orange) binds HuR at the level of the mRNA binding cleft, maintaining the protein in a closed conformation, preventing the binding of the RNA (blue ribbons). D) DHTS impairs the binding between HuR and its target TNF. RNA Immunoprecipitation experiments show as upon DHTS treatment TNF mRNA binds less to HuR. E) Tumor growth of colon cancer cell lines HCT116 wild-type and HuR KO xenografts in nude mice treated with DHTS (10 mg/kg) or vehicle (DMSO) and F) Representative tumor excised after 31 days. In all experiments p-value is * <0.05, **<0.01, ***<0.001, n.s. = not significant.

4.2 Characterization of DHTS mechanism of inhibition for the generation of a more potent family of HuR inhibitors.

In order to achieve the goal mentioned above, we evaluated the ability of DHTS to interfere between the interaction of HuR with its target mRNAs, by applying a transcriptome-wide approach.

In collaboration with Myriam Gorospe's group at the NIH, by performing a RIP-chip experiment in Hela cells, treated with DHTS (1 μ M) and DMSO for three hours, we observed that among 2306 mRNAs found bound to HuR, DHTS impairs the binding of a minimal part of the targets, represented by 79 transcripts. On the contrary, 558 mRNAs have been found enriched after DHTS treatment (Figure 7).

Due to these unexpected results, since an HuR inhibitors should display the overall HuR binding to its targets, we decided to characterize the structural properties of the 3'UTRs and the binding sites

inside HuR targets. Our hypothesis was that DHTS, by competing with the RNA for the binding, as previously demonstrated, displaces the binding with mRNAs that have a lower affinity to HuR, than DHTS itself. On the contrary, DHTS is not able to interplay between HuR binding to the targets that have a higher affinity for the protein, paradoxically these kind of mRNAs with major affinity for HuR have been found to bind it in high copy numbers and thus resulting enriched after RIP-chip. The mRNAs structural analysis strongly supported our ideas, since, as expected the HuR-bound mRNAs had a relative higher frequency of U/AU rich segments compared to the frequency in the overall transcriptome (Silanes *et al.*, 2004), but the U/AU density in the UTRs in the enriched mRNAs was significantly higher than that in the downregulated mRNAs. Indeed, the relevant differences were evaluated at the level of the 3'UTR (Figure 7A), where the percentage of AU increased from 58% (depleted) to 65% (enriched).

Moreover, considering the length of the 3'UTRs, but not the 5'UTRs of these mRNAs, we observed that the ones belonging to the enriched group were significantly longer than the 3'UTRs of the depleted transcripts, while we have observed no differences in the density of secondary structure elements (Figure 7B/C). Furthermore, we analysed the nature of these targets, by performing functional analysis. For what concerns the depleted genes, no analysis was provided, due to the small size of the set and because was partially composed by unannotated mRNAs. Meanwhile, enriched transcripts (Figure 7D and 7E) encoded for proteins involved in the regulation of the gene expression, cell cycle progression and apoptosis. To validate these data, I have performed RNA immunoprecipitation (RIP) experiments followed by qRT-PCR in a biological triplicate, investigating on the enrichment or depletion in binding of a subset of mRNAs enrolled in the processes mentioned above and they are respectively: *PABPC1*, *YTHDF1*, *UPF2*, *CASC3* and *BRIP1*. Figure 7F shows microarray analysis for the selected targets for the validation.

Enrichment or depletion of the targets, is represented by the value "change in binding", meaning that data have been obtained by applying a first normalization on the IgG, as a background, and then we calculated the ratio between the treated sample over the control, represented by DMSO. In Figure 7G, the validation of the data obtained by RIP followed by RT-qPCR is reported and significantly confirmed what observed in the microarray experiment. Transcripts with a longer 3'UTR and high content of U/AU rich sites are tightly bound by HuR and this binding can't be disrupted by DHTS. Instead, the compound displaces HuR interaction with mRNAs containing a shorter 3'UTR structure with a low number of ARE sites, without changing the total expression level of each target considered (Figure 7H).

These results I have obtained so far, have been important for a better understanding of DHTS in a mechanistic way of action and have put the basis for a rational design of synthetic inhibitors to improve their potency in displays HuR-RNA complex formation.

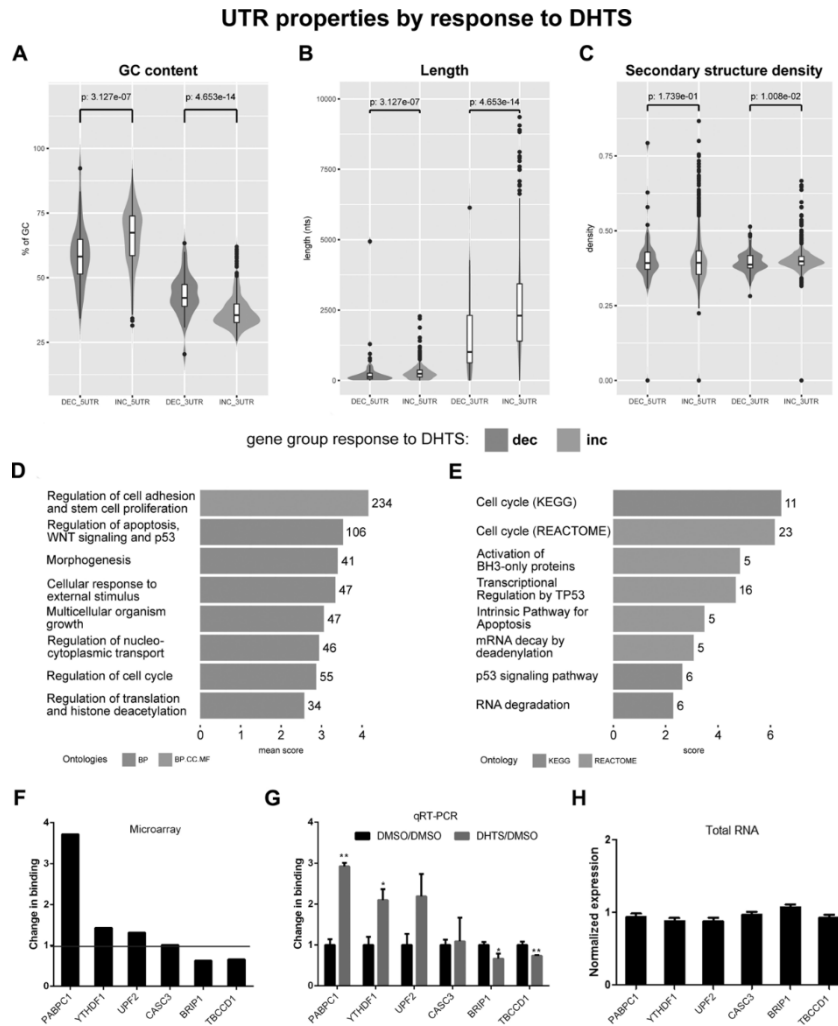


Figure 7. Depleted and enriched mRNAs and UTRs structural properties affecting DHTS action.

A) GC content distribution for decreased (dec) and enriched (inc) UTRs, differences of the data analyzed with Wilcoxon test-P-values Distribution. B) UTRs' length distribution for decreased (dec) and enriched (inc) mRNAs, with Wilcoxon test-P-values of the differences. C) Decreased (dec) and enriched (inc) UTRs Secondary structure density (computed as fraction of unpaired nucleotides). Differences of the data analyzed with Wilcoxon test-P-values Distribution. D) Enrichment analysis performed with Gene Ontology (GO) for enriched gene group. Each terms cluster is represented by the corresponding bar. Mean score represents the mean of Enrichr combined score for all belonging terms. GO classes found in each cluster are represented by the bars color. E) For the enriched set pathway enrichment analysis were performed with KEGG and REACTOME. Number of gene belonging to each pathway is shown at the end of the corresponding bar. The score is the Enrichr combined score for the pathway. Bars color indicate the pathway database of each entry. (Bioinformatic analysis were performed by Dr. Erik Dassi)

RNA Immunoprecipitation (RIP) of HuR after treatment with DHTS in HeLa cells.

F) Gene selected emerged from Microarray data. Fold enrichment of each mRNA upon treatment is reported, microarray values are represented by black bars. Microarray experiments performed by the lab of Genetics, Head by Dr. Miriam Gorospe (NIH, Baltimore)

G) RT-qPCR performed to validate microarray data. Fold enrichments of each mRNA, during DHTS treatment normalized on control condition (DMSO) are represented by gray bars. Comparison between microarray F) and RT-qPCR data G) shows similar results for enriched transcripts (*PABPC1*, *YTHDF1* and *UPF2*), unchanged transcripts (*CASC3*) and depleted transcripts (*BRIP1* and *TBCCD1*). RPLP0 mRNA was used as an endogenous control mRNA that is not bound by HuR. Error bars represent SD. P-value is <0.05 . <0.001 . Microarray experiments were done in duplicate ($n = 2$), qRT-PCR in triplicate ($n = 3$). H) RT-qPCR analysis of HuR non-targets, showing no changes in total expression levels after DHTS treatment. RPLP0 mRNA was used as an endogenous control for normalization. Error bars represent SD. Experiments were done in triplicate ($n = 3$). (Experiments performed by me) (Lal *et al.*, 2017)

4.3 Tanshinone Mimics (TMs): identification and evaluation of a new class of HuR inhibitors.

The design and synthesis of an array of DHTS analogs have been possible thanks to the contribution and support of Prof. Seneci, from the University of Milan.

They used a function-oriented synthesis (FOS) (Wender, Quiroz and Stevens, 2015) aiming at the design of less structurally complex molecules exploiting the structure-activity relationship properties of the ancestor natural compounds, setting the basis for the design of more potent but simpler synthetic analogs.

We, me included, tested the molecules produced by our collaborators for their capability of inhibiting the binding between HuR and RNA at different levels (biochemical and biological). This allowed us to generate for the first time structure activity relationships (SARs) for HuR inhibitors (not shown) (Manzoni *et al.*, 2018). SARs have been pivotal to assign to a structural chemical element, biological and functional activity properties, providing solid guidelines for the generation of highly effective HuR disruptors and some hints will be presented along this section. For simplicity, TMs can be divided into two classes: a) first (TMs-I) and b) second generation (TMs-II). I will indicate with the number 6 followed by different alphabetic letters, the TMs belonging to the first generation, while using the number 7 and letters, the ones of the second one.

Once these molecules have been synthesized, in collaboration with other members of our group, we have first carried a biochemical characterization of the first generation of Tanshinone Mimics (TMs). In particular, through Alpha Screen assay, we evaluated the ability of TMs to inhibit the rHuR and the biotinylated U/AU RNA probe in condition of binding saturation. Thus, for the majority of the compounds, it has been possible to calculate a constant, K_i , representing their inhibitory efficiency. A summary of the values obtained (from high to low) of the most significant molecules is shown in Table 4. From this and Figure 8A, showing representative Alpha Screen, compounds 6a and 6n have K_{is} of respectively 12.8 nM and 15 nM, appearing to be more effective than DHTS, indicated as 1 in Table 4. Further validations have been performed through RNA EMSA assays, as reported in Figure 8B. The lane indicated as (-) represents the RNA probe only, that is the unbound RNA fragment. The addition of the recombinant protein to the RNA in control (DMSO) condition, indicated as (+), leads to the formation of a complex made by protein and RNA that is higher and more complex in its molecular weight, reflecting in a shifting up of the corresponding band on the polyacrylamide gel. The addition of the TMs (from 6a to o) at the concentration of 5 μ M, causes a reduction in the shifted RNA probe, suggesting the presence of an inhibitory effect on the formation of the HuR-RNA complex (Figure 8B).

Table 4. Abilities of Tanshinone Mimics to Inhibit the rHuR–Bi–AU Complex Formation (Manzoni *et al.*, 2018).

| Cpd | Structure | K _i , ¹ nM | Cpd | Structure | K _i , ¹ nM |
|-----|-----------|----------------------------------|-----|-----------|----------------------------------|
| 1 | | 50 | 6a | | 12.8 |
| 6b | | Interfering* | 6c | | >100 |
| 6d | | >200 | 6e | | >200 |
| 6f | | Interfering* | 6g | | >100 |
| 6h | | 48 | 6i | | >100 |
| 6k | | 81 | 6l | | 56 |
| 6m | | Interfering* | 6n | | 15 |
| 6o | | Interfering* | 6p | | >100 |
| 6q | | >100 | 6r | | 41 |
| 6s | | 55 | 6t | | >200 |
| 6w | | >300 | | | |

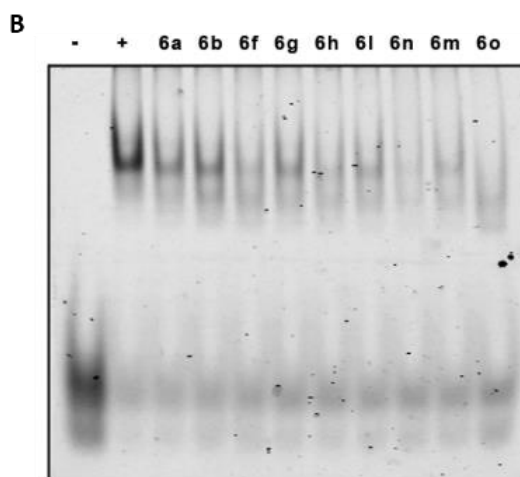
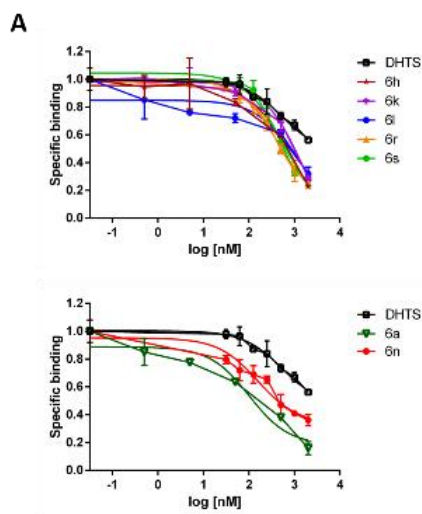


Figure 8. TMs disrupt HuR-RNA *in vitro*. A) Alpha screen with relative K_i (inhibition constant) calculation of the specific binding of the His-tagged HuR and AU-rich biotinylated RNA. K_is have been calculated with respect to a K_D (dissociation constant) of 2.5 nM for the rHuR–Bi–AU interaction and normalized to control (DMSO). Data fit nonlinear regression fitting curves according to a 1-site binding model in GraphPad Prism. Plotted bars are mean ± SD of two independent experiments. B) REMSA showing disruption by TMs of HuR binding. Recombinant HuR was incubated for 30 min with 75 fmol of 5'-DY681-labeled RNA probe. (-) indicates the incubation with RNA probe only without the protein, (+) indicates the presence of rHuR with RNA probe and DMSO as a positive control for the binding. TMs first generation (6) were incubated at 5 μM dose. (Experiments in A) and B) were entirely performed by Lal P. and Zucal C.)

Apart from some exceptions, such as 6b, 6f, 6m and 6o showing a lower potency in REMSA, there is concordance between the two set of experiments. 6a and 6n seem to be the most potent compound, thus being the leading compounds for the synthesis of the new generation ones. Furthermore, as confirmed by REMSA and by Circular Dichroism assays (data not shown) we have been able to demonstrate that compound 6a is not interacting with the RNA probe (Manzoni *et al.*, 2018), suggesting that the compound does not interfere with the probe fluorescence or change its conformation. Moreover, we further investigated on 6a, the most potent among the compounds, in order to provide insights on its mechanism of action, as we did for DHTS. Indeed, we demonstrated that 6a directly binds to HuR. By testing truncated version of the recombinant protein HuR, formed only by the first two RRM (RRM1-2), we confirmed, as we did for DHTS (D' Agostino *et al.*, 2015), that 6a is able to interact with the first two RRM domains of the protein, but not with either RRM3 or the probe (Manzoni *et al.*, 2018). In collaboration with Mario Negri's Institute in Milan, through Dynamic Mass Redistribution (DMR) approach, we were able to demonstrate a direct interaction between the protein and the compound (6a) at the equilibrium and in label-free conditions (Figure 9A). Full length rHuR was immobilized in the plate, exploiting the amine-coupling chemical features. Increasing amounts of compound were added to the wells and the mass of the complexes was measured after 30 minutes of incubation. A dose-dependent binding was observed in the 0.3-10 μM range, enough to detect saturation. The affinity constant (K_D) has been estimated to be around 4.5 μM (Figure 9A) (Manzoni *et al.*, 2018). Moreover, as reported for DHTS (Lal *et al.*, 2017), the level of interaction, evaluating the precise residues of the protein interacting with 6a, has been revealed with NMR and molecular docking studies. NMR (data not shown) suggested that 6a has a similar binding mechanism to DHTS, involving 8 aminoacidic residues in the β -platform of the first two RRM. Considering the general decreasing in the signal intensity and by looking at the distribution along the extent β -platform surface, we proposed a model of interaction for 6a similar to DHTS, stabilizing HuR in a closed conformation. In order to better understand, precisely define the binding position and model and to point out differences with DHTS-HuR interaction, a combination of NMR, SARs, docking calculations and extended molecular dynamics (MD) simulations (data not shown) was performed. These different approaches gave rise to a conclusive binding mode for 6a (Figure 9B), in which, differently from what described for DHTS, it appears that the interaction between 6a occurs at the level of the interdomain linker region between the first two RRM, thus strengthening the stabilization of HuR in a closed conformation (Manzoni *et al.*, 2018).

As depicted in Figure 9B, SARs seems to be in accordance with NMR and molecular modeling data, being of pivotal importance, providing insights into the binding mode and mechanism of action of this family of molecules. Therefore, they can be exploited for introducing modifications and improvements to the rational synthesis and design of more potent HuR inhibitors.

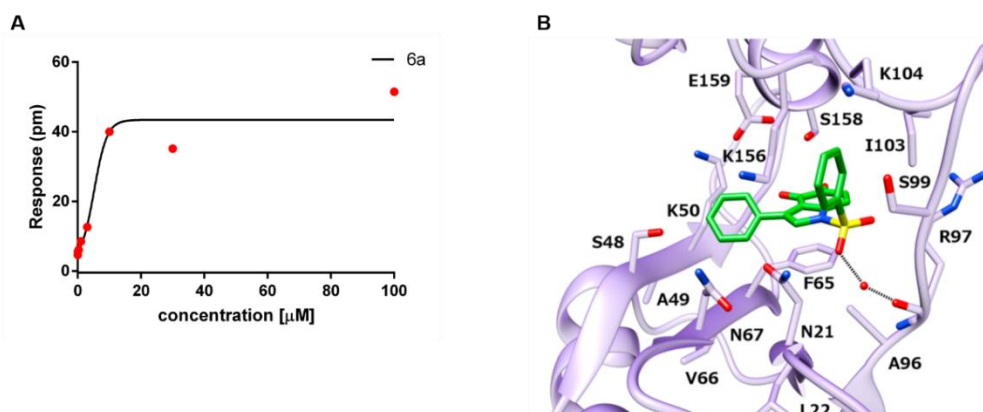


Figure 9. Compound 6a directly binds HuR with a predicted binding mode. A) rHuR was previously immobilized in label free microplate, and different concentrations of compound 6a were added to the plate. Measurements were performed before adding the compounds, in order to define a baseline and after. The final response (pm) signal, was obtained by subtracting the one from the baseline. The signal for each well, was calculated by subtracting the signal obtained from a reference protein coated surface area, with a not coated one. The fitting curve (black line) of the data (red dots) assumes a sigmoid function using a 4-parameter logistic (4-PL) non linear regression model: $R^2=0.944$; $p = 0.009$. Data have been entirely performed by Elezgarai S. in collaboration with Mario Negri Institute in Milan. B) Structural modeling of predicted binding mode of 6a (green sticks) to HuR (purple cartoons), coming from the last 500 ns of the MD stimulation. HuR residues participating in the interplay with 6a are displayed as sticks (Manzoni *et al.*, 2018)

4.4 TMs affect viability and migration of cancer cells by modulating HuR post transcriptional activity, without changing its subcellular localization.

In order to investigate on TMs biological activity and anticancer properties, we first evaluated their toxicity in a dose-dependent manner in different cancer cell lines. In particular, we focused our attention on testing them on breast cancer cell lines, as MCF7 and MDA-MB-231 or pancreatic ductal adenocarcinoma cell line, PANC-1. We have evaluated the cytotoxicity of the molecules after 72 hours of treatments at different doses (1, 5, 10, 25 and 50 μM) and as depicted in Figure 10, compounds 6a and 6n affect cell viability along with the other TMs (6b, 6m, 6k, 6l and 6t), yet the latter 5 seem to be less toxic. IC_{50} was evaluated and values are shown in Figure 10 for each compound, ranging from 20 to 50 μM for 6a, 6b, 6n, and 6m, although PANC-1 reflect to be more sensitive than the other lines (Manzoni *et al.*, 2018). Subsequently, in order to investigate on the inhibitory activity exerted by 6a, leading compound among the TMs and another one for comparison, 6t, towards the direct formation of HuR-RNA complex, I have performed an RNA Immunoprecipitation (RIP) assay in MCF7 cells. In particular, in order to compare 6a and 6t activity with DHTS, I treated MCF7 cells with both 6a and 6t at the subtoxic dose of 5 μM and DHTS at 1 μM for 6 hours, as previously reported (D' Agostino *et al.*, 2015; Lal P. *et al.*, 2017) and DMSO was used as control. After lysis of the cells and RNA precipitation with either HuR antibody and the relative IgG isotype as control, I have performed quantitative real time PCR (qRT-PCR) to evaluate the enrichment or depletion of *CTNNB1*, *ERBB2* and *VEGF*, three well known HuR targets, encoding for protein exerting key oncogenic functions, as already described (see Introduction paragraph 2.3).

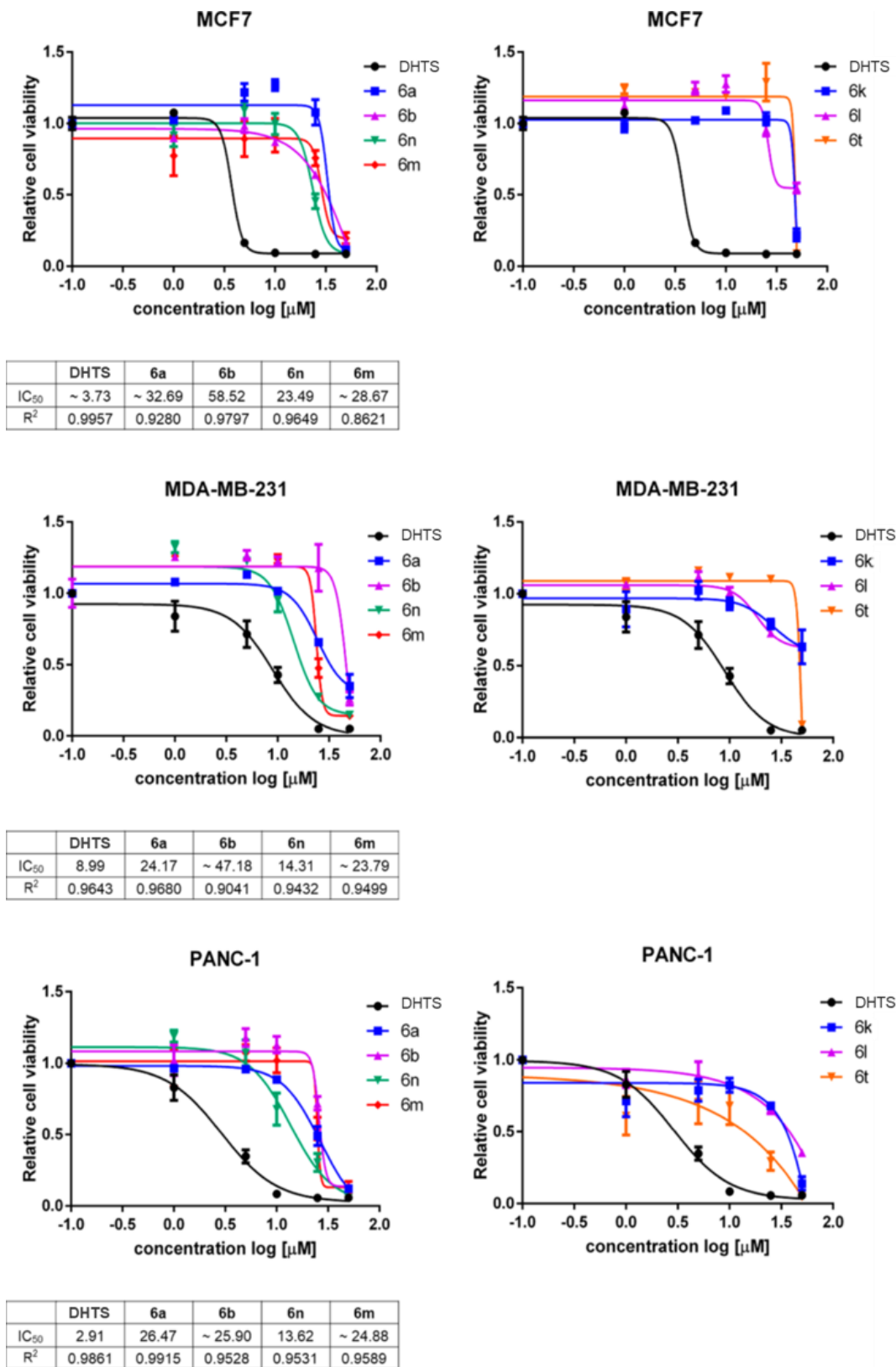


Figure 10. Tanshinone mimics (TMs) affect cell viability in a dose dependent manner. Cell viability was evaluated with OZBlue kit after 72 hours of treatments. Doses range were from 0 to 50 μ M. Plotted bars are mean \pm SD of a biological duplicate, normalized to control (DMSO). Relative IC₅₀ and R² were calculated by nonlinear regression curve fitting. (I have performed these experiments in collaboration with Thongon N. and Zucal C.) (Manzoni *et al.*, 2018)

As represented in Figure 11A, DHTS, 6a and 6t show to interfere with the binding between HuR and its targets, as suggested by the decreasing in the mRNAs fold enrichment. Fold enrichment of each sample, is indicated as a result between the value obtained after HuR precipitation, normalized on the corresponding one in which IgG have been precipitated, after subtracting *RPLP0* values in both cases. In Figure 11A data are plotted as relative to the DMSO sample that we used as control. At the RNA total levels, we wanted to investigate if the reduction of the HuR-mRNA target complex formation observed after TMs treatment was reflecting in a decreasing in the total transcription of the considered targets. To this aim, I have treated MCF7 cells with 6a (5 μ M) for 6 hours and then by qRT-PCR I have evaluated whether there was a decrease at the transcription level of *CTNNB1*, *ERBB2* and *VEGF* compared to DMSO. Results are shown in Figure 11B, and compound 6a, by interacting with HuR *in vitro* and in cellular contexts prevents the binding with its targets, inducing a subsequent mRNAs downregulation. As further controls, we checked the expression of *HPRT1* and *RPLP0* two mRNAs that are not bound by HuR and indeed, after treatments, we did not observe changes in their expression level, suggesting again, that the effect observed is related exclusively to a deregulation of HuR binding activity.

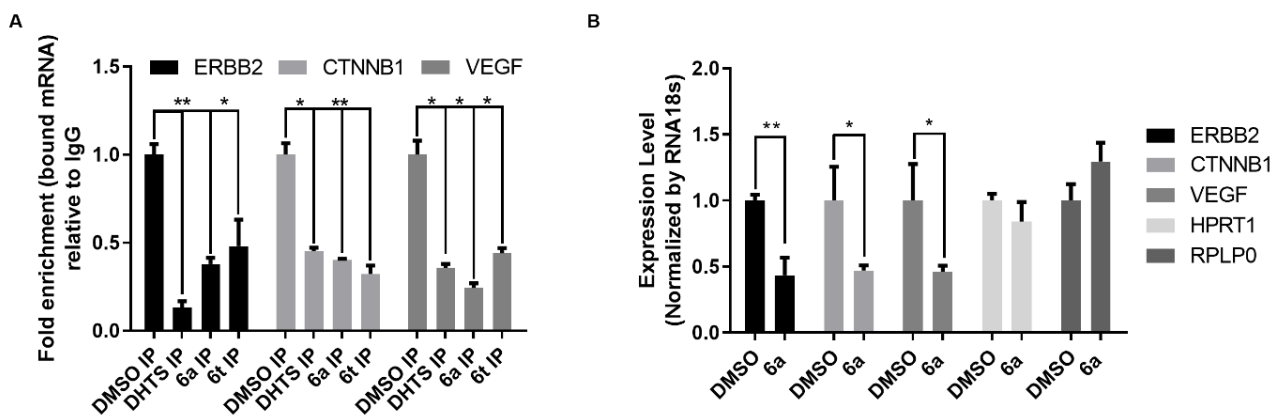


Figure 11. TMs directly modulate HuR post-transcriptional activity. A) RNA Immunoprecipitation assay (RIP) followed by real time PCR (qRT-PCR). MCF7 were treated for 6 hours with DMSO (CTRL) as control, DHTS (1 μ M) and 6a (5 μ M) and 6t (10 μ M). Afterwards cells were lysed and RNA precipitated with HuR antibody (IP) and IgG isotype (IgG) as negative control. Changes in the mRNAs bound to HuR in the control (CTRL) or treatment (DHTS or 6a) were evaluated through qRT-PCR and normalized on the corresponding values obtained with IgG, as negative control. The obtained numbers indicate the Fold enrichment, obtained after normalization with IgG and subtracting the value of the housekeeping gene *RPLP0*. B) MCF7 cells were treated with 6a (5 μ M) for 6 hours to investigate on changes in the total mRNA expressions of well-known HuR targets, as *ERBB2*, *CTNNB1* and *VEGF*. *RPLP0* and *HRPT1* mRNA levels was assessed as control, knowing that they are not bound by HuR. The expression levels obtained are normalized on the housekeeping gene *RNA18S*. Data are presented as mean \pm SD of a biological triplicate (*p < 0.05 and **p < 0.01 versus CTRL). (All the experiments have been performed by me)

Moreover, as already described, HuR has been shown to promote cell migration and invasiveness during cancer progression, in pancreatic ductal adenocarcinoma cells (see Introduction paragraph 2.3) (Jimbo *et al.*, 2015), subsequently we assessed if TMs were able to modulate these events by blocking HuR activity. Therefore, we have mainly evaluated TMs properties of reducing cancer cell migration and in order to do this, we have performed *in vitro* scratch assay using MDA-MB-231, a human breast cancer cell line known to be highly aggressive and invasive (Liang, Park and Guan, 2007). Cells were treated for 24 hours and 48 hours with increasing concentration of 6a and DMSO as control. The scratch width separating the cells inside the plate has been measured, therefore we have been able to assess that after 48 hours treatments, 6a prevents the closure of the wound area compared to control, suggesting that cells undergo a decrease migration capability in 6a dose dependent manner (Figure 12A) (Manzoni *et al.*, 2018). Same assays have been performed by treating the cells with other compounds, respectively 6b, 6n and 6t and results are shown in Figure 12B. TMs, in particular 6n and 6z at 10 μ M dosage, reduce significantly at 48 hours and 24 hours invasion of breast cancer cells.

These experiments suggest that TMs, by inhibiting the activity of HuR, downregulate migration and motility properties of MDA-MB-231, chosen as a reference since it is known to be a highly aggressive and metastatic cancer cell line (Relda Cailleau, 1978). For 6a, same experiments have been repeated using another cells, pancreatic carcinoma cell line (PANC-1), and similar results have been obtained (data not shown) (Manzoni *et al.*, 2018).

Nevertheless, scratch assays, although if informative, show many limitations, indeed they could be complemented with other assays, such as Matrigel invasion assays (Jimbo *et al.*, 2015). Moreover, further evidences may be acquired by performing similar assays, evaluating the capability of the molecules to counteract the mobility of the cells when exposed to a chemoattractant agent. Considering that HuR regulates the expression of different transcripts encoding for protein as cytokines, chemokines, such as *TNF α* or *CCL5* (see Introduction paragraph 2.6) taking advantages of techniques as real-time cellular analysis (RTCA) would be useful for the study of TM effects. Specifically, by exposing the migrating cells to different media belonging to cells pre-treated with TMs, would lead to the downregulation of different chemo-attractants in the medium, reflecting in a strong reduction of cells invasion. Vice versa, treating the cells with TMs would prevent their migration towards a chemoattractant media, confirming what observed with scratch assay. These set of experiments, have been previously performed for DHTS by D'Agostino et al in 2015, where RTCA was performed using MDA-MB-231 as a read out, exposed to MCF7 conditioned medium, where cells were previously treated with DHTS at 1 μ M dose. Results demonstrated that the treatment impaired the migration of the cells, as expected. In order to demonstrate HuR dependency of what observed, HuR depletion or HuR overexpression was performed in MCF7. The conditioned medium belonging to the HuR depleted cells, showed the same effect of retarding MDA-MB-231 migration as observed when cells where treated with DHTS, on the contrary, the rescue of the

migration capability of the cells was evaluated when the conditioned medium belonged to MCF7 overexpressing HuR (D' Agostino *et al.*, 2015). These kind of evidences, have to be collected for TMs and indeed these experiments with TMs are still ongoing.

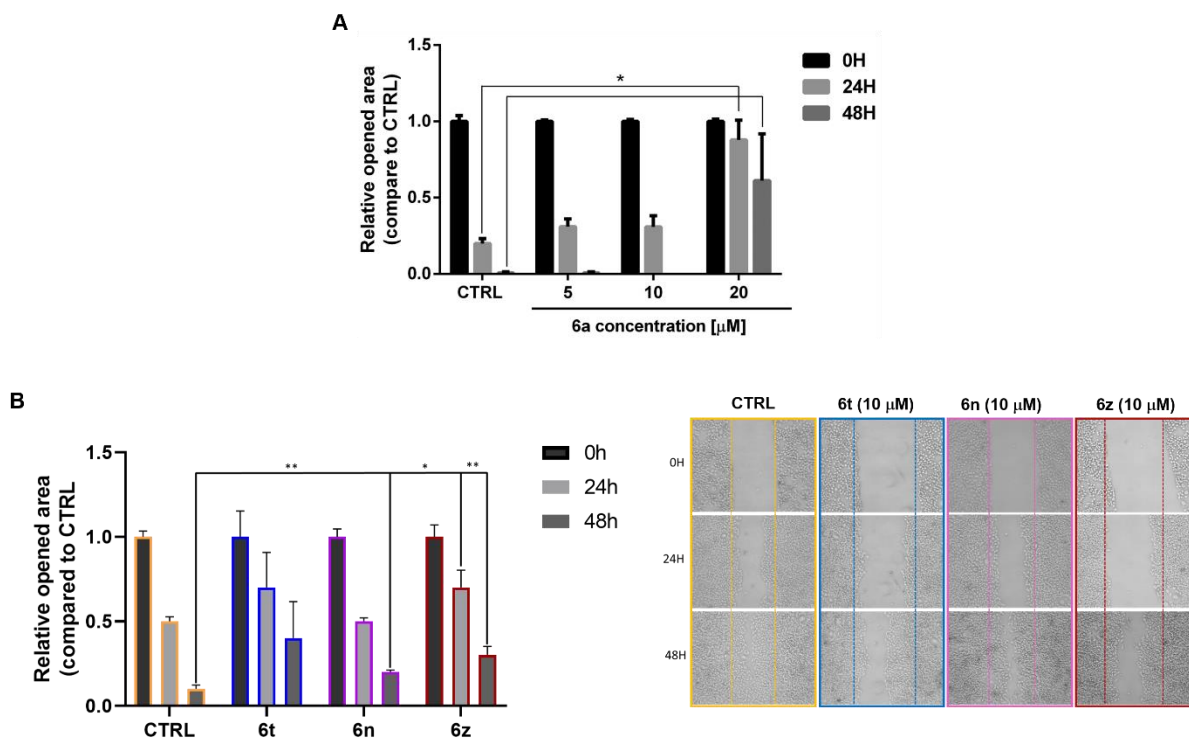


Figure 12. TMs repress migration in breast cancer cell lines. A) Scratch assay in MDA-MB-231. Cells were treated either with DMSO (CTRL) or 6a at different doses (Manzoni *et al.*, 2018).

B) Scratch assay in MDA-MB-23. Cells were treated with 6a-derivative TMs at the dose 10 μM , in particular: 6z, 6n and 6t, in order to investigate on their efficacy in reducing cell migration, representative images showing cells invasion in control and treatment conditions at the different time points (unpublished data).

In both A) and B) Wound with a consistent shape in each well were generated with a 200 μl tip. Images of invasive cells at 0, 24 and 48 hours after scratching and treatments, were taken from a time-laps sequence, after scratching sequence of cell migration

Residual open area at different time points has been calculated with ImageJ software (* $p < 0.05$).

(I have performed these experiments with Thongon N.)

Based on the data previously shown, concerning the effectiveness of TMs, 6a in particular, in inducing toxicity and reducing migration and invasiveness in cancer cell lines, downregulating HuR-mRNA complex formation, *in vitro* and *in vivo* towards HuR targets, we wondered about other anticancer properties of our compounds.

As described in the Introduction (paragraph 2.3), another critical step in cancer progression represented by the chemo and radio-resistance acquired by the cancer cells and reflecting in failure of the vast majority therapies. Farther, recently, it has been shown that pancreatic cancer cell lines co-treated with PARP inhibitors and the HuR inhibitor MS-444 (see Introduction paragraph 2.5) were showing an increasing toxicity if compared with the single treatment with PARP inhibitors. This reflects in a downregulation of HuR post-transcriptional function in stabilizing polyADP-ribose

glycohydrolase mRNA encoding for a protein involved in DNA repair, that thus was impaired. Notably, same effect has been observed through a synthetic lethality approach in which PARP inhibition was coupled with HuR KO (Chand *et al.*, 2017). This turned out to be a starting point for us, testing our molecules in combination with chemotherapeutic agents. In collaboration with other members of the lab, I used Olaparib that is a PARP inhibitor, as an example, to investigate its efficiency in single or co-treatment with 6a. In MIA PaCa2 and MDA-MB231, pancreatic and breast cancer cell lines respectively, viability was reduced up to 50% compared to control, when treatments were performed with Olaparib and 6a for 72 hours (Figure 13). This is just a promising preliminary experiment, that drives to further investigate on checking whether the combination with our TMs with other already-in-use therapeutics could be an advantage in clinical approaches.

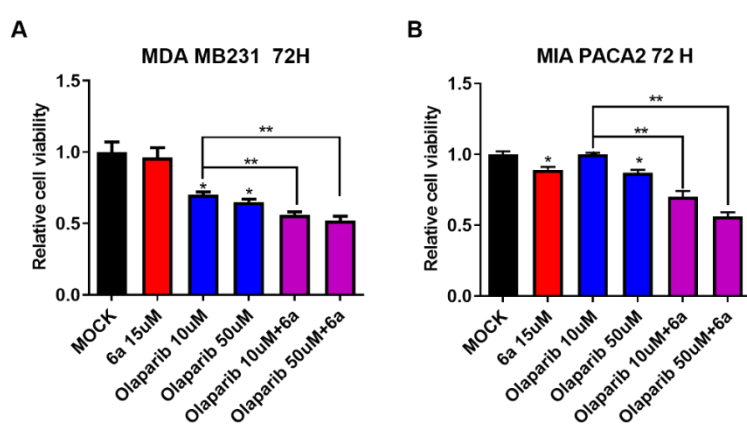


Figure 13. Cell viability on MDA MB231, MIA PaCa2. Cells were treated with indicated concentrations of Olaparib (1-50 μ M) and compound 6a for 72 hours. Cell viability was analyzed by Ozblue Cell Viability kit. Relative cell viability as compared to Mock (DMSO) were shown. (* p <0.05, and ** p <0.01). (These experiments were performed by Thongon N.)

Meanwhile, to further investigate on the mechanism of action of these molecules in cellular context, we wanted to investigate whether TMs activity was affecting HuR localization inside the cells. As mentioned in the Introduction section (see paragraph 2.5) many drugs have been described so far impacting on HuR activity by preventing its translocation in the cytoplasm or promoting it (Actinomycin D), thus we decided to investigate if TMs' behaviour was the same. To do this, as previously demonstrated for DHTS (D' Agostino *et al.*, 2015), I treated MCF7 with the following TMs: 6a, 6t, 6n and 6z for 3 hours at 10 μ M dose, adding DMSO (CTRL) as negative control and Actinomycin D (Act-D) at 2.5 μ M, as positive control, known to stimulate HuR translocation from the nucleus to the cytoplasm.

Then, I have performed Immunofluorescence (IF) to detect HuR and its nuclear or cytoplasmic localization inside the cells and results are shown in Figure 13, where a representative IF and relative quantification are reported. As previously evaluated for DHTS, HuR localization did not change during TM treatments with respect to control (CTRL) and remain nuclear, compared to Act-D where a significant translocation to the cytoplasm is observed (Figure 14). Same effects were further confirmed with other TMs (data not shown) (Manzoni *et al.*, 2018) and further demonstrate that the

inhibition of HuR is connected with a modulation induced by TMs on the binding activity of HuR and not via a changing in its expression level or distribution in the cell.

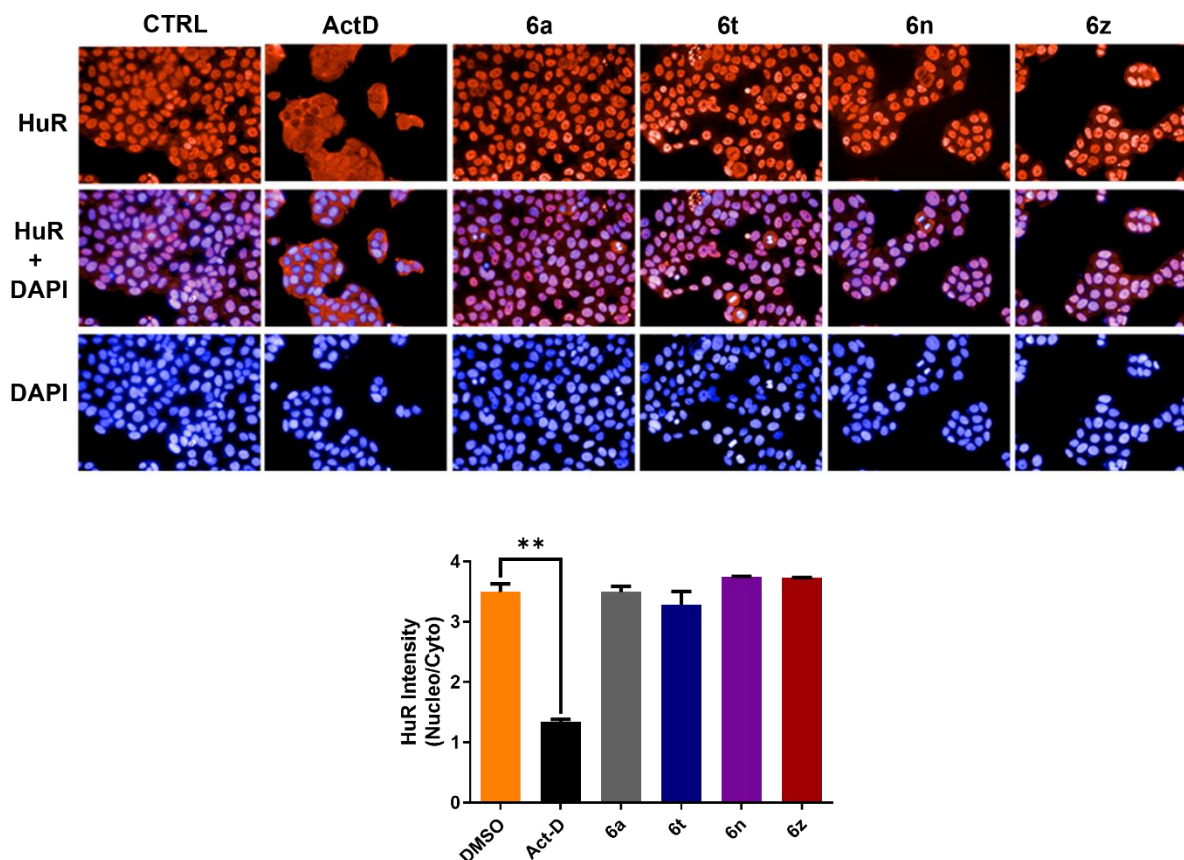


Figure 14. TMs do not influence HuR subcellular localization. Representative immunofluorescence showing HuR localization inside the cells not changing upon treatments with different TMs: the leading compound 6a, 6t, 6n and 6z. I have treated the cells for 3 hours both with compounds at 10 μ M, 2.5 μ M of Actinomycin D (Act-D) as positive control and finally DMSO (CTRL) as negative control. In the graph, the ratio of HuR fluorescent signal between nucleus and cytoplasm (N/C) is plotted. For image acquisition (40 \times high NA objective), Operetta was used and evaluation by selecting 13 fields/well. The ratio N/C represents the mean \pm SD of single cells for every well (** $p < 0.01$) (unpublished data). (I have entirely performed these set of experiments).

Taking these data together, we concluded this part showing TMs having biological properties in different cancer cell lines. They displayed toxicity at higher doses, and when cells have been treated at subtoxic ones, TMs showed different anticancer activity strictly impacting on HuR post-transcriptional function inhibition. In fact, treatment with 6a, leading compound of the family of these small molecules, reduced directly the binding between HuR and its targets: *VEGF*, *ERBB2* and *CTNNB1* encoding for proteins determinant for cancer processes (see Introduction, paragraph 2.3). We have shown that this reflected in a downregulation of the total mRNA expression of these targets, suggesting that HuR post-transcriptional function of stabilizing and enhancing the translation of these targets is deregulated by the TMs.

Investigations on impairments on the stability of the transcripts at the level of mRNAs and pre-mRNAs have been described for what concerns DHTS by D'Agostino *et al.*, 2015. In fact, it has been demonstrated with Act-D treatments, inhibition of transcription, allows to study mRNA decay

mechanism counteracted by a stabilization effect given by HuR activity, enabling the evaluation of the stability of the transcripts (Koba and Konopa, 2005). Thus, MCF7 cells were treated with Act-D and with DHTS and DMSO as control, afterwards level of *TNF* and other mRNAs was detected. Upon DHTS treatments a decreasing in the stability of the transcripts was observed, rescued by the HuR overexpression. Same experiments have to be performed by looking at the stability of HuR mRNAs targets after treatments with 6a and the most promising compounds.

For what concerns a reduction in the translational efficacy induced by TMs treatment in an HuR dependent manner, the loading on polysome of *VEGF*, *ERBB2* and *CTNNB1* mRNAs could be pivotal for the evaluation and quantification of the effective reduction in the translation. Moreover, the effect of TMs on global translation should be investigated, knowing that HuR regulates a variety of transcripts, a blockage of its activity could reflect in a diminishing of the global translation and these experiments are still ongoing in the lab. Polysome profiling and loading upon treatments with TMs-I, in order to quantify and detect the translational reduction of each targets above mentioned, still remain to be performed, but some insights concerning impairment in the stability of HuR targets and their translation, will be provided in the paragraphs investigating on the anti-inflammatory properties of the compounds. On the other end, our group has previously shown that, after treatments with DHTS, no changes in the polysomal profile were observed compared to the control, but *TNF* mRNA polysomal loading was significantly reduced after treatment and a corresponding increase in the sub-total fraction was observed (D' Agostino *et al.*, 2015).

4.5 Characterization of TMs-II and 7n, leading compound with a biochemical and biological activity in cancer cell lines.

From the previous paragraphs, the biochemical and biological activity of TMs belonging to the 1st generation (TMs-I) from which 6a is the most potent hit, have been described.

Anyway, these molecules present some limitations: deriving from a natural compound, specificity and solubility issues need to be overcome. For these reasons, this family of chemicals can be considered as the founder for pursuing our current aim, that is generation of more potent set of compounds, to implement the SARs already presented, thus improving the efficacy of the modulatory activity towards HuR, with anti-cancer and anti-inflammatory properties, in the cellular context but mostly *in vivo*. Subsequently, along with 6a, we selected also 6n as one of the most representative TMs-I and these two, have been modified and ameliorated, thus producing 7a and 7n that we have tested at the biochemical and biological level to evaluate their activity.

To this aim, other members of our group, performed REMSAs and Alpha Screen assays, of which the most representative have shown in Figure 15 A and C. REMSA in Figure 15A shows the biochemical inhibition capability of 7a, derivative of 6a in comparison with its precursor. The potency of both the compounds appears to be the same, with a slight additive strength shown by 6a. In Figure 15B another representative REMSA shows 6n and 7n disruption of HuR-RNA complex, and also in

this case 6n shows higher activity compared to 7n. However, both 7a and 7n show better solubility compared to their ancestor molecules. 6n and 7n have been also evaluated in their HuR-RNA binding impairment properties with Alpha Screen assays and a K_i has been calculated, while for 7a, the assigned K_i was higher (data not shown). Among the TMs-II screened, we choose 7n as the leading compound of the TMs-II and its HuR-RNA complex formation inhibition properties was again observed by performing a dose-response REMSA (Figure 15D). Along with increasing doses, 7n is able to interfere with the interaction between HuR and ARE probe, giving, at the higher concentration, a complete abolishment of the binding.

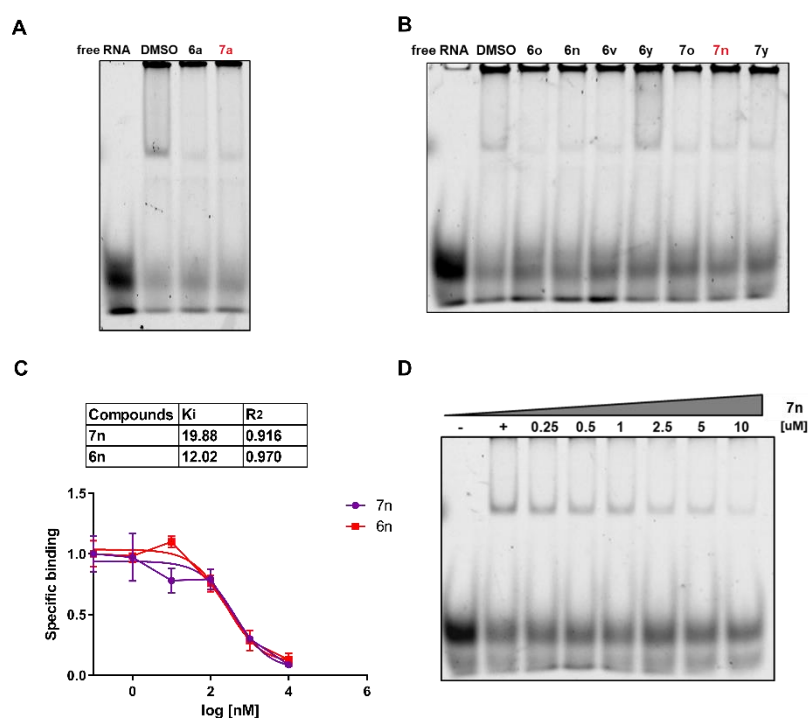


Figure 15. TM-II shows inhibitory activity towards HuR in vitro.

A) and B) Representative REMSAs showing HuR-RNA binding impairment induced by TMs, in particular 7a (red) and 7n (red). rHuR was incubated for 30 min with either 75 fmol of 5'-DY681-labeled RNA probe alone, or together with DMSO used as control, or TMs at 5 μ M doses. B) Alpha screen with relative K_i (inhibition constant) calculation of the specific binding of the His-tagged HuR and AU-rich biotinylated RNA. K_i have been calculated with respect to a K_D (dissociation constant) of 2.5 nM for the rHuR-Bi-AU interaction and normalized to control (DMSO). Data fit nonlinear regression fitting curves according to a 1-site binding model in GraphPad Prism. Plotted bars are mean \pm SD of two independent experiments. (Experiments in A) and B) were entirely performed by Digilio R. and Zucal C.)

Furthermore, we started checking biological activity in breast cancer cell line (Figure 16). As we did for TMs-I, we first assessed if the molecules affect the viability of MCF7. To this aim, we performed viability assay (Figure 16A). In this set of experiments we tested also 8n, that a chemical improvement of 7n, but until now we have poorly characterized it especially from the biochemical point of view.

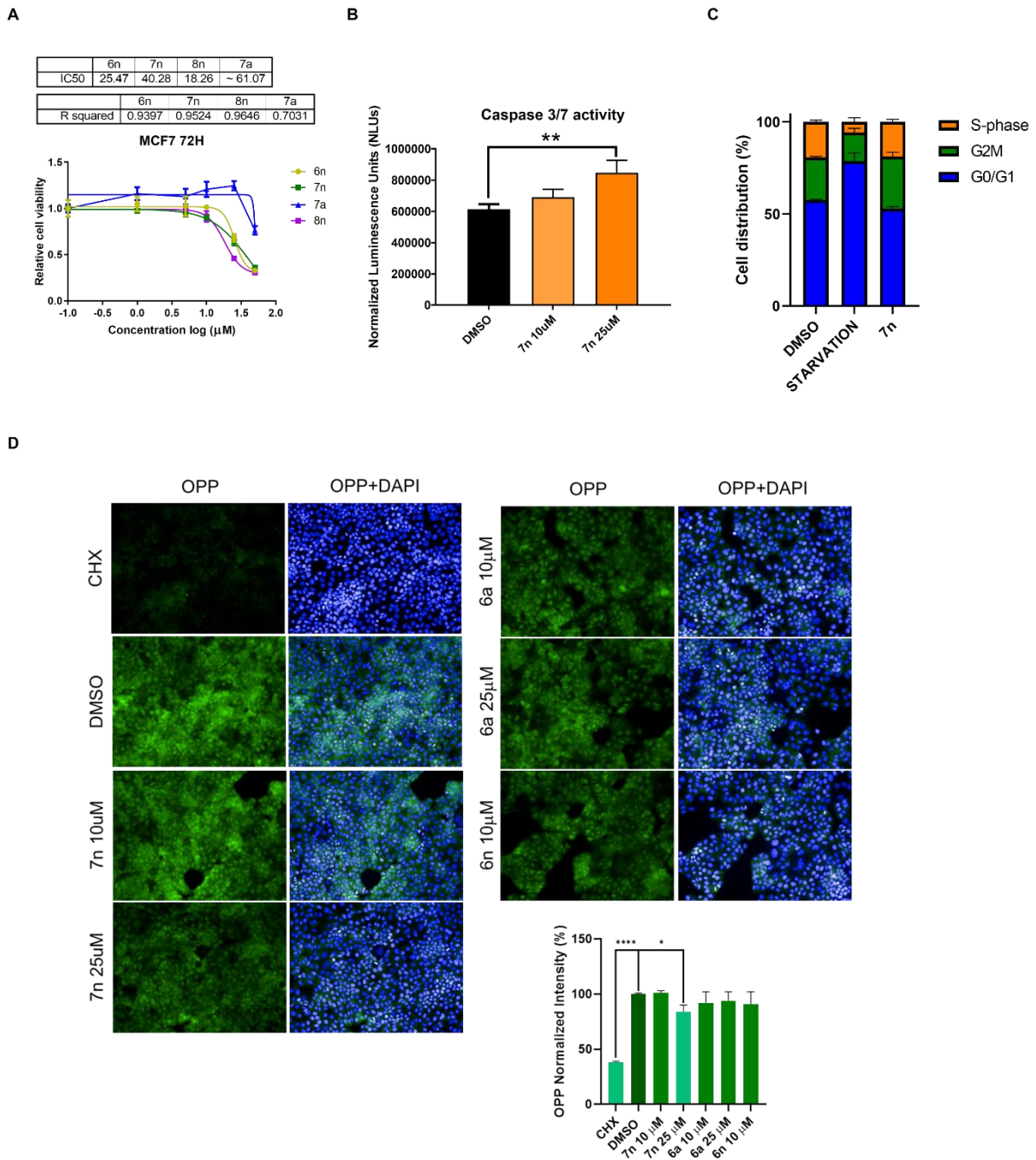


Figure 16. TMs-II show toxicity in MCF7 cancer cell line and among all, 7n induces apoptosis and slightly affect cell cycle progression. A) Cell viability was evaluated with OZBlue kit after 72 hours of treatments. Doses were from 0 to 50 μ M. Plotted bars are mean \pm SD of a biological duplicate, normalized to control (DMSO). Relative IC50 and R2 were calculated by nonlinear regression curve fitting. B) Caspase 3/7 activity was measured in MCF7 cells treated with 10 and 25 μ M dose of 7n for 24 h, using DMSO as control. Data have been plotted as mean \pm SD of a biological triplicates, ** p-value <0.01. C) Cell cycle analysis were performed with PI staining of the nuclei after 24 hours treatments with 7n at 10 μ M dose. Overnight serum starvation is shown as positive control of induced cell cycle synchronization in G0/G1 phase. Histograms quantify the cell cycle phase distribution. Flow-cytometry experiments were carried out on two biological replicates. Cell cycle phase analysis was done using ModFit LT 3.2 software and the Sync Wizard model. D) Representative immunofluorescence of PPP Click-iT assays. Cells have been treated with DMSO as control, CHX as positive control and 6a, 7n at 10 and 25 μ M, while 6n at 10 μ M doses. O-propargyl-puromycin (OPP) was added to the culture medium to label nascent peptides which were visualized with immunofluorescence after fixation by fluorescent Click-iT reaction chemistry between OPP and Alexa488 picolyl-azide. Data have been represented as mean OPP intensity normalized on the control \pm SD of a biological triplicates *p<0.05; ****p<0.0001 (I have performed these experiments in collaboration with Zucal C.).

The complete evaluation of its biochemical and biological activity is still ongoing in the lab. However, we treated MCF7 for 72 hours, with increasing doses of 6n, 7n, 7a and 8n (1, 5, 10, 25 and 50 μM) and DMSO in a single dose as control. Apart from 7a, that is revealed to be the less toxic compound, with an ambiguous IC_{50} around 60 μM , 6n, 7n show a comparable IC_{50} between 25 and 41 μM . On the contrary, 8n shares equal solubility properties of 7n, but is more toxic than the other analogues, with an IC_{50} around 18 μM , and the related implications should be investigated.

Moreover, considering these data as the starting points, we checked whether 7n shows anticancer activity mainly focusing our attention in the induction of apoptosis and of cell cycle blockage in cancer cell line. To this purpose, to evaluate apoptosis insurgence, we investigated on the activation of caspase enzymes, which are responsible for the cleavage of protein substrates and disruption of the cells (Shi, 2004). More deeply, upon checking caspases activation, we have treated MCF7 for 24 hours with two different doses of 7n, 10 and 25 μM along with DMSO as control. After, we have measured levels of caspase 3 and 7 with luminescent Caspase-Glo® 3/7 Assay from Promega (Figure 16B). Notably, a significant activation of caspases signal has been detected in 25 μM treated samples compared to control, suggesting that in cancer cell line 7n induces apoptosis response.

Furthermore, we evaluated 7n capability of provoking cell cycle arrest in breast cancer cell line. Precisely, we treated MCF7 cells for 24 hours with 7n (10 μM), using DMSO as control and cell starvation as positive control. Figure 16C shows preliminary Results, suggesting that starvation properly synchronizing the cells in G0G1 but, 7n, compared with the control, induces a marginal accumulation in G2M phase and we are currently in the process of validating and repeating these assays in order to verify if what observed could be revealed a significative effect.

All these evidences, suggest that the 2nd generation of HuR inhibitors, have been confirmed to block HuR *in vitro*, with similar efficacy than the precursors, among them, 7n appeared to show higher potency. Accordingly, they have shown similar toxicity in MCF7 cells compared to their precursors and 7n appears to affect cancer cell viability by activating apoptotic response, with emerging implications in cell cycle arrest induction. More observations have to be collected aiming at a deep characterization of 7n *in vitro* and anti-cancer properties in cellular context. As a consequence, from a biochemical point of view, with thermal-shift calorimetry approach (Ramsay and Tipton, 2017) we aim at measuring a direct interaction between the molecule and HuR, rather than performing DMR assay, in order to overcome technical issues found for HuR recombinant protein, mainly in the plate-immobilization steps. On the other end, we are currently performing RNA Pull-Down and RNA Immunoprecipitation to investigate on the inhibitors capability of disrupt HuR-targets binding, by confirming evidences that TMs induce a downregulation of cancerogenic factors, in particular, by performing Actinomycin-D and polysome profiling assays, we will evaluate if TMs affect stability and/or translational efficacy in HuR dependent manner. Nevertheless, further analysis on TMs effects on the global translation and transcription should be appreciated, before investigating on single target perturbation. Therefore, we obtained a first evidence, by using OPP Click-IT assay,

basically by treating MCF7 cells for 48 hours with 6a (10 and 25 μM), 7n (10 and 25 μM) and 6n (10 μM), DMSO as a control and Cycloheximide (CHX) (10 μM) for 4 hours as a positive control of translation blockage (Schneider-poetsch *et al.*, 2010). Afterwards, we monitored protein biosynthesis by adding O-propargyl L-puromycin (OPP; 10 μM) to the cell culture media and incubated for 30 minutes. Intensity of OPP was measured after performing immunofluorescence conjugating via Click-IT reaction OPP and Alexa 488 picolyl-azide (Figure 16D). Data represented in Figure demonstrated that 7n at 25 μM at 48 hours significantly downregulated about 20% of the global protein synthesis, whereas other TMs treatments result to be not effective. For what concerns global transcription, we are currently focused in collect some evidences. These data, with the purpose of checking the TMs' effect in the fate of specific HuR-targets both at protein and mRNA level, could give insights on TMs specificity and strength in inhibiting HuR. Since, DHTS has been shown to affect the binding of only a subset of HuR transcripts (paragraph 3.2), synthetic analogs provoking a significant abolishment of the HuR-mRNA formation could be selected not only by looking at single targets, but through investigations on the global translation and transcription perturbation. Furthermore, as we did for TMs-I, we need to investigate deeper on TMs-II capability of modulating cancer traits, such as cell invasiveness diminishing and reduction of the resistance induced by TMs-I, when administrated in combination with single chemotherapeutic agents. Finally, considering the reduction of invasive capability shown for TMs-I and the slight accumulation in G2M phase of the cell cycle induced by TMs-II, we should investigate on TMs implication in regulating cell proliferation.

4.6 Evidences on TMs anti-inflammatory properties: TMs show toxicity in macrophages cell lines, as well as reduction in cytokines expression.

Cancer progression, along with worst prognosis, is related with an establishment of an erroneous crosstalk between cancer and the inflammatory response (Introduction paragraph 2.4) (Epithalamion and Pinka, 2012). In fact, tumour microenvironment is maintained by inflammatory cells, that, at the end, participate in the neoplastic process, inducing proliferation, survival and migration. Furthermore, tumour cells exploiting signalling molecules coming from the immune system, such as cytokines, chemokines and their receptor, promote invasion migration and metastasis (Epithalamion and Pinka, 2012; Zhang *et al.*, 2017). HuR, as described in the paragraph 2.4 of the Introduction, is responsible and directly involved in the proper development and response of the myeloid lineage, monocytes and Natural Killer cells (Yiakouvaki *et al.*, 2012; Shang and Zhao, 2017) B and T cells maturation and response (Papadaki *et al.*, 2009; Diaz-Muñoz *et al.*, 2015; Turner and Díaz-Muñoz, 2018). Nevertheless, playing a pleiotropic function HuR promotes and represses macrophages, neutrophils infiltration, astrocytic proliferation, inflammation and neuroinflammation in different circumstances (Brauß *et al.*, 2017; Chen *et al.*, 2017; Kwan *et al.*, 2017). In this context, we started exploring TMs' effects on innate immune response, specifically on macrophages, pushed by the emerging

evidences above mentioned, HuR is being better characterized in this cell lineage both in physiological development and in the inflammation response. Furthermore, it is now clear that the crosstalk between cancer and myeloid cells is crucial and dynamic. Tumour Associated Macrophages (TAMs), for example, have been demonstrated to play different roles as positive and negative regulators in cancers, depending on the different phenotypes they acquire (M0, M1 and M2) (Pathria, Louis and Varner, 2019). Based on this model, our idea is to promptly evaluate the simultaneous TMs effect on HuR modulation both in cancer cells and macrophages infiltrates. For what concerns this part, we choose to focus our attention on CXCL10 and TNF α for the following reasons. CXCL10 and TNF α are now recognized to be key markers belonging to macrophages into the differentiation status of M1 phenotype (Mantovani *et al.*, 2002) and are main mediators in promoting macrophage invasion, in order to harm and trigger progress of diseases, such as fibrosis and tumour formation (Müller-Quernheim *et al.*, 2012). With a reduced extent, we used CXCL2 as a read-out for our experiments, because it has been shown that CXCL2 is generally secreted by TAMs and mediates tumour invasiveness (Hashimoto *et al.*, 2016). TNF α mRNA is a well-known HuR target (see Introduction), while CXCL2 has been recently confirmed to be recognized by HuR (Ke *et al.*, 2017) and together with CXCL10 mRNA, they are both competitively bound by HuR and TTP (Tiedje *et al.*, 2016). Indeed, PAR-Clip experiments, have shown that their 3' UTRs have been found to share binding sites for both TTP and HuR (Sedlyarov *et al.*, 2017).

To this aim, we first evaluated TMs toxicity in two different macrophage cell lines: a human one, represented by THP 1, that is a monocyte cell line, but after stimulation with PMA differentiates in macrophages and a murine one, RAW 264.7 (Figure 17A). I have tested for cells viability assay, the compounds: 6a and 7n, leading compound of respectively the first and the second generation, 6n, that is the chemical precursor of 7n and 8n and lastly 7a that is an ameliorated version of 6a belonging to the TMs-II. The graphs showing the tests in Figure 17B have been organized by dividing the drugs based on the chemical nature of the compounds, previously explained (6a;7a and 6n;7n;8n). In order to assess whether the simultaneous stimuli of proliferation given by PMA but also its low toxicity level could impair the assay read out, we performed viability assay also on THP1, the human monocyte cell line before the stimulation (Figure 17B).

Indeed, THP1 receiving for 72 hours both PMA (100 ng/ml) and TMs treatments seemed to be more sensitive, as represented by the IC50 values. In both these cases THP1 were tested only for 6a and 7n the leading compounds of the two generations, already described. In both A) and B) it has been possible to calculate the precise or a prospective IC50 for all the compounds, ranging from 16-25 μ M, lower doses if compared with the one calculated for the cancer cell lines, shown in the paragraph 3.3. Figure 17C, shows explorative experiment performed in THP1 cells after stimulation with PMA (100 ng/ml) for 24 hours followed by 4 hours co-treatments with LPS (1 μ g/ml) and 6a and 7n at 10 μ M doses respectively and LPS+DMSO as control.

DMSO alone was used as a control to check the proper activation of the cytokines after LPS response. After RNA extraction a qRT-PCR was performed, in order to evaluate if the treatments with both the compounds were able to counteract the LPS induction of expression. Indeed, considering *TNF α* and *CXCL2*, a significant reduction of the mRNA expression of both the targets is observed upon treatments with 6a and 7n.

These experiments, appeared to be highly promising, thus we deeply investigated on the response to LPS and TMs effect on macrophages. Since THP1 cell line showed highly toxicity to PMA, optimization is still ongoing in the lab, and, therefore, I will present results obtained using murine RAW 264.7 as macrophages model.

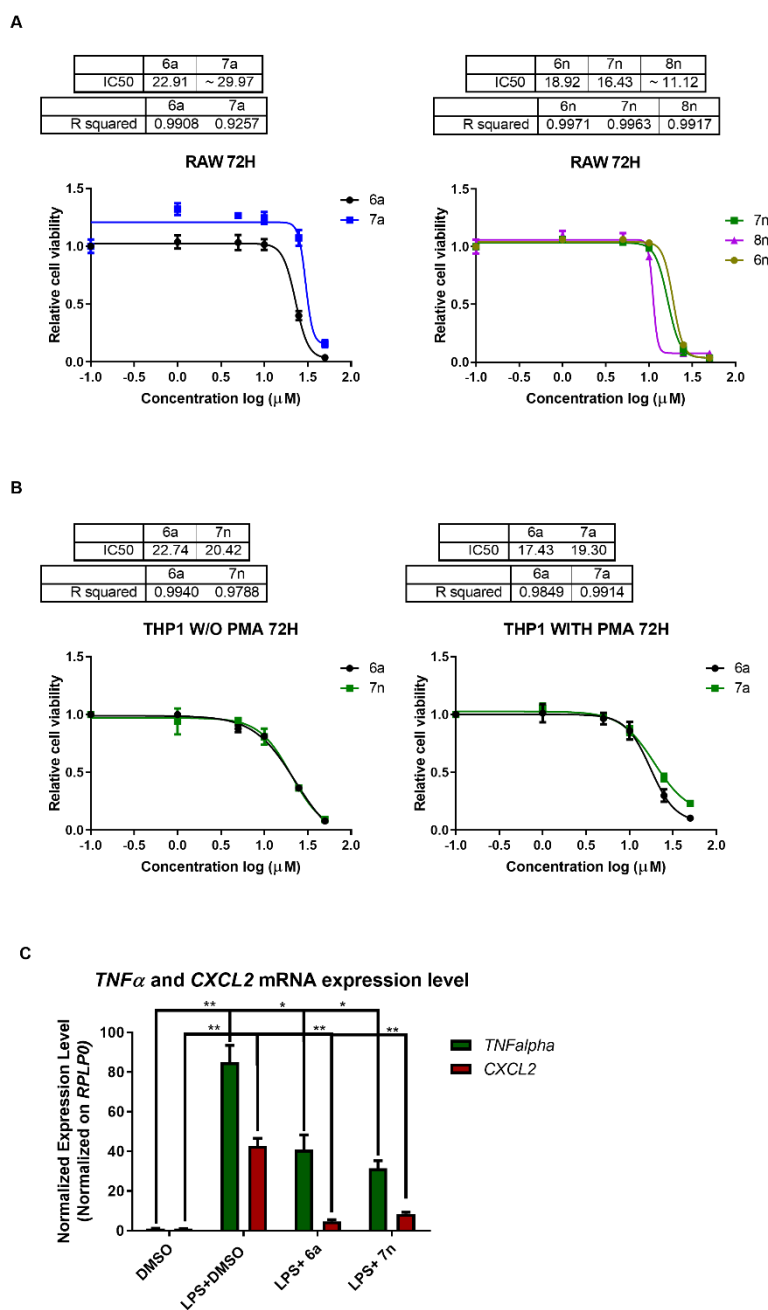


Figure 17. TMs cause toxicity in RAW cells and THP1 with and w/o PMA, further downregulating the expression of *CXCL2* and *TNF α* after LPS response. A)

RAW Cell viability was evaluated with OZBlue kit after 72 hours of treatments. Doses were from 0 to 50 μ M. Plotted bars are mean \pm SD of a biological duplicate, normalized to control (DMSO). Relative IC50 and R2 were calculated by nonlinear regression curve fitting. (I have performed these experiments in collaboration with Zucal C). B) THP1 cells were either activated for 24 hours with PMA (100 ng/ml), or not as a control for PMA toxicity and treated for 72 hours with molecules at doses ranging from 0 to 50 μ M. Plotted bars are mean \pm SD of a biological duplicate, normalized to control (DMSO). Relative IC50 and R2 were calculated by nonlinear regression curve fitting, cells viability was evaluated with OZBlue kit. (I have entirely performed the experiments).

C) Preliminary data, in which THP1 cells were stimulated with PMA (100 ng/ml) for 24 hours, and then were co-treated with LPS (1 μ g/ml) for 4 hours and with HuR inhibitors at 10 μ M dose and DMSO as control. After RNA extraction, qRT-PCR was performed and *CXCL2* and *TNF α* mRNA expression levels were evaluated. mRNA levels were normalized on *RPLP0* mRNA as housekeeping gene and data have been normalized on DMSO as control and plotted represent Mean \pm SD (n=2; *p<0.05 ** p < 0.01). (I have entirely performed the experiments)

4.7 TMs affect HuR post-transcriptional function by downregulating cytokines production and release in RAW 264.7

Innate Immune response is activated to counteract pathogen constituents and lipopolysaccharides (LPS), is one of the components of the outer membrane of gram-positive bacteria. LPS is sensed by macrophages mainly, thanks to the recognition by the TLR4 receptor located on the membrane of these cells. This process activates the MAPK signalling cascade ending in turn with the activation of the transcription factor NF- κ B, resulting in a reorganization at the level of gene expression, stimulating the production of pro-inflammatory cytokines and chemokines (Medzhitov and Horng, 2009; Takeuchi and Akira, 2010; Smale, 2012; Vaure and Liu, 2014). This reflects in drastic changes at the genome-wide level in macrophages expression (Reynier *et al.*, 2012; Rutledge *et al.*, 2012), that need a strict post-transcriptional control, ensuring appropriate response from the immune system (Carpenter *et al.*, 2014; Kafasla, Skliris and Kontoyiannis, 2014). RBPs are emerging to be the pivotal factors regulating these processes, TTP and HuR in particular (see Introduction) (Fu and Blackshear, 2017; García-Mauriño *et al.*, 2017; Díaz-Muñoz and Turner, 2018; Mino and Takeuchi, 2018; Turner and Díaz-Muñoz, 2018). Thus, taking into account preliminary data previously shown, we decided to investigate the impact given by our TMs in response to LPS in murine macrophages RAW 264.7. Basically, we firstly co-treated RAW cells with the leading compounds of respectively the first and second generation of TMs, 6a and 7n (10 μ M), with LPS (1 μ g/ml) by performing different time points at respectively 1, 4 and 6 hours (Figure 18). The expression levels of *CXCL10* and *TNF α* were checked by qRT-PCR and data have been normalized on the expression level of the housekeeping *RPLP0*, using DMSO as the reference sample.

In Figure 18, notwithstanding the different time points, comparing the sample LPS+DMSO and DMSO, LPS induces activation of the expression of the cytokines, furthermore *CXCL10* and *TNF α* mRNA levels appeared to be significantly downregulated at 4h co-treatments, by both 6a and 7n. The same is not observed at 1h, that, indeed we considered as an early time points, where only 6a, seemed to counteract LPS stimuli. This may be due to the low expressions of the cytokines compared to the 4h and 6h. On the other end, after 6h, LPS seemed to be already a late stage; although it is possible to observe a downregulation of the cytokines, the levels of decreasing are not significant, this may do the variability of the experiments that is intrinsically high.

Based on these data, in order to put some insights in the molecular mechanism of 6a, that has been shown to be effective after 1 and 4 hours LPS treatments, other colleagues performed some preliminary experiments. To further investigate if the downregulation of the cytokines mRNAs was related to a decrease in the stability of the transcripts impairing HuR post-transcriptional function, using Actinomycin-D chase experiments, kinetics of these targets have been performed.

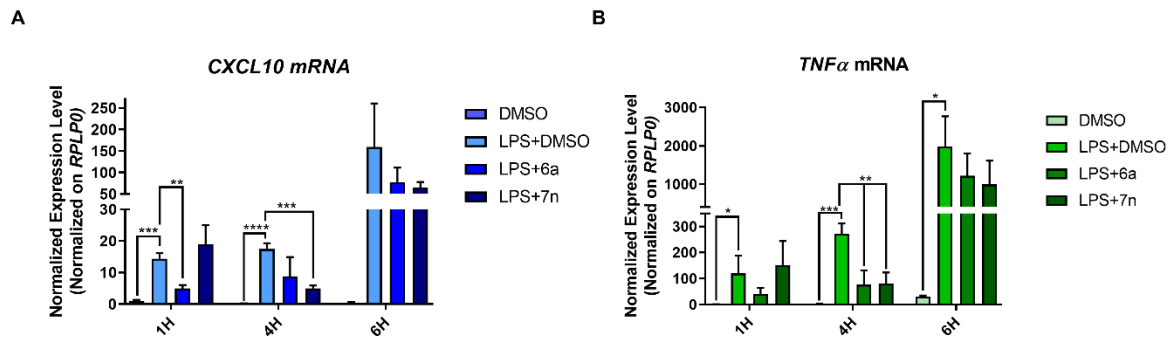


Figure 18. 6a and 7n treatments downregulate cytokines mRNA expression level in RAW 264.7. RAW cells were treated with both LPS (1 μ g/ml) and 6a, 7n (both 10 μ M) and DMSO as control, at different time points: 1h, 4h, 6h. *CXCL10* and *TNF α* mRNA level were assessed by qRT-PCR and data have been normalized on the control samples (DMSO) and the housekeeping gene, *RPLP0* mRNA level. Data represent mean \pm SD of a biological triplicate (* p <0.05, and ** p <0.01) (Experiments entirely performed by me)

In particular, the level of the remaining *TNF α* and *CXCL10* mRNAs in RAW 264.7 was estimated after 3 hours of LPS treatments (1 μ g/ml) co-treated with DMSO (as control), Actinomycin D (2.5 μ M) with DMSO and in combination with DHTS (1 μ M) and 6a (5 μ M). In Figure 19A, both the compounds show to decrease mRNA stability of both *TNF α* and *CXCL10* compared to samples treated with Act-D only. These experiments, showed that the half-life of all the transcripts is affected by DHTS and 6a treatment, acting by interfering with HuR post-transcriptional function as a stabilizer of these targets. Moreover, polysome profiling has been performed to check if a decrease in the stability due to a reduction of the binding between HuR and *TNF α* mRNA brought to a reduce transcripts loading on polysome with a subsequent depletion in the translation. Figure 19B shows the distributions of the mRNAs copies along the polysomal fractions of the following samples: DMSO, LPS+DMSO, LPS+6a. DMSO alone was used as a control for *TNF α* activation after LPS stimuli, that indeed is confirmed. The polysome profiling of ACTIN was used as a control and as it is shown in the Figure 19B without changes on ACTIN, *TNF α* was reduced during co-treatments suggesting that the decrease in copy number of *TNF α* mRNA affected the translation of the mRNA itself.

To give some insights on the HuR dependency, we checked the level of expression of *TNF α* and *CXCL10* in a RAW 264.7 cells in which HuR expression has been silenced. HuR depletion has been obtained by transfection of siRNA against HuR and scramble as control for 72 hours, then we first detected HuR expression both at the mRNA and protein level (Figure 19C-left panel). Afterwards we co-treated the cells with LPS (1 μ g/ml), DMSO alone or in combination with LPS, with DHTS (1 μ M) and 6a (10 μ M) for three hours and *TNF α* and *CXCL10* mRNA levels were assessed by performing qRT-PCR. Results are shown in Figure 19C-right panel, notably DHTS and 6a downregulated LPS cytokines induction, as observed when HuR expression is depleted. All these experiments suggest that, as was already shown for DHTS in MCF7, DHTS and 6a negatively modulate the cytokines expressions after LPS induction in RAW 264.7, affecting HuR post-transcriptional function.

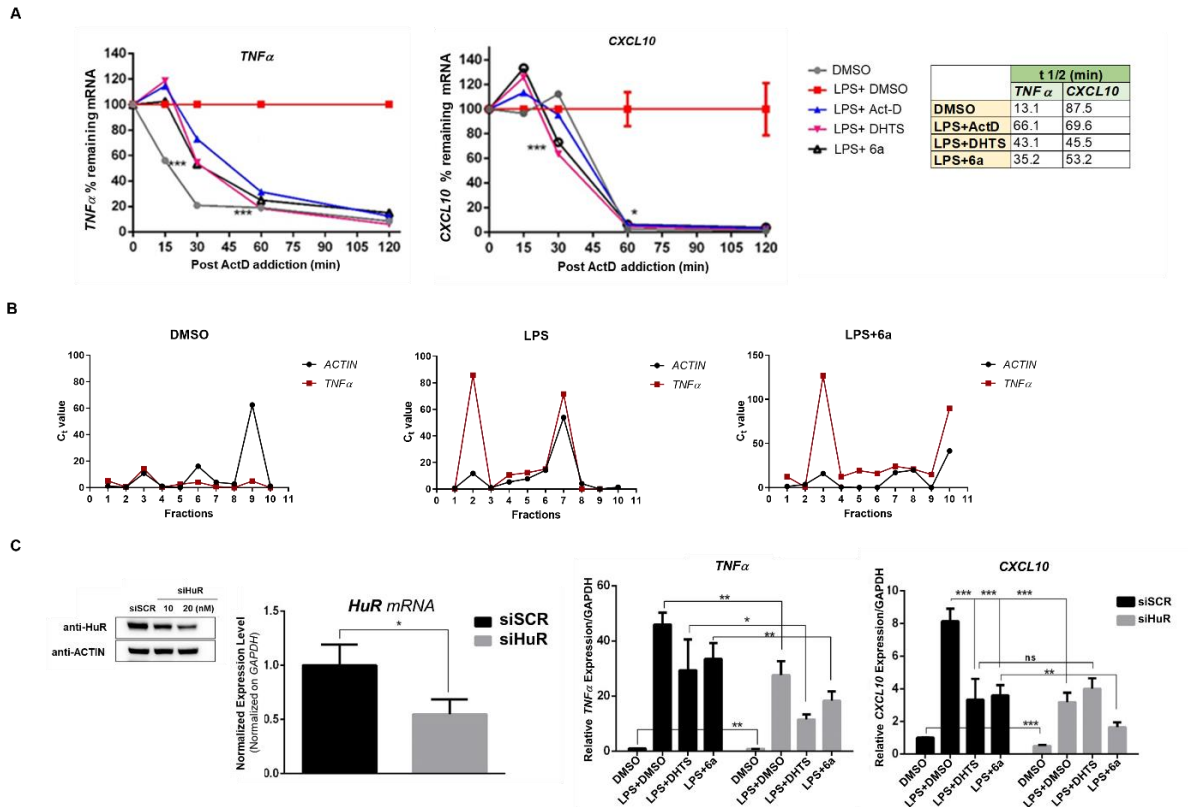


Figure 19. 6a downregulates TNF and CXCL10 in a HuR dependent manner.

A) RAW264.7 cells were co-treated with DMSO, LPS+DMSO, LPS+DHTS and LPS+6a for 0, 15, 30, 60 and 120 min. RT- qPCR was performed to quantify the remaining *TNF α* and *CXCL-10* mRNA levels. The half-lives of the targets in the different samples are indicated in the table and has been calculated using GraphPad Prism, nonlinear regression analysis and then choosing one phase decay function to calculate the half-life of each mRNAs. Each replicate was plotted and compared using Dunnett's Multiple Comparison Test showing P values * $P \leq 0.05$, *** $P \leq 0.001$. B) RT-qPCR analysis of actin and *TNF α* mRNA levels in polysomal RNA fractions in RAW 264.7 after co-stimulation with LPS (1 μ g/ml) and 6a treatment (5 μ M) for 3 hours. TNF different polysome profiles can be appreciated for DMSO, LPS+DMSO and LPS+6a conditions, ACTIN has been used as normalizer. C) On the left, western blot analysis and RT-qPCR showing around 50% decreasing in HuR expression level after siRNA transfection against HuR with different doses and scramble as control. On the right, *TNF α* and *CXCL10* mRNAs in siSCR and siHuR after 3 hours of co-treatment with LPS 1mg/ml, DMSO and DMSO alone to control LPS stimulation, DHTS (1 μ M) and 6a (5 μ M) in RAW cells. Data have been plotted as Mean, and SD obtained are from 3 independent experiments and were analyzed by one-way ANOVA. * $p \leq 0.05$, ** $p \leq 0.01$, *** $p \leq 0.001$; ns, not significant. (Experiments in A) B) and C) have been all performed by Lal P.)

Taking into account these data, we decided to perform experiments aimed on investigating the cytokines both at the level of the secreted proteins and most importantly we wanted to challenge the activity of other molecules belonging to TMs-I and TMs-II.

Thus, in order to give an exhaustive description regarding the chemical nature of the molecules, in order to strengthen the already presented structure-activity relationships, I decided to repeat the previous experiment focusing on 6h LPS, but treating the cells with the following compounds: 6a and 7a; 6n and 7n, in order to investigate on the comparison between analogues belonging to the 1st and 2nd generations (6a and 6n; 7a and 7n) and evaluate the differences in the efficacy of activity between the precursor and the ameliorated derivative (6a and 7a; 6n and 7n). RAW 264.7 cells were treated for 6 hours with the inhibitors at 10 μ M, along with LPS and DMSO alone used as control. Notably, Results are shown in Figure 20A-B, LPS is confirmed to activate the expression of the cytokines

(LPS+DMSO vs DMSO), while 7n reduces significantly the expression of both CXCL10 and *TNF α* mRNA. 6n and 7n (precursor of the 1st generation and derivative of the 2nd generation) both seems to affect significantly *TNF α* expression. On the contrary, 6a and 7a do not change mRNA expression level, resulting to be ineffective. This may due to the time point, concerning what described above, repeating this experiment by performing treatments and LPS stimulation for 4 hours, and, considering the IC50 of 6a and 7a, increasing the dose of treatments could be enough to appreciate an inhibitory effect. Furthermore, we wanted to investigate on the level of TNF protein secreted, in order to confirm if a reduction observed in the mRNA transcription corresponds in a downregulation of the translated protein and a succeeding deregulated secretion, suggesting generally that the pro-inflammatory response is impaired. On this purpose, we performed ELISA assays to detect protein level released in the supernatant of the cells, co-treated with LPS and TMs at different time points: 1, 4, and 6 hours. Unfortunately, CXCL10 levels were low even at 6 hours LPS. Indeed, one of the ongoing works in the lab is now focused in analyzing CXCL10 secretion after 18 hours of LPS and TMs treatment in RAW cells. For what concerns TNF (Figure 20C), TMs downregulate protein secretion after 1 hour treatments and LPS activation, 6n, 7a and 7n confirm to reduce the secretion even at 4 hours treatments, but after 6 hours only 7n is capable or reducing TNF α release. DMSO alone has not been plotted since it was under the limit of detection, suggesting that at the steady state TNF level is not secreted as expected and DMSO does not affect the cytokine production when combined with LPS.

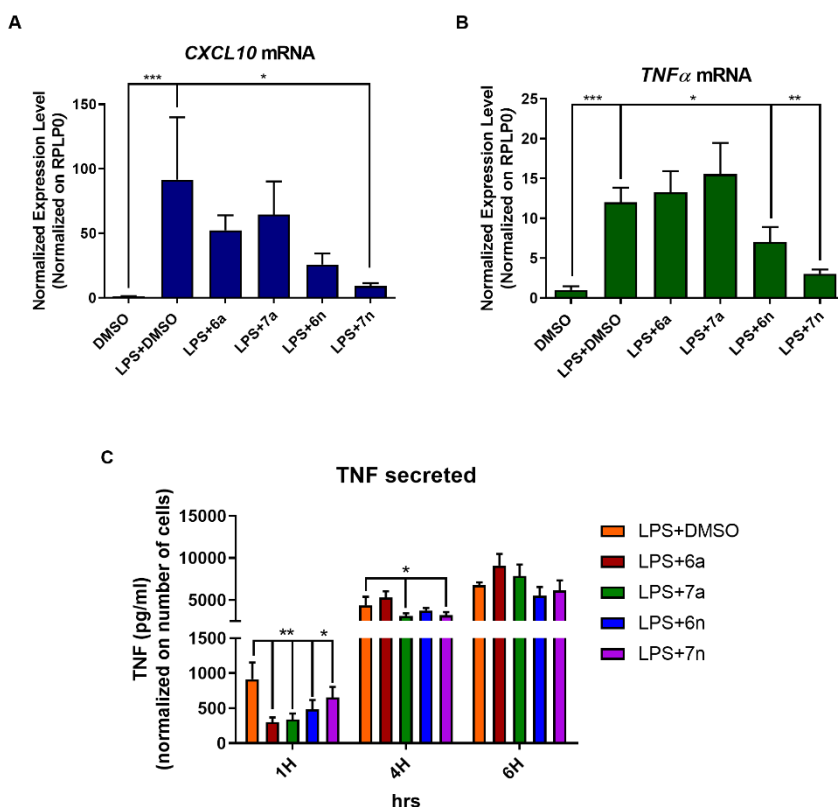


Figure 20. TMs reduce CXCL10 and TNF α level of expression and TNF protein secretion with different efficacy. A) and B) RAW cells were co-treated for 6 hours with compounds at 10 μ M doses, LPS (1 μ g/ml) and DMSO as control. mRNA levels of the cytokines has been assessed through qRT-PCR using *RPLP0* as an housekeeping gene and data have been normalized on DMSO condition, in order to evaluate the effect of LPS. Data gave been plotted as mean \pm SD of a biological triplicate (* p <0.05, and ** p <0.01). C) TNF protein levels measured with ELISA. DMSO alone treatment has not been plotted since the levels of the protein (pg/ml) were under the limit, cell supernatants were diluted 1:3. Relative pg/ml obtained for each sample have been normalized on the number of cells obtained by performing crystal violet assay. Data represent as mean \pm SD of a biological triplicate (* p <0.05, and ** p <0.01) (Experiments have been performed entirely by me)

All these data together have suggested that, among the TMs, 6a, as well as DHTS, affects the stability of *CXCL10* and *TNF α* mRNAs as emerged by preliminary Act-D chase experiments. Furthermore, 6a appeared to decrease the polysomal loading of *TNF α* , resulting in a hypothetical reduction in the translation of the related protein, that has to be deeper investigated. Nonetheless, the downregulation of *CXCL10* and *TNF α* inferred by 6a appeared to be HuR-dependent, as hinted by the HuR silencing experiments performed in RAW 264.7 cells (Figure 19C-left and right panel). Significant additive effects occurring when simultaneously treating the cells with the molecule and HuR silencing, may be due to the inhibition of a residual expression of HuR, subsequently, by generating a HuR complete knockout by using techniques, such as CRSPR/cas9 could help to demonstrate this hypothesis, taking into account that HuR complete ablation is related with high cell toxicity implications. In order to collect more validations, TMs-II and especially the leading compound 7n should be challenged for the same assays. To do this, blocking mRNAs transcription by using inhibitors to evaluate targets stability, reflects to be toxic for cells, in most of the cases. To overcome this issue, using inducible promoters or different mRNA labelling techniques such as 4-thiouridine (4sU) method, could improve the limitations given by using chemicals (Wada and Becskei, 2017), considering also that Actinomycin-D indirectly act on HuR by forcing its translocation to the cytoplasm (see Introduction paragraph 2.5). As described above (paragraph 3.4), nascent RNA labelling techniques could be pivotal to give insights on the strength capacity towards HuR inhibition, or provide some specificity evidences, by assessing whether these molecules could infer a blocking of the transcription *per se*. Moreover, I have shown in Figure 20 A) and B) that RAW 264.7 co-treated with LPS and selected HuR inhibitors downregulate, with different efficacies, *CXCL10* and *TNF α* mRNA expression. This could be explained by taking into account the treatments time points. I have evaluated 6a activity at 1, 4 and 6 hours. 6a affects HuR targets expression at 1, 3 (taking into account Act-D, polysome and HuR silencing experiments), 4 but not at 6 hours treatments. It is well known that LPS stimuli reflects in a change in gene expression divided in early and late response, suggesting that 6a impacts the early phase of inflammatory response rather than the late one (Sharif *et al.*, 2007; Lawrence and Natoli, 2011). Surprisingly, 7n, TMs-II reference molecule appears to have a major effect between 4 and 6 hours after LPS administration. Although if further characterizations are needed, what observed for 7n could be due to a major chemical stability and potency for HuR inhibition, reflecting in a prolonged blockage of its activity, related to a progressive counteraction of LPS response.

However, as already mentioned, increasing doses of the other TMs tested (e.g. 6a) could reflect in stronger effects. Further efforts should be put in investigating on TNF, plus *CXCL10* translation, starting from checking whether treatments with 6a and 7n cause mRNA translation downregulation, and by performing polysome profiling, we will quantify any differences in the number of transcripts copies loaded on the translational machinery, taking into account that treatments could affect the global translation profile compared to the control condition.

4.8 Upon LPS response, TMs do not affect NF- κ B localization in the cells, but directly impair HuR-mRNA binding.

LPS stimuli results mainly in the activation of macrophages and initiate when LPS-Binding protein (LBP) binds CD14 receptor on their surface (Sweet and Hume, 1996). Thus, the LPS-CD14 via Toll-like receptor 4 (TRL4) induces a signaling pathway that involves NF- κ B as well as the extracellularly-regulated kinase, c-Jun N-terminal, and p38 mitogen-activated protein kinases, all of which activate the production of inflammatory factors (Scott *et al.*, 2000). NF- κ B acts as a transcription factor (TF), thus promoting the expression of many cytokines and chemokines, but its function is related to its translocation in the nucleus stimulated by TRL4 signaling cascade which involves other protein activity, such as MyD88 and TRIF (Sakai *et al.*, 2017). *CXCL10* and *TNF α* mRNA are just two among the variety of NF- κ B targets (Hl, 1999; Yeruva, Ramadori and Raddatz, 2008; Ostareck *et al.*, 2019), thus we decided to investigate if, what observed so far, was related to an aberrant NF- κ B subcellular localization caused by HuR inhibitors after LPS stimuli. To this aim, we performed immunofluorescence in RAW 264.7 co-treated with LPS (1 μ g/ml) and 6a, 6n, 7a and 7n (10 μ M) for 3 hours, plus DMSO alone or in combination with LPS, as a control for treatments and LPS proper stimuli occurrence. Moreover, we used Actinomycin-D (2.5 μ M) simultaneously with LPS as a positive control, in order to stimulate a high induction of NF- κ B in the nucleus.

Results are shown in Figure 21, LPS significantly promotes NF- κ B (green) nuclear localization, along with additional effect given by the co-treatment with Actinomycin-D, while TMs do not show any significant counteracting or addictive action, proving that their capability of downregulate *CXCL10* and *TNF α* mRNA, showed in the previous paragraph, is not dependent by a changing in NF- κ B subcellular localization, suggesting that its activity as TF is not impaired.

Previously we demonstrated that TMs do not promote any HuR shuttling from the nucleus to the cytoplasm in MCF7 cells (Figure 13), that instead, is provoked upon Act-D treatments. Furthermore, it has been suggested that LPS induces HuR cytoplasmic translocation (Lin *et al.*, 2006), subsequently, we wondered whether we could observe any changes in HuR localization after LPS stimuli and after TMs treatments alone or in combination with LPS. To this purpose, we co-treated RAW 264.7 cells with LPS, 6n and 7n (10 μ M), or each TMs without LPS induction for 3 hours, plus DMSO alone as control and with LPS to verify the stimuli occurrence.

In Figure 22A, representative Immunofluorescence shows a slight HuR (red) accumulation in the cytoplasm as previously reported, thus we asked if TMs in combination with LPS could counteract this event. We treated the cells only with TMs (w/o LPS) to evaluate if TMs alone could influence HuR localization in RAW 264.7 We demonstrated that 7n and 6n single treatment do not alter HuR cell distribution (vs DMSO), whereas, no changes in HuR localization were observed in LPS+7n and LPS+6n samples compared to LPS+DMSO (Figure 22A). Moreover, we wondered the same for Actinomycin-D, investigating if TMs were able to neutralize HuR mis-regulation promoted by Act-D.

In Figure 22B Results are shown through representative immunofluorescence performed in RAW 264.7 treated simultaneously with Act-D (2.5 mM) and TMs (10 μ M) for 3 hours, using DMSO as control. We observed that Actinomycin-D+DMSO stimulates HuR localization outside the nucleus, not rescued by the addition of TMs. These data suggest that, in any case, TMs acts independently from changing NF-kB cellular localization induced by LPS, and are not able to stimulate HuR rescue in the nucleus as once inferred by drugs like Actinomycin-D, suggesting once again that TMs mechanism of HuR targets downregulation is exclusively related on the affection of HuR activity.

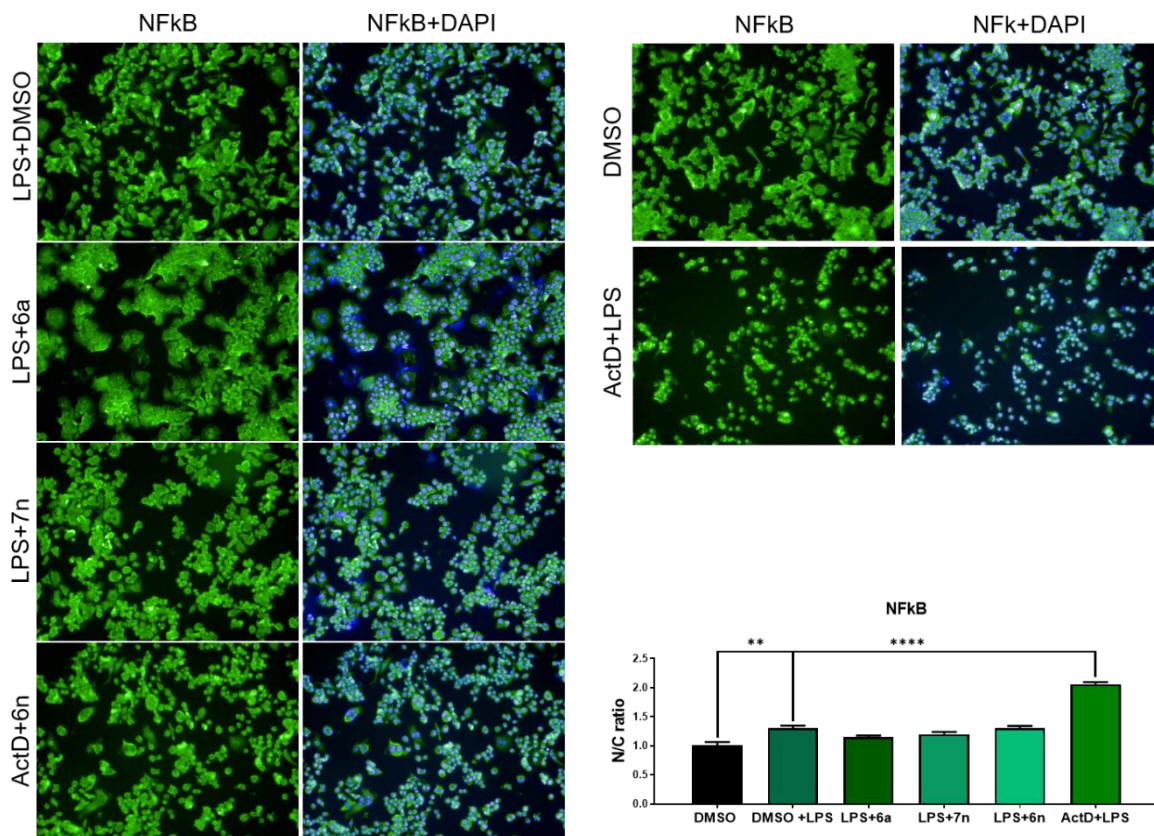
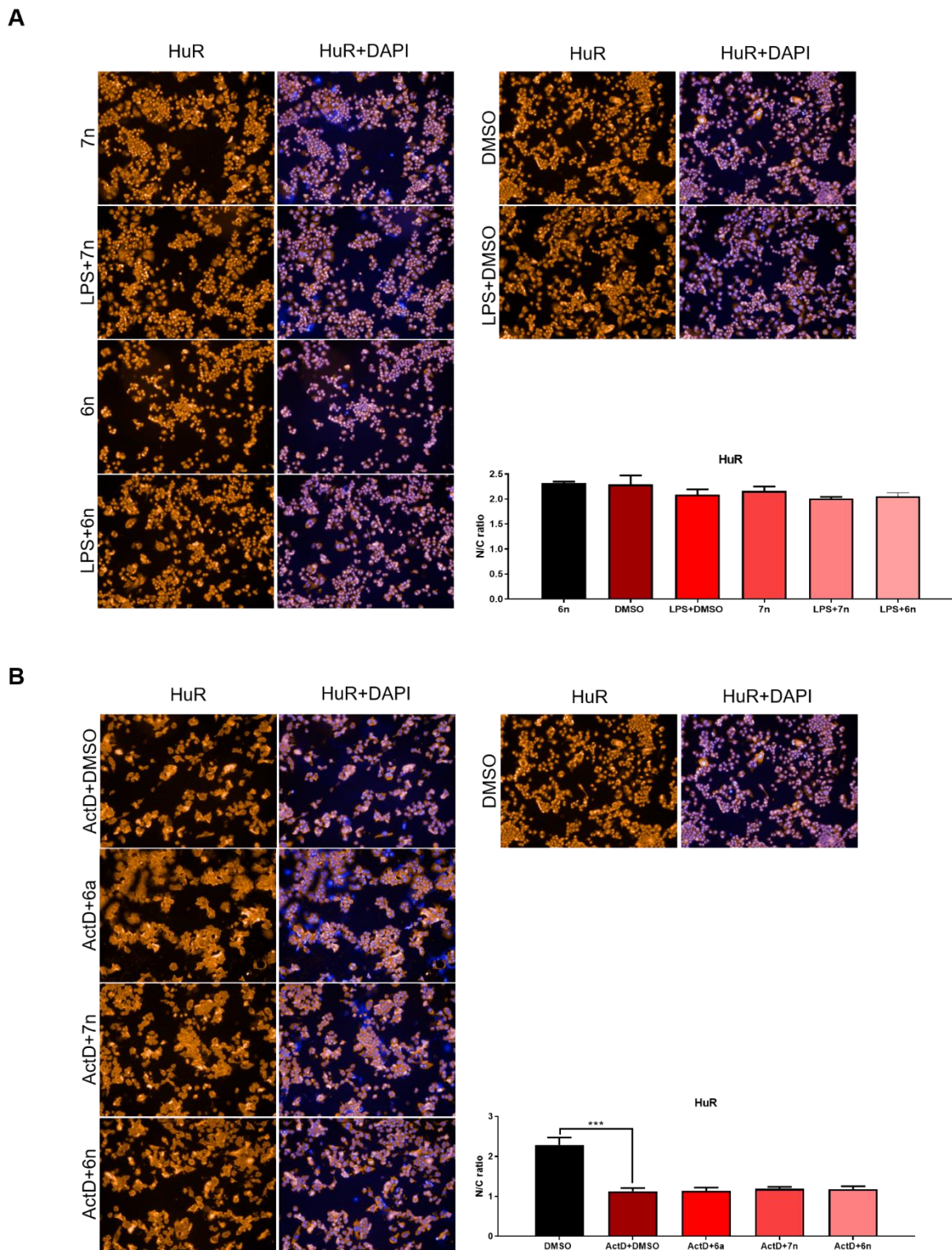


Figure 21. TMs do not change NFkB subcellular localization upon LPS stimuli. Representative immunofluorescence showing that N-kB nuclear translocation inside the cells induced by LPS is not changing upon treatments with different TMs (10 μ M). Cells have been treated for 3 hours in combination with LPS (1 μ g/ml). In order to obtain a positive control given by a high induction of NFkB related with a massive shuttling in the nucleus, we treated the cells with 2.5 μ M of Actinomycin D (Act-D), and DMSO (CTRL) either alone or with LPS was used as negative control. In the graph, the ratio of NFkB fluorescent signal between nucleus and cytoplasm (N/C) is plotted. For image acquisition (40 \times high NA objective), Operetta was used and evaluation by selecting 13 fields/well. The ratio N/C represents the mean \pm SD of single cells for every well (** p < 0.05; p < 0.0001) (unpublished data). (Experiments performed with Zucal C.)



In order to investigate deeply if what observed on *TNF α* and *CXCL10* in macrophages is due to TMs inhibition of HuR-RNA complex formation, we performed RNA Pull-Down assays along with RNA IP preliminary experiments. For these assays, we decided to use 7n, since it appears to be the most promising and lead compounds among the 2nd generation of chemicals. Results are plotted in Figure 23A, we performed RNA Pull-Down in RAW 264.7 pre-treated with 7n for 6 hours and DMSO as control. After 6 hours, cells were lysed and incubated with two different biotinylated probes: one containing 3' ARE sequence belonging to *TNF α* 3'UTR known to be bound by HuR and another one, as negative control containing sequence that is not recognized by HuR. After incubation for two hours at 4 degree, probes were precipitated with streptavidin beads. Afterall, HuR level were assessed by Western Blot analysis (Figure 23A). As expected, no signal for HuR has been measured in the negative control, in which the lysate was incubated with the negative probe, whereas HuR signal in the treated sample precipitated with the ARE sequence is significantly decreased (~ 50%) compared to the positive control, in which cells were treated with DMSO and lysates precipitated with ARE probe. This suggests that upon treatments 7n competes with HuR target RNAs for HuR binding within cells. Furthermore, as observed for *CTNNB1*, *ERBB2* and *VEGF* in MCF7 treated with 6a and 6t (Figure 11A), we performed preliminary experiments aim at evaluating the decrease in the binding between HuR and its target *CXCL10* inferred by 7n. Thus, I have performed RNA IP assays, by co-treating cells with LPS and 7n for 6 hours, using DMSO alone or in combination with LPS as control, according to what previously described. Results are represented in Figure 23B, which shows a depletion on *CXCL10* (~ 30%) fold enrichment in 7n treated HuR-IP samples, suggesting that it reduces HuR-*CXCL10* interaction. As described previously (see Introduction paragraph 2.4), TTP and HuR have been proposed to play key functions in modulating mRNA expression changes at the genome wide level in macrophages during immune response induced by LPS. This process is mainly regulated by a fine tune balance between these two RBPs, of which different or common targets as well as binding sites have been characterized (Ostareck *et al.*, 2019). Furthermore, as mentioned in the Introduction (see Introduction paragraph 2.4), through PAR-iCLIP assays TTP and HuR binding sites and targets in RAW 264.7 and in primary murine macrophages cells stimulated with LPS have been identified (Sedlyarov *et al.*, 2016; Tiedje *et al.*, 2016). Considering this and our data, we are currently pursuing the goal of performing a RIP-seq on RAW 264.7 and Figure 22C represents schematically the workflow. Notably, we decided to challenge 7n for RIP-seq experiments, that will be carried out in cells treated for 6 hours with 7n in combination with LPS, plus LPS with DMSO as control and DMSO alone to check the proper inflammatory response insurgence (Figure 22C). Summarizing, we have observed the downregulation of the expression of HuR cytokine target mRNA by 7n and a decrease of TNF protein secretion level. Furthermore, we observed a subsequent reduction in the binding between HuR recognition sequence and the protein in RAW 264.7 via Pull Down assay. Finally, we provided insights concerning a decrease in the direct interaction between HuR and *CXCL10* by performing RIP, therefore our hypothesis is that 7n counteracts LPS

inflammatory response, in an HuR dependent manner, by disrupting its binding to the targets defining a new rearrangements genome-wide, mainly by downregulating the expression of pro-inflammatory factors. Performing a RIP-seq experiment in native condition, will lead us to identify dynamic interactions between HuR and RNAs defining its target transcripts and precise binding sites eventually impaired by 7n inhibitory activity. These genome-wide experiments will be pivotal to determine precisely our compounds mechanism of action and mainly it will help us to dig deeply into the characterization of the TMs anti-inflammatory properties in macrophages driven immune response.

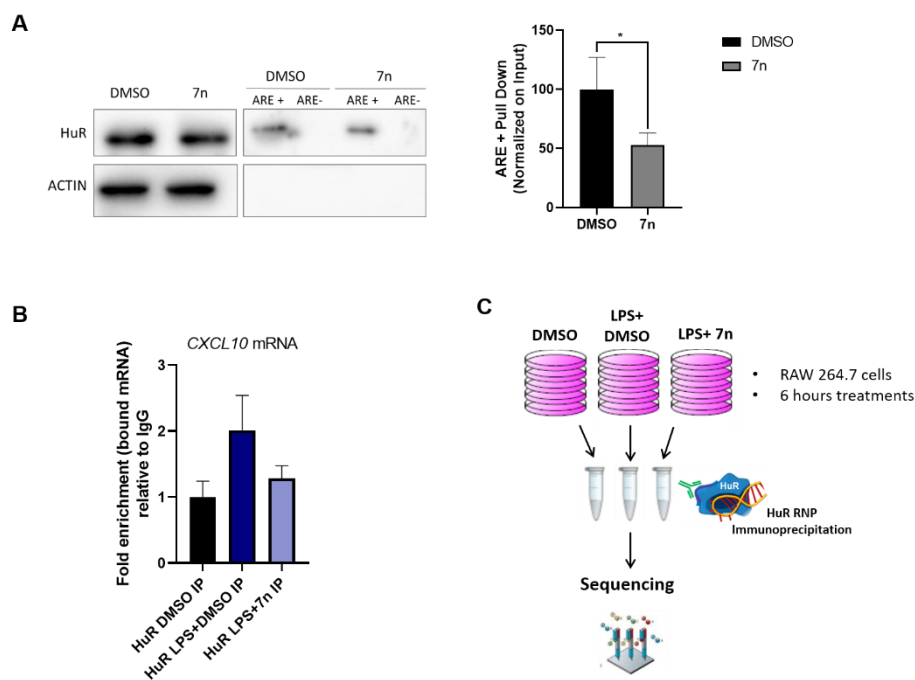


Figure 23. 7n directly interplay between HuR-RNA binding causing its disruption.

A) Pull Down assays performed in RAW 264.7 cells pre-treated with 7n or DMSO as control for 6 hours. Cell lysates were incubated for 1 hour at 4°C with either a biotinylated probe containing HuR consensus sequence, either a probe not supposed to bound by HuR as a negative control. Precipitations of the probes have been carried out with streptavidin beads and HuR level have been detected by WB analysis. HuR signal have been quantify on the Input (10%) and Data have been plotted as mean mean \pm SD of three independent experiments * $p < 0.05$. (I have performed these assays with the collaboration of Micaelli M.) B) RNA Immunoprecipitation assay (RIP) followed by real time PCR (qRT-PCR). RAW 264.7 cells were treated for 6 hours with DMSO as control and 7n at 10 μ M dose. Afterwards cells were lysed and RNA precipitated with HuR antibody (IP) and IgG isotype (IgG) as negative control. Changes in the mRNAs bound to HuR in the control or treatment were evaluated through qRT-PCR and normalized on the corresponding values obtained with IgG, as negative control. The obtained numbers indicate the Fold enrichment, obtained after normalization with IgG and subtracting the value of the housekeeping gene RPLP0, experiments were performed in a biological duplicate. C) Schematic representations of the ongoing RIP-seq workflow. RAW 264.7 cells have been treated with DMSO, LPS+DMSO and LPS+7n for 6 hours. Cell lysis and Immunoprecipitation with HuR antibody and the negative isotype as control have been followed by RNA sequencing. Data in process.

(I have entirely performed and currently performing experiments in B and C)

4.9 Evaluation of TMs effects in primary murine macrophages derived from bone marrow (BMDMs), with *in vivo* evidences.

Notwithstanding several advantages given using a cell line as a model, RAW 264.7 application presents some limitations. In fact, cell lines derive from transformation and immortalization processes, acquiring genetic and phenotypic differences if compared with the corresponding primary ones. As a consequence, cell lines often developed genomic instability, hybrid phenotypes and altered signalling pathways, making them a not reliable system for physiologically investigations and for *in vivo* proof of principles (Andreu *et al.*, 2017). As an example, different studies have revealed a substantial difference in the induced cytokines response if comparing RAW 264.7 macrophage cell line with the primary counterpart (Merly and Smith, 2017). According to this, we decided to begin to extend assays performed in RAW264.7 in a more appropriate primary cell culture system, that is represented by murine Bone Marrow Derived Macrophages (BMDMs).

Macrophages are essential not only for immune defence, but also for embryo development and adult homeostasis, therefore, macrophages reside in different tissues, bringing different nomenclature and features, such as: microglial cells (brain), Kupffer cells (liver), alveolar macrophages (lung), peritoneal macrophages (peritoneum), foam cells (blood vessel plaques), Langerhans cells (skin) (Mills, 2012). Usually, primary macrophages used *in vitro* are harvested from peritoneal cavity (PEMs) or Bone marrow (BMDMs) (Macrophages *et al.*, 2015). We decided to use BMDMs, extracting monocytes from bone marrow and performing macrophages differentiation *in vitro*, in order to avoid a premature and uncontrolled polarization associated with the use of pro-inflammatory agents, such as Brewer's thioglycollate broth or proteose peptone, pivotal for the stimulation of macrophages rushing in the peritoneal cavity (Ding *et al.*, 2017). Moreover, many evidences have been collected highlighting the differences between PEMs and BMDMs, revealing that BMDMs often results in a more reliable systems for *in vivo* aims (Bisgaard *et al.*, 2016), consequently we decide to use BMDMs as our model. I have harvested BMDMs from 6 to 12 weeks old C57BL6/j wild type mice according to the protocol presented in the Materials and Methods section. After differentiation *in vitro* of the monocytes into macrophages (Materials and Methods), I have performed viability test in BMDMs, treating the cells for 24 hours with increasing doses of the TMs-I and TMs-II leading compounds, 6a and 7n, in order to evaluate differences of toxic dosages previously measured in RAW 264.7. Viable cells have been checked after 24 hours and not after 72 hours as we did for the other cell lines, because being a primary lineage, extended times of culture would have caused an additive toxicity effect. Graphs representing toxicity curves are shown in Figure 24A, for 6a it has been possible to calculate an IC₅₀ around 12 μ M, whereas 7n appeared less toxic than 6a.

Farther, I have repeated the assays as performed in RAW 264.7 cells. Hence, I have firstly co-treated BMDMs for 6 hours, with LPS (1 μ g/ml) and selected TMs-I and TMs-II: 6a, 7a, 6n, 7n at 10 μ M dose, along with DMSO alone, in order to verify inflammatory activation and in combination with LPS as a control for treatments. Afterwards, I have extracted total RNA and through qRT-PCR I have

investigated on *CXCL10* and *TNF α* mRNA expression level. Results are shown in Figure 24B, upon treatments a significantly downregulation of the two transcripts have been observed, *CXCL10* (right panel) is reduced more than 50% in all treatments with different efficacy following a good relation between precursors and derivatives compounds (6a;7a/6n;7n) and the same can be appreciated also considering *TNF α* (left panel). Moreover, we investigated if downregulation of cytokines levels of expression was related with a decreasing of the secreted proteins. To this aim, I have performed ELISA assays from BMDMs with LPS (1 μ g/ml), compounds (10 μ M) plus DMSO alone or in combination with LPS, at different time points: 1 hour; 4 hours and 6 hours. Due to the poor signal for *CXCL10* released protein, I have been able to detect only TNF secretion level and Figure 24C shows Results obtained. DMSO alone is not plotted because values were under the limits of detection in all the ELISA assays I have performed.

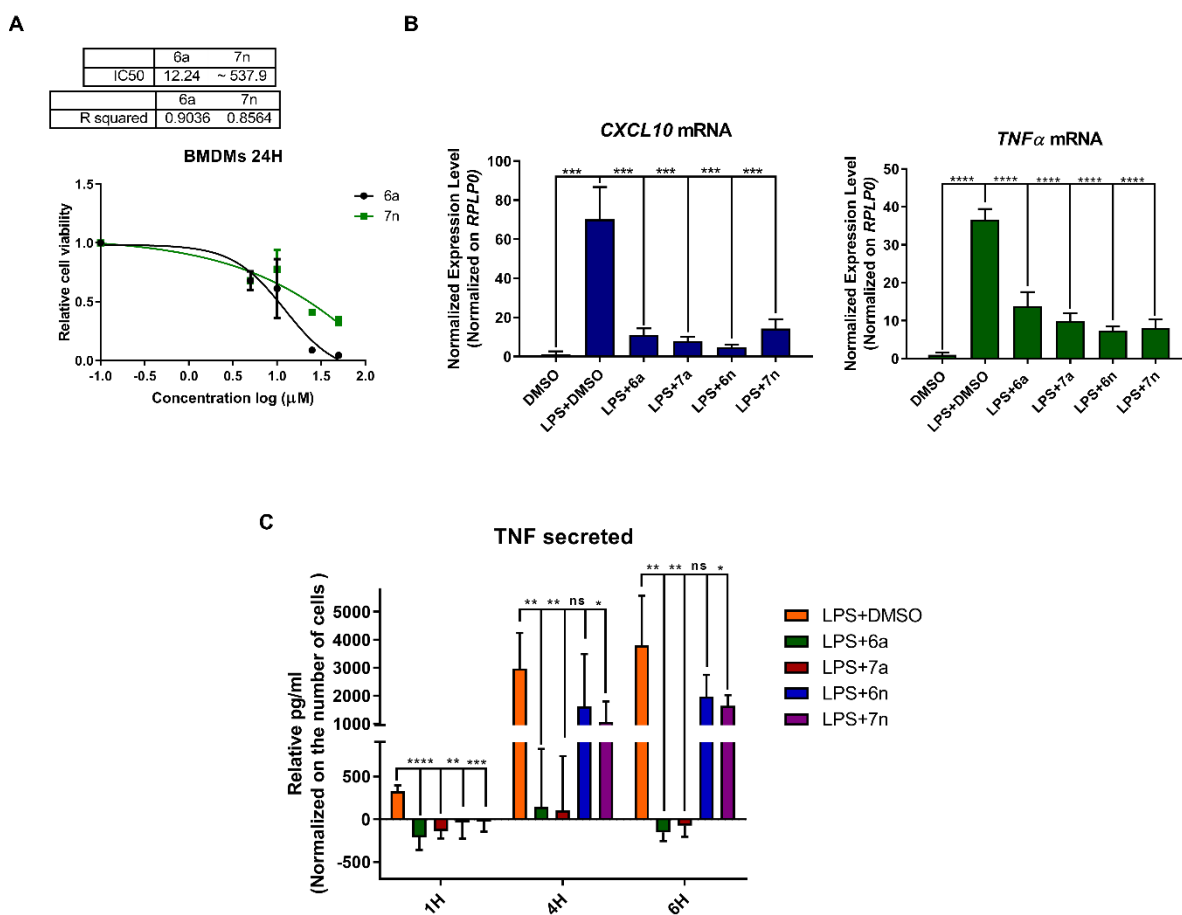


Figure 24. TMs downregulates mRNA expression level of cytokines regulated by HuR and TNF secretion in BMDMs. A) BMDMs viability was evaluated with OZBlue kit after 24 hours of treatments. Doses were ranging from 0 to 50 μ M. Plotted bars are mean \pm SD three independent experiments performed in technical duplicate, normalized to control (DMSO). Relative IC50 and R2 were calculated by nonlinear regression curve fitting. B) BMDMs were co-treated for 6 hours with compounds at 10 μ M doses, LPS (1 μ g/ml) and DMSO as control. mRNA levels of the cytokines has been assessed through qRT-PCR using *RPLP0* as an housekeeping gene and data have been normalized on DMSO condition, in order to evaluate the effect of LPS. Data gave been plotted as mean \pm SD of a biological quadruplicate (* p <0.05, ** p <0.01, *** p <0.001, **** p <0.0001). C) TNF protein levels measured with ELISA. DMSO alone treatment has not been plotted since the levels of the protein (pg/ml) were under the limit, cell supernatants were diluted 1:3. Relative pg/ml obtained for each sample have been normalized on the number of cells obtained by performing crystal violet assay. Data represent as mean \pm SD of a biological triplicate (* p <0.05, and ** p <0.01 *** p <0.001, **** p <0.0001) (Experiments have been performed entirely by me)

Surprisingly and differently for what observed in RAW 264.7, all the molecules significantly affected TNF protein secretion, but 6a and 7a showed a stronger activity almost abolishing the total protein release. Negative values have been obtained because considering stringent dilutions, aimed at loading equal cell supernatant quantities, lead to immediate signal saturation of LPS+DMSO sample, keeping the signal coming from the supernatants belonging to treated samples under the limit of detection. However, experiments will be repeated in order to overcome these issues. Moreover, for a better characterization of what observed so far, we are currently replicating these data by extending time points to 18 hours, for a better detection of CXCL10.

However, our compounds show high potency in downregulating cytokines transcripts and the secretion of TNF protein, suggesting that they can have anti-inflammatory properties. Once enough data will be collected for CXCL10, in order to deeply investigate on the anti-inflammatory properties of the compounds other targets should be measured, such as IL1 β or IL-6. Anyway, the results coming from RIP-seq performed on RAW 264.7 should open the horizons for the proper selection of the targets. These data suggested also that there is a different downregulation strength and outcome observed in RAW 264.7 compared to BMDMs. Furthermore, previously in the lab, other members, in collaboration with the lab of Dr. Gaestel in Hannover, checked downregulations of different cytokines transcripts upon stimulation with LPS and treatments with DHTS and 6a in immortalized BMDMs in which TTP expression was depleted, and results (not shown) suggested that reduced expression level of the targets considered was not dependent from TTP expression.

As before mentioned by describing TAMs, macrophages are not homogenous and these phenotypic heterogeneity is given by different local environments (Bashir *et al.*, 2015) and is referred as polarization. In particular, three different groups of macrophages can be distinguished: naïve (M ϕ ; also called M0) that can differentiate into two other different sub-types: pro-inflammatory (M1) and anti-inflammatory (M2) (Scheme in Figure 25A) (Abumaree *et al.*, 2013; Y. Wang *et al.*, 2019). Not only related with cancer infiltrations, generally M1 and M2 macrophages play two different roles in mediating the inflammatory response: M1, classical activated macrophages respond to TLR ligands upon LPS or INF γ stimuli and are characterized by high antigen presentation and expression of pro-inflammatory cytokines such as TNF α , in a physiological context, they have been reported to have inflammatory activity, responsible for the defense against microbial attack and tumor insurgence (Barros *et al.*, 2013; Wang *et al.*, 2014). On the other end, M2, also called alternatively activated macrophages have different functions, including apoptotic cell clearance, tissue repairing, since they produce high levels of VEGF and are also responsible for the release of anti-inflammatory molecules (Murray and Wynn, 2011; Atri, Guerfali and Laouini, 2018). Since implied in a variety processes, dysregulations, such as hyperactivation of the macrophagic response is linked to the development and exacerbation of several disease conditions (e.g. cancer), as mentioned previously. Indeed, recently, different compounds have been identified to modulate an aberrant activation of the both kind of macrophages (Y. Wang *et al.*, 2019).

Considering this, we decided to collect some insights to check whether our HuR inhibitors, showing anti-inflammatory properties, could impair and interfere with polarization of pro-inflammatory macrophages M1. To this aim, I have extracted BMDMs and further polarized them *in vitro* from naïve macrophages towards M1 phenotype through 24 hours stimulation with LPS (100 ng/ml) and IFN γ (10 ng/ml). In order to define sub-toxic dose of the compounds to use, I have first performed viability assay on M1, as I have done for BMDMs with increasing doses of 6a and 7n, to check whether after activation and proliferation stimuli, IC₅₀ for BMDMs was not the same for M1. Results are shown in Figure 25B, 6a similarly to BMDMs, shows an IC₅₀ of around 12 μ M, while 7n at 18 μ M. Once defined the subtoxic doses, I have polarized naïve macrophages towards M1 phenotype co-treating the cells with the following compounds (10 μ M): 6a, 7a, 6n, 7n and 8n, for 24 hours, plus DMSO as control. Afterwards, in order to check impairment on the M1 polarization, I have performed Nitric Oxide (NO) assay, that consists in the measurements of the level of the gas (NO) released by the cells, that is a marker of M1 macrophage differentiation (Scheme, Figure 25A). Results are plotted in Figure 25C, showing a highly significant reduction, more than 50%, in the NO production in M1 treated with all the compounds. Notably, I have used naïve macrophages treated with DMSO as a negative control of the assay and to check if a proper activation occurred.

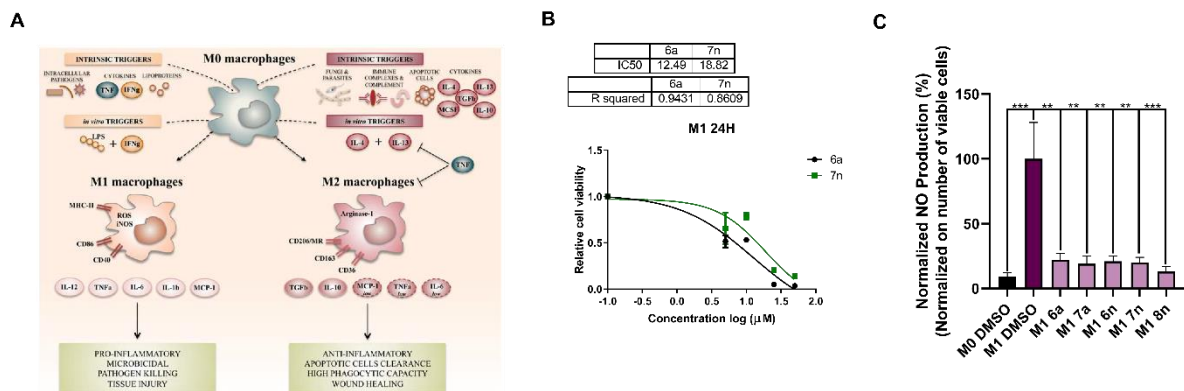


Figure 25. TMs affect NO production in primary M1 macrophages. A) Scheme representing the different macrophage differentiation lineage (M0, M1 and M2) with the related characteristics (Atri *et al.*, 2018). B) BMDMs were stimulated towards M1 with LPS (100 ng/ml) and IFN γ (10 ng/ml) for 24 hours co-treating with DMSO as control and increasing doses ranging from 0 to 50 μ M of compounds. Viability was evaluated with OZBlue kit and plotted bars are mean \pm SD of three independent experiments performed in technical duplicate, normalized to control (DMSO). Relative IC₅₀ and R² were calculated by nonlinear regression curve fitting C) BMDMs were stimulated towards M1 with LPS (100 ng/ml) and IFN γ (10 ng/ml) for 24 hours co-treating with DMSO as control and compounds at 10 μ M. Nitric Oxide release has been quantified with Griess Reagent. As technical and control for polarization the NO signal of naïve macrophages plus DMSO has been measured. NO quantity has been plotted as percentage normalized on the number of cells quantified with crystal violet assay. Data have been plotted as mean \pm SD of four independent experiments (I have performed the entire experiments).

Lastly, our ongoing work is focused on giving some insights about the application of TMs *in vivo*. We are currently in the phases of the optimization of the experimental model, of which I will show several results. More precisely, starting from what observed in RAW 264.7 and primary macrophages, we decided to refer to LPS-induced peritonitis mouse model (Qin *et al.*, 2016). Specifically, we evaluated TMs properties of reducing cytokines release in the serum of mice in which inflammatory response has been stimulated with LPS intraperitoneal injection (i.p) for 2 hours. TMs were all administrated via i.p. at the dose of 10 mg/kg, using reported DHTS dose as a reference (Lal *et al.*, 2017). In a first instance, TMs tested, have shown different solubility properties, in particular, TMs-I seemed to be less soluble than the ones belonging to TMs-II (Table 5), so far, 7n reflects to be the most soluble compounds. In Table 5, DHTS, 6a and 7n have been presented according to their solubility condition, for DHTS and 6a we added BSA at 0,03 mM in order to help solubilization, avoiding to increase DMSO to help this process, considering its toxicity. We have chosen using BSA, among different reagents commonly used, because they appeared to be ineffective, such as NMP.

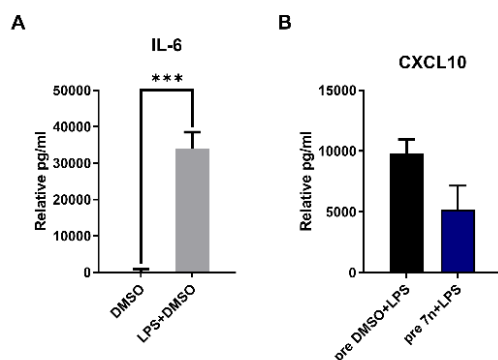
Group of 6-8 mice 8 weeks old, have been treated with sub-lethal dose of LPS (150 µg/20 g of body weight) in co-treatments, post-treatments and pre-treatments with different TMs (protocol in details in Material and Methods section). After 2 hours, mice blood was collected through cardiac puncture, serum purified from plasma and cytokines detected with ELISA assays. In Figure 26A preliminary experiments show the functionality and reproducibility of the model, inflammation response has been checked by detecting the level of IL-6, comparing LPS+DMSO mice group with DMSO treatment alone as control.

Among the three conditions already presented and TMs challenged, we obtained promising hints from experiments performed with 7n pre-treating the mice 30 minutes before LPS administration (Figure 26B). According to what represented in the Figure (26B) CXCL10 levels in the serum are decreased compared in sera derived from mice pre-treated with 7n, compared to the control condition (LPS+DMSO).

Although this promising evidence, we are currently facing steps of method optimization, in order to establish the most accurate time point of TMs treatment, in order to reduce the great variability found among the experiments and experimental groups. Nevertheless, we are putting our efforts in stabilizing and checking the bioavailability and stability of our compounds in mice blood in order to overcome reproducibility issues. Once the method will be solid, anti-inflammatory properties of our compounds will be investigated not only considering CXCL10, in which we are interested the most, but we would like to investigate on TMs capability of downregulating other cytokines known to be HuR targets as TNF, IL1β but also challenging inflammatory factors not reported to be HuR-regulated, such as IL-6. Moreover, in order to evaluate the HuR dependency, this model should be applied by using mice conditional KO for HuR.

| Compound (10 mg/kg) | DMSO (%) | BSA (mM) | Solubility |
|---------------------|----------|----------|-------------|
| DHTS | 10 | 0.03 | Fine Powder |
| 6a | 5 | 0.03 | 100% |
| 7n | 5 | / | 100% |

Figure 26. 7n preliminary activity in LPS-induced peritonitis mouse model.



A) LPS-induced peritonitis model optimization: Cytokine levels in sera from C57BL/6j wild type mice after administration of LPS (150 µg/25 g of body weight) for 2 hours, DMSO alone has been used as a control of LPS inflammatory response insurgence. IL-6 secreted protein has been detected with ELISA assay and bar graphs depict mean values ± SD from 6-8 mice per group. ***p ≤ 0.001. B) CXCL10 levels in the sera from C57BL/6j wild type mice after administration of LPS (150 µg/25 g of body weight) for 2 hours, with 30 minutes of pre-treatment with 7n (10mg/kg). DMSO alone has been used as a control of LPS inflammatory response insurgence and LPS+DMSO has been considered being drug vehicle. IL-6 secreted protein has been detected with ELISA assay and bar graphs depict mean values ± SD from 4 mice per group. (Experiments performed by me).

4.10 Ongoing work: TMs activity in adaptive immunity

In conclusion, HuR has been reported to be important in the maturation and homeostasis of B, T cells (see Introduction paragraph 2.4) (Papadaki *et al.*, 2009; Chen *et al.*, 2013; Techasintana *et al.*, 2017; Díaz-Muñoz and Turner, 2018). Furthermore, HuR has been proposed to regulate migration of T cells, in particular Th17 cells during neuroinflammation by regulating the mRNA of CCR6, receptor on the surface of this cell lineage (see Introduction, paragraph 2.4) (Chen *et al.*, 2017).

Thus, we started to collect some explorative data, investigating on TMs effect on cytokine release in human PBMCs stimulated with PMA/Ionomycin (50 ng/ml/1 µM) for 24 hours. Precisely we collected PBMCs from 4 different donors and subsequently we cultured the cells together with PMA/Ionomycin and different TMs (5 µM). Afterwards, we measured with ELISA assays TNF secreted level (Figure 27A). Notably, TMs reduce the secretion of TNF about the 50%, suggesting their activity in modulating the cytokines after an unspecific T-cell activation signal. Moreover, I first performed viability assay with CellTiter-Glo® Luminescent Cell Viability Assay on murine splenocytes unstimulated for 24 hours (Figure 27B) and then, I have investigated on primary murine splenocytes without any further activation or stimulation, at subtoxic doses, if 6a downregulates cytokines expression after 24 hours of treatment, reproducing what observed in macrophages and THP1.

Figure 27C shows the results and as expected 6a significantly downregulates *TNFα* and *CXCL2* in murine primary splenocytes.

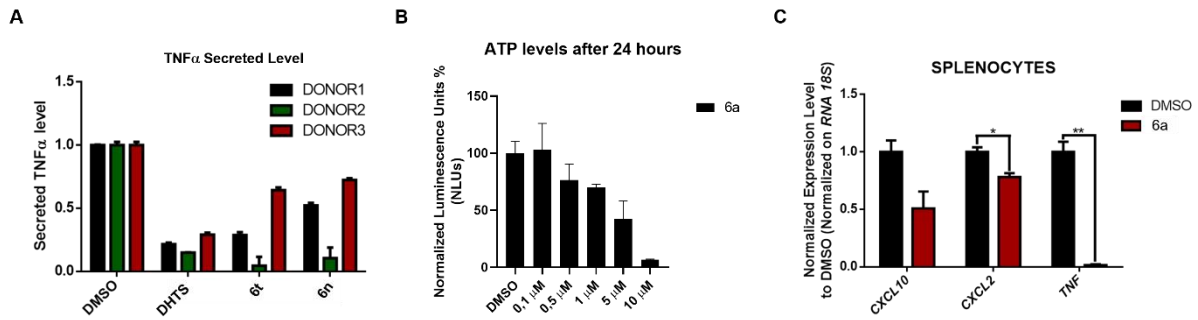


Figure 27. TMs downregulate TNF secretion in T-cells activated human PBMCs and a subtoxic dose 6a deregulated cytokines mRNA expression level.

A) TNF α secreted from supernatants of human PBMCs coming from 4 different donors, stimulated with PMA/Ionomycin for 24 hours and treated with DHTS, 6t and 6n (5 μ M). secreted protein has been detected with ELISA assay and bar graphs depict mean values \pm SEM a technical duplicate for each donor. Experiments performed in collaboration with Caffa I from Prof. Nencioni's lab, at the Hospital San Martino, Genova, Italy.

B) viability of primary murine splenocytes has been assessed by ATP level measurements performed with CellTiter-Glo. Cells were treated with increasing doses of 6a and DMSO as control. Data have been normalized on DMSO treated cells, thus expressed as Normalized Luminescence Units (NLUs). Graph plotted as mean values \pm SD of a duplicate. C) Preliminary evidences on 6a downregulating acidity towards cytokines mRNA expression in primary murine splenocytes. Cells have been harvested from the spleen of C57BL6/j wild-type mice and cultured for 24 hours with DMSO and 6a (2.5 μ M). Total RNA has been extracted and transcripts level evaluated by qRT-PCR. Data have been plotted as mean values \pm SD of a duplicate. (I have performed all the experiments)

Taking this as the starting point plus reported evidences concerning HuR function in T-lineage subset (see Introduction, paragraph 2.4), I have investigated with pilot experiments TMs activity towards mainly Th1 and Th17 polarized T cells, in which HuR roles evidence have been reported so far.

With this purpose, I have extracted splenocytes from wild-type C57BL6/j mice, I have polarized them *in vitro* according to the protocol shown in detail in the Material and Methods section towards respectively Th1 and Th17 phenotypes.

On the other end, in order to evaluate if 6a could affect at subtoxic doses the polarization capability of the cells, during differentiation of the cells *in vitro*, 6a (2.5 μ M) was simultaneously added (protocol in Material and Methods). Results are shown in Figure 28A, the cells have been checked by transcription profiling evaluating the level of expression of different mRNAs encoding for specific markers of the both cell lines. Furthermore, HuR protein levels have been measured by Western blot analysis of cell lysates belonging to either Th1 or Th17 treated with DMSO as control and 6a, and two different concentration of the lysates have been loaded on the gel (1;2) (Figure 28B). Moreover, I have first checked the viability of the cells after 96 hours of stimulation and treatment with DMSO as control and 6a (2.5 μ M) and then I have evaluated with Flow Cytometry Analysis, if cells acquired the proper phenotype in control condition (DMSO) and with treatment (6a) (Figure 28D). Notably, I have measured the intensity of specific marker for Th17, CCR6 and a specific one for T cell subset,

that is CD4. Th1 cells, were used as negative control, as they should be negative for CCR6 expression but positive for CD4.

These data suggest that Th1 and Th17 polarization properly occurred, no differences in HuR expression level have been observed, in both Th1 and Th17. Moreover, low doses of 6a do not impair the proper Th17 differentiation.

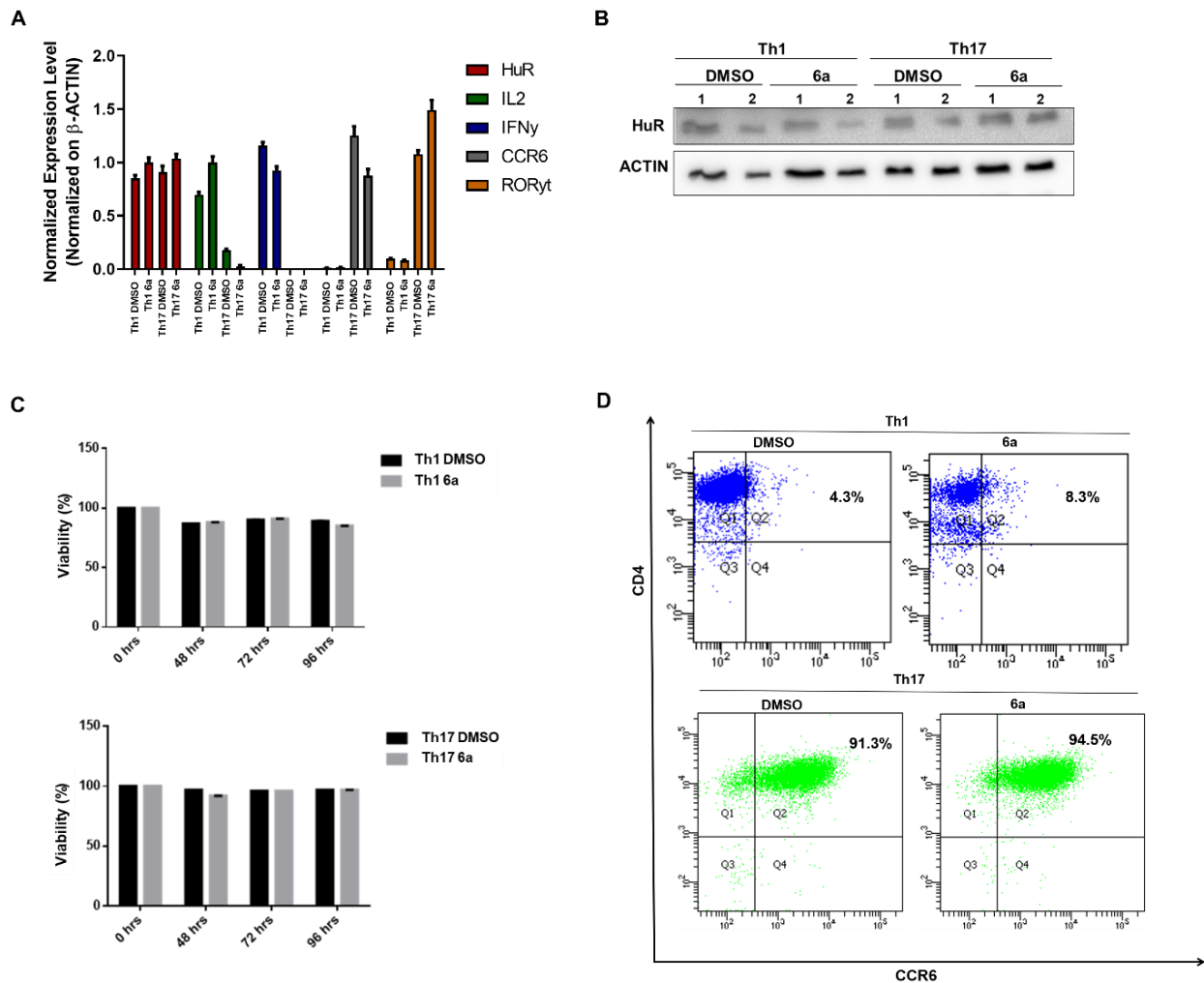


Figure 28. HuR expression in Th1 and Th17 is not changing among the lineages and 6a treatments do not impair T-cells proper polarization. A) Naive CD4⁺ T-cells have been harvested from wild type C57BL6/j mice and polarized with different factors (see protocol in Material and Methods). After 96 hours of stimulation and treatments with DMSO as control and 6a (2.5 μ M) added every 48 hours, cells were harvested and RNA extracted and markers checked with qRT-PCR. Data are plotted as mean values \pm SD of a duplicate. B) Representative WB analysis of protein lysates of Th1 and Th17 cells, obtained as previously described. 1 and 2 represented two different concentrations of lysates loaded on gel (15 and 30 μ g). C) Th1/Th17 Cells viability assessed with trypan blue, cells were cultured and treated as expressed in A). Data are plotted as % of viability, mean values \pm SD of a duplicate. D) Expressions of CCR6 and CD4 on Th1 and th17 analyzed by flow cytometry, one representative experiments shown among a duplicate. Mean intensity represented in the figure. (I have performed all the experiments)

Considering that 6a does not impair Th17 and Th1 polarization and viability (Figure 28C), counting the cells with trypan blue suggested that the total number of cells was decreased in the treated samples during 96 hours (Figure 29A), therefore I have decided to investigate on 6a effect towards Th1 and Th17 proliferation. In order to do this, through CFSE staining, I have measured cellular proliferation during 96 hours differentiation. Results are shown in Figure 29B for Th1 and 29C for Th17 cells, surprisingly 6a has anti-proliferative effect in Th1 cells, related with the complete disappearance of the last two generation (9th and 10th) and an accumulation of 3rd generation (Figure 29B). With a lesser extent, this effect was also present in Th17 cells (Figure 29C). Lastly, I have confirmed the results obtained so far, repeating CFSE staining in splenocytes activated with two different non-specific T-cell stimulating factors, PHA (100 ng/ml) and PMA (50 ng/ml)/Ionomycin (1 μ M). Results are shown in Figure 29D cells have been harvested after 48 hours of staining with CFSE and PHA or PMA/Iono stimulations in combinations with treatments with 6a and another TMs-II compound 7c. A further sample, NTC has been added and represents cells that are CFSE positive but unstimulated and untreated, meaning that they are not supposed to proliferate by their own. Indeed, 6a and 7c treatments reduce proliferation in cells compared to control (PHA/PMA+ DMSO), as the signal in the last generation is almost abolished comparable to the unstimulated sample, whereas a stationary increasing in the signal in 3rd generation is measured.

These evidences show a clear activity of TMs towards T cells, Th1 and Th17 lineages in particular. We have shown, that with a solid protocol, 6a co-administration with stimulation factors does not impact on the polarization properties and viability of murine primary cells, instead they highly reduce proliferation in Th1 and splenocytes not specifically activated with PHA and PMA. Migration of T cells, in particular Th17 cells, is linked with the insurgence and maintenance of neuro-inflammation processes (see Introduction, paragraph 2.4) (Chen *et al.*, 2017), thus downregulation of the proliferation could reflect in impairment in migration of these cell population, further experiments *in vivo* could have relevance for therapeutic implications (see Future perspectives).

On the other end, more investigations are needed in order to evaluate whether these effects observed are linked with HuR activity inhibition. In Figure 28A *CCR6* is downregulated, but as already described *CCR6* mRNA has been recognized as HuR targets and is responsible for Th17 migration, for this reason other targets regulated by HuR should be deeply characterized, (e.g. *IFN γ*) (Fan *et al.*, 2011).

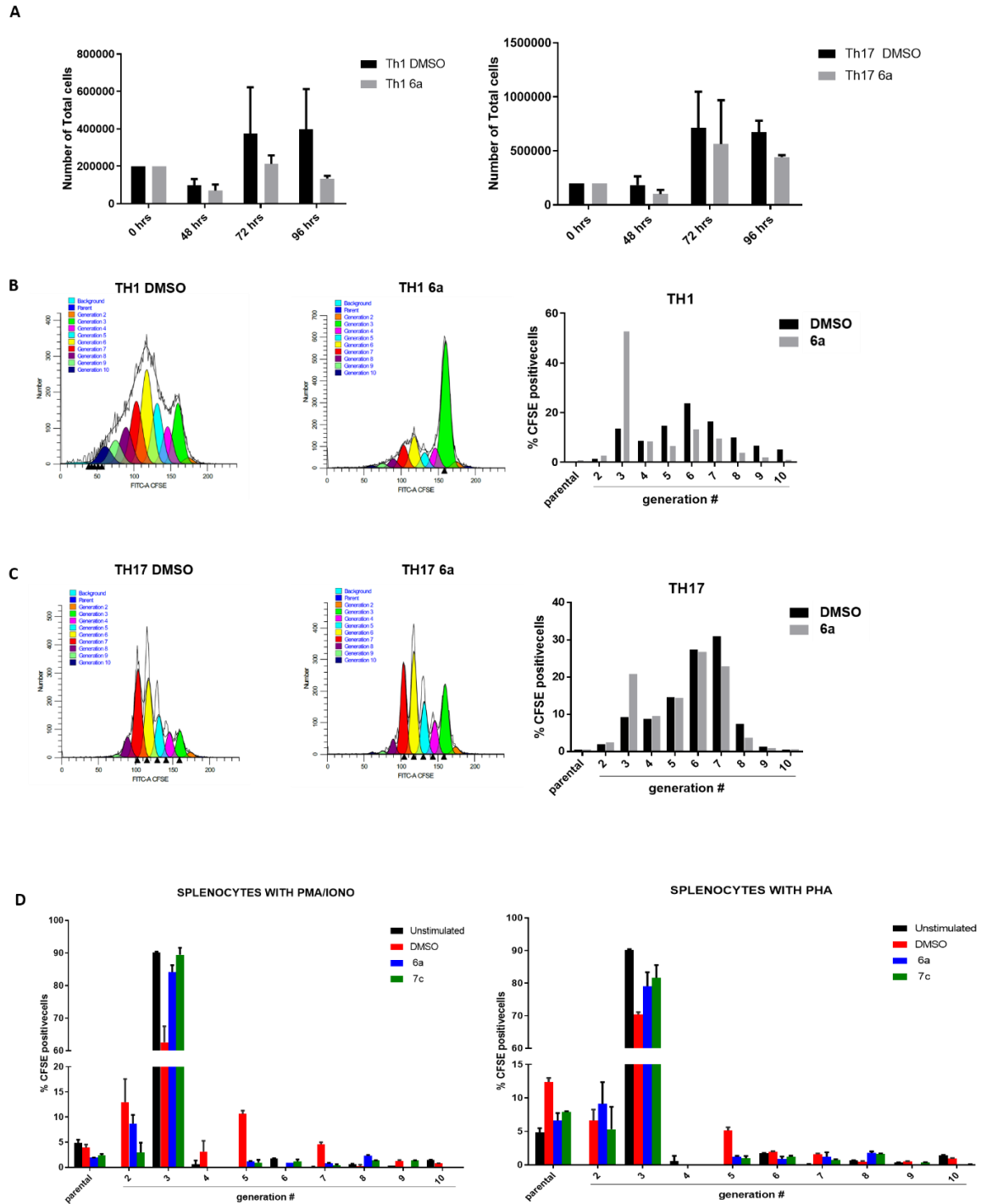


Figure 29. 6a affect Th1 proliferation, as well as T-cell stimulated splenocytes with PHA or PMA/Iono. A) Number of total primary cells (Th1/Th17), assessed with Trypan Blue. Th1 and Th17 were treated with 6a (Data represented as mean values \pm SD of a duplicate. B and C) Th1 and Th17 were stained with CFSE (2 μ M) for 10 minutes at 37°C and then left in culture for additional 72 hours in addition with polarizing stimuli (see protocol in Material and Methods) and treatments with DMSO as control and 6a (2.5 μ M) added every 48 hours. Proliferation has been measured with Flow Cytometry Analysis together with CXCR6, CD4 and live/dead staining. CFSE data have been represented as the fitted model for proliferation obtained with ModFit LT 3.2 and relative quantifications, showing mean \pm SD of a duplicate. D) primary Splenocytes were stained with CFSE (2 μ M) for 10 minutes at 37°C and then left in culture for additional 48 hours in addition with PMA/Iono or PHA and treatments with DMSO as control and 6a (2.5 μ M). Proliferation has been measured with Flow Cytometry Analysis together live/dead staining. CFSE data have been quantified using proliferation modelling obtained with ModFit LT 3.2 and relative quantifications, are shown as mean \pm SD of a duplicate (I have performed the experiments).

5. Discussion and Future Aims

In Eukaryotes, regulation of gene expression occurs at different levels, of which post-transcriptional control plays a pivotal role. RBPs are the most important actors defining these processes (Moore, 2005; Otsuka *et al.*, 2019; Zanzoni *et al.*, 2019), thus, aberrant modulation of RBPs function provokes subsequent alteration in the post-transcriptional control of gene expression, leading to the insurgence of complex and controversial phenotypes and diseases.

Hence, targeting RBPs found de-regulated in different pathologies remains a fascinating and challenging aim (Hong *et al.*, 2017; D'Agostino *et al.*, 2019; Peña, Song and Campbell, 2019).

Concerning targeting strategies, the approaches applied so far are mainly based in using molecular tools as RNA interference and antisense oligonucleotides (ASO) against different RBPs or in the identification of small compounds inhibiting their activity (Hence *et al.*, 2017).

On the other end, most of the RBPs shares common structure, thus, designing molecules with binding specificity towards a single protein still remain an issue (D'Agostino *et al.*, 2019).

Furthermore, since RBPs play a variety of functions, being pivotal in development and tissue homeostasis, their targeting could arise several side and unwanted effects, due to their pleiotropic and heterogeneous involvement in different cellular mechanisms (Hence *et al.*, 2017; D' Agostino *et al.*, 2019).

Here, I have presented HuR, one of the most studied RBP, ubiquitously expressed in the cells and evolutionary conserved among mammals (Ma *et al.*, 1996; Zucal *et al.*, 2015). Together with TTP, HuR binds mRNAs harboring AU/U rich elements located mainly in the 3'UTR. By counteracting the destabilizing effect given by TTP, HuR mainly promotes transcripts stability and translation enhancement (Tiedje *et al.*, 2012). HuR modulates transcripts encoding for protein involved in different cellular processes: cell cycle progression, proliferation, immune response and inflammation, differentiation and angiogenesis, senescence and apoptosis (Zucal *et al.*, 2014).

Thus, HuR regulates gene expression, being pivotal for development, cells and tissue homeostasis and physiology.

Therefore, HuR aberrant expression and mis-regulation leads to the insurgence of different disorders, it has been indeed associated with a variety of cancer types and inflammatory pathologies (Wang *et al.*, 2016; Grammatikakis, Abdelmohsen and Gorospe, 2017; Zhang *et al.*, 2019).

Although some evidences assigned to HuR anti-inflammatory properties (Yiakouvaki *et al.*, 2012; Brauß *et al.*, 2017) ascribing it as a controversial factor, HuR has been mainly found associated with different pathological conditions, thus lot of efforts have been put searching for inhibitors (see Introduction, paragraph 2.5).

Among all the studies performed so far, in 2015 our group, by using High Throughput Screening based on Alpha screen approach, identified DHTS, a natural compound inhibiting HuR activity. We have been able to ascribe to it a biochemical mechanism of inhibition and we have identified the

sites of interaction between HuR and DHTS, through NMR studies, molecular docking and molecular dynamics simulations. In fact, we demonstrated that DHTS stabilizes HuR in a closed conformation, preventing the RNA binding (Figure 6). We have been able to define DHTS anti-cancer properties in cancer cell lines. In particular, DHTS directly impairs the binding between HuR and its targets, such as *TNF α* , reflecting in a decrease mRNA stability and translation. Moreover, in collaboration with Dixon's group, at the University of Kansas, we proved that HuR dysregulation induced by DHTS produces a strong anti-cancer activity *in vivo*, in a xenograft model of colon cancer (HCT116 cells), in an HuR dependent manner (Figure 6).

My contribution in this project has been to identify the effects of the disruption of mRNA-HuR complex formation provoked by DHTS at a genome-wide level.

In collaboration with Myriam Gorospe group at NIH, we performed a RIP-Chip assay in HeLa cells treated for 3 hours with DHTS, and then we investigated on the genome-wide level the impact inferred by DHTS. Surprisingly, we have found that DHTS disrupts the binding of mRNAs with short 3'UTRs containing low ARE sites density. On the contrary, HuR has been found enriched in the binding with targets composed of a long 3'UTR with high density of ARE sequences in their structure (Figure 7) (Lal P *et al.*, 2017). In this way, we collected evidences for a better understating on DHTS mechanism and strength level of the inhibition, putting the basis for the rational design of a more potent family of inhibitors called Tanshinone Mimics (TMs). The synthesis of these molecules have been performed by our collaborators at the University of Milan, by the group headed by Prof. Seneci. Specifically, they carried out a functional-oriented synthesis (FOS) by designing less structurally complex molecules, aimed at increasing their potency and specificity for HuR targeting.

In this way, we identified, by testing these compounds at the biochemical and biological level, the structure-activity relationships (SARs) of this new class of HuR inhibitors (Manzoni *et al.*, 2018).

These SARs played key-role that have led us to provide guidelines for the generation of more potent inhibitors, that we have divided into two generation: TMs-I and TMs-II.

With the contribution of other members in the lab, these compounds have been characterized for the biochemical point of view by performing REMSA and Alpha Screen assays and for the majority of the TMs-I we have been able to calculate a K_i in the nanomolar range (Figure 8). Among the vast number of TMs-I tested, 6a revealed to show higher potency. We have been able to perform DMR measuring a K_d around the micromolar range, NMR, and computational studies, identifying the binding site of 6a towards HuR. Hence, 6a is more potent compared to DHTS, induces HuR stabilization in an inaccessible-to-RNA conformation (Figure 9) (Manzoni *et al.*, 2018). We have characterized the biological activity of these compounds, proving a direct HuR-dependent behavior. To do this, firstly we have evaluated anticancer activity of TMs, starting from determining the toxicity of these molecules in breast cancer cell line MCF7, and pancreatic cancer cell lines PANC1, and we calculated IC_{50} for most of TMs-I (Figure 10) (Manzoni *et al.*, 2018). Afterwards, we demonstrated by performing RIP experiments, that TMs (6a, 6t) directly interfere with the binding between HuR

and its target mRNAs coding for proteins involved in cancer insurgence and progression as *VEGF*, *ERBB2* and *TNF α* (Figure 11A). We also further evaluated 6a ability to downregulate the total expression level of these transcripts, in an HuR specific manner, since we have checked total expression level of *HPRT1* and *RPLP0*, not bound by HuR, and we observed no changes in their expression level after treatments (Figure 11B). Moreover, by performing migration assays in MDA-MB231, a breast highly metastatic cell line, and PANC-1, we showed that TMs treatments at subtoxic doses reduce invasiveness (Figure 12). Then, as previously shown for MS-444, the first HuR inhibitors discovered so far (Meisner *et al.*, 2007), combination treatments with PARP-inhibitors have shown increasing toxicity in pancreatic cancer cell lines if compared with the single treatment with PARP-inhibitors. Therefore, we decided to investigate if TMs own equal or stronger inhibitory behavior than MS-444. To this aim, we proved that 6a treatments in combination with chemotherapeutic agent, Olaparib, affect MIA Paca2 and MDA-MB231 viability 50% more compared to Olaparib single treatment (Figure 13).

All these data together suggest that TMs-I show inhibitory activity towards HuR *in vitro* and in cellular context. TMs disrupt HuR-mRNA complexes in cancer cells, and considering the nature of the targets evaluated, they have shown anti-cancer properties, reinforced by phenotypical experiments evaluating the reduction of invasiveness of highly migrant cells and increasing toxicity in combination with chemotherapeutics. Therefore, these data suggest that it would be worth full to investigate whether combination with TMs and already in use chemotherapeutics could have an additive ameliorating effect in clinics.

Since many drugs indirectly affect HuR function by modulating its subcellular localization (e.g. Actinomycin-D, Doxorubicin), we have demonstrated that TMs do not affect HuR localization, proving that their activity its only focused on targeting directly the protein and its post-transcriptional function (Figure 14).

Taking this as the starting point, our aim is to expand the SARs for the generation of optimized HuR inhibitors suitable for *in vivo* applications. Considering 6a, the leading compound of TMs-I, and 6n, TMs-II have been synthesized and biochemically characterized as already described (Figure 15). Generally, TMs-II have shown a slight decrease in the biochemical potency, but they appear to be more soluble and more stable, pivotal parameters suggesting an increase in the bioavailability. Among the tested ones, we have identified 7n that has shown higher biochemical activity, abolishing HuR binding to the target sequence in a dose-dependent manner *in vitro* (Figure 15D). Thus, we have put our efforts on characterizing 7n biological activity, considering the other selected compound 7a for comparison. We have demonstrated that 7n affected viability in cancer cell lines significantly inducing apoptosis after 48 hours in MCF7 (Figure 16A+B). Moreover, we observed that 7n slightly affects cell cycle in MCF7 (Figure 16C), and to confirm these data, more evidences should be collected to evaluate if even the observed slight retardation in the cell cycle progression could be significant and reflect in a decrease in the cancer cell proliferation.

Lastly, we have demonstrated that 7n after 48 hours treatment significantly reduces about the 20% of the global translation in MCF7 (Figure 16D).

Taking all these data together, our future aim concerns the deeply characterization of TMs activity at different level. Firstly, we would provide insights on TMs specificity towards HuR protein. Previously, our group showed, by performing several REMSA assays challenging DHTS interaction with other RBPs, such as TTP, LIN28B, TDP43, that DHTS is highly specific in binding HuR. DHTS was also affecting the activity of HuD (D'Agostino *et al.*, 2015). Indeed, since HuR belongs to ELAVL protein family and the structure organization is conserved among the family, an un-specific binding by TMs towards other ELAVL proteins could represent an issue.

However, considering that we have identified the binding sites between HuR and both DHTS and 6a, describing SARs that are driving the current rational design of new inhibitors, we hope to increase the specificity for HuR with the future compounds. As we did for 6a, we will calculate all parameters defining the inhibition strength (e.g, K_i) by using Alpha Screen assay, but furthermore we are currently putting our efforts in the measurements of K_D for the TMs-II shown so far (e.g. 7n) through DMR approaches. However, as the the immobilization on the plates of the recombinant HuR is challenging, due to its precipitation tendency, we are now planning to perform K_D measurements through thermal-shift calorimetry approach. Furthermore, as was done for DHTS and 6a, molecular interaction between the most potent TMs-II and HuR will be defined by using NMR and computational studies. Moreover, the specificity towards HuR inhibition will be also defined by using biotinylated TM compounds for Mass Spectrometry assays and/or Alpha Screen and Biotin Pull Down *in vitro*. For what concerns this last approach, we are currently optimizing the technique with biotinylated compounds available in the lab.

Regarding TMs anti-cancer properties, we have shown direct impairment induced by TMs of HuR:targets binding, of transcripts encoding for protein involved in cancer progression. As previously shown, we demonstrated that DHTS interferes specifically with HuR post-transcriptional activity provoking a destabilization and reduction in the loading of HuR-regulated mRNA (*TNF α*) on the polysome machinery (D'Agostino *et al.*, 2015). We have to further address for TMs (e.g. 6a;7n) the capability on reducing HuR transcripts stability and translational rate, in order to dig deeper in their mechanism of action highlighting the consequences of inhibiting HuR post-transcriptional activity. Nevertheless, considering what observed for 7n perturbation of the global translation, we have to evaluate if 7n impacts also on the general transcription, in order to clarify the precise HuR function affected by TMs. It is known that HuR regulates alternative splicing events (Akaike *et al.*, 2015; Dutertre *et al.*, 2014), thus we aim at investigating whether TMs could affect HuR nuclear function interfering with its regulation of the pre-mRNA processing or if TMs interferes exclusively with HuR post-transcriptional function.

As a consequence of HuR impairment, TMs regulates cancer cells phenotypic traits. In particular, we have shown reduced viability and activation of apoptosis after treatments in cancer cell line and

a reduction in the cell cycle progression and invasion capabilities. As we assess if TMs affect also cancer cell proliferation, we should evaluate TMs mechanism of action in cells in which HuR expression is depleted or overexpressed as already performed for DHTS (D'Agostino *et al.*, 2015), to further prove if phenotypic changes in cancer cell lines inferred by TMs are strictly HuR-dependent. Once this will be fulfilled and a complete characterization of TMs will be performed, our next aim is to exploit TMs activity to collect some *in vivo* evidences. Specifically, as was performed for DHTS (Figure 6E/F), our first efforts will be put in the evaluation of TMs toxicity in reducing tumor mass growth in xenograft models. We will use HCT116 cells as model and as control, since already established HuR KO in HCT116 cells will help to evaluate HuR dependency of TMs *in vivo*. These experiments will be pivotal to extend TMs application to more complex tumor *in vivo* models.

A key-regulatory role for cancer progression and development is exerted by a sustained and uncontrolled immune response giving rise to an unresolved inflammation process (Epithalamion and Pinka, 2012)

Considering HuR involvement in this process, as previously described, we decided to evaluate TMs anti-inflammatory properties in HuR dependent manner.

Knowing that tumors are characterized by highly infiltration of Tumor-associated macrophages (Pathria, Louis and Varner, 2019), we have first considered HuR modulation by TMs in innate immunity, using macrophage RAW 264.7 cell line as our model.

We have demonstrated that at subtoxic doses (Figure 17), in a time point dependent manner, in co-treatment with LPS used to stimulate the inflammatory response, 6a and 7n regulates the total mRNA expression of two HuR-regulated pro-inflammatory cytokines, drivers of the macrophages inflammatory response, *TNF α* and *CXCL10* (Figure 18) (Sedlyarov *et al.*, 2016; Tiedje *et al.*, 2016). Through several experiments, we have shown that 6a induced mRNA downregulation was HuR-dependent, as proved by HuR depletion with shRNAs in RAW 264.7 cells (Figure 19 C). In addition, we have shown that downregulation of these targets induced by 6a corresponds to a decrease in *CXCL10* and *TNF α* mRNA stability and *TNF α* loading on polysomes, suggesting that, also in this case, 6a interferes with HuR post-transcriptional function (Figure 19 A+B).

Furthermore, we have focused our attention in investigating on a reduction in the TNF protein secretion, as a consequence of TMs downregulatory activity described above. Surprisingly, we have shown a significant downregulation at both mRNA levels (Figure 18; Figure 20 A/B) and protein secretion level induced by TMs during the early LPS time points, less evident when considering prolonged LPS administration time (6 hours) (Figure 20).

What observed suggested us to focus on 7n, that instead revealed to be, along with its precursor, the molecule whose treatments resulted to be efficient in reducing cytokines at both the mRNA and protein levels (Figure 20). Indeed, an increased stability proper of TMs-II (7n) could explain in part the more efficient effect we observed compared with TMs-I (6a) (Figure 29).

Moreover, we have been focused on describing deeply the mechanism of action of these compounds. First, we evaluated if TMs reduced mRNAs expression level after LPS stimulus was provoked by a perturbation in the activity of NF- κ B. To this aim, we have demonstrated that TMs do not change NF- κ B localization in the cells, thus suggesting that no impairment on its nuclear TF functions occurred (Figure 21). As already described, we further demonstrated that TMs do not interfere with changes in HuR slight cytoplasmic accumulation promoted by LPS (Figure 22A), suggesting once again that TMs affect HuR activity exclusively by binding to it. To put everything together, in first instance, we demonstrated that 7n directly impairs HuR binding to the target, by performing Pull Down experiments in RAW 264.7 cells (Figure 23A) and then we evaluated that 7n directly interferes between HuR: *CXCL10* mRNA complex formation, by performing a RIP assays. These promising data led us to a further attempt in understanding the mechanism of action of TMs at the genome wide level, during LPS response, considering what observed so far. To this aim, we have decided to perform RIP-seq experiments in RAW 264.7 cells co-stimulated with LPS and 7n for 6 hours (Figure 23C). From this approach, we will evaluate specific targets modulated by TMs in a HuR dependent manner after an inflammatory response insurgence, and moreover we will have information concerning the strength and efficacy of TMs activity. By using RIP approach, we aim at exclusively investigate dynamic binding between HuR and its target mRNAs. To consider the effects of our compound into a native cellular context, we excluded the utilization of a cross-linking step (e.g. CLIP) , although if aimed at reinforcing RBP and target binding leading to the identification of the specific binding site sequence and structure, indeed, CLIP assay could be potentially very helpful in deciphering which RNA sequences, if any, are preferentially displaced by TMs.

On the other end, to collect proof of concepts for *in vivo* applications, we have decided to extend our data in primary murine macrophage cells. To this aim, we have provided evidences on the anti-inflammatory activity of TMs (6a, 7a, 6n and 7n) in BMDMs derived for C57BL6/j wild-type mice. In particular, differently from RAW 264.7 cells, we have demonstrated that TMs significantly downregulate already mentioned cytokines transcripts in response to LPS stimuli, and corresponding TNF secretion level (Figure 24). Considering what observed in RAW 264.7 and the future experiments we are going to perform, a further validation in primary cell lines is needed to confirm the strength of TMs activity.

Our aim nowadays, in order to identify more cytokines modulated by HuR, is to perform customized multiplex ELISA assays, in order to build up a panorama of the factors impaired by TMs. Nevertheless, considering what previously observed and once the cytokines will be selected from RIP-seq assay results, transcripts stability and translational impairments for the targets should be evaluated in order to achieve a better understanding of the down-regulatory mechanism inferred by the compounds, for example by performing Act-D experiments and polysome profiling assays. Farther, we have to collect some evidences in cells with a genetic background depleted for HuR expression. Due to the poor time extent of the primary cells culturing, using directly BMDMs coming

from conditional knockout mice in the myeloid cell line (Yiakouvaki *et al.*, 2012) would be the most proper solution. However, the data collected so far have been very promising suggesting us to put our effort to reach our next goal. Considering that, tumor associated macrophages are divided into two sub-types, M1 and M2 (Figure 24A), the insurgence of inflammatory un-resolved processes in cancer starts with a recruitment of M1 cells in the tumor microenvironment that stimulates a strong anti-inflammatory response, as a consequence M2 macrophages function is to repair damaged tissue and when associated to cancer, as a response to the inflammatory stimuli, they are responsible for a sustained angiogenesis, tumor vascularization (Quatromoni and Eruslanov, 2012). Thus, considering our previous data, we decided to challenge our TMs by starting to evaluate their effect on M1 population first. Hence, we demonstrated that *in vitro* M1 polarization was impaired after TMs treatments. Although if this potential anti-differentiation effect of the compounds has to be deeply investigated (e.g. checking other M1 targets), we aim at evaluating whether the anti-polarizing effect is HuR dependent. Possible experiments are based on the investigation of the rescue of TMs effects' by overexpressing HuR during treatments and the repetition of NO assay in macrophages downregulating or Knockout for HuR expression to check for similarities with TMs treatments (e.g. derived from conditional KO mice). In order to assess whether deregulation of HuR impairs with M1 differentiation, treatments with TMs in cells with a HuR null genetic background could put some insights about their specificity and elucidate if the presence of other factors, especially other RBPs, could be involved in M1 differentiation process, that still remains a poorly characterized field. Once this aim will be achieved, impairments inferred by TMs towards M2 polarization will be observed. Once described, this will be of pivotal importance since it will help us to better understand the extent of TMs anti-inflammatory properties, also considering that M1 macrophages characterize the early inflammatory processes, whereas M2 act mainly in a later one. Moreover, our main aim is to put together the dual TMs anti-cancer and anti-inflammatory activity shown so far, and to do this we will set-up a co-culture system. Precisely, we aim at evaluating the efficacy of TMs in reducing the crosstalk between infiltrating macrophages, provoking a cytotoxic effect in cancer cells. Specifically, primary murine macrophages will be pre-treated with TMs and stained for tracking cell migration, and then added to murine cancer cell line (e.g. breast cancer: 4T1). After all, the level on infiltration of the macrophages will be measured. Vice versa, pre-treating the cancer cells and adding murine macrophages properly differentiated (M1; M2) to the culture will help to understand the signaling pathway coming from the two cells population pivotal for cancer progression and affected by TMs. Furthermore, by using trans-well assays, polarized primary macrophages and murine cancer cells will be treated with TMs, evaluating a cytotoxic effect on the cancer cell line and measuring the releasement of cytokines, that we will identify with multiplexing assay. To further evaluate HuR dependency, these assays will be repeated harvesting macrophages from bone marrows derived from conditional HuR KO or OE mice (Yiakouvaki *et al.*, 2012), or modulating HuR expression in primary macrophages with molecular biology tools (e.g. siRNAs /HuR OE vectors). On

the other way around, we will perform assays in the context of HuR expression modulation in murine cancer cells lines, in order to understand if a different effect can be observed, understanding whether the role of HuR result to be most relevant in TMs effect.

Meanwhile, same assays can be optimized and implemented by using human cell lines as THP1 or eventually human PBMC differentiated in macrophages M1 and M2 lineages, co-cultured with human cancer cell lines, such as MCF7 (Brauß *et al.*, 2017). However, given the complexity of the tumor microenvironment, is likely that the effect of TMs on macrophages observed with a reductionist approach could be different from what will be observed *in vivo*. To solve this issue, one possible approach would be the utilization of a syngeneic system of cancer donors and immunocompetent recipient animals to allow the direct activation of the immune system.

Taking into account M1 anti-polarizing effects and cytokines modulation inferred by TMs in BMDMs stimulated with LPS, we started to collect proof of concepts of TMs activity *in vivo*. To pursue this aim, by using LPS-induced peritonitis mouse model, we have been able to provide a TMs regulatory effect on downregulating CXCL10 secretion in mice sera (Figure 26). We are currently optimizing the approach mostly by evaluating the stability and the bioavailability of the compound. In this case too, we are planning to reinforcing our data by identifying more cytokines modulated by HuR and TMs in the sera taking advantage of using multiplex ELISAs.

This will be the starting point to extend LPS treatment duration in mice, exacerbating the inflammatory response in sub-lethal manner, in order to investigate (considering TMs effects in the *in vitro* cell populations) on TMs affecting the blood cell population distribution, migration and polarization, by performing flow cytometry assays combined with histological studies mainly on liver and lung, in order to measure amelioration in LPS-induced peritonitis onset, according to Qin *et al.*, 2016.

Moreover, once results will be obtained, we will compare them with experiments performed in mice in which HuR expression is depleted or overexpressed, in order to finally prove HuR dependency, thus opening promising therapeutic implications for TMs (Katsanou *et al.*, 2005; Yiakouvaki *et al.*, 2012).

Lastly, we have further shown TMs importance in the modulation of T-cells. As reported, HuR has a pivotal role in T cells homeostasis and maintenance (Papadaki *et al.*, 2009; Diaz-Muñoz *et al.*, 2015). Furthermore Chen *et al.*, 2017 demonstrated that HuR regulates Th17 migration by binding CCR6. Subsequently, we aimed at investigating TMs impairment in Th-lineages differentiation. Chen *et al* 2017 checked HuR expression level among Th1, Th2, Th17 and Treg cells: they found that HuR is increasing its expression in Th17, whereas we observed that HuR is expressed at same level among the Th1 and Th17 lineages considering both the transcript and the protein quantity (Figure 28B), thus we decided to consider both the lineages. Moreover, at subtoxic doses, we observed that TMs do not compromise Th1/Th17 polarization (Figure 28), but through CFSE cell pre-staining, we showed that TMs affect T-cells proliferation (Figure 29). To further confirm this, we evaluated

proliferation impairment with TMs treatments in murine splenocytes, differentiated in T-cell subset with non-specific PMA/Ionomycin and PHA stimuli, previously stained with CFSE. These experiments represent the starting point for *in vivo* therapeutic studies. As reported by Chen *et al.*, we will test TMs in murine Experimental Autoimmune Encephalomyelitis (EAE) as a model for multiple sclerosis (MS). In collaboration with Prof. Uccelli group in Genova, we aim at demonstrating if administration every 48 hours of one selected TM (7n) for 15 to 30 days could help to reduce Th17 migration in the Central Nervous System (CNS), thus ameliorating disease onset, further coupled with histological tissue and blood cell population analysis, in order to check if there is a decrease in the massive inflammatory processes inferred by EAE insurgence.

However, taking all these together, generally HuR deletion leads to different consequences strongly depending on the gene expression program in the immune cells under examination. As an example, it has been reported that HuR mice conditional KO in the B-cells precursor lineage, strongly affect the number of properly mature and circulating B-cells. By controlling the mRNAs splicing in B cells, HuR regulates the expression of metabolic genes, acting as a key factor for the proper metabolic switch and cell growth during B cell maturation, its deletion reflected in the induction of apoptosis in these cells (Díaz-Muñoz *et al.*, 2015; DeMicco *et al.*, 2015). In, HuR conditional KO in thymocytes, T-cells development is strongly inhibited as HuR is an essential factor required for TCR signaling pathway. Indeed, in its absence, cell cycle factors and death receptors are strongly downregulated, leading to an erroneous accumulation of immature cells in the thymus (Papadaki *et al.*, 2009).

Furthermore, considering that HuR acts a stabilizer factor balancing the destabilizing activity of TTP, studies exploiting conditional mice KO models revealed the existence of a more intricate and complex network (Díaz-Muñoz and Turner, 2018; Turner and Díaz-Muñoz, 2018). As a consequence, HuR revealed to be a regulator of both pro-inflammatory and anti-inflammatory factors, with ambiguous activity and strongly depending on the cell-lineage and context. For example, HuR deletion in the myeloid cell type resulted in an exacerbation of inflammatory phenotypes with a corresponding increasing in the production of inflammatory mRNAs (Katsanou *et al.*, 2005). Other findings correlated HuR expression with an increase of the stability and translation of TNF and other pro-inflammatory cytokines mRNAs (Dean *et al.*, 2001; Tiedje *et al.*, 2012; Chen *et al.*, 2013; Techasintana *et al.*, 2017). As already mentioned, HuR sustained over-stabilization and production of IL17 mRNA in activated Th17 cells promoted their migration and EAE pathology insurgence. However, in disease context, recently it has been shown that HuR deletion attenuates glioblastoma tumor growth and survival, affecting its microenvironment represented by tumor associated macrophages and microglia cells. Furthermore, in GL261 mouse glioma models, HuR deletion attenuates mRNA and protein production of macrophages (e.g. M1) pro-inflammatory markers as *TNF*, *IL-6* and *CXCL2* (J. Wang *et al.*, 2019). Recent studies, exploiting intestinal inflammation mice models in which HuR has been deleted in the IEC (Intestinal epithelial cells) and in myeloid derived immune compartments, highlighted once again the controversial role played by

HuR. In the IEC, HuR KO provoked a decrease in cell survival and a promotion of the cell death, confirming that HuR as a role in the maintenance of the intestinal barrier integrity and homeostasis. Meanwhile, HuR absence in myeloid lineage increased the inflammation process exacerbating the pathological condition (Christodoulou-Vafeiadou *et al.*, 2018). In 2017, other finding concerning HuR targeting as a therapeutic strategy, pointed out the existence of intricate complexity still poorly understood (Lang *et al.*, 2017). In this study, in contrast with the previous one, authors, by using HuR inhibitor MS-444 in inflammation-bowel disease (IBD) mice model (AOM/DSS), observed an augmented induced weight loss and increased tumor multiplicity, size and invasiveness capability, due to a diminished number of tumor-associated eosinophils and a decreasing in IL-18 and eotaxin-1 production. In the same work, authors claimed that HuR inhibition in a mice model of colon cancer and familial adenomatous polyposis (FAP), diminished the number of small intestinal tumors development (Lang *et al.*, 2017). Taking all these together, we conclude that the pleiotropic functions exerted by HuR could explain the different and conflicting evidences emerged so far, and that the existence of other RNA regulons could explain what observed so far. For example, the exacerbation of the inflammation status due to HuR loss reported in some reports, could be may explained with correlated counteracting effects generated by the altered expression of RNA regulons (e.g. other RBPs) still to be fully characterized (Díaz-Muñoz and Turner, 2018). Furthermore, HuR deletion effects, strictly depend on the cellular context. We observed anti-cancer effects in different cancer cell models and a reduction in inflammatory cytokine production in primary macrophages and a retard in T cells proliferation upon TMs treatments, suggesting us that targeting HuR with TMs could be considered as a promising therapeutic strategy. Considered data collected so far and by using a genome wide approach (e.g. RIP-seq on RAWs), we aim to obtain a better understanding regarding the mechanism of action of our TMs for a certain set of targets and it will help us for the choice of the proper model.

Finally, for what concerns the controversial effects observed with MS-444 treatments previously shown, features concerning it specificity and bioavailability are still under debate. As mentioned previously, deeply investigations that we aim to perform concerning our TMs specificity towards HuR and chemical improvements regarding their solubility and bioavailability will be pivotal for a better understanding of the pros, cons and side effects regarding HuR targeting as a new therapeutic strategy.

6. Conclusion

Through this thesis, we have entirely characterized previously discovered DHTS activity towards the inhibition of the HuR Binding Protein. In particular, we have described its mechanism of action, identifying the aminoacidic residues involved in its inhibitory mechanism, demonstrating that DHTS directly binds HuR stabilizing the protein in a closed conformation, inaccessible for mRNA binding. We further characterized, at the genome wide level, targets impaired by DHTS activity and lastly, we have been able to show *in vivo* activity in reducing tumor growth inferred by DHTS in an HuR dependent manner, in xenograft mouse model.

In collaboration with the group of Prof. Seneci in the University of Milan, we used DHTS to synthesize a new family of HuR inhibitors called TM (TMs-I, TMs-II).

We have been able to describe SARs for the new compounds, with the aim of synthesizing more potent and specific compounds. Among them, 6a revealed to be the most promising hit and with this aim we have characterized sites of interaction between HuR and the molecule with NMR, molecular docking and computational dynamics and calculated a dissociation constant (KD) through DMR.

TM6a and other TMs-I have been tested to quantify their biochemical potency with Alpha Screen and REMSA assays. Furthermore, we have selected the most biochemically potent molecules and we have explored their anti-cancer activity. We have demonstrated that these molecules show cytotoxicity in cancer cell lines and directly impair the binding between HuR and several targets encoding for protein involved in cancer progression and onset (*VEGF*, *TNF α* , *ERBB2*), reflecting in a downregulation of the total expression level of the selected targets. We showed that TMs-I reduce invasiveness capability in breast cancer cell line, without changing HuR subcellular localization. Subsequently, 6a has been considered the leading compound for the generation of ameliorated HuR inhibitors, named TMs-II.

Among TMs-II, from a biochemical point of view, we demonstrated that 7n showed higher potency, thus we investigated in its anticancer activity. We have shown that 7n induces a global reduction of the protein synthesis in cancer cell line, showing cytotoxic effect and activation of apoptosis, with a slight but promising arrest of the cell cycle progression in G2/M phase, thus we future aim at testing TMs anti-cancer properties *in vivo*.

Taking into account HuR importance in regulating inflammation processes during cancer progression, we have shown anti-inflammatory properties of TMs inferred in an HuR dependent manner, and we have firstly considered RAW 264.7 cells and LPS stimulation as model for inflammatory response driven by macrophages, the master regulators in innate immunity. We have shown that TMs reduce cytokines mRNA (*CXCL10*, *TNF α*) expression levels, comparable with what observed in RAW 264.7 cells depleted for HuR expression. Furthermore, we have shown that TMs (TMs-I and TMs-II) treatments, without changing both HuR and NF- κ B subcellular localization, induced a reduction in mRNA stability, *TNF α* loading on polysome and subsequent protein secretion.

We have shown that, among TMs-II, the leading compound 7n directly impairs the binding between HuR and its target sequence, by performing RNA Pull Down assay and RIP experiments. We aim to carry out RIP-seq assays in samples treated with LPS and 7n, with the needed control, in order to identify, at the genome wide level, the mechanism of action of the molecules and targets affected by the impairment with HuR binding, digging deeply in the TMs anti-inflammatory properties. Furthermore, we have moved to primary murine macrophages (BMDMs), and we have shown that, with higher potency, TMs modulated cytokines mRNA expression level and TNF protein secretion. We have been able to show that TMs impaired M1 polarization in primary macrophages, putting the bases for investigating compounds effects in a co-culture system, in order to evaluate simultaneously the cytotoxic effect inferred by TMs and the corresponding reduction in cytokines release and macrophages infiltration rate. Then, we have shown 7n *in vivo* activity, in mice with induced LPS-peritonitis. We have shown that 7n pre-treatment downregulated CXCL10 secretion level in mice sera. With the identification of other cytokines modulated by HuR and the optimization of the model, we will be able to reveal a TMs pivotal implication for a therapeutic point of view. Lastly, we have shown that TMs-I (6a) impaired T cell proliferation, in particular T-cells stimulated with PMA and PHA, Th1 and Th17 in a reduced extent, without affecting cell viability and polarization properties. These data represented the starting point for *in vivo* future aims focused on testing TMs capability of downregulating T cells migration in the CNS promoting neuroinflammation in mice affected by EAE. Taking all these data together, I have presented a new class of HuR inhibitors with *in vitro*, in cells and *in vivo* properties, with potent HuR inhibitory activity and anti-cancer and inflammatory properties, suitable for *in vivo* analysis and further therapeutic implications.

7. Materials and Methods

7.1 AlphaScreen and RNA-Electrophoretic Mobility Shift Assays (REMSAs).

Amplified Luminescent Proximity Homogeneous Assay (ALPHA Screen), have been performed using histidine (nickel) chelate detection kit (PerkinElmer, 6760619), exploiting the binding between an His-tagged HuR protein and a biotinylated single strand RNA (BITEG-RNA), see D'Agostino *et al.*, 2013, for extended protocol. Expression of the full-length version of HuR recombinant protein has been carried out in E.coli Rosetta DH5 α , according to the protocol described by D' Agostino *et al.*, 2015. Calculation of the Hook point curves, with 50 nM of BITEG-RNA probe, have been previously assessed, to test its activity after purification and dialysis. Dissociation equilibrium constants (K_i) were measured with respect to a K_D of 2.5 nM for the Bi-AU ligand interaction, in the presence of 0.5% DMSO (relative control) and TMs and no interference with the assay has been appreciated when reacting the same quantity of acceptor and donor beads (20 μ g/mL/well) with biotinylated-His molecule in the same assay conditions. GraphPad Prism software v5.1 has been used for fitting calculation and statistical significance. Eventual rHuR expressed in HEK293T has been purified according to a previously published protocol.

REMSAs were performed as previously indicated by D'Agostino *et al.*, 2013. After HuR recombinant protein purification as previously described, 10-fold excess was incubated for 30 min with either 75 fmol of 5'-DY681-labeled AU-rich RNA probe or with 25 nM of 5'-FAM-labeled RNA probe or with 500 nM of Cy-3-RNA probe and DMSO as control or TMs at their indicated doses. Afterwards, samples have been loaded on 4% native polyacrylamide gel, image was developed with Odyssey infrared Imaging System (LI-COR Biosciences) for DY681-labeled RNA or in Typhoon Trio scanner (GE Healthcare) at high resolution for FAM and Cy-3 probe.

I was not involved in performing these experiments, for extensive protocol, see D'Agostino *et al.*, 2013; D'Agostino *et al.*, 2015; Lal *et al.*, 2017; Manzoni *et al.*, 2018)

7.2 NMR, DMR, Molecular modelling and Computational Dynamics.

NMR either for DHTS either for 6a HuR interaction, DMR for 6a ad well as molecular docking, computational dynamics have been performed by our collaborators, thus, for extensive protocol, refer to Lal et al 2017 and Manzoni et al., 2018.

7.3. RNA Immunoprecipitation (RIP) assays.

Five million of MCF7 cells/sample, Hela cells/sample or 10 to 30 million of RAW 264.7 were used for each RIP experiments followed by qRT-PCR or NGS sequencing (ongoing) that have been performed following the protocol published by Keene et al., 2006, without cross-linking steps and using 1-15 μ g/mL of anti-HuR antibody (Santa Cruz, 71290) or same amount of mouse normal IgG isotype (negative control, Santa Cruz 2025). Cells have been harvested after treatments with LPS,

DHTS, TMs or DMSO as control depending on each cases presented in the Results section and lysed with 20 mM Tris–HCl at pH 7.5, 100 mM KCl, 5 mM MgCl₂, and 0.5% NP-40 for 10 min on ice and centrifuged at 15 000 × g for 10 min at 4°C. Lysates were incubated with Pierce A/G beads (Thermo Scientific Pierce 88847-88848) for pre-clearing steps 1 hour at 4°C, in parallel 80% A and 20% G beads each sample have been incubated either with HuR or IgG antibodies for ab-coating step for 1 hour at RT. After all lysates were incubated with antibodies and beads for further 4 hours at 4°C. Finally, samples have been washed (6 times, 5 minutes each wash) with NT2 buffer. TRIzol reagent was added directly to the beads for HuR-bound RNA isolation as described in paragraph 7.4 and processed for qRT-PCR analysis or sequencing. 1-5% of the total lysate of each sample has been stored as input.

Quantitative PCRs have been performed after cDNA Synthesis (Thermo Scientific, K1612) were performed using Universal SYBR Master Mix (KAPA Biosystems, KR0389) on CFX-96/384 thermal cyclers (BIO-RAD) as described in paragraph 7.6. Fold enrichment for *VEGF*, *ERBB2*, *TNF α* , *CTNNB1* and *CXCL10* has been calculated using the eq $2^{-\Delta\Delta Ct}$, where the Ct value for HuR and IgG IP was subtracted from the Ct value of the housekeeping gene RPLP0 to yield the ΔCt value. For each condition, ΔCt value for the HuR and IgG IP sample were evaluated in triplicate. The delta Ct value for HuR in the IgG IP samples were calculated in the same way. Then delta–delta Ct values were calculated from the difference between HuR IP samples and IgG IP samples.

7.4 RIP-Chip protocol.

To evaluate the DHTS effect on HuR with endogenous mRNAs interactions RNA immunoprecipitation (IP) of endogenous HuR ribonucleoprotein complexes was performed as described previously (Abdelmohsen et al., 2009). Briefly, HeLa cells were harvested after 3 hours treatment with DHTS (1 μ M) and DMSO as control. After all, cell have been lysed in 20 mM Tris–HCl at pH 7.5, 100 mM KCl, 5 mM MgCl₂, and 0.5% NP-40 for 10 min on ice and centrifuged at 15 000 × g for 10 min at 4°C. The supernatants were further incubated for 2 h at 4°C with protein G Sepharose beads (GE Healthcare) coated either with anti-HuR or with control IgG antibodies (both from Santa Cruz Biotechnology). The beads have been washed several times (6 times, 5 minutes incubation each wash) with NT2 buffer (50 mM Tris–HCl [pH 7.5], 150 mM NaCl, 1 mM MgCl₂, 0.05% NP-40), followed by incubation with RNase-free DNase I for 15 min at 37°C to remove the DNA. 0.1% SDS–0.5 mg/ml proteinase K incubation for 15 min at 55°C with in order to digest proteins was performed. Microarray analysis was performed in biological duplicate (GEO number GSE94360). The RNA belonging to IP samples was extracted using phenol–chloroform, precipitated, and used for cDNA microarray analysis or RT-qPCR validation.

RT-qPCR validation conditions have been followed as described in paragraph 7.6 and Fold enrichment from immunoprecipitated (IP) samples has been calculated as $2e^{-\Delta\Delta CT}$, where the Ct value for either the HuR or IgG IP was subtracted from the Ct value of RPLP0 as a control to yield

the ΔC_t value. For each sample condition, the ΔC_t value for the HuR and IgG IP were evaluated in duplicate and averaged to give one $\Delta\Delta C_t$ value per sample. Data have been represented in the graph as “change in binding” values, calculated as ratio between $2e^{-\Delta\Delta C_t}$ obtained for the treatment condition over control per sample. Total RNA extracted from each sample was analysed by quantitative RT-PCR as described in paragraph 7.8.

(RIP assay followed by microarray analysis have been performed by Gorospe group at NIH).

7.5 Analysis of enriched mRNAs

GC content, length and secondary structure density (computed as the fraction of unpaired nucleotides) for the UTRs of DEC and INC genes were obtained from the AURA 2 database (Dassi *et al.*, 2014) and plotted with the R software. The enrichment of post-transcriptional regulatory elements, Gene ontology and pathway enrichment analyses were entirely performed by Dassi E. and for full protocols refer to Lal *et al.*, 2017

7.6 Total RNA extraction and qRT-PCR

Total RNA has been extracted either with Zymo research extraction kit, according to the manufacturer instructions or with Trizol, chloroform precipitation followed by RNase free-DNase I treatments, 15 min at 37°C. qRT-PCR conditions were the following: 95°C for 2 minutes, followed by 40 cycles of 95°C for 15 seconds alternating with 60°C for 15 seconds. Melting curve analysis was performed on every reaction to confirm a single amplicon. after CDNA synthesis (ThermoScientific) with equimolar mix of random and oligo-dT primers and 1 microgram of the template RNA. Quantitative RT-PCR was performed with the list of primer and conditions as previously described. Normalized expression level for each selected genes was calculated as $2e^{-\Delta\Delta C_t}$, where C_t value for either control and treatment condition was subtracted from the C_t value of the housekeeping genes (*ACTIN*, *RNA18s*, *GAPDH*, *RPLP0*) expression level to yield the ΔC_t value, then ΔC_t value for treatment and control were computed in duplicate and averaged to give one $\Delta\Delta C_t$ value per sample. Table 6 shows both human and mouse primers used in all the experiments.

Table 6. List of Primer used for all the experiments

| Human gene | Sequence | |
|---------------|--------------------------|-------------------------|
| | Forward (5'-3') | Reverse (5'-3') |
| RPLP0 | CATTCTCGCTTCCTGGAG | CTTGACCTTTTCAGCAAGTGG |
| ERBB2 | GGTACTGAAAGCCTTAGGGAAGC | ACACCATTGCTGTTCCCTCCTC |
| VEGFA | CCGCAGACGTGTAATGTTCTCT | CGGCTTGTACATCTGCAAGTA |
| CTNNB1 | GACCTCATGGATGGGCTGCCT | GATTTACAATAGCCTAAACCAC |
| RNA18s | GCAGCTAGGAATAATGGAATAG | TGGCAAATGCTTTCGCTCTG |
| HPRT1 | TGACACTGGCAAAACAATGCA | GGTCCTTTTACCAGCAAGCT |
| UPF2 | GAAGATTATCAAGAAATGTTGCAG | CAACGTCTCCTCCCACCA |
| YTHDF1 | GACAACAACCCGGTCACAAAC | TTTCGACTCGCCGTTCCCTTG |
| PABC1 | AGCAAATGTTGGGTGAACGGCT | TTCATCAACCTTAGAACGGAGT |
| BRIP1 | GGCCCTTGGTAGATGTATTAGAC | CCCATTTAGAAAGTCCAGATATA |
| TBCCD1 | TTTGACAAAGGATCAAAGGAAGC | ATGTAAGATCCTTATCCAGCTG |
| CASC3 | ATACACAGGCCCCATCACAG | TGCTTACAACCTCAGGTGGA |
| GAPDH | AGAAGGCTGGGGCTCATT | CAGGAGGCATTGCTGATGAT |
| TNF α | CCATGTTGTAGCAAACCCCTCAA | AGGTACAGGCCCTCTGAT |
| RNA 18s | GCAGCTAGGAATAATGGAATAG | TGGCAAATGCTTTCGCTCTG |
| CXCL2 | CCGAAGTCATAGCCACACT | AGTTGGATTTGCCATTTTTCAGC |
| HuR | GAATTTGATCGTCAACTACC | GCTGATGTACAAGTTGGCGT |

| Mouse gene | Sequence | |
|----------------|--------------------------|-------------------------|
| | Forward (5'-3') | Reverse (5'-3') |
| IFN- γ | GCCAAGTTTGAGGTCACAA | CAGCAGCGACTCCTTTTTC |
| IL-2 | CCAAGCAGGCCACAGAAT | GTCAGAGCCCTTTAGTTTTAC |
| CCR5 | CAGAGACTCTTGAATGACA | CAGGATTGCTTGTCTGGAA |
| CCR6 | CAGAGCAATCCGAGTCGT | GACTTTCTCGGTGCTGCA |
| ROR γ T | CCGCTGAGAGGGCTTCAC | TGCAGGAGTAGGCCACATTACA |
| CXCL2 | GACAGAAGTCATAGCCACTCT | AGCCTTGCCTTTGTTTCAGTA |
| CXCL10 | TGTTGAGATCATTGCCACGA | GGAGCCCTTTTAGACCTTTTT |
| TNF α | AGGGATGAGAAGTCCCAA | CTTGGTGGTTTGTCTACGAC |
| RPLP0 | TTTCTGGAGGGTGTCCGCAA | GCCTTGACCTTTTCAGTAAGT |
| ACTIN | AGATCAAGATCATTGCTCCTC | TAGAAGCACTTTCGGGTGCA |
| HuR | ATGAAGACCACATGGCCGAAGACT | AGTTCACAAGCCATAGCCCAAGC |

7.7 Biotinylated RNA Pull Down assay

For RNA pull-down assays, 5-10 million RAW264.7 cells were lysed in Polysome Extraction Buffer (PEB) (20 mM Tris-HCl (pH 7.5), 100 mM KCl, 5 mM MgCl₂ and 0.5% NP-40 plus RNase and protease inhibitors) and incubated for 1 h at 4 °C with 0.5 μ M of positive (BiTNF) or negative biotinylated (BiTNF_{neg}, 5' -ACCACCCACCACCCACCCACCCACCCA) RNA probes (D'Agostino et al., 2013) in the TENT buffer (20 mM Tris-HCl (pH 8.0), 2 mM EDTA (pH 8.0), 500 mM NaCl 1% (v/v), Triton X-100 plus RNase and protease inhibitors), according to Panda, Martindale and Gorospe, 2016. Solutions were incubated for further 2 h with 30 μ l/samples of streptavidin magnetic beads (Life technologies, 11205D). 10% of the total lysates for each sample has been stored as Input. Specific protein enrichments in beads-precipitated samples were analyzed by immunoblotting (paragraph 7.8) and densitometric analysis obtained using Image J 1.4 software (NIH).

7.8 Immunoblotting analysis

RAW 264.7 or primary murine T-cells were lysed for 5 min on ice in RIPA lysis buffer supplemented with Protease Inhibitor Cocktail (SigmaAldrich). After clarification, Laemmli Buffer (6X) was diluted

into equal amounts of proteins (15-30 μg), then separated by SDS-PAGE and blotted onto PVDF membranes (Immobilon-P, Millipore). Membranes were then incubated with the following antibodies: rabbit anti-HuR (Millipore, 07-468) or mouse anti-HuR (Santa Cruz, sc-71290) and mouse anti- β -ACTIN antibody (3700, Cell Signaling) 1 hour at RT or overnight at 4°C. Secondary antibodies (Santa Cruz) were used for protein detection using a ECL select western blotting detection reagent (RPN2235; GE healthcare). Immunoblotting for β -actin as a control for the homogeneous amount of loaded protein. Densitometric analysis of immunoreactive bands was analyzed using ImageJ software (NIH, USA).

7.9 Immunofluorescence and OPP Click-IT assay

8,000 MCF7/RAW264.7 cells/well were seeded in a 96-well plate and after treatments (see Results) they were fixed with 3.7% paraformaldehyde (PFA) for 15 min at RT. Cells were permeabilized for 10 min with permeabilization buffer (0.2% Triton X-100 in PBS), and incubated with blocking solution (2% Bovine Serum Albumin in PBS) for 15 min. Primary antibody anti-HuR 1:250 in 3% BSA, anti-NF- κB 1:250 in 3% BSA and secondary fluorophore conjugated (Alexa 594 Red or Alexa 488) antibody (1:500) were diluted in PBS + BSA 0.6%. DAPI Blue (1.5 $\mu\text{g}/\text{mL}$) in PBS + BSA 0.6% was used to detect nuclei. PerkinElmer image plate reader Operetta was used for image acquisition and evaluation by selecting 13 fields/well. The ratio between nuclear and cytoplasmic signal represents the mean of single cells for every well.

8,000 MCF7 cells/well were used to perform Click-iT assays. O-propargyl L-puromycin (OPP; OPP; 10 μM) (Life Technologies) was added to the cells and incubated for 30 minutes. Cells were washed in PBS and then fixed and permeabilized as described above. Alexa-Fluor-488 was conjugated to OPP as described in the manufacturer's instructions. As a control, cells were treated with cycloheximide for 4 hours before OPP addition. PerkinElmer image plate reader Operetta was used for image acquisition and evaluation by selecting 13 fields/well, the signal represents the mean of single cells for every well.

7.10 Polysome profiling assays

RNA fractionation and polysome profiling were performed in MCF7 by D'Agostino VGA according to the protocol published in D'Agostino et al., 2015.

RNA fractionation and polysome profiling in RAW264.7 cells have been performed by Lal P. in the Hannover in collaboration with Gaestel group, according to the protocol published in Tiedje C *et al.*, 2016.

7.11 Flow cytometry and Enzyme-linked immunosorbent assay (ELISA)

In order to perform Flow cytometry analysis, staining for surface antibody was performed from single cell suspensions prepared from Th1/Th17 cells polarized *in vitro* and previously extracted from C57BL6/j mice spleen. Before antibodies staining, we incubated the cells with CD16/CD32 (Mouse), purified (Mouse BD Fc Block™), purchased from BD Biosciences # 553141, in order to block unspecific binding. Afterwards, anti-mouse CCR6-PE conjugated (BioLegend # 129803), anti-mouse CD4-APC conjugated (BioLegend # 100411) and LIVE/DEAD reagent APC-Cy7 (ThermoFischerScientific) to check viability were incubated with FACs buffer (0.2% BSA in PBS) for 30 minutes at 4°C in protected by the light. Finally, before Flow cytometry analysis cells were fixed with 3% paraformaldehyde (PFA). Cells were detected using FACSCantoll and data were analyzed using FACSDIVA (V.3; BD Biosciences).

ELISA for murine TNF were carried out on mice sera, RAW264.7 and BMDMs supernatants diluted respectively 1:5 (serum), 1:3 (cell supernatants), according to manufacturer's instructions TNF kit (Mouse TNF-alpha DuoSet ELISA # DY410, R&D systems), for detection of the signal, TMB solution (ThermoFischerScientific) was used as a substrate. Reaction was then stopped with 2N of H₂SO₄ and read at Tecan microplate reader at wavelength corresponding to 450 nm.

7.12 Cell lines and primary cell cultures.

Human cervical adenocarcinoma HeLa cells (ATCC® CCL2™), human breast adenocarcinoma MCF7 (ICLC; HTL95021) and MDA-MB-231 (ICLC; HTL99004) and pancreatic carcinoma PANC-1 (kindly provided by G. Feldmann), human monocytes THP1 (Biobank, Genova), murine macrophages RAW264.7 (Biobank, Genova) and murine fibroblasts L929 (Sigma 85011425) cell lines were maintained in high glucose Dulbecco's modified Eagle's medium (DMEM) by adding 10% fetal bovine serum (FBS, Lonza), 2 mM L-glutamine, 100 U/ml penicillin-streptomycin (Lonza) in standard growth conditions.

The derivation of murine bone marrow-derived macrophages (BMDM) was performed according to Warren and Vogel (1985) from C57BL6/j 6-12 weeks old mice sex balanced. BMDMs were maintained in Roswell Park Memorial Institute (RPMI) 1640 Medium by adding 5% fetal bovine serum (FBS, Lonza), 2 mM L-glutamine, 100 U/ml penicillin-streptomycin (Lonza) in standard growth conditions.

Single murine splenocytes were harvested from C57BL6/j 6-12 weeks old mice, by using 70µm nylon mesh cell strainer and *in vitro* Naive CD4⁺ T cells were purified from splenocytes using CD4 negative selection kits (Miltenyi Biotec S.r.l. #130-104-454) and maintained in 5% FBS in RPMI supplemented by 50 µM β- mercaptoethanol and Sodium Pyruvate (Sigma)

7.13 Primary murine naïve, M1 macrophages, Th1/Th17 T-cells in vitro differentiation and reagents used for cell treatments.

In order to differentiate BMDMs into naïve macrophages, cells have been cultured for 7 days with 7-10% of L929 fibroblast supernatant medium (Kontoyiannis *et al.*, 1999; Warren and Vogel 1985). M1 macrophages have been obtained by 24 hours BMDMs stimulation with LPS (Sigma # L5418) (100ng/ml) and IFN γ (PeproTech # 315-05).

For Th1/Th17 cell polarization, purified naïve CD4 $^+$ T Cells were activated with plate-bound anti-CD3 (10 μ g/ml) (14-0032, eBioscience) and anti-CD28 (3 μ g/ml) (14-0281, eBioscience). For Th1 polarization, IL-12 (10 ng/ml) (419-ML-010, R&D system Inc.) and anti-IL-4 (10 μ g/ml) (16-7041, eBioscience) were added for 96 hours. For Th17 polarization, TGF- β (3 ng/ml) (rH100-21, PeproTech), IL-6 (20 ng/ml) 9216-6, PeproTech), IL-23 (20 ng/ml) (14-8231, eBioscience), anti-IFN- γ (10 μ g/ml) (16-7312, eBioscience) and anti-IL-4 (10 μ g/ml) were additionally used, according to Chen *et al.*, 2017.

Murine splenocytes extracted as previously described (paragraph 7.12) were cultured for 48 hours, after lysis of Red Blood Cells (RBC) with RBC Lysis Buffer (CSH protocols) were activated with non-specific T-cells stimuli, PMA (50 ng/ml)(Invivogen), Ionomycin (1 mM) (Invivogen) or PHA (100 ng/ml) (Invivogen).

Reagents used for cells treatments have been the following: LPS (1 μ g/ml)(Sigma #L5418) DMSO (ThermoFischer Scientific), CHX (10 μ M) (Sigma), Act-D (2.5 μ M)(A9400).

7.14 NO and Caspase 3/7 detection assays

Measurements of Nitric Oxide released by M1 macrophages have been performed using Griess's assay according to Green *et al.*,1982 and assay signals have been detected with Tecan microplate reader at wavelength corresponding to 540-550 nm.

In order to detect apoptosis signal, MCF7 cells Caspase-Glo 3/7 Assay (Promega) was used according to the manufacturer's instructions.

7.15 Cell viability assays

To test cell viability, were seeded and treated in 96 well-plate for 24-48-72 hours, as indicated in the Results section. Viability was assessed with OZBlue assay, Trypan Blue cells counting, Crystal violet staining and CellTiter-Glo assay. For what concerns OZB Briefly, OZBlue was added at 10% volume of culture media to each well and cells were further incubated at 37°C, until color signal developing was observed. Fluorescence was then determined (excitation 560 and emission 590 nm) by a Tecan microplate reader. Cell survival was calculated with respect to control (DMSO), and IC50 values were determined by fitting with GraphPad Prism software v5.1.

Splenocytes and Th1/Th17 cells viability was evaluated with CellTiter-Glo luminescent assay (Promega # CellTiter-Glo luminescent assay (Promega# G7570) according to manufacturer's instructions and percentage of viable cells has been calculated after normalization on DMSO treated control condition. Moreover, Trypan Blue has been used to count and determine viability percentage (%) of Th17/Th17 cells. Cells were diluted (1:2) in Trypan Blue and viable cells were calculated with Burker's chamber, and percentage of viable cells was calculated by normalization on DMSO control condition.

Crystal violet to determine cell number for ELISA/NO assay normalization, was performed according to (Feoktistova, Geserick and Leverkus, 2016).

7.16 Cell cycle, proliferation and migration assays.

For cell cycle analysis, cells at density of 2×10^5 to 1×10^6 cells /well were treated with TMs or DMSO as control as shown in the Results section, starvation was performed by overnight removing of FBS from cell media. Afterwards, cells were harvested and centrifuged at 1200 rpm for 5-10 min, washed twice in ice-cold PBS and fixed by incubating the cells 30 minutes or overnight at -20°C with 70% ethanol. Cells were then washed with ice-cold PBS and resuspended in 250 μl PI/RNase staining solution (Sigma P4874). The cell cycle position was evaluated by FACS using an excitation laser set at 480 nm and a detection wavelength of 575 nm. A minimum of 20.0000 events/sample was analyzed.

Cell proliferation assay, has been carried out using vibrant CFDA-SE Cell Tracer Kit (Thermo Fisher # V12883), briefly, murine CD4⁺ T cells, or splenocytes were incubated at the ratio of 1×10^6 cells per 2 μM of CFSE for 30 minutes at 37°C . After several washes in PBS cells were seeded and after 48-96 hours cell analysis was performed with FACS using excitation/emission wavelengths respectively of 492/517 nm. A minimum of 30.0000 was analyzed.

In both cases, cell cycle phase and cell proliferation analysis were performed using ModFit LT 3.2 software and the Sync Wizard models.

Lastly, migration assays, cells were seeded and treated with different conditions as indicated in Results section. Images of the same field were acquired immediately, $t=0$, after 24 and 48 h using a Leica DM IL Led microscope (5 \times magnification) and wounded-open areas were measured using ImageJ software.

7.17 Animal inflammation models and sera collection

C57BL6/j mice have been purchased from Charles River Laboratories were bred and maintained in the animal facilities of the Department of CIBIO, I under specific-pathogen-free conditions.

For measurement of inflammatory factors (TNf) secretion, 8 weeks old C57BL6/j mice were injected i.p. with LPS (Sigma L3755) at 150 $\mu\text{g}/25$ g body weight. Bloods were collected 90 minutes later by

cardiac puncture and after 30 minutes of RT sitting, two serial centrifuges were performed in order to collect sera, respectively 3000 rpm at 4°C and 6000 rpm both for 10 minutes

7.18 Statistical analysis

Statistical analysis Experiments were performed in number of biological replicates indicated in all experiments described in the Results section. t-tests were used to calculate final p-values, without assuming variances to be equal (Welch's t-test). P-value <0.05, < 0.01, <0.001 and <0.0001 were indicated with *, **, ***, **** symbols, respectively.

References

- Abdelmohsen, K. *et al.* (2007) 'Posttranscriptional orchestration of an anti-apoptotic program by HuR', *Cell Cycle*, 6(11), pp. 1288–1292. doi: 10.4161/cc.6.11.4299.
- Abdelmohsen, K. *et al.* (2008) 'Posttranscriptional gene regulation by RNA-binding proteins during oxidative stress: Implications for cellular senescence', *Biological Chemistry*, 389(3), pp. 243–255. doi: 10.1515/BC.2008.022.
- Abdelmohsen, K. *et al.* (2009) 'Ubiquitin-mediated proteolysis of HuR by heat shock', *EMBO Journal*. Nature Publishing Group, 28(9), pp. 1271–1282. doi: 10.1038/emboj.2009.67.
- Abumaree, M. H. *et al.* (2013) 'Human Placental Mesenchymal Stem Cells (pMSCs) Play a Role as Immune Suppressive Cells by Shifting Macrophage Differentiation from Inflammatory M1 to Anti-inflammatory M2 Macrophages', *Stem Cell Reviews and Reports*, 9(5), pp. 620–641. doi: 10.1007/s12015-013-9455-2.
- Akaike, Y. *et al.* (2014) 'HuR Regulates Alternative Splicing of the TRA2 Gene in Human Colon Cancer Cells under Oxidative Stress', *Molecular and Cellular Biology*, 34(15), pp. 2857–2873. doi: 10.1128/MCB.00333-14.
- Al-Ahmadi, W. *et al.* (2009) 'Alternative polyadenylation variants of the RNA binding protein, HuR: Abundance, role of AU-rich elements and auto-Regulation', *Nucleic Acids Research*, 37(11), pp. 3612–3624. doi: 10.1093/nar/gkp223.
- Amadio, M. *et al.* (2010) 'The PKC β /HuR/VEGF pathway in diabetic retinopathy', *Biochemical Pharmacology*, 80(8), pp. 1230–1237. doi: 10.1016/j.bcp.2010.06.033.
- Anderson, P. (2010) 'Post-transcriptional regulons coordinate the initiation and resolution of inflammation', *Nature Reviews Immunology*. Nature Publishing Group, 10(1), pp. 24–35. doi: 10.1038/nri2685.
- Andreu, N. *et al.* (2017) 'Primary macrophages and J774 cells respond differently to infection with Mycobacterium tuberculosis', *Scientific Reports*. Nature Publishing Group, 7(October 2016), pp. 1–12. doi: 10.1038/srep42225.
- Atasoy, U. *et al.* (1998) 'ELAV protein HuA (HuR) can redistribute between nucleus and cytoplasm and is upregulated during serum stimulation and T cell activation.', *Journal of cell science*, 111 (Pt 2, pp. 3145–56. Available at: <http://www.ncbi.nlm.nih.gov/pubmed/9763509>.
- Atri, C., Guerfali, F. Z. and Laouini, D. (2018) 'Role of human macrophage polarization in inflammation during infectious diseases', *International Journal of Molecular Sciences*, 19(6). doi: 10.3390/ijms19061801.
- Auweter, S. D., Oberstrass, F. C. and Allain, F. H. T. (2006) 'Sequence-specific binding of single-stranded RNA: Is there a code for recognition?', *Nucleic Acids Research*, 34(17), pp. 4943–4959. doi: 10.1093/nar/gkl620.
- Badawi, A. *et al.* (2017) 'Silencing of the mRNA-binding protein HuR increases the sensitivity of colorectal cancer cells to ionizing radiation through upregulation of caspase-2', *Cancer Letters*, 393(February), pp. 103–112. doi: 10.1016/j.canlet.2017.02.010.
- Bakheet, T. *et al.* (2018) 'The AU-rich element landscape across human transcriptome reveals a large proportion in introns and regulation by ELAVL1/HuR', *Biochimica et Biophysica Acta - Gene Regulatory Mechanisms*. Elsevier, 1861(2), pp. 167–177. doi: 10.1016/j.bbagr.2017.12.006.

Baltz, A. G. *et al.* (2012) 'The mRNA-Bound Proteome and Its Global Occupancy Profile on Protein-Coding Transcripts', *Molecular Cell*, 46(5), pp. 674–690. doi: 10.1016/j.molcel.2012.05.021.

Barbisan, F. *et al.* (2009) 'Overexpression of ELAV-like Protein HuR is Associated with Increased COX-2 Expression in Atrophy, High-grade Prostatic Intraepithelial Neoplasia, and Incidental Prostate Cancer in Cystoprostatectomies', *European Urology*, 56(1), pp. 105–112. doi: 10.1016/j.eururo.2008.04.043.

Barros, M. H. M. *et al.* (2013) 'Macrophage polarisation: An immunohistochemical approach for identifying M1 and M2 macrophages', *PLoS ONE*, 8(11), pp. 1–11. doi: 10.1371/journal.pone.0080908.

Bisgaard, L. S. *et al.* (2016) 'Bone marrow-derived and peritoneal macrophages have different inflammatory response to oxLDL and M1/M2 marker expression - Implications for atherosclerosis research', *Scientific Reports*. Nature Publishing Group, 6(October), pp. 1–10. doi: 10.1038/srep35234.

Brauß, T. F. *et al.* (2017) 'The RNA-binding protein HuR inhibits expression of CCL5 and limits recruitment of macrophages into tumors', *Molecular Carcinogenesis*, 56(12), pp. 2620–2629. doi: 10.1002/mc.22706.

Brennan, C. M. and Steitz, J. A. (2001) 'Brennan et al 2001.pdf', 58, pp. 266–277.

Carpenter, S. *et al.* (2014) 'Post-transcriptional regulation of gene expression in innate immunity', *Nature Reviews Immunology*. Nature Publishing Group, 14(6), pp. 361–376. doi: 10.1038/nri3682.

Chae, M. J. *et al.* (2009) 'Chemical inhibitors destabilize HuR binding to the AU-rich element of TNF- α mRNA', *Experimental and Molecular Medicine*, 41(11), pp. 824–831. doi: 10.3858/emm.2009.41.11.088.

Chand, S. N. *et al.* (2017) 'Posttranscriptional regulation of PARG mRNA by HuR facilitates DNA repair and resistance to PARP inhibitors', *Cancer Research*, 77(18), pp. 5011–5025. doi: 10.1158/0008-5472.CAN-16-2704.

Chang, N. *et al.* (2010) 'HuR Uses AUF1 as a Cofactor To Promote p16INK4 mRNA Decay', *Molecular and Cellular Biology*, 30(15), pp. 3875–3886. doi: 10.1128/mcb.00169-10.

Chen, J. *et al.* (2013) 'Posttranscriptional Gene Regulation of IL-17 by the RNA-Binding Protein HuR Is Required for Initiation of Experimental Autoimmune Encephalomyelitis', *The Journal of Immunology*, 191(11), pp. 5441–5450. doi: 10.4049/jimmunol.1301188.

Chen, J. *et al.* (2017) 'The RNA-binding protein HuR contributes to neuroinflammation by promoting C-C chemokine receptor 6 (CCR6) expression on Th17 cells', *Journal of Biological Chemistry*, 292(35), pp. 14532–14543. doi: 10.1074/jbc.M117.782771.

Cheng, Y.-C. *et al.* (2013) 'MPT0B098, a Novel Microtubule Inhibitor That Destabilizes the Hypoxia-Inducible Factor-1 mRNA through Decreasing Nuclear-Cytoplasmic Translocation of RNA-Binding Protein HuR', *Molecular Cancer Therapeutics*, 12(7), pp. 1202–1212. doi: 10.1158/1535-7163.mct-12-0778.

Cherry, J. O. Y. *et al.* (2008) '911Cherry', 24, pp. 1–7. Available at: [papers3://publication/uuid/DB4D594E-F8DA-4C62-80F9-0136AF6A5C39](https://pubmed.ncbi.nlm.nih.gov/14532/).

Chou, S. D. *et al.* (2015) 'HSF1 regulation of β -catenin in mammary cancer cells through control of HuR/elavL1 expression', *Oncogene*. Nature Publishing Group, 34(17), pp. 2178–2188. doi: 10.1038/onc.2014.177.

- Christodoulou-Vafeiadou, E. *et al.* (2018) 'Divergent innate and epithelial functions of the RNA-binding protein HuR in intestinal inflammation', *Frontiers in Immunology*, 9(NOV), pp. 1–19. doi: 10.3389/fimmu.2018.02732.
- Cléry, A., Blatter, M. and Allain, F. H. T. (2008) 'RNA recognition motifs: boring? Not quite', *Current Opinion in Structural Biology*, 18(3), pp. 290–298. doi: 10.1016/j.sbi.2008.04.002.
- Cuadrado, A. *et al.* (2003) 'Role of HuR in Skeletal Myogenesis through Coordinate Regulation of Muscle Differentiation Genes', *Molecular and cellular biology*, 23(14), pp. 4991–5004. doi: 10.1128/MCB.23.14.4991.
- D'Agostino, V. G. *et al.* (2015) 'Dihydrotanshinone-I interferes with the RNA-binding activity of HuR affecting its post-transcriptional function', *Scientific Reports*. Nature Publishing Group, 5(October), pp. 1–15. doi: 10.1038/srep16478.
- D'Agostino, V. G. *et al.* (2019) 'Screening Approaches for Targeting Ribonucleoprotein Complexes: A New Dimension for Drug Discovery', *SLAS Discovery*, 24(3), pp. 314–331. doi: 10.1177/2472555218818065.
- D'Agostino, V. G., Adami, V. and Provenzani, A. (2013) 'A Novel High Throughput Biochemical Assay to Evaluate the HuR Protein-RNA Complex Formation', *PLoS ONE*, 8(8), pp. 1–9. doi: 10.1371/journal.pone.0072426.
- Dassi, E. *et al.* (2014) 'AURA 2: Empowering discovery of post-transcriptional networks', *Translation*, 2(1), p. e27738. Available at: <http://www.landesbioscience.com/journals/translation/article/27738/>.
- DeMicco, A. *et al.* (2015) 'B Cell–Intrinsic Expression of the HuR RNA-Binding Protein Is Required for the T Cell–Dependent Immune Response In Vivo', *The Journal of Immunology*, 195(7), pp. 3449–3462. doi: 10.4049/jimmunol.1500512.
- Díaz-Muñoz, M. D. *et al.* (2015) 'The RNA-binding protein HuR is essential for the B cell antibody response', *Nature Immunology*, 16(4), pp. 415–425. doi: 10.1038/ni.3115.
- Díaz-Muñoz, M. D. and Turner, M. (2018) 'Uncovering the role of RNA-binding proteins in gene expression in the immune system', *Frontiers in Immunology*, 9(MAY). doi: 10.3389/fimmu.2018.01094.
- Ding, X. *et al.* (2017) 'Comparison of the characteristics of macrophages derived from murine spleen, peritoneal cavity, and bone marrow', *Journal of Zhejiang University-SCIENCE B*, 18(12), pp. 1055–1063. doi: 10.1631/jzus.b1700003.
- Dixon, D. A. *et al.* (2001) 'Altered expression of the mRNA stability factor HuR promotes cyclooxygenase-2 expression in colon cancer cells', *Journal of Clinical Investigation*, 108(11), pp. 1657–1665. doi: 10.1172/JCI12973.
- Dong, R. *et al.* (2007) 'Stabilization of Snail by HuR in the process of hydrogen peroxide induced cell migration', *Biochemical and Biophysical Research Communications*, 356(1), pp. 318–321. doi: 10.1016/j.bbrc.2007.02.145.
- Dreyfuss, G., Kim, V. N. and Kataoka, N. (2002) 'Messenger-RNA-binding proteins and the messages they carry', *Nature Reviews Molecular Cell Biology*, 3(3), pp. 195–205. doi: 10.1038/nrm760.
- Dutertre, M. *et al.* (2014) 'A recently evolved class of alternative 3'-terminal exons involved in cell cycle regulation by topoisomerase inhibitors', *Nature Communications*, 5, pp. 1–12. doi: 10.1038/ncomms4395.

- Epithalamion, S. and Pinka, P. G. (2012) 'Donne , Somerset G . Pinka', *Nature*, 90(1), pp. 58–73. doi: 10.1038/nature01322.Inflammation.
- Fan, J. *et al.* (2005) 'The role of post-transcriptional regulation in chemokine gene expression in inflammation and allergy', *European Respiratory Journal*, 26(5), pp. 933–947. doi: 10.1183/09031936.05.00120204.
- Fan, X. C. and Steitz, Joan A (1998) 'HNS, a nuclear-cytoplasmic shuttling sequence in HuR (nuclear localization RNA degradation nuclear export)', *Biochemistry*, 95(December), pp. 15293–15298. doi: 10.1073/pnas.95.26.15293.
- Fan, X. C. and Steitz, Joan A. (1998) 'Overexpression of HuR, a nuclear-cytoplasmic shuttling protein, increases the in vivo stability of ARE-containing mRNAs', *EMBO Journal*, 17(12), pp. 3448–3460. doi: 10.1093/emboj/17.12.3448.
- Feoktistova, M., Geserick, P. and Leverkus, M. (2016) 'Crystal violet assay for determining viability of cultured cells', *Cold Spring Harbor Protocols*, 2016(4), pp. 343–346. doi: 10.1101/pdb.prot087379.
- Fernández-Ramos, D. and Martínez-Chantar, M. L. (2015) 'NEDDylation in liver cancer: The regulation of the RNA binding protein Hu antigen R', *Pancreatology: official journal of the International Association of Pancreatology (IAP) ... [et al.]*, 15(4), pp. S49–S54. doi: 10.1016/j.pan.2015.03.006.
- Freeberg, M. A. *et al.* (2013) 'Pervasive and dynamic protein binding sites of the mRNA transcriptome in *Saccharomyces cerevisiae*', *Genome Biology*. BioMed Central Ltd, 14(2), p. R13. doi: 10.1186/gb-2013-14-2-r13.
- Fu, M. and Blackshear, P. J. (2017) 'RNA-binding proteins in immune regulation: A focus on CCCH zinc finger proteins', *Nature Reviews Immunology*. Nature Publishing Group, 17(2), pp. 130–143. doi: 10.1038/nri.2016.129.
- Gabut, M., Chaudhry, S. and Blencowe, B. J. (2008) 'SnapShot: The Splicing Regulatory Machinery', *Cell*, 133(1), pp. 192-192.e1. doi: 10.1016/j.cell.2008.03.010.
- García-Mauriño, S. M. *et al.* (2017) 'RNA Binding Protein Regulation and Cross-Talk in the Control of AU-rich mRNA Fate', *Frontiers in Molecular Biosciences*, 4(October), pp. 1–9. doi: 10.3389/fmolb.2017.00071.
- Gerstberger, S., Hafner, M. and Tuschl, T. (2014) 'A census of human RNA-binding proteins', *Nature Reviews Genetics*. Nature Publishing Group, 15(12), pp. 829–845. doi: 10.1038/nrg3813.
- Ghosh, M. *et al.* (2009) 'Essential role of the RNA-binding protein HuR in progenitor cell survival in mice', *Journal of Clinical Investigation*, 119(12), pp. 3530–3543. doi: 10.1172/JCI38263.
- Van Der Giessen, K. *et al.* (2003) 'RNAi-mediated HuR Depletion Leads to the Inhibition of Muscle Cell Differentiation', *Journal of Biological Chemistry*, 278(47), pp. 47119–47128. doi: 10.1074/jbc.M308889200.
- Glisovic, T. *et al.* (2008) 'RNA-binding proteins and post-transcriptional gene regulation', *FEBS Letters*, 582(14), pp. 1977–1986. doi: 10.1016/j.febslet.2008.03.004.
- Good, P. J. (2006) 'A conserved family of elav-like genes in vertebrates.', *Proceedings of the National Academy of Sciences*, 92(10), pp. 4557–4561. doi: 10.1073/pnas.92.10.4557.
- de Graaf, M. *et al.* (2008) 'B and T cell imbalances in CSF of patients with Hu-antibody associated PNS', *Journal of Neuroimmunology*, 195(1–2), pp. 164–170. doi: 10.1016/j.jneuroim.2008.01.007.

- Grammatikakis, I., Abdelmohsen, K. and Gorospe, M. (2017) 'Posttranslational control of HuR function', *Wiley Interdisciplinary Reviews: RNA*, 8(1), pp. 1–15. doi: 10.1002/wrna.1372.
- Gu, L. *et al.* (2017) 'Reconstitution of HuR-Inhibited CUGBP1 Expression Protects Cardiomyocytes from Acute Myocardial Infarction-Induced Injury', *Antioxidants & Redox Signaling*, 27(14), pp. 1013–1026. doi: 10.1089/ars.2016.6880.
- Guo, X., Wu, Y. and Hartley, R. S. (2009) 'MicroRNA-125a represses cell growth by targeting HuR in breast cancer.', *RNA biology*, 6(5), pp. 575–583. doi: 10.4161/rna.6.5.10079.
- Guttinger, S. *et al.* (2004) 'From The Cover: Transportin2 functions as importin and mediates nuclear import of HuR', *Proceedings of the National Academy of Sciences*, 101(9), pp. 2918–2923. doi: 10.1073/pnas.0400342101.
- Hamosh, A. *et al.* (2005) 'Online Mendelian Inheritance in Man (OMIM), a knowledgebase of human genes and genetic disorders', *Nucleic Acids Research*, 33(DATABASE ISS.), pp. 514–517. doi: 10.1093/nar/gki033.
- Hanahan, D. and Weinberg, R. A. (2011) 'Hallmarks of cancer: the next generation.', *Cell*. Elsevier Inc., 144(5), pp. 646–74. doi: 10.1016/j.cell.2011.02.013.
- Hashimoto, O. *et al.* (2016) 'Collaboration of cancer-associated fibroblasts and tumour-associated macrophages for neuroblastoma development', *Journal of Pathology*, 240(2), pp. 211–223. doi: 10.1002/path.4769.
- Heinonen, M. *et al.* (2011) 'Role of RNA binding protein HuR in ductal carcinoma in situ of the breast', *Journal of Pathology*, 224(4), pp. 529–539. doi: 10.1002/path.2889.
- Hentze, M. W. *et al.* (2018) 'A brave new world of RNA-binding proteins', *Nature Reviews Molecular Cell Biology*. Nature Publishing Group, 19(5), pp. 327–341. doi: 10.1038/nrm.2017.130.
- Herjan, T. *et al.* (2013) 'HuR Is Required for IL-17-Induced Act1-Mediated CXCL1 and CXCL5 mRNA Stabilization', *The Journal of Immunology*, 191(2), pp. 640–649. doi: 10.4049/jimmunol.1203315.
- Hi, P. (1999) 'Activators and target genes of Rel/NF-kappaB transcription factors', *Oncogene*, 18(49), pp. 6853–66.
- Hong, S. (2018) 'RNA Binding Protein as an Emerging Therapeutic Target for Cancer Prevention and Treatment', *Journal of Cancer Prevention*, 22(4), pp. 203–210. doi: 10.15430/jcp.2017.22.4.203.
- Jeyaraj, S. C. *et al.* (2010) 'Transcriptional control of human antigen R by bone morphogenetic protein', *Journal of Biological Chemistry*, 285(7), pp. 4432–4440. doi: 10.1074/jbc.M109.062216.
- Jimbo, M. *et al.* (2015) 'Targeting the mRNA-binding protein HuR impairs malignant characteristics of pancreatic ductal adenocarcinoma cells', *Oncotarget*, 6(29). doi: 10.18632/oncotarget.4743.
- Jiménez, F. and Campos-Ortega, J. A. (1987) 'Genes in subdivision IB of the drosophila melanogaster x-chromosome and their influence on neural development', *Journal of Neurogenetics*, 4(1), pp. 179–200. doi: 10.3109/01677068709102340.
- Kafasla, P., Skliris, A. and Kontoyiannis, D. L. (2014) 'Post-transcriptional coordination of immunological responses by RNA-binding proteins', *Nature Immunology*, 15(6), pp. 492–502. doi: 10.1038/ni.2884.
- Kang, M. J. *et al.* (2008) 'NF-κB Activates Transcription of the RNA-Binding Factor HuR, via PI3K-AKT Signaling, to Promote Gastric Tumorigenesis', *Gastroenterology*. AGA Institute American

- Gastroenterological Association, 135(6), pp. 2030-2042.e3. doi: 10.1053/j.gastro.2008.08.009.
- Katsanou, V. *et al.* (2005) 'HuR as a negative posttranscriptional modulator in inflammation', *Molecular Cell*, 19(6), pp. 777–789. doi: 10.1016/j.molcel.2005.08.007.
- Katsanou, V. *et al.* (2009) 'The RNA-Binding Protein Elavl1/HuR Is Essential for Placental Branching Morphogenesis and Embryonic Development', *Molecular and Cellular Biology*, 29(10), pp. 2762–2776. doi: 10.1128/mcb.01393-08.
- Kaur, K. *et al.* (2017) 'The fungal natural product azaphilone-9 binds to HuR and inhibits HuR-RNA interaction in vitro', *PLoS ONE*, 12(4), pp. 1–18. doi: 10.1371/journal.pone.0175471.
- Ke, Y. *et al.* (2017) 'PARP1 promotes gene expression at the post-transcriptional level by modulating the RNA-binding protein HuR', *Nature Communications*. Nature Publishing Group, 8, pp. 1–15. doi: 10.1038/ncomms14632.
- Keene, J. D. (2007) 'RNA regulons: Coordination of post-transcriptional events', *Nature Reviews Genetics*, 8(7), pp. 533–543. doi: 10.1038/nrg2111.
- Keene, J. D. *et al.* (2011) 'Integrative Regulatory Mapping Indicates that the RNA-Binding Protein HuR Couples Pre-mRNA Processing and mRNA Stability', *Molecular Cell*, 43(3), pp. 327–339.
- Khera, T. K., Dick, A. D. and Nicholson, L. B. (2010) 'Mechanisms of TNF α regulation in uveitis: Focus on RNA-binding proteins', *Progress in Retinal and Eye Research*. Elsevier Ltd, 29(6), pp. 610–621. doi: 10.1016/j.preteyeres.2010.08.003.
- Koba, M. and Konopa, J. (2005) '[Actinomycin D and its mechanisms of action].', *Postepy higieny i medycyny doswiadczalnej (Online)*, 59, pp. 290–8. Available at: <http://www.ncbi.nlm.nih.gov/pubmed/15995596>.
- Kontoyiannis, D. *et al.* (1999) 'TNF α mice construct.pdf', 10, pp. 387–398.
- Kotb Abdelmohsen (2013) 'Post-transcriptional regulation of cancer traits by HuR NIH Public Access', 1(2), pp. 1–24. doi: 10.1002/wrna.4.Post-transcriptional.
- Kotta-Loizou, I., Giaginis, C. and Theocharis, S. (2014) 'Clinical significance of HuR expression in human malignancy', *Medical Oncology*, 31(9), pp. 1–19. doi: 10.1007/s12032-014-0161-y.
- Kwan, T. *et al.* (2017) 'Astrocytic expression of the RNA regulator HuR accentuates spinal cord injury in the acute phase', *Neuroscience Letters*. Elsevier Ireland Ltd, 651, pp. 140–145. doi: 10.1016/j.neulet.2017.05.003.
- Lal, P. *et al.* (2017) 'Regulation of HuR structure and function by dihydrotanshinone-I', *Nucleic Acids Research*. Oxford University Press, 45(16), pp. 9514–9527. doi: 10.1093/nar/gkx623.
- Lang, M. *et al.* (2017) 'HuR small-molecule inhibitor elicits differential effects in adenomatous polyposis and colorectal carcinogenesis', *Cancer Research*, 77(9), pp. 2424–2438. doi: 10.1158/0008-5472.CAN-15-1726.
- Lawrence, T. and Natoli, G. (2011) 'Transcriptional regulation of macrophage polarization: Enabling diversity with identity', *Nature Reviews Immunology*. Nature Publishing Group, 11(11), pp. 750–761. doi: 10.1038/nri3088.
- Lebedeva, S. *et al.* (2011) 'Transcriptome-wide Analysis of Regulatory Interactions of the RNA-Binding Protein HuR', *Molecular Cell*, 43(3), pp. 340–352. doi: 10.1016/j.molcel.2011.06.008.
- Lee, J. Y. *et al.* (2014) 'A novel cantharidin analog N-Benzylcantharidinamide reduces the expression

of MMP-9 and invasive potentials of Hep3B via inhibiting cytosolic translocation of HuR', *Biochemical and Biophysical Research Communications*. Elsevier Inc., 447(2), pp. 371–377. doi: 10.1016/j.bbrc.2014.04.035.

Levadoux-Martin, M. *et al.* (2003) 'Impaired gametogenesis in mice that overexpress the RNA-binding protein HuR', *EMBO Reports*, 4(4), pp. 394–399. doi: 10.1038/sj.embor.embor803.

Levy, N. S. *et al.* (1998) 'Hypoxic stabilization of vascular endothelial growth factor mRNA by the RNA-binding protein HuR', *Journal of Biological Chemistry*, 273(11), pp. 6417–6423. doi: 10.1074/jbc.273.11.6417.

Liang, C.-C., Park, A. Y. and Guan, J.-L. (2007) 'In vitro scratch assay: a convenient and inexpensive method for analysis of cell migration in vitro.', *Nature protocols*, 2(2), pp. 329–33. doi: 10.1038/nprot.2007.30.

Lin, F. Y. *et al.* (2006) 'The role of human antigen R, an RNA-binding protein, in mediating the stabilization of toll-like receptor 4 mRNA induced by endotoxin: A novel mechanism involved in vascular inflammation', *Arteriosclerosis, Thrombosis, and Vascular Biology*, 26(12), pp. 2622–2629. doi: 10.1161/01.ATV.0000246779.78003.cf.

Linder, P. and Jankowsky, E. (2011) 'From unwinding to clamping the DEAD box RNA helicase family', *Nature Reviews Molecular Cell Biology*. Nature Publishing Group, 12(8), pp. 505–516. doi: 10.1038/nrm3154.

Lu, Y. C. *et al.* (2014) 'ELAVL1 Modulates Transcriptome-wide miRNA Binding in Murine Macrophages', *Cell Reports*, 9(6), pp. 2330–2343. doi: 10.1016/j.celrep.2014.11.030.

Lu, Z. *et al.* (2006) 'Transcriptional and posttranscriptional down-regulation of the imprinted tumor suppressor gene ARHI (DRAS3) in ovarian cancer', *Clinical Cancer Research*, 12(8), pp. 2404–2413. doi: 10.1158/1078-0432.CCR-05-1036.

Lukong, K. E. *et al.* (2008) 'RNA-binding proteins in human genetic disease', *Trends in Genetics*, 24(8), pp. 416–425. doi: 10.1016/j.tig.2008.05.004.

Lunde, B. M., Moore, C. and Varani, G. (2007) 'RNA-binding proteins: Modular design for efficient function', *Nature Reviews Molecular Cell Biology*, 8(6), pp. 479–490. doi: 10.1038/nrm2178.

Ma, W. J. *et al.* (1996) 'Cloning and characterization of HuR, a ubiquitously expressed Elav-like protein', *Journal of Biological Chemistry*, 271(14), pp. 8144–8151. doi: 10.1074/jbc.271.14.8144.

Ma, W. J. and Furneaux, H. (1997) 'Localization of the human HuR gene to chromosome 19p13.2', *Human Genetics*, 99(1), pp. 32–33. doi: 10.1007/s004390050305.

Macrophages, P. *et al.* (2015) 'Methods in Mouse Atherosclerosis', 1339, pp. 101–109. doi: 10.1007/978-1-4939-2929-0.

Mantovani, A. *et al.* (2002) 'Macrophage polarization: tumor-associated macrophages as a paradigm for polarized M2 mononuclear phagocytes', *Trends in Immunology*, 23 No.11(11), pp. 549–555. doi: 10.1002/cber.188301601200.

Manzoni, L. *et al.* (2018a) 'Interfering with HuR-RNA Interaction: Design, Synthesis and Biological Characterization of Tanshinone Mimics as Novel, Effective HuR Inhibitors', *Journal of Medicinal Chemistry*, 61(4), pp. 1483–1498. doi: 10.1021/acs.jmedchem.7b01176.

Manzoni, L. *et al.* (2018b) 'Interfering with HuR-RNA Interaction: Design, Synthesis and Biological Characterization of Tanshinone Mimics as Novel, Effective HuR Inhibitors', *Journal of Medicinal*

Chemistry, 61(4), pp. 1483–1498. doi: 10.1021/acs.jmedchem.7b01176.

Marasa, B. S. *et al.* (2010) 'MicroRNA profiling in human diploid fibroblasts uncovers miR-519 role in replicative senescence', *Aging*, 2(6), pp. 333–343. doi: 10.18632/aging.100159.

Di Marco, S. *et al.* (2005) 'NF- B-Mediated MyoD Decay during Muscle Wasting Requires Nitric Oxide Synthase mRNA Stabilization, HuR Protein, and Nitric Oxide Release', *Molecular and Cellular Biology*, 25(15), pp. 6533–6545. doi: 10.1128/mcb.25.15.6533-6545.2005.

Matsumiya, T. *et al.* (2010) 'Characterization of Synergistic Induction of CX3CL1/Fractalkine by TNF- and IFN- in Vascular Endothelial Cells: An Essential Role for TNF- in Post-Transcriptional Regulation of CX3CL1', *The Journal of Immunology*, 184(8), pp. 4205–4214. doi: 10.4049/jimmunol.0903212.

Mazroui, R. *et al.* (2008) 'Caspase-mediated cleavage of HuR in the cytoplasm contributes to pp32/PHAP-I regulation of apoptosis', *Journal of Cell Biology*, 180(1), pp. 113–127. doi: 10.1083/jcb.200709030.

Medzhitov, R. and Horng, T. (2009) 'Transcriptional control of the inflammatory response', *Nature Reviews Immunology*. Nature Publishing Group, 9(10), pp. 692–703. doi: 10.1038/nri2634.

Meisner, N. C. *et al.* (2007) 'Identification and mechanistic characterization of low-molecular-weight inhibitors for HuR', *Nature Chemical Biology*, 3(8), pp. 508–515. doi: 10.1038/nchembio.2007.14.

Meng, Z. *et al.* (2005) 'The ELAV RNA-stability factor HuR binds the 5'-untranslated region of the human IGF-IR transcript and differentially represses cap-dependent and IRES-mediated translation', *Nucleic Acids Research*, 33(9), pp. 2962–2979. doi: 10.1093/nar/gki603.

Merly, L. and Smith, S. L. (2017) 'Murine RAW 264.7 cell line as an immune target: are we missing something?', *Immunopharmacology and Immunotoxicology*, 39(2), pp. 55–58. doi: 10.1080/08923973.2017.1282511.

Mills, C. D. (2012) 'M1 and M2 Macrophages: Oracles of Health and Disease.', *Critical reviews in immunology*, 32(6), pp. 463–88. Available at: <http://www.ncbi.nlm.nih.gov/pubmed/23428224>.

MINO, T. and TAKEUCHI, O. (2018) 'Post-transcriptional regulation of immune responses by RNA binding proteins', *Proceedings of the Japan Academy, Series B*, 94(6), pp. 248–258. doi: 10.2183/pjab.94.017.

Moore, M. J. (2005) 'From birth to death: The complex lives of eukaryotic mRNAs', *Science*, 309(5740), pp. 1514–1518. doi: 10.1126/science.1111443.

Müller-Quernheim, U. C. *et al.* (2012) 'Tumor-Cell Co-Culture Induced Alternative Activation of Macrophages Is Modulated by Interferons In Vitro', *Journal of Interferon & Cytokine Research*, 32(4), pp. 169–177. doi: 10.1089/jir.2011.0020.

Murray, P. J. and Wynn, T. A. (2011) 'Protective and pathogenic functions of macrophage subsets', *Nature Reviews Immunology*. Nature Publishing Group, 11(11), pp. 723–737. doi: 10.1038/nri3073.

Nabors, L. B. *et al.* (2001) 'HuR, a RNA stability factor, is expressed in malignant brain tumors and binds to adenine- and uridine-rich elements within the 3' untranslated regions of cytokine and angiogenic factor mRNAs', *Cancer Research*, 61(5), pp. 2154–2161.

Nakano, S. *et al.* (2005) 'Messenger RNA degradation may be inhibited in sporadic inclusion body myositis', *Neurology*, 65(3), pp. 420–425. doi: 10.1212/01.wnl.0000171341.76482.15.

- Nussbacher, J. K. *et al.* (2015) 'RNA-binding proteins in neurodegeneration: Seq and you shall receive', *Trends in Neurosciences*. Elsevier Ltd, 38(4), pp. 226–236. doi: 10.1016/j.tins.2015.02.003.
- Ostareck, D. H. and Ostareck-Lederer, A. (2019) 'RNA-Binding Proteins in the Control of LPS-Induced Macrophage Response', *Frontiers in Genetics*, 10(February), pp. 1–10. doi: 10.3389/fgene.2019.00031.
- Otsuka, H. *et al.* (2019) 'Emerging Evidence of Translational Control by AU-Rich Element-Binding Proteins', *Frontiers in Genetics*, 10(May), pp. 1–10. doi: 10.3389/fgene.2019.00332.
- Pabis, M. *et al.* (2019) 'HuR biological function involves RRM3-mediated dimerization and RNA binding by all three RRMs', *Nucleic acids research*, 47(2), pp. 1011–1029. doi: 10.1093/nar/gky1138.
- Panda, A., Martindale, J. and Gorospe, M. (2016) 'Affinity Pulldown of Biotinylated RNA for Detection of Protein-RNA Complexes', *Bio-Protocol*, 6(24), pp. 1–10. doi: 10.21769/bioprotoc.2062.
- Pang, L. *et al.* (2013) 'Loss of CARM1 is linked to reduced HuR function in replicative senescence', *BMC Molecular Biology*. BMC Molecular Biology, 14(1), p. 1. doi: 10.1186/1471-2199-14-15.
- Papadaki, O. *et al.* (2009) 'Control of Thymic T Cell Maturation, Deletion and Egress by the RNA-Binding Protein HuR', *The Journal of Immunology*, 182(11), pp. 6779–6788. doi: 10.4049/jimmunol.0900377.
- Pathria, P., Louis, T. L. and Varner, J. A. (2019) 'Targeting Tumor-Associated Macrophages in Cancer', *Trends in Immunology*. Elsevier Ltd, 40(4), pp. 310–327. doi: 10.1016/j.it.2019.02.003.
- Peña, J. B. I. de la, Song, J. J. and Campbell, Z. T. (2019) 'RNA control in pain: Blame it on the messenger', *Wiley Interdisciplinary Reviews: RNA*, (April), pp. 1–19. doi: 10.1002/wrna.1546.
- Pereira, B., Billaud, M. and Almeida, R. (2017) 'RNA-Binding Proteins in Cancer: Old Players and New Actors', *Trends in Cancer*. Elsevier Inc., 3(7), pp. 506–528. doi: 10.1016/j.trecan.2017.05.003.
- Pullmann, R. *et al.* (2007) 'Analysis of Turnover and Translation Regulatory RNA-Binding Protein Expression through Binding to Cognate mRNAs', *Molecular and Cellular Biology*, 27(18), pp. 6265–6278. doi: 10.1128/mcb.00500-07.
- Qin, X. *et al.* (2016) 'Micheliolide inhibits LPS-induced inflammatory response and protects mice from LPS challenge', *Scientific Reports*. Nature Publishing Group, 6, pp. 1–13. doi: 10.1038/srep23240.
- Quatromoni, J. G. and Eruslanov, E. (2012) 'Tumor-associated macrophages: function, phenotype, and link to prognosis in human lung cancer.', *American journal of translational research*, 4(4), pp. 376–89.
- Ramsay, R. R. and Tipton, K. F. (2017) *Assessment of Enzyme Inhibition: A Review with Examples from the Development of Monoamine Oxidase and Cholinesterase Inhibitory Drugs*, *Molecules (Basel, Switzerland)*. doi: 10.3390/molecules22071192.
- Relda Cailleau, M. O. and Q. V. J. C. (1978) 'Long-Term Human Breast Carcinoma Cell Lines of Metastatic Origin: Preliminary Characterization', *In Vitro*, Vol. 14, pp. 911–915.
- Reynier, F. *et al.* (2012) 'Gene Expression Profiles in Alveolar Macrophages Induced by Lipopolysaccharide in Humans', *Molecular Medicine*, 18(9), pp. 1303–1311. doi: 10.2119/molmed.2012.00230.
- Riaz, N. *et al.* (2016) 'HHS Public Access', 118(24), pp. 6072–6078. doi:

10.1002/cncr.27633.Percutaneous.

Rutledge, H. R. *et al.* (2012) 'Gene expression profiles of RAW264.7 macrophages stimulated with preparations of LPS differing in isolation and purity', *Innate Immunity*, 18(1), pp. 80–88. doi: 10.1177/1753425910393540.

Sakai, J. *et al.* (2017) 'Lipopolysaccharide-induced NF- κ B nuclear translocation is primarily dependent on MyD88, but TNF α expression requires TRIF and MyD88', *Scientific Reports*. Springer US, 7(1), pp. 1–9. doi: 10.1038/s41598-017-01600-y.

Samson, M. L. (2008) 'Rapid functional diversification in the structurally conserved ELAV family of neuronal RNA binding proteins', *BMC Genomics*, 9, pp. 1–11. doi: 10.1186/1471-2164-9-392.

Saunus, J. M. *et al.* (2008) 'Posttranscriptional regulation of the breast cancer susceptibility gene BRCA1 by the RNA binding protein HuR', *Cancer Research*, 68(22), pp. 9469–9478. doi: 10.1158/0008-5472.CAN-08-1159.

Schneider-poetsch, T. *et al.* (2010) 'Cycloheximide mechanism', 6(3), pp. 209–217. doi: 10.1038/nchembio.304.Inhibition.

Schulz, S. *et al.* (2013) 'Domain-specific phosphomimetic mutation allows dissection of different protein kinase C (PKC) isotype-triggered activities of the RNA binding protein HuR', *Cellular Signalling*. Elsevier Inc., 25(12), pp. 2485–2495. doi: 10.1016/j.cellsig.2013.08.003.

Scott, M. G. *et al.* (2000) 'An α -Helical Cationic Antimicrobial Peptide Selectively Modulates Macrophage Responses to Lipopolysaccharide and Directly Alters Macrophage Gene Expression', *The Journal of Immunology*, 165(6), pp. 3358–3365. doi: 10.4049/jimmunol.165.6.3358.

Sedlyarov, V. *et al.* (2016) 'Tristetraprolin binding site atlas in the macrophage transcriptome reveals a switch for inflammation resolution.', *Molecular systems biology*, 12(5), p. 868. doi: 10.15252/msb.20156628.

Seko, Y. *et al.* (2006) 'The role of cytokine mRNA stability in the pathogenesis of autoimmune disease', *Autoimmunity Reviews*, 5(5), pp. 299–305. doi: 10.1016/j.autrev.2005.10.013.

Shang, J. and Zhao, Z. (2017) 'Emerging role of HuR in inflammatory response in kidney diseases', *Acta Biochimica et Biophysica Sinica*, 49(9), pp. 753–763. doi: 10.1093/abbs/gmx071.

Sharif, O. *et al.* (2007) 'Transcriptional profiling of the LPS induced NF- κ B response in macrophages', *BMC Immunology*, 8, pp. 1–17. doi: 10.1186/1471-2172-8-1.

Shi, Y. (2004) 'Caspase activation, inhibition, and reactivation: A mechanistic view', *Protein Science*, 13(8), pp. 1979–1987. doi: 10.1110/ps.04789804.

de Silanes, I. L. *et al.* (2004) 'Identification of a target RNA motif for RNA-binding protein HuR', *Proceedings of the National Academy of Sciences*, 101(9), pp. 2987–2992. doi: 10.1073/pnas.0306453101.

de Silanes, I. L. *et al.* (2008) 'Hu proteins regulate polyadenylation by blocking sites containing U-rich sequences', *Journal of Biological Chemistry*. Nature Publishing Group, 283(3), pp. 479–490. doi: 10.1038/s41590-017-0028-4.

Skliris, A. *et al.* (2015) 'Neuroprotection requires the functions of the RNA-binding protein HuR', *Cell Death and Differentiation*. Nature Publishing Group, 22(5), pp. 703–718. doi: 10.1038/cdd.2014.158.

Smale, S. T. (2012) 'Transcriptional regulation in the innate immune system', *Current Opinion in*

- Immunology*, 24(1), pp. 51–57. doi: 10.1016/j.coi.2011.12.008.
- Soller, M., Li, M. and Haussmann, I. U. (2010) 'Determinants of ELAV gene-specific regulation', *Biochemical Society Transactions*, 38(4), pp. 1122–1124. doi: 10.1042/bst0381122.
- Srikantan, S. and Gorospe, M. (2011) 'UneCLIPsing HuR Nuclear Function', *Molecular Cell*. Elsevier Inc., 43(3), pp. 319–321. doi: 10.1016/j.molcel.2011.07.016.
- Sun, L. *et al.* (2011) 'Triptolide inhibits COX-2 expression by regulating mRNA stability in TNF- α -treated A549 cells', *Biochemical and Biophysical Research Communications*. Elsevier Inc., 416(1–2), pp. 99–105. doi: 10.1016/j.bbrc.2011.11.004.
- Sweet, M. J. and Hume, D. A. (1996) 'Endotoxin signal transduction in macrophages', *Journal of Leukocyte Biology*, 60(1), pp. 8–26. doi: 10.1002/jlb.60.1.8.
- Takeuchi, O. and Akira, S. (2010) 'Pattern recognition receptors and inflammation.', *Cell*. Elsevier Inc., 140(6), pp. 805–20. doi: 10.1016/j.cell.2010.01.022.
- Tan, S. *et al.* (2017) 'Post-transcriptional regulation of ERBB2 by miR26a/b and HuR confers resistance to tamoxifen in estrogen receptor-positive breast cancer cells', *Journal of Biological Chemistry*, 292(33), pp. 13551–13564. doi: 10.1074/jbc.M117.780973.
- Tang, K., Breen, E. C. and Wagner, P. D. (2015) 'Hu protein R-mediated posttranscriptional regulation of VEGF expression in rat gastrocnemius muscle', *American Journal of Physiology-Heart and Circulatory Physiology*, 283(4), pp. H1497–H1504. doi: 10.1152/ajpheart.00813.2001.
- Techasintana, P. *et al.* (2017) 'The RNA-Binding Protein HuR Posttranscriptionally Regulates IL-2 Homeostasis and CD4 + Th2 Differentiation', *ImmunoHorizons*, 1(6), pp. 109–123. doi: 10.4049/immunohorizons.1700017.
- Tiedje, C. *et al.* (2016) 'The RNA-binding protein TTP is a global post-transcriptional regulator of feedback control in inflammation', *Nucleic Acids Research*, 44(15), pp. 7418–7440. doi: 10.1093/nar/gkw474.
- Tran, H., Maurer, F. and Nagamine, Y. (2003) 'Stabilization of urokinase and urokinase receptor mRNAs by HuR is linked to its cytoplasmic accumulation induced by activated mitogen-activated protein kinase-activated protein kinase 2.', *Molecular and cellular biology*, 23(20), pp. 7177–88. doi: 10.1128/MCB.23.20.7177.
- Turner, M. and DÍaz-Muñoz, M. D. (2018) 'RNA-binding proteins control gene expression and cell fate in the immune system review-article', *Nature Immunology*, 19(2), pp. 120–129. doi: 10.1038/s41590-017-0028-4.
- Valverde, R., Edwards, L. and Regan, L. (2008) 'Structure and function of KH domains', *FEBS Journal*, 275(11), pp. 2712–2726. doi: 10.1111/j.1742-4658.2008.06411.x.
- Vaure, C. and Liu, Y. (2014) 'A comparative review of toll-like receptor 4 expression and functionality in different animal species', *Frontiers in Immunology*, 5(JUL). doi: 10.3389/fimmu.2014.00316.
- Viiri, J. *et al.* (2013) 'Autophagy Activation Clears ELAVL1/HuR-Mediated Accumulation of SQSTM1/p62 during Proteasomal Inhibition in Human Retinal Pigment Epithelial Cells', *PLoS ONE*, 8(7), pp. 1–16. doi: 10.1371/journal.pone.0069563.
- Wada, T. and Becskei, A. (2017) 'Impact of methods on the measurement of mma turnover', *International Journal of Molecular Sciences*, 18(12). doi: 10.3390/ijms18122723.

- Wang, H. *et al.* (2013) 'The structure of the ARE-binding domains of Hu antigen R (HuR) undergoes conformational changes during RNA binding', *Acta Crystallographica Section D: Biological Crystallography*, 69(3), pp. 373–380. doi: 10.1107/S0907444912047828.
- Wang, H. *et al.* (2016) 'Dysregulation of TTP and HuR plays an important role in cancers', *Tumor Biology*. *Tumor Biology*, 37(11), pp. 14451–14461. doi: 10.1007/s13277-016-5397-z.
- Wang, J. *et al.* (2013) 'Multiple functions of the RNA-binding protein HuR in cancer progression, treatment responses and prognosis', *International Journal of Molecular Sciences*, 14(5), pp. 10015–10041. doi: 10.3390/ijms140510015.
- Wang, J. *et al.* (2019) 'Deletion of the RNA regulator HuR in tumor-associated microglia and macrophages stimulates anti-tumor immunity and attenuates glioma growth', *Glia*, (June), pp. 1–16. doi: 10.1002/glia.23696.
- Wang, W. *et al.* (2000) 'Wang,W., Caldwell,M.C., Lin,S., Furneaux,H. and Gorospe,M. (2000) HuR regulates cyclin A and cyclin B1 mRNA stability during cell proliferation. *EMBO J.*, 19, 2340–23450..pdf>', 19(10).
- Wang, W. *et al.* (2002) 'Loss of HuR Is Linked to Reduced Expression of Proliferative Genes during Replicative Senescence', *Molecular and Cellular Biology*, 21(17), pp. 5889–5898. doi: 10.1128/mcb.21.17.5889-5898.2001.
- Wang, Y. *et al.* (2014) 'Simultaneous reduction of aldehyde group to hydroxymethyl group in palladium-catalyzed Suzuki cross-coupling reaction', *Chemical Research in Chinese Universities*, 30(4), pp. 614–618. doi: 10.1007/s40242-014-3562-8.
- Wang, Y. *et al.* (2019) 'M1 and M2 macrophage polarization and potentially therapeutic naturally occurring compounds', *International Immunopharmacology*. Elsevier, 70(January), pp. 459–466. doi: 10.1016/j.intimp.2019.02.050.
- Wang, Z., Bhattacharya, A. and Ivanov, D. N. (2015) 'Identification of Small-Molecule Inhibitors of the HuR/RNA Interaction using a fluorescence polarization screening assay followed by NMR validation', *PLoS ONE*, 10(9), pp. 1–13. doi: 10.1371/journal.pone.0138780.
- Wender, P. A., Quiroz, R. V. and Stevens, M. C. (2015) 'Function through Synthesis-Informed Design', *Accounts of Chemical Research*, 48(3), pp. 752–760. doi: 10.1021/acs.accounts.5b00004.
- Wu, X. *et al.* (2015) 'Identification and Validation of Novel Small Molecule Disruptors of HuR-mRNA Interaction', *ACS Chemical Biology*, 10(6), pp. 1476–1484. doi: 10.1021/cb500851u.
- Wu, X. *et al.* (2017) 'A-44G transition in SMN2 intron 6 protects patients with spinal muscular atrophy', *Human Molecular Genetics*, 26(14), pp. 2768–2780. doi: 10.1093/HMG/DDX166.
- Yeruva, S., Ramadori, G. and Raddatz, D. (2008) 'NF- κ B-dependent synergistic regulation of CXCL10 gene expression by IL-1 β and IFN- γ in human intestinal epithelial cell lines', *International Journal of Colorectal Disease*, 23(3), pp. 305–317. doi: 10.1007/s00384-007-0396-6.
- Yiakouvaki, A. *et al.* (2012) 'Myeloid cell expression of the RNA-binding protein HuR protects mice from pathologic inflammation and colorectal carcinogenesis', *Journal of Clinical Investigation*, 122(1), pp. 48–61. doi: 10.1172/JCI45021.
- Yoo, Mulkeen and Cha (2006) 'Post-transcriptional regulation of vascular endothelial growth factor: Implications for tumor angiogenesis', *World Journal of Gastroenterology*, 12(31), pp. 4937–4942.
- Yu, C. *et al.* (2015) 'Human antigen R mediated post-transcriptional regulation of epithelial-

mesenchymal transition related genes in diabetic nephropathy', *Journal of Diabetes*, 7(4), pp. 562–572. doi: 10.1111/1753-0407.12220.

Yu, T. X. *et al.* (2011) 'Chk2-dependent HuR phosphorylation regulates occludin mRNA translation and epithelial barrier function', *Nucleic Acids Research*, 39(19), pp. 8472–8487. doi: 10.1093/nar/gkr567.

Yuan, Z. *et al.* (2011) 'Knockdown of human antigen R reduces the growth and invasion of breast cancer cells in vitro and affects expression of cyclin D1 and MMP-9', *Oncology Reports*, 26(1), pp. 237–245. doi: 10.3892/or.2011.1271.

Zanzoni, A. *et al.* (2019) 'Post-transcriptional regulatory patterns revealed by protein-RNA interactions', *Scientific Reports*. Springer US, 9(1), pp. 1–13. doi: 10.1038/s41598-019-40939-2.

Zhang, F. *et al.* (2019) 'Multiple functions of HuR in urinary tumors', *Journal of Cancer Research and Clinical Oncology*. Springer Berlin Heidelberg, 145(1), pp. 11–18. doi: 10.1007/s00432-018-2778-2.

Zhang, J. *et al.* (2012) 'Macrophage β 2integrin-mediated, HuR-dependent stabilization of angiogenic factor-encoding mRNAs in inflammatory angiogenesis', *American Journal of Pathology*, 180(4), pp. 1751–1760. doi: 10.1016/j.ajpath.2011.12.025.

Zhang, Z. *et al.* (2017) 'HuR promotes breast cancer cell proliferation and survival via binding to CDK3 mRNA', *Biomedicine and Pharmacotherapy*. Elsevier Masson SAS, 91, pp. 788–795. doi: 10.1016/j.biopha.2017.04.063.

Zhou, A. *et al.* (2018) 'HuR-mediated SCN5A messenger RNA stability reduces arrhythmic risk in heart failure', *Heart Rhythm*. Heart Rhythm Society, 15(7), pp. 1072–1080. doi: 10.1016/j.hrthm.2018.02.018.

Zucal, C., D'Agostino, V., Loffredo, R., Mantelli, B., Thongon, N., *et al.* (2015) 'Targeting the Multifaceted HuR Protein, Benefits and Caveats.', *Current drug targets*, 16(February), pp. 1–17. doi: 10.2174/1389450116666150223163632.

Zucal, C., D'Agostino, V., Loffredo, R., Mantelli, B., NatthakanThongon, *et al.* (2015) 'Targeting the Multifaceted HuR Protein, Benefits and Caveats', *Current Drug Targets*, 16(5), pp. 499–515. doi: 10.2174/1389450116666150223163632.

APPENDIX

During my PhD, my work has been mainly focused on characterization of inhibitors towards RNA binding protein HuR/ELAVL1 activity, this led to the listed publications:

Screening Approaches for Targeting Ribonucleoprotein Complexes: A New Dimension for Drug Discovery.

D'Agostino VG, Sighel D, Zucal C, **Bonomo I**, Micaelli M, Lolli G, Provenzani A, Quattrone A, Adami V.

SLAS Discov. 2019

Interfering with HuR-RNA Interaction: Design, Synthesis and Biological Characterization of Tanshinone Mimics as Novel, Effective HuR Inhibitors.

Manzoni L, Zucal C, Maio DD, D'Agostino VG, Thongon N, **Bonomo I**, Lal P, Miceli M, Baj V, Brambilla M, Cerofolini L, Elezgarai S, Biasini E, Luchinat C, Novellino E, Fragai M, Marinelli L, Provenzani A, Seneci P.

J Med Chem. 2018

The Natural Carotenoid Crocetin and the Synthetic Tellurium Compound AS101 Protect the Ovary against Cyclophosphamide by Modulating SIRT1 and Mitochondrial Markers.

Di Emidio G, Rossi G, **Bonomo I**, Alonso GL, Sferra R, Vetuschi A, Artini PG, Provenzani A, Falone S, Carta G, D'Alessandro AM, Amicarelli F, Tatone C.

Oxid Med Cell Longev, 2017.


Regulation of HuR structure and function by dihydrotanshinone-I.

Lal P, Cerofolini L, D'Agostino VG, Zucal C, Fuccio C, **Bonomo I**, Dassi E, Giuntini S, Di Maio D, Vishwakarma V, Preet R, Williams SN, Fairlamb MS, Munk R, Lehmann E, Abdelmohsen K, Elezgarai SR, Luchinat C, Novellino

E, Quattrone A, Biasini E, Manzoni L, Gorospe M, Dixon DA, Seneci P, Marinelli L, Fragai M, Provenzani A.

NAR, 2017

Screening Approaches for Targeting Ribonucleoprotein Complexes: A New Dimension for Drug Discovery

SLAS Discovery
1–18
© 2019 Society for Laboratory
Automation and Screening
DOI: 10.1177/2472555218818065
journals.sagepub.com/home/jbx


Vito Giuseppe D'Agostino¹, Denise Sighel¹, Chiara Zucal¹, Isabelle Bonomo¹, Mariachiara Micaelli¹, Graziano Lolli¹, Alessandro Provenzani¹, Alessandro Quattrone¹, and Valentina Adami²

Abstract

RNA-binding proteins (RBPs) are pleiotropic factors that control the processing and functional compartmentalization of transcripts by binding primarily to mRNA untranslated regions (UTRs). The competitive and/or cooperative interplay between RBPs and an array of coding and noncoding RNAs (ncRNAs) determines the posttranscriptional control of gene expression, influencing protein production. Recently, a variety of well-recognized and noncanonical RBP domains have been revealed by modern system-wide analyses, underlying an evolving classification of ribonucleoproteins (RNPs) and their importance in governing physiological RNA metabolism. The possibility of targeting selected RNA–protein interactions with small molecules is now expanding the concept of protein “druggability,” with new implications for medicinal chemistry and for a deeper characterization of the mechanism of action of bioactive compounds. Here, taking SF3B1, HuR, LIN28, and Musashi proteins as paradigmatic case studies, we review the strategies applied for targeting RBPs, with emphasis on the technological advancements to study protein–RNA interactions and on the requirements of appropriate validation strategies to parallel high-throughput screening (HTS) efforts.

Keywords

RBP, RNP, RNA–protein interaction, HTS, RBP targeting

Introduction

The posttranscriptional control of gene expression in eukaryotic cells defines all the steps related to mRNA metabolism, from its maturation/processing to its subcellular localization and decoding for protein production. The RNA-binding proteins (RBPs) participate in the formation of ribonucleoprotein (RNP) complexes by recognizing and dynamically binding to both coding and noncoding selective RNA targets, thus profoundly influencing gene expression.¹ Recently, genome-wide identification of RBPs and their RNA targets has been facilitated by unbiased and high-throughput approaches, such as next-generation sequencing and mass spectrometry. A census published in 2014 reports 1542 human RBPs interacting with all known classes of RNAs.² The majority of RBPs are found ubiquitously expressed and directly or indirectly implicated in the process of protein synthesis, while at least one-third of them have yet unrevealed biological functions.² RBPs bind to defined motifs in target RNA via RNA-binding domains.³ These motifs are distinguished as RNA recognition motifs (RRMs), which are the most abundant protein domains in

eukaryotes,⁴ the heterogeneous nuclear RNP (hnRNP) K homology domains (KH),⁵ the DEAD box helicase domains,⁶ the double-stranded RNA-binding motifs (DSRMs), or the zinc-finger domains.⁷ The analysis of the RNA *cis* elements among 205 genes from 24 diverse eukaryotes indicated a good correlation between sequence specificities and protein domain similarities.⁸ Recent studies have uncovered hundreds of RBPs lacking conventional RNA-binding domains. This reveals the potential for novel types of RNA-binding modules mediated by new interaction modes. These could

¹University of Trento, Department of Cellular, Computational and Integrative Biology (CIBIO), Trento, Italy

²University of Trento, HTS Core Facility, Department of Cellular, Computational and Integrative Biology (CIBIO), Trento, Italy

Received Aug 1, 2018, and in revised form Oct 18, 2018. Accepted for publication Nov 19, 2018.

Corresponding Author:

Valentina Adami, University of Trento, HTS Core Facility, Department of Cellular, Computational and Integrative Biology (CIBIO), via Sommarive 9, 38123 Trento, Italy.
Email: valentina.adami@unitn.it

be favored by intrinsically disordered regions, protein–protein interaction (PPI) interfaces, and enzymatic cores.⁹

Interestingly, RBP-focused pharmacological studies have highlighted the existence of a significant posttranscriptional impact mediated by small molecules exerting antitumor properties. For instance, the antitumor activity of resveratrol has been associated with the production of pro-inflammatory cytokines via modulation of the far upstream element-binding protein 2 (KHSRP)¹⁰ and more recently via activation of the mRNA-decay factor tristetraprolin (TTP).¹¹ The small molecule PTC-299¹² or PTC-510¹³ has been reported to target the 3'-untranslated region (UTR) of vascular endothelial growth factor (VEGF) mRNA in tumor cells. Furthermore, the antibacterial compound enoxacin has been proven to enhance the stability of selected miRNAs (premiR-125a, prelet-7, and premiR-30a), acting as tumor suppressors by binding to the TAR RNA-binding protein 2 (TRBP2).¹⁴ This evidence suggests that the enhancement or inhibition of the activity of RNPs can be exploited to modulate the posttranscriptional control of gene expression with potential benefits in disease-related states.

In the Online Mendelian Inheritance in Man (OMIM) database, ~150 RBPs targeting both mRNAs and noncoding RNAs (ncRNAs) are linked to human diseases.⁷ However, the majority of RBPs lack traditional enzymatic pockets or functional epitopes that could classify them as canonical “druggable targets.” Indeed, the explored drug targets are largely biased toward enzymes, easily assayable in high-throughput screening (HTS) format, and often use small-molecule cofactors inspiring the design of drug-like molecules. This bias has been reinforced by the hectic popularity of “hot” targets and by pharmaceutical companies often competing for the very same target families, that is, G-protein-coupled receptors, protein kinases, metallopeptidases, proteases, nuclear hormone receptors, and phosphodiesterases.¹⁵ Proof of this biased approach is that 90% of the 823,179 drug-like compounds targeting human proteins are directed against 278 targets, which are classical enzymes or membrane protein targets.¹⁶ These results are associated with the exploring of narrow chemical spaces corresponding to the “accessible doped space” so far considered.¹⁷ This triggers a vicious circle where commercial libraries used in HTS fail to produce useful compounds for new targets, corroborating the notion of their undruggability.

The most striking example of the recent enlargement of the druggable space is the development of several compounds interfering with PPIs, especially targeting epigenetic reader domains such as bromodomains, chromodomains, PHD zinc finger, and Tudor domains. While the majority of PPI surfaces have undruggable features (shallow and polar), a number of them become pharmacologically attractive. The above-mentioned epigenetic reader domains have aromatic and hydrophobic binding sites for neutralized lysines

(acetylated or methylated), which recognize their substrates with affinities in the low micromolar range. Therefore, competition through small molecules is a reasonably achievable task.¹⁸ Indeed, various bromodomain inhibitors are currently in clinical trials for the treatment of solid and hematological malignancies. Another class of traditionally classified undruggable targets is represented by the transcription factors, whose activity has been proven to be successfully modulated by several strategies, including the blockage of protein–DNA binding.¹⁹ Small compounds are probably not able to disrupt the transcription factor–DNA interaction, given the large interacting surface, but they can instead interfere with the dynamics of the DNA-binding domains (DBDs) and impede the subsequent molecular recognition of their target sequence.²⁰

In this context, RNPs represent a new, largely unexplored, druggable space. The challenge of targeting RNPs relies on the application of new strategies to identify and interfere with dynamic protein–RNA surfaces. Indeed, the notions uncovered with PPIs may be viewed as the archetype for the development of small molecules interfering with other types of molecular recognitions, in particular for RNP complexes and specifically for RNA reader/protective domain rather than RNA modifying enzymes (**Fig. 1**). RNA reader/protective domains have aromatic and hydrophobic pockets or channels recognizing nucleobases whose polarity can be further reduced by epitranscriptomic modifications. For RNP disruption, the well-known purine-mimicking chemical space (i.e., fragment libraries and kinase inhibitors) is of possible advantage. The above considerations expand the concept of druggability, even implying the possibility of multiple downstream effects elicited by the RNP after interference by the small molecule, in a cell-specific context.

Here we review the current high-throughput experimental approaches to probe RNA–protein interaction in RNPs. An interesting proof of principle that interfering with the binding of RBPs to their target RNA is a promising strategy in drug discovery has been recently provided by the SF3b spliceosome complex and is outlined in the next section. We also describe the physiological roles and clinical relevance of other important RNP targets, with the most successful screening strategies employed so far to identify small molecules interfering with them.

In Vitro Approaches to Study and Challenge RNA–Protein Interactions

High-resolution structural insights of macromolecular complexes provide valuable biological information on the specific interaction between the ligands. However, techniques such as x-ray crystallography, nuclear magnetic resonance (NMR), and cryo-electron microscopy (cryo-EM) have to be complemented by studies probing the dynamics and

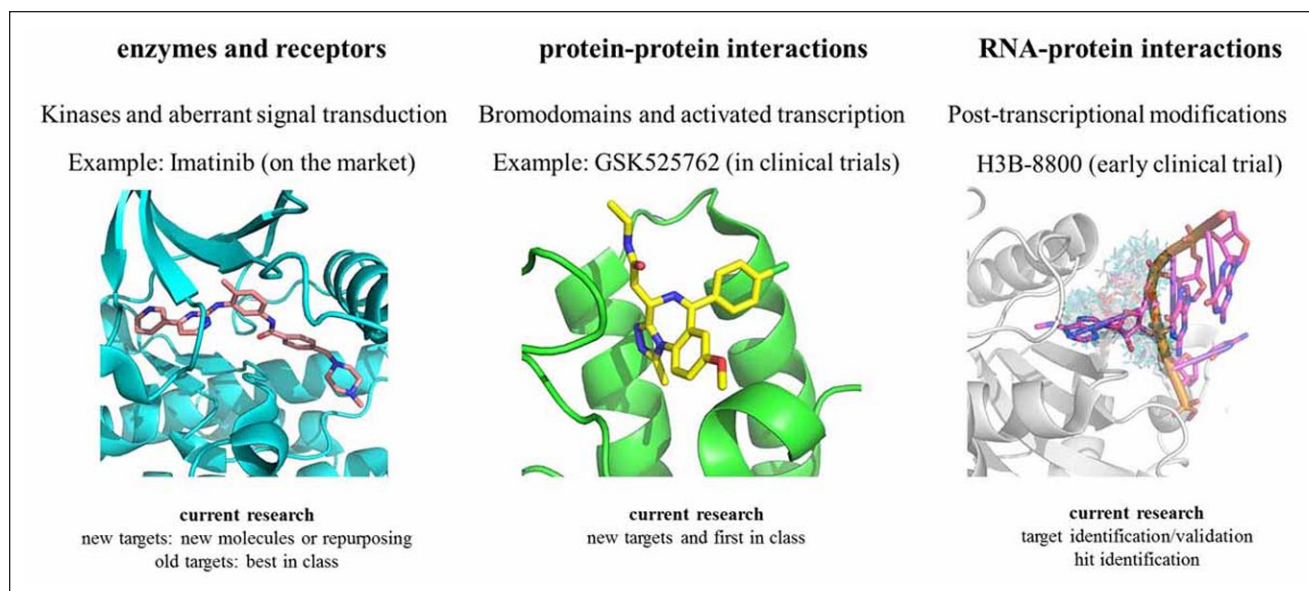


Figure 1. Expanding view of druggability: from the traditional concept of druggability, targeting enzymes or recognized epitopes, to the druggable interface responsible for RNA–protein interactions.

flexibility of a RNA–protein complex formation.²¹ A complete picture about the integrated biophysical and structural methods used to capture the structure and dynamics of RNPs is reviewed by Schlundt et al.²² Briefly, the dynamic features require solution techniques such as NMR, small-angle scattering, or fluorescence spectroscopy to complement structural analysis based on crystallography, NMR, and cryo-EM.

Several biochemical and biophysical techniques have been successfully employed to assay RNA–protein interactions *in vitro* and challenge their inhibition by small molecules. A combination of different approaches is usually adopted to unravel the mechanism by which the inhibition is exerted. Nevertheless, a primary screening assay should be able to identify both classes of interactors, binding to either the RNA or the protein, the first being more unspecific and prone to off-target effects (**Fig. 2b**). The challenging approaches aiming at identifying small molecules specifically binding RNA are well described by Deigan Warner et al. in a recent review.²³ In addition, small molecules might act by altering the protein conformation and changing the RNA binding site (**Fig. 2c**).

The common assays employed in screening campaigns are biochemically based, involving the purification, labeling, and/or immobilization of one or both the binding partners. In **Table 1** we describe the screening methods for small molecules interfering with RNA–protein interactions and those used for secondary assays and hit validation, including emerging techniques that could be adopted for screening purposes. Given the size difference of the two partners and the low complexity of the assay,

fluorescence polarization (FP) has frequently been selected in HTS campaigns, while electrophoresis mobility shift assay (EMSA), even coupled with fluorescent or infrared probes, still represents one of the standard orthogonal tests for hit confirmation. Recently, the establishment of nonradioactive bead-based assays, such as AlphaScreen (Amplified Luminescent Proximity Homogeneous Assay), and of new high-throughput instruments has improved the screening power of technologies such as microfluidic capillary mobility shift assay (MMSA) or surface plasmon resonance (SPR).

Additionally, fragment screening is nowadays possible with a low-medium throughput, also by NMR, and especially by x-ray crystallography. The latter allows obtaining the structural details required for the subsequent fragment-growing campaign, with the limitation of being applicable only to targets easily and reproducibly crystallizable.^{24,25} The throughput/molecular details and the success ratio are optimal when two or more strategies (molecular docking, HTS, NMR, and x-ray crystallography) are used in combination.^{26–28}

The success of these biochemical and biophysical approaches also depends on the combination with cell-based methods addressing the activity of RBPs at the intracellular level. The analysis of subcellular localization of RBPs, participation in nuclear transcriptional and/or post-transcriptional events, cytoplasmic accumulation in functional compartments, and the exerted effect on cargo RNA decay and translation require multiple approaches, enabling the quantification of the intracellular effects of a small molecule interfering with an RBP.

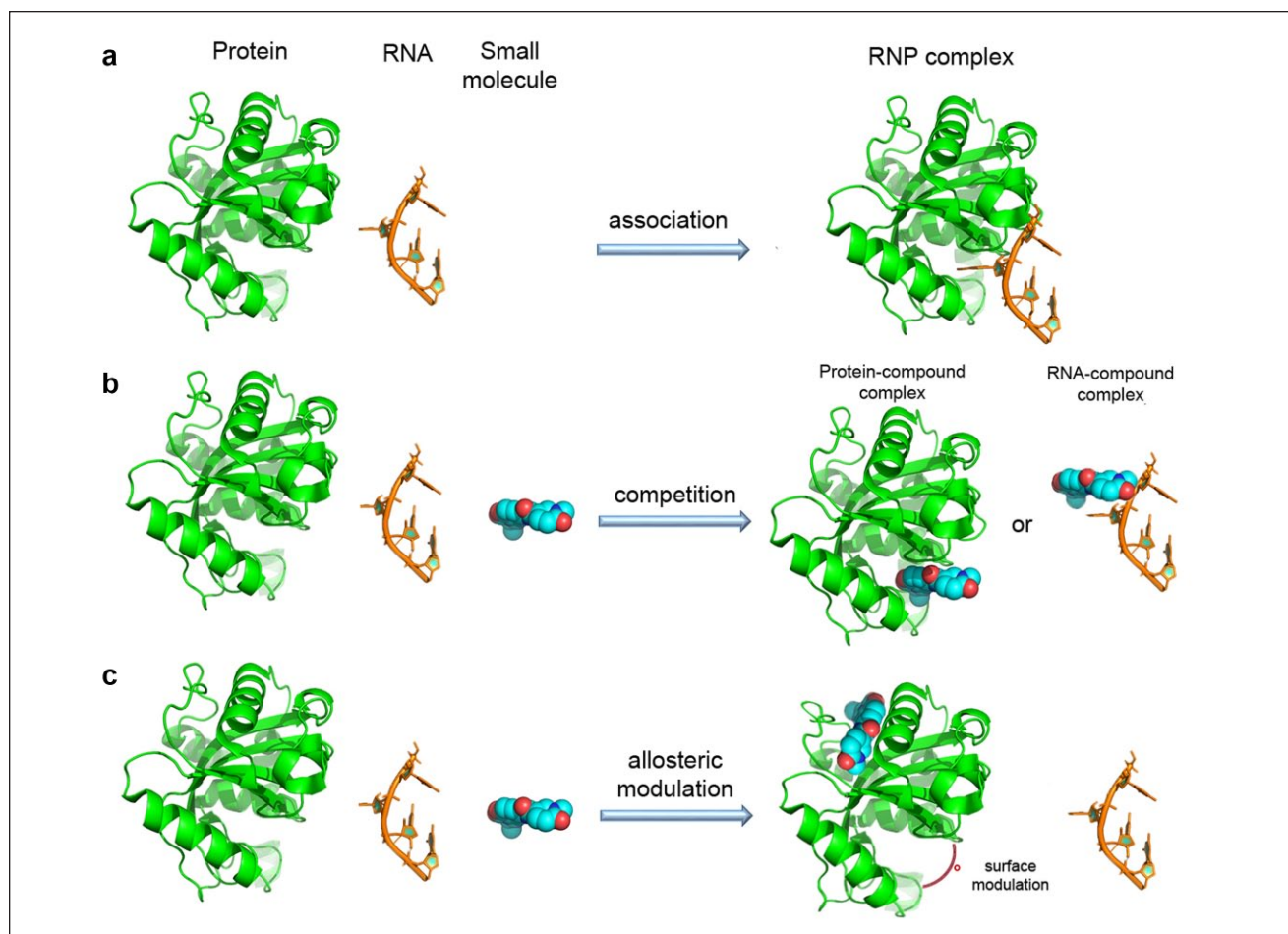


Figure 2. Multiple mechanisms by which a small molecule can interfere with the RNA–protein complex. (a) RNA–protein complex. (b) The molecule can bind directly to the target RNA, compete with RNA for the RNA binding site in the RBP, or (c) bind to another region of the protein, causing a conformational change.

Current methods developed to track RNA–protein interactions in the context of the cells include Foerster resonance energy transfer (FRET)²⁹ and trimolecular fluorescence complementation (TriFC), a novel method based on the well-established bimolecular fluorescence complementation (BiFC) technique (Fig. 3).³⁰ Both techniques allow for imaging of molecular interactions by using fluorescent probes: while FRET measures the intensity change of a dual fluorescence spectrum, fluorescence complementation only measures the specific fluorescence, with advantages in reducing the background noise. Despite the promising technical asset, no screenings have been so far reported using the TriFC assay, probably due to the technical challenges still associated with the fluorescent complementation: the low temperature required by many FC systems (below 37 °C), the self-assembly tendency of the split fragments that increases the background, and the irreversibility of fluorescent protein complementation.³¹

Initially, the idea of targeting RNA–protein interactions arose from the study of viruses like HIV. This represents a paradigmatic example of a complex system under strict control of a few “simple” RNA–protein interactions and extends the possibility to directly interfere with the surface of the molecules that evolved to bind to selected RNA motifs.³² Tat and Rev are small viral proteins involved in the mechanisms of transcriptional activation and posttranscriptional regulation (splicing, transport, etc.) and exert their function through interaction with their respective RNA targets, trans-activation-responsive element (TAR) and Rev-responsive element (RRE).³³ Because the Tat-TAR axis is essential to HIV viral transcription, it has been the subject of intense efforts aimed at developing therapeutic interventions. Since 1985, several screening campaigns have been performed.^{34–36} The aminoglycoside class of antibiotics has been proven to inhibit the Tat-TAR complex, by binding TAR RNA, and neomycin derivatives have been proposed as leads for multitarget HIV inhibition.³³

Table 1. Biochemical, Biophysical, and Cell-Based Techniques Used to Assay the RNA–Protein Binding and Its Modulation by Small Molecules.

| | Throughput | Reference | Detection Principle | Ligand Phase | Label ^a | Instrumentation |
|---|------------|------------------|---|---------------------------|--|---|
| Screening Methods | | | | | | |
| Filter binding assay | High | 179 | Absorption of the complex on cellulose filter | Surface immobilization | Fluorescence ×1 | Plate reader |
| Foerster resonance energy transfer (FRET)/TR-FRET | High | 131, 133 | FRET caused by proximity of the binding partners | Solution | Fluorescence ×2 | Plate reader |
| Fluorescence polarization (FP)/anisotropy | High | 180 | Fluorescence changes linked to rotational diffusion | Solution | Fluorescence ×1 | Plate reader with FP |
| Scintillation proximity assay (SPA) | High | 34 | Energy conversion of radioactive decay | Bead-based immobilization | Radioactive | Beta counter |
| AlphaScreen | High | 35, 104 | Energy transfer caused by proximity of the binding partners | Bead-based immobilization | Tag ×2 | Plate reader with Alpha |
| Differential scanning fluorimetry (thermal shift assay) | High | 181 | Change in protein-binding dye fluorescence intensity | Solution | Fluorescent molecule or intrinsic protein fluorescence | Fluorescence PCR |
| Microfluidic capillary mobility shift assay (MMSA) | High | 37 | Change in electrophoretic mobility in microfluidics | Solution | Fluorescence ×1 | Microfluidic gel electrophoresis system |
| Dynamic mass redistribution (DMR) | High | 107, 182 | Changes of refractive index at binding equilibrium | Surface immobilization | Label-free | Plate reader with Epic module |
| Biolayer interferometry (BLI) | High | 183 | Change of interference pattern of white light | Surface immobilization | Label-free or tag ×1 | Optical system with tip biosensors |
| Trimolecular fluorescence complementation (TriFC) | High | 30, 38 | Fluorescence reporter is reconstituted upon binding in living cells | Solution (tagged) | Fluorescence ×2 | Automated microscope |
| Validation Methods | | | | | | |
| Surface plasmon resonance (SPR) | Medium | 184, 185 | Change of refractive index during binding | Surface immobilization | Label-free or tag ×1 | Optical system with microfluidic chip |
| Electromobility shift assay (EMSA) | Low | 186 | Change in electrophoretic mobility in nondenaturing gel | Solution | Radioactive/fluorescence ×1 | Gel electrophoresis |
| Microscale thermophoresis (MST) | Low | 187, 188 | Change in motion of molecules in temperature gradient | Solution | Fluorescence ×1 | Fluorescence-microfluidic chamber heating |
| Isothermal titration calorimetry (ITC) | Low | 189 | Enthalpy of binding in a titration experiment | Solution | Label-free | Calorimeter |
| Nuclear magnetic resonance (NMR) | Low-medium | 21, 24, 190, 191 | Perturbation in chemical shift upon binding | Solution | Label-free | NMR spectrometer |
| Crystallography | Low-medium | 21, 25, 192–194 | X-ray diffraction | Crystals | Label-free | X-ray diffractometer |
| Cryo-electron microscopy (cryo-EM) | Low | 21, 45 | TEM imaging | Frozen solution | Label-free | Cryo-electron microscope |

^aLabel type and number of labeled ligands.

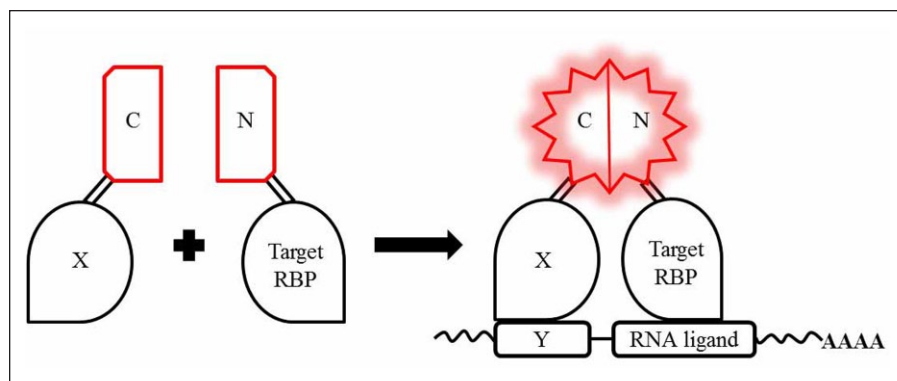


Figure 3. TriFC system for the detection of RNA–protein interaction. The C fragment of the fluorescent protein is attached to a protein X involved in a known RNA–protein interaction (X–Y). The complementing fragment N is fused to the target RBP. If the RBP interacts with a sequence of interest within the reporter mRNA close to the Y sequence, the two fragments N and C are brought into proximity to fold into a fluorescent product.

Interestingly, the high-affinity binding between Tat and TAR has been exploited by several authors to validate novel methods for RNA–protein interactions.^{37,38}

Other viral RNA–protein interactions, such as NS1 protein–influenza virus RNA,³⁹ HIV-1–Matrix protein,⁴⁰ HIV Rev–RRE,^{35,36} and HCV-IRES,⁴¹ have been targeted by biochemical assays for screening small molecules. **Table 2** reports these references, together with the other target RBPs described in the following paragraphs.

SF3b Complex and the First-in-Class Small Molecule in Clinical Trial

Splicing and alternative splicing of mRNA precursors is necessary for the removal of introns and the production of mature mRNAs. These events involve almost the entire human transcriptome and strongly contribute to the regulation of cellular gene expression programming. In the spliceosome machinery, the splicing factor 3B subunit 1 (SF3B1) protein is the largest component of the heptameric SF3b subcomplex in the U2 small nuclear RNP (snRNP) and supports the splicing via the recognition and selection of the branch point adenosine (BPA).^{42,43} SF3B1 is functionally associated with PHD finger protein 5A (PHF5A), SF3B3, and SF3B5 and forms a scaffold complex of ~250 kDa that allows the subsequent recruitment of additional splicing factors.⁴⁴ SF3B1 is composed of 20 HEAT repeats that form a superhelical spiral. This spiral wraps around PHF5A and establishes contact regions with the polypyrimidine tract of the pre-mRNA and the BPA. In the *apo* form, the SF3B1 protein assumes an open conformation. Binding to the RNA induces SF3B1 to close up on the RNA itself.⁴⁵

Aberrations in RNA splicing, leading, for example, to intron retention, are common across cancers in comparison to the normal counterpart.^{46,47} Somatic mutations in genes encoding core spliceosomal proteins and associated RNA splicing factors, such as SF3B1, U2 small nuclear RNA auxiliary factor 1 (U2AF1), and SRF2, are commonly present in several cancers, including myelodysplastic syndromes (MDSs),⁴⁸ chronic myelomonocytic leukemia

(CMML),⁴⁸ and chronic lymphocytic leukemia (CLL),⁴⁹ and in a number of solid tumors, including breast,⁵⁰ lung,⁵¹ uveal melanoma,⁵² and pancreatic carcinomas.⁵³ Mutated splicing factors confer a strong vulnerability to the associated cancer type as shown by genetic and pharmacological perturbation of the splicing process.^{54,55} These mutations represent a genetic link between dysfunction of the splicing machinery and cancer, thus providing a strong rationale for targeting the spliceosome as a new anticancer therapy.⁵⁶

The development of spliceosome-targeting small molecules accelerated when potent anticancer natural compounds isolated from bacteria as FR901464, herboxiedenes, and pladienolides^{57–59} turned out to target the SF3b subcomplex of U2 snRNP and to interrupt early stages of spliceosome assembly. Using biotinylated chemical probes, spliceostatin, a methylated pladienolide derivative of FR901464 and E7107, was found to exert antitumor activity by modulating the splicing process via the SF3B complex.^{60,61} Later efforts have led to the chemical synthesis of herboxiedenes⁶² and of FR901464 analogs, a new class of small molecules called sudemycins, that showed similar splicing inhibition as spliceostatin.⁶³

Based on important preclinical indications,^{54,64} E7107 entered clinical trials for locally advanced or metastatic solid tumors (Study E7107-A001-101; trial registration ID: NCT00499499).^{65,66} Unfortunately, the trials were suspended due to toxic bilateral optic neuritis.

The ability of E7107 to modulate the spliceosome activity has been readily explained by structural studies using cryo-EM: E7107 binds to the branch point of the adenosine-binding pocket, at the interface of SF3B1, namely, the HR domains 15–17, and PHF5A, in a hydrophobic region. Comparison of the *apo* form of the tetrameric (SF3B1, PHF5A, SF3B3, SF3B5) complex with the bound ligands showed that E7107 binds to the pre-mRNA-unbound form or the so-called open conformation of the complex. The cryo-EM data indicate that E7107 directly competes with pre-mRNA for binding to the *apo* form of the complex, suggesting that E7107 would more easily inhibit weaker pre-mRNA substrates.⁴⁵

Table 2. Screening and Screening Assays to Identify Small Molecules Interfering with RNA–Protein Interactions.

| Target | Reference | Year | Screening Assay | Throughput ^a | Validated Compounds ^b |
|--------------------------------|-----------|------|---|-------------------------|---|
| HuR-IL2 ARE | 72 | 2007 | Confocal fluctuation spectroscopic (anisotropy) | 50,000 | MS-444, okicenone |
| HuR-TNF α ARE | 103 | 2009 | RNA EMSA and filter binding assays | 179 | Quercetin, b-40, b-41 |
| HuR-TNF α ARE | 104 | 2013 | AlphaScreen | 2000 | Mitoxantrone |
| HuR-TNF α ARE | 105 | 2015 | AlphaScreen | 107 | Dihydrotanshinone-I |
| HuR-MSII ARE | 109 | 2015 | FP | 6000 | CMLD 1-6, NCI-3 |
| HuR-C-Fos ARE | 108 | 2015 | FP | 1597 | C10 |
| HuR-MSII ARE | 110 | 2017 | FP | 2000 | Azaphilone-9 (AZA-9) |
| LIN28-pre-let-7f-1 | 132 | 2018 | FP | 101,017 | DAQ-BI (demethylasterriquinone), BVT-948, gossypol, LI20, LI71, TPEN |
| LIN28-pre-let-7a-2 | 133 | 2016 | FRET | 16,000 | <i>N</i> -methyl- <i>N</i> -[3-(3-methyl[1,2,4]triazolo[4,3- <i>b</i>]pyridazin-6-yl)phenyl]acetamide (compound 1632) |
| LIN28-pre-let-7g | 134 | 2016 | FP | 2768 | Aurintricarboxylic acid, 6-hydroxy-DL-DOPA, Reactive Blue 2, SB/ZW/0065 |
| LIN28-pre-let-7a-1 | 131 | 2016 | FRET | 4500 | Benzopyranylpyrazole based |
| MSI-RNA | 155 | 2014 | FP | 6208 | Inhibitors 1, 2, 3 |
| MSI-RNA | 195 | 2018 | FP | Assay validation | Ro 08-2750 (Ro) |
| NHP2LI-U4 | 68 | 2018 | TR-FRET | 10,173 | Topotecan |
| Translation initiation factors | 196 | 2009 | FP | 30,000 | Thiol reactive compound |
| MDM2 - XIAP | 158 | 2017 | FP | 141,394 | MX69, MX3 |
| La-cyclin D1 RNA | 197 | 2017 | FP | 50,080 | 8-(Isobutoxycarbonyl)-3a,4,5,9b-tetrahydro-3 <i>H</i> -cyclopenta[<i>c</i>]quinoline-4-carboxylic acid, 2-(2-hydroxy-4-methylbenzoyl)benzoic acid |
| CsrA-RNA | 184 | 2016 | SPR and FP | 1000 | MM14, NAT31-454537 |
| HCV-IRES | 41 | 2013 | FRET | 97 | Benzoxazole derivative |
| HIV-1 Matrix protein–RNA | 40 | 2013 | Plate binding and FP | 14,000 | Thiadiazolanes |
| HIV Tat-TAR | 34 | 1997 | SPA and filtration | 150,000 | Aminoglycoside neomycin B |
| HIV Tat-TAR and Rev-RRE | 36 | 2001 | Dual-labeled plate assay | 110,000 | Ba13338, Ba18945E |
| HIV Tat-TAR and Rev-RRE | 35 | 2007 | AlphaScreen and FP | 5500 | Propidium iodide, glutathione analog, suramin, suramin analog (NFI10) |
| Influenza virus NSI-RNA | 39 | 2008 | Flashplate (radioactivity) | 27,520 | Molecules A, B, and C |
| Influenza virus NSI-RNA | 38 | 2013 | TriFC | Assay validation | |

Csr = carbon storage regulator; La = La autoantigen (La, LARP3); MDM2 = Mouse Double Minute 2.

^aNumber of molecules tested in the primary screening, when applicable.

^bPrimary screening hits confirmed by using secondary in vitro or in vivo assays.

Starting from E7107, an orally available modulator of the SF3b complex, called H3B-8800, was generated by medicinal chemistry. The competitive mechanism of action of H3B-8800 is similar to that of pladienolide, and H3B-8800 potently binds and inhibits splicing catalysis by both WT SF3B1 and its mutant forms in vitro. However, differently from pladienolide, H3B-8800 preferentially kills spliceosome-mutant epithelial and hematologic tumor cells.

Mutations of either SF3B1, SRSF2, or U2AF1 confer to cancer cells a dependency on the remaining WT spliceosome. H3B-8800 causes the enrichment of short, GC-rich intron retention in mRNAs encoding RNA splicing factors, providing an explanation for H3B-8800's preferential killing of spliceosome-mutant tumor cells.⁶⁷

H3B-8800 has been proposed for the treatment of genetically defined subsets of cancer with RNA splicing factor

mutations. H3B-8800 is currently being tested in a phase 1 clinical trial (NCT02841540) for MDSs, acute myeloid leukemia, and CMML. Notably, H3B-8800 and E7107 well represent the first-in-class small molecules that modulate the activity of RNP complexes with a therapeutic outcome and a precise indication of use.

Interestingly, other well-known drugs, such as topotecan, have been recently shown to inhibit RNA splicing.⁶⁸ In this work Diouf et al. report a time-resolved (TR)-FRET screening to find small molecules disrupting the interaction between NHP2L1 protein and U4, revealing an additional posttranscriptional activity of this drug.

HuR

Human antigen R (HuR; also known as ELAVL1) is among the most widely studied RBP. It regulates the splicing, stability, and translation of thousands of coding and noncoding RNAs.^{69–71} The posttranscriptional function has been described for a wide number of transcripts bearing AU-rich elements (AREs), whose turnover is critical for tissue differentiation and cell physiology.

HuR protein comprises three RNA-recognition motifs (RRMs): RRM1, RRM2, and RRM3. The N-terminal ones are arranged in tandem (RRM1–RRM2), whereas RRM2 and RRM3 are joined by a hinge region. While the first two regions are involved in the binding to target RNAs,⁷⁰ RRM3 has been reported to bind to poly-A tail and to be involved in protein oligomerization.^{72,73} The HuR crystal structure of RRM1–RRM2 was solved in both the RNA-free and RNA-bound form of the protein and revealed a conformational change undergone by HuR after RNA binding.⁷⁴

HuR is ubiquitously expressed, is normally located in the nucleus, and shuttles to cytoplasm upon cell stresses as DNA damage or hypoxia.⁷⁵ In the nucleus, it exerts posttranscriptional functions such as splicing^{76,77} and alternative polyadenylation.⁷⁸

HuR is fundamental during the development of the embryo, as its deletion leads to embryonic lethality, and affects the adult tissue homeostasis.^{79,80} It plays a role in the maturation of lymphocytes (B and T) and macrophages and regulates the expression of specific chemokines and cytokines.^{81–83} By binding to AREs in target mRNAs, it modulates the expression of specific transcripts coding for proteins involved in inflammation,^{83,84} cell division,⁸⁵ angiogenesis,^{86,87} senescence,⁸⁸ apoptosis,^{89,90} immune,^{91,92} and hypoxia response.⁹³ Therefore, HuR is involved in the cellular response to different stimuli and impairment of its related gene expression can impact different disease processes. HuR was reported to be implicated in cancer and chronic inflammation and linked to cardiovascular, neurological, and muscular pathologies.⁹⁴

HuR posttranscriptional regulation can sustain cancer traits, such as increased cell proliferation and survival,

elevated local angiogenesis, immune recognition evasion, tumor cell invasion, and metastasis, due to its stabilizing function of many key mRNA encoding proteins implicated in carcinogenesis.⁹⁵ Furthermore, overexpression of HuR or its cytoplasmic localization is associated with tumor progression and poor prognosis in various cancer types, including breast,^{96,97} colon,^{98,99} ovarian, prostate, pancreatic, and oral cancer.⁹⁵ HuR nucleo-cytoplasmic translocation in malignant cells has been reported for many tumors and correlated with advanced clinicopathological parameters and decreased patient survival rate.¹⁰⁰ Moreover, observations from animal models confirm a critical role for HuR in sustaining colon cancer formation and progression.¹⁰¹ Therefore, HuR has been proposed as a valuable drug target based on all the reported posttranscriptional regulations involved in different pathologies and its ubiquitous expression in malignant samples.¹⁰²

The pivotal role of HuR in several diseases, such as inflammation and cancer, led to searching for inhibitors/modulators able to impact HuR activity.¹⁰² Different compounds have been identified as able to interfere at the level of RNA–HuR complex formation.

In 2007, Meisner et al. identified the first low-molecular-weight HuR inhibitors. The authors screened 50,000 compounds using a confocal fluctuation spectroscopic assay with a shortened variant of recombinant HuR. The most potent hits that have been found were dehydromutactin, MS-444, and okicenone. The mechanism of action of these compounds has been proposed through mathematical and experimental analysis and resulted in the prevention of HuR homo-dimerization by binding the first two RRM. This is reflected by inhibiting HuR activity as nucleus–cytoplasm shuttling, cytokine expression, and primary T-cell line activation.⁷²

In 2009, Chae et al. identified chemical inhibitors of the interaction between HuR and the ARE of tumor necrosis factor alpha (TNF α) mRNA using RNA-EMSA and a filter binding assay.¹⁰³ In particular, they generated a recombinant glutathione S-transferase (GST) fusion protein with HuR and TTP, and used these recombinant proteins and radiolabeled RNA containing the ARE sequence from TNF α to perform RNA-EMSA. From the screening of a total of 179 chemicals, three compounds, quercetin, b-40, and b-41, respectively, showed a half-maximal inhibitory concentration (IC₅₀) below 10 μ M. The IC₅₀ values of the three compounds were 1.4, 0.38, and 6.21 μ M, respectively, for the binding between HuR protein and TNF α mRNA. Further experiments were performed in RAW264.7 cells treated with lipopolysaccharide (LPS), quercetin, and b-40, and a decrease in the stability of TNF α mRNA and the secreted protein was observed.¹⁰³

A novel biochemical assay to study *in vitro* HuR protein–RNA complex formation, feasible for HTS, has been proposed in 2013. This assay is based on AlphaScreen

technology, in which the binding efficacy is evaluated between a purified human HuR protein and a probe with the sequence of TNF α ARE. This method allowed to calculate HuR binding parameters under saturation binding and kinetic conditions, quantifying HuR-RNA Kd in the low nanomolar range. The results were further validated by fluorescent probe-based RNA-EMSA. In this work, 2000 small molecules were screened, and after a secondary validation with RNA-EMSA, mitoxantrone was identified as a modulator of the RNA-binding activity.¹⁰⁴

Furthermore, in 2015 the same group identified the natural compound dihydrotanshinone-I (DHTS), belonging to the family of tanshinones, as interfering with HuR binding activity. DHTS was further validated with complementary assays such as the EMSA, NMR titration, and molecular dynamics simulation, demonstrating that DHTS interacts with HuR at the level of the mRNA binding site, thus preventing the complex formation.^{105,106} The in cellulo confirmation has been performed with different cell lines toward the control of TNF α , CTNNB1, and ERBB2 mRNA targets.¹⁰⁵

Recently, DHTS has been demonstrated to inhibit in vivo xenograft tumor growth in a HuR-dependent model without systemic toxicity.¹⁰⁶ As a consequence, DHTS has been considered the leading compound for the synthesis of analogs, called tanshinone mimics, in order to enhance the efficacy in inhibiting HuR activity.¹⁰⁷

In 2015, Wang et al. presented an integrated approach to select inhibitors of HuR-RNA interaction using fluorescence-based HTS. This method was used to screen a library of 1597 compounds and hit validation was performed through the NMR method with saturation transfer difference (STD) detection. In this case, the authors identified the mechanism of action of these compounds, based on the disruption of HuR oligomerization, thus blocking the RNA binding.¹⁰⁸

A further screening was performed in 2015 by FP assay, using HuR protein and an ARE oligo from Musashi RNA-binding protein 1 (MSI1) mRNA, a HuR target. Wu et al. performed an HTS of about 6000 compounds; the potential disruptors were then validated by AlphaLISA, SPR, RNP immunoprecipitation (IP) assay, and luciferase reporter studies. These compounds inhibit HuR-ARE interactions at the nanomolar range and prevent HuR function by competitive binding with HuR.¹⁰⁹

Lastly, in 2017, through another FP competition HTS assay, Kaur et al. isolated the compound azaphilone-9 (AZA-9) that derives from the fungal natural product asperbenzaldehyde. AZA-9 is able to bind to HuR and inhibit HuR-ARE interaction with an IC₅₀ of 1.2 μ M. Data were validated with SPR, in which the authors were able to verify the direct binding of AZA-9 to HuR. NMR methods identified the involvement of critical RNA-binding residues in binding with AZA-9. Computational docking was then applied to propose a predictive binding site for AZA-9 in

the RNA-binding cleft of HuR.¹¹⁰ Similar to others, this work was able to identify HuR-RNA disruptors in vitro.

Considering the structural diversity of the compounds discovered so far and their mechanisms of interfering with ELAV protein-mRNA complexes, the structure-activity relationship is still a challenge.

LIN28

LIN28 protein was first described in *Caenorhabditis elegans* in association with its important role in development and in developmental timing.¹¹¹ LIN28 is highly expressed in the early developmental stages and in stem cells, decreases upon differentiation, and is normally absent in most differentiated cells in the adult.^{112,113}

The mammalian genome encodes for two LIN28 paralogs: LIN28A and LIN28B. The term *LIN28* will be used to refer collectively to LIN28A and LIN28B in this section. The human LIN28A protein, which is composed of 209 amino acids, and the human LIN28B protein, which consists of 250 amino acids, share a high degree of homology in their structure and function.¹¹⁴ Both LIN28A and LIN28B proteins present a cold-shock domain (CSD) and a zinc knuckle domain (ZKD), composed of two CysCysHisCys (CCHC) zinc finger domains.¹¹⁵⁻¹¹⁸ These highly conserved regions are responsible for interacting and binding with target miRNAs and mRNAs.

The let-7 family of miRNAs is the most studied LIN28 interactor and consists of different members, including let-7a-i, mir-98, and mir-202. LIN28 binds to precursor forms of let-7 (pri- and pre-let-7) using both the CSD, which binds to let-7 terminal loops and contributes to most of the LIN28-let-7 binding affinity, and the ZKD, which recognizes a highly conserved GGAG sequence motif.¹¹⁷ Upon binding, LIN28 prevents let-7 maturation and leads to decreased levels of mature let-7, which in turn cannot exert its tumor suppressor activity on its multiple target genes, such as RAS, MYC, and high-mobility group-A2 (HMGA2).¹¹⁴ LIN28A initiates pre-let-7 degradation via recruitment of the terminal uridylyltransferases (TUTases) TUT4 and TUT7, which oligouridylylate the pre-let-7 RNA in the cytoplasm.¹¹⁹⁻¹²¹ The mechanism of LIN28B-mediated let-7 inhibition, as well as its cellular localization, remains controversial. LIN28B has been shown to directly bind to precursor let-7 transcripts in the nucleus and to prevent the pri-let-7 cleavage mediated by Microprocessor,^{122,123} but also to bind to pre-let-7 in the cytoplasm and prevent its processing mediated by Dicer.¹²⁴ Furthermore, LIN28B has also been demonstrated to promote pre-let-7 uridylation by TUT7.¹²¹ Compelling evidence shows that LIN28 also acts by directly binding to target mRNAs presenting GGAGA sequences enriched within their loop structures.¹²⁵

LIN28 is a recognized oncogenic driver, which is abnormally expressed in ~15% of human cancer cell lines and has

been associated with a dismal prognosis.¹²⁶ High levels of LIN28 are found in different tumor types, such as glioblastoma, prostate, gastric, ovarian, and breast cancers.¹¹⁴ Its overexpression has been shown to induce different tumors, such as Wilms tumor,¹²⁷ neuroblastoma,¹²⁸ and hepatocellular cancer,¹²⁹ in mouse models. LIN28 has also been demonstrated to have an important role in cancer stem cell formation and tumor metastasis.¹³⁰ LIN28A and/or LIN28B are useful cancer stem cell biomarkers in several cancer types.¹³⁰ Moreover, their expression has been associated with resistance to chemotherapy in several cancers.¹¹⁴

In recent years, four HTSs aimed at identifying molecules able to disrupt LIN28-let-7 interaction have been reported.^{131–134}

Using a FRET assay based on a GFP-LIN28B donor and a black-hole quencher-labeled let-7 acceptor, Roos et al. screened 16,000 small drug-like molecules and selected 203 molecules, which were reevaluated in triplicate in a new screen. Different secondary assays, including a luciferase reporter gene assay; RT-qPCR on let-7a, let-7f, and let-7g; and enzyme-linked immunosorbent assay (ELISA), were performed to validate the 14 confirmed molecules. *N*-Methyl-*N*-[3-(3-methyl[1,2,4]triazolo[4,3-*b*]pyridazin-6-yl)phenyl]acetamide, which displayed an IC₅₀ value of 8 μM, was selected. The molecule was proven to bind to LIN28A and not to the let-7 RNA in a pull-down experiment. The selected molecule was able to induce differentiation in murine embryonic stem cells (ESCs) and to decrease clonogenic growth of four different cancer cell lines.¹³³

Lim and colleagues also developed a FRET-based assay to identify small molecules able to inhibit the LIN28-let7 interaction. Forty-five hundred drug-like molecules were screened and the primary hits were validated using EMSA. A benzopyranylpyrazole-based molecule, which presented IC₅₀ values in the low micromolar range in FRET and EMSA, was selected as a hit. Structure–activity relationship studies revealed that the carboxylic group in the *para* position in the phenyl ring attached to the pyrazole was essential for the inhibitory activity. The selected molecule was proven to bind to the CSD of LIN28A by SPR and differential scanning fluorimetry. Finally, the cellular effects of the molecule were demonstrated by miRNA level quantification through qRT-PCR, a reporter gene assay, and Western blot analysis.¹³¹

Lightfoot et al. developed an FP assay, through which they screened 2768 small molecules. The 64 primary hits were retested using the same assay to assess for reproducibility, and the 21 confirmed hits were then validated in a radioactivity-based EMSA. Next, the four validated hits were tested for their ability to prevent LIN28 blockage of pre-let-7 cleavage by Dicer. 6-Hydroxy-DL-DOPA was able to completely restore Dicer processing of pre-let-7g and another compound, SB/ZW/0065, partially restored it.¹³⁴

Very recently, Wang and colleagues also used an FP assay to screen 101,017 compounds belonging to 17 different libraries in order to identify small-molecule inhibitors of both the CSD and ZKD of LIN28A. Since CSD has a higher affinity for the target RNA compared with the ZKD, compounds able to selectively interfere with ZKD-RNA binding are difficult to detect with assays using native full-length LIN28A. Therefore, in order to increase the sensitivity in detecting ZKD-RNA inhibitors, a point mutation able to weaken CSD-RNA binding was introduced in the LIN28A protein structure. The HTS identified 350 molecules, which were then prioritized based on their IC₅₀ values calculated by performing a dose–response FP titration. Evaluation of the ability of the most potent compounds to prevent TUT4-mediated uridylation allowed to select six promising compounds. Structural studies performed by NMR and/or STD spectroscopy experiments elucidated the mechanism of action and the binding site of two compounds, with TPEN binding to the ZKD and LI71 binding to the CSD.¹³²

Musashi

Musashi (MSI) protein was first identified in *Drosophila* as an essential factor for correct asymmetrical division of cell precursors generating external sensory organs.¹³⁵ In mammals, two orthologs have been identified, both described as critical regulators of stem cell differentiation.^{136,137} The MSI1 protein has been found selectively expressed in neural stem cells, while MSI2 has been found in a variety of other tissues, including hematopoietic stem cells (HSCs). MSI2 has also been demonstrated as an independent factor able to enhance the regenerative potential of HSCs through a posttranscriptional mechanism that negatively regulates the aryl hydrocarbon receptor (AHR) signaling and induces a pro-self-renewal phenotype.¹³⁸

Musashi proteins belong to the A/B hnRNP class. They are characterized by two N-terminal RRM1s that are responsible for binding to the UAG-context sequence in the 3'-UTR of target RNAs.¹³⁹ Both proteins interact with RNA by RRM1, in a molar ratio of 1:1, as demonstrated in complex with *Numb5* RNA,¹⁴⁰ and the RRM2 adds affinity.¹⁴¹ Other structural insights relate to the minimal recognition sequence, UAGGUAG, required to interact with RNA.¹⁴²

The global reprogramming capacity has prompted the investigation of Musashi proteins in cancer. Accumulating evidence from many aggressive forms of solid tumors, such as colorectal adenocarcinomas; breast, lung, pancreatic, glioblastoma, or endometrial cancer;¹⁴³ and hematologic malignancies,¹⁴⁴ suggest that Musashi proteins are potential markers of cancer stem cells (CSCs).¹⁴⁵ On the basis of maintaining cancer stem cell populations, Musashi proteins have been proposed to regulate cancer invasion, metastasis, and the development of more aggressive cancer phenotypes,

with modulation of drug resistance.¹⁴⁵ Elevated levels of MSI2 were found in non-small cell lung cancer (NSCLC) tumor specimens, and its higher expression was associated with disease progression, positively correlating with the metastatic potential of tumor cells through the regulation of TGF- β R1/SMAD3 signaling.¹⁴⁶ Different reports have indicated that MSI2 overexpression can be detected in 70% of AML patients and correlates with poor prognosis.^{147,148} The same trend of clinical outcome has been demonstrated in gastric cancer for MSI1,¹⁴⁹ or in cervical cancer,¹⁵⁰ colon cancer,¹⁵¹ and breast cancer¹⁵² for MSI2. In addition, the overexpression of MSI2 strongly influenced the chemoresistance of ovarian cancer cells, NSCLC cells, and pancreatic cancer cells;¹⁴⁵ consistently, the downregulation of MSI2 sensitized ovarian cancer and acute myeloid leukemia cells to the pharmacological treatment.^{153,154}

These findings suggest that Musashi proteins can be a promising therapeutic target for cancer, and their modulation can also represent a potential strategy to optimize conventional therapeutics.

Recombinant MSI1 and MSI2 proteins were used for an FP-based drug screening of more than 6000 compounds.¹⁵⁵ The small molecule Ro 08-2750 (Ro) was identified as an inhibitor of the RNA-protein interaction by FP and EMSA, with IC_{50} in the low micromolar range.¹⁵⁶ By microscale thermophoresis (MST), the K_d of Ro was evaluated around 12 μ M, with appreciated selectivity in comparison with an evolutionarily related RBP, SYNCRIP. Structural data also demonstrated that the amino acids F66 and R100 are crucially involved in Ro binding. The validation of biochemical data has been performed using leukemia cell lines, where Ro induced differentiation and apoptosis together with a transcriptional program resembling MSI2 depletion. In addition, Ro inhibited leukemogenesis in an MLL-AF9 mouse model.

MSI1 targets include the mRNA encoding for the tumor suppressor protein APC, and one strategy to interfere with Wnt and Notch pathways was to identify compounds that could inhibit MSI1 RNA-binding activity. Also in this case, the screening was performed by FP using GST recombinant MSI1 protein and the natural product gossypol was identified with an inhibitory equilibrium dissociation constant in the high nanomolar range.¹⁵⁷ Complementary approaches, including SPR, confirmed a direct interaction of gossypol with the protein. The inhibition of MSI1-RNA interaction was effectively observed *in vivo* with inhibition of colon cancer growth upon oral administration of gossypol.

Intriguingly, Gu et al. found gossypol to be among the top hits of an HTS done with the aim of identifying inhibitors of the interaction between mouse double minute 2 (MDM2) RING and XIAP IRES. They later demonstrated gossypol's inhibitory activity on the MDM2-VEGF 3'-UTR interaction.^{158,159} Through isothermal titration calorimetry (ITC) and fluorescence titration techniques, the

investigators were able to determine whether the selected screening hits bind to the protein or to the RNA and found that gossypol binds to MDM2 RING, with a K_d of 5.21 μ M.¹⁵⁹ Indeed, the biological effects of gossypol and some analogs have been shown in different cell lines and models,¹⁶⁰ demonstrating anti-inflammatory effects,¹⁶¹ antiproliferative capacity through direct interference with the kinase domain of EGFR,¹⁶² pro-apoptotic effects by enhancing the levels of Bcl-2,¹⁶³ and autophagic effects through activation of LC3.¹⁶⁴ This compound also induces an accelerated hemolytic toxicity when administered *in vivo*.¹⁶⁵ The interference with RBPs represents an additional perspective that contributes to defining the broad mechanism of action of gossypol and its preferential intracellular targets at the tissue-specific level.

Other RNPs Suggested as Potential Therapeutic Targets

TDP-43 is a nuclear protein of 414 amino acids, with two highly conserved RRM1 and RRM2 domains resembling the architecture of the members of the hnRNP family. TDP-43 participates in different processes, including DNA replication, repair, mRNA splicing, and translation. Mechanistically, TDP-43 recognizes both DNA and RNA *cis* elements. This protein is crucial for correct embryonic development and its role has been extensively investigated in neurodegeneration, starting from the identification of rare TDP-43 mutations in cases of sporadic and familial amyotrophic lateral sclerosis (ALS) and cases of frontotemporal lobar degeneration (FTLD).¹⁶⁶ TDP-43 mutations are the cause of disease for 6.5% of familial ALS cases, while in the rest of ALS and FTD patients no mutations have been found but the presence of TDP-43 aggregates. Other functional studies have demonstrated that TDP-43 is associated with aberrant exon 9 skipping, as the case of the cystic fibrosis transmembrane conductance regulator (CFTR) gene in cystic fibrosis.¹⁶⁷

An increased accumulation of this protein is surprisingly found in the cytoplasm of affected neurons, where TDP-43 aggregates have been demonstrated to be hyperphosphorylated, ubiquitinated, and cleaved at the C-terminus.¹⁶⁸ However, the pathogenetic role of this protein, in terms of specific neurotoxic effects, remains to be clarified.¹⁶⁹ The mislocalization in the cytoplasm suggests a loss of all the functions concerning transcriptional regulation, splicing, and mRNA stability.

Among RBPs, TDP-43 is certainly considered an interesting target to address neurodegeneration. However, the elucidation of the basic molecular functions of the protein and of the effects of their alteration after mutation and aggregation is required for a targeted approach. Technically, the interaction of TDP-43 with nucleic acids has already been explored with high-throughput assays.¹⁷⁰ Interestingly, the inhibition of TDP-43 aggregate formation has been

explored by suppressing ataxin-2 expression (necessary for TDP-43 aggregate formation), by reversing translational suppression, by stimulating autophagic processing, or by decreasing TDP-43 mitochondrial localization.¹⁷¹

Tristetraprolin (TTP) is an RBP containing tandem CCH zinc finger (TZF) domains. It strongly binds to ARE sequences, mainly enriched in the 3'-UTR of mRNAs, regulating their stability and decay. TTP interacts with the CCR4-CNOT1 deadenylase complex and favors the decay of ARE containing mRNAs, including the ones encoding pro-inflammatory cytokines. TNF α is one of the main targets of TTP, which causes the specific degradation of this transcript, as clearly observed in macrophages.¹⁷² Interestingly, the downregulation of TTP in mice leads to the development of autoimmune diseases due to the increased release of TNF α .¹⁷³ For these reasons, TTP has been proposed as a therapeutic target in inflammatory diseases, with the goal of enhancing its expression using small molecules.¹⁷⁴ In a more complex paradigm, TTP loss has been reported in several tumors and associated with poor prognosis for enhanced cancer cell proliferation, epithelial-mesenchymal transition, and tumor aggressiveness, as summarized by Guo et al.¹⁷⁵

Discussion/Conclusions

In conclusion, in recent years a number of reports have highlighted the role of alterations of the posttranscriptional control of gene expression in disease, and the multiple reasons why specific RBPs could be attractive drug targets. The advantages of targeting RBPs reside in their intrinsic pleiotropy and in their ability to simultaneously control entire subsets of mRNAs, which could in principle allow the small molecules interfering with them to affect complex cellular programs deranged in disease. Another attractive feature of RBPs is that several of them act as repressors of gene expression, or as activators that compete with ncRNAs. In this case, the inhibition of their activity by small molecules would in principle produce enhancement of the expression of the RBP targets. This would open up potential therapeutic solutions for single-gene haploinsufficiency diseases, to reconstitute physiological levels of expression of pathologically repressed genes.

Despite these exciting perspectives, the strategies to develop therapeutic approaches against RNPs face several challenges. The first directly relies on the RBP pleiotropy, which exposes any pharmacological interventions to the risk of unwanted effects, involving a fine tuning in the medicinal chemistry phase to reach the required specificity. Medicinal chemistry campaigns are also likely necessary for the development of lead compounds requiring large hydrophobic cores, as several of the RBP hits are predicted to contain. Again, in terms of selectivity, one of the main

biological challenges of RNP complexes is first related to the strong avidity (often detected in the nanomolar range) that limits the competition kinetics of small molecules at the levels of the association between the ligands with a weak or no effect on the dissociation. Second, the presence of homologous protein domains shared by RBPs can be responsible, by competition, for a limited intracellular efficacy of the small molecules. It is worth noting that the efficient activity as well as the subcellular localization of an RBP is a result of the global protein conformation that assists the RNA recognition and is often posttranslationally modified to confer target preferences.

Future screening strategies should take care to use chemical libraries as diverse as possible and include noncanonical chemotypes (i.e., violating Lipinski's rule of five), such as various natural compounds or macrocycles, as well as using fragment libraries to identify useful chemical scaffolds and hot spots in protein pockets.¹⁷⁶

Furthermore, computational predictions can be successfully applied to RNPs, analyzing targets with known 3D structure and scanning their shape in search of pockets with favorable physicochemical and geometrical properties (hydrophobicity, size, compactness, hydrogen bond donor and acceptor surface areas, and amino acid composition in pockets) or running fragment-based virtual screening.^{177,178} These methods are cost-saving and timely with respect to the experimental approach, with the drawbacks of being limited to targets with known structures and hardly applicable when significant flexibility and conformational adaptivity are present at the binding site.

These challenges can be successfully addressed when deep structural insights about the ligands are available and the dynamics of the biological process involving that specific RNA-RBP interaction is elucidated. For these reasons, compounds identified through primary and counter HTSs need to be validated by at least two rounds of complementary approaches: (1) a technical validation only successfully achieved by the smart combination of different (in principle) assays, and (2) a biological validation of the small molecule in cellular and in *in vivo* models where the pathophysiology of the RBP is known to generate specific readouts. These integrated approaches will be necessary to understand the pathological relevance of specific RBPs and their effect in regulating constitutive pathways, whose inhibition might result in potential toxicities when administered at the systemic level, as showed by the case of the drug E7107 targeting SF3B1.

In order to deal effectively with these obstacles, a number of tailored strategies can be suggested. The attempts so far conducted to explore the RNP as targets have generated important advancements in understanding their biochemical activity and additional efforts should be undertaken to implement novel technologies, suitable for HTS, to study

the interactions and their dynamics at the intracellular level, with the final goal of discovering novel drugs or developing chemical probes as powerful research tools.

Declaration of Conflicting Interests

The authors declared no potential conflicts of interest with respect to the research, authorship, and/or publication of this article.

Funding

The authors disclosed receipt of the following financial support for the research, authorship, and/or publication of this article: A.P. gratefully acknowledges funding from Associazione Italiana per la Ricerca sul Cancro (AIRC) (17153), CARITRO Riposizionamento Farmaci (40102838), and CARIPLO, ricerca biomedica sulle malattie legate all'invecchiamento (40102636). A.Q. acknowledges AIRC (17026). V.G.D. acknowledges MIUR-FFABR-17.

References

1. Dreyfuss, G.; Kim, V. N.; Kataoka, N. Messenger-RNA-Binding Proteins and the Messages They Carry. *Nat. Rev. Mol. Cell Biol.* **2002**, *3*, 195–205.
2. Gerstberger, S.; Hafner, M.; Tuschl, T. A Census of Human RNA-Binding Proteins. *Nat. Rev. Genet.* **2014**, *15*, 829–845.
3. Lunde, B. M.; Moore, C.; Varani, G. RNA-Binding Proteins: Modular Design for Efficient Function. *Nat. Rev. Mol. Cell Biol.* **2007**, *8*, 479–490.
4. Cléry, A.; Blatter, M.; Allain, F. H.-T. RNA Recognition Motifs: Boring? Not Quite. *Curr. Opin. Struct. Biol.* **2008**, *18*, 290–298.
5. Valverde, R.; Edwards, L.; Regan, L. Structure and Function of KH Domains. *FEBS J.* **2008**, *275*, 2712–2726.
6. Linder, P.; Jankowsky, E. From Unwinding to Clamping—The DEAD Box RNA Helicase Family. *Nat. Rev. Mol. Cell Biol.* **2011**, *12*, 505–516.
7. Hamosh, A.; Scott, A. F.; Amberger, J. S.; et al. Online Mendelian Inheritance in Man (OMIM), a Knowledgebase of Human Genes and Genetic Disorders. *Nucleic Acids Res.* **2005**, *33* (Database issue), D514–D517.
8. Ray, D.; Kazan, H.; Cook, K. B.; et al. A Compendium of RNA-Binding Motifs for Decoding Gene Regulation. *Nature* **2013**, *499*, 172–177.
9. Hentze, M. W.; Castello, A.; Schwarzl, T.; et al. A Brave New World of RNA-Binding Proteins. *Nat. Rev. Mol. Cell Biol.* **2018**, *19*, 327–341.
10. Bollmann, F.; Art, J.; Henke, J.; et al. Resveratrol Post-Transcriptionally Regulates Pro-Inflammatory Gene Expression via Regulation of KSRP RNA Binding Activity. *Nucleic Acids Res.* **2014**, *42*, 12555–12569.
11. Lee, S.-R.; Jin, H.; Kim, W.-T.; et al. Tristetraprolin Activation by Resveratrol Inhibits the Proliferation and Metastasis of Colorectal Cancer Cells. *Int. J. Oncol.* **2018**, *53*, 1269–1278.
12. Tonra, J. R.; Hicklin, D. J. Targeting the Vascular Endothelial Growth Factor Pathway in the Treatment of Human Malignancy. *Immunol. Invest.* **2007**, *36*, 3–23.
13. Cao, L.; Weetall, M.; Bombard, J.; et al. Discovery of Novel Small Molecule Inhibitors of VEGF Expression in Tumor Cells Using a Cell-Based High Throughput Screening Platform. *PLoS One* **2016**, *11*, e0168366.
14. Melo, S.; Villanueva, A.; Moutinho, C.; et al. Small Molecule Enoxacin Is a Cancer-Specific Growth Inhibitor That Acts by Enhancing TAR RNA-Binding Protein 2-Mediated microRNA Processing. *Proc. Natl. Acad. Sci. U.S.A.* **2011**, *108*, 4394–4399.
15. Hopkins, A. L.; Groom, C. R. The Druggable Genome. *Nat. Rev. Drug Discov.* **2002**, *1*, 727–730.
16. Southan, C.; Boppana, K.; Jagarlapudi, S. A.; et al. Analysis of In Vitro Bioactivity Data Extracted from Drug Discovery Literature and Patents: Ranking 1654 Human Protein Targets by Assayed Compounds and Molecular Scaffolds. *J. Cheminform.* **2011**, *3*, 14.
17. Dandapani, S.; Marcaurette, L. A. Grand Challenge Commentary: Accessing New Chemical Space for “Undruggable” Targets. *Nat. Chem. Biol.* **2010**, *6*, 861–863.
18. Knapp, S. Emerging Target Families: Intractable Targets. *Handb. Exp. Pharmacol.* **2016**, *232*, 43–58.
19. Hagenbuchner, J.; Ausserlechner, M. J. Targeting Transcription Factors by Small Compounds—Current Strategies and Future Implications. *Biochem. Pharmacol.* **2016**, *107*, 1–13.
20. Chen, W.; Hill, H.; Christie, A.; et al. Targeting Renal Cell Carcinoma with a HIF-2 Antagonist. *Nature* **2016**, *539*, 112–117.
21. Jones, S. Protein–RNA Interactions: Structural Biology and Computational Modeling Techniques. *Biophys. Rev.* **2016**, *8*, 359–367.
22. Schlundt, A.; Tants, J. N.; Sattler, M. Integrated Structural Biology to Unravel Molecular Mechanisms of Protein-RNA Recognition. *Methods* **2017**, *118–119*, 119–136.
23. Deigan Warner, K.; Hajdin, C. E.; Weeks, K. M. Principles for Targeting RNA with Drug-Like Small Molecules. *Nat. Rev. Drug Discov.* **2018**, *17*, 547–558.
24. Wu, B.; Zhang, Z.; Noberini, R.; et al. HTS by NMR of Combinatorial Libraries: A Fragment-Based Approach to Ligand Discovery. *Chem. Biol.* **2013**, *20*, 19–33.
25. Patel, D.; Bauman, J. D.; Arnold, E. Advantages of Crystallographic Fragment Screening: Functional and Mechanistic Insights from a Powerful Platform for Efficient Drug Discovery. *Prog. Biophys. Mol. Biol.* **2014**, *116*, 92–100.
26. Lolli, G.; Cafilisch, A. High-Throughput Fragment Docking into the BAZ2B Bromodomain: Efficient In Silico Screening for X-Ray Crystallography. *ACS Chem. Biol.* **2016**, *11*, 800–807.
27. Marchand, J.-R.; Lolli, G.; Cafilisch, A. Derivatives of 3-Amino-2-Methylpyridine as BAZ2B Bromodomain Ligands: In Silico Discovery and In Crystallo Validation. *J. Med. Chem.* **2016**, *59*, 9919–9927.
28. Spiliotopoulos, D.; Wamhoff, E.-C.; Lolli, G.; et al. Discovery of BAZ2A Bromodomain Ligands. *Eur. J. Med. Chem.* **2017**, *139*, 564–572.
29. Huranová, M.; Jablonski, J. A.; Benda, A.; et al. In Vivo Detection of RNA-Binding Protein Interactions with Cognate RNA Sequences by Fluorescence Resonance Energy Transfer. *RNA* **2009**, *15*, 2063–2071.
30. Zhang, X. E.; Cui, Z.; Wang, D. Sensing of Biomolecular Interactions Using Fluorescence Complementing Systems in Living Cells. *Biosens. Bioelectron.* **2016**, *76*, 243–250.

31. Han, Y.; Wang, S.; Zhang, Z.; et al. In Vivo Imaging of Protein-Protein and RNA-Protein Interactions Using Novel Far-Red Fluorescence Complementation Systems. *Nucleic Acids Res.* **2014**, *42*, e103.
32. Emerman, M.; Malim, M. H. HIV-1 Regulatory/Accessory Genes: Keys to Unraveling Viral and Host Cell Biology. *Science* **1998**, *280*, 1880–1884.
33. Abulwerdi, F. A.; Le Grice, S. F. J. Recent Advances in Targeting the HIV-1 Tat/TAR Complex. *Curr. Pharm. Des.* **2017**, *23*, 4112–4121.
34. Mei, H. Y.; Mack, D. P.; Galan, A. A.; et al. Discovery of Selective, Small-Molecule Inhibitors of RNA Complexes. I. The Tat Protein/TAR RNA Complexes Required for HIV-1 Transcription. *Bioorganic Med. Chem.* **1997**, *5*, 1173–1184.
35. Mills, N. L.; Shelat, A. A.; Guy, R. K. Assay Optimization and Screening of RNA-Protein Interactions by AlphaScreen. *J. Biomol. Screen.* **2007**, *12*, 946–955.
36. Hamy, F.; Felder, E.; Lipson, K.; et al. Merged Screening for Human Immunodeficiency Virus Tat and Rev Inhibitors. *J. Biomol. Screen.* **2001**, *6*, 179–187.
37. Fourtounis, J.; Falgueyret, J. P.; Elie Sayegh, C. Assessing Protein-RNA Interactions Using Microfluidic Capillary Mobility Shift Assays. *Anal. Biochem.* **2011**, *411*, 161–163.
38. Yin, J.; Zhu, D.; Zhang, Z.; et al. Imaging of mRNA-Protein Interactions in Live Cells Using Novel mCherry Trimolecular Fluorescence Complementation Systems. *PLoS One* **2013**, *8*, e80851.
39. Maroto, M.; Fernandez, Y.; Ortin, J.; et al. Development of an HTS Assay for the Search of Anti-Influenza Agents Targeting the Interaction of Viral RNA with the NS1 Protein. *J. Biomol. Screen.* **2008**, *13*, 581–590.
40. Alfidhli, A.; McNett, H.; Eccles, J.; et al. Analysis of Small Molecule Ligands Targeting the HIV-1 Matrix Protein-RNA Binding Site. *J. Biol. Chem.* **2013**, *288*, 666–676.
41. Zhou, S.; Rynearson, K. D.; Ding, K.; et al. Screening for Inhibitors of the Hepatitis C Virus Internal Ribosome Entry Site RNA. *Bioorg. Med. Chem.* **2013**, *21*, 6139–6144.
42. Gozani, O.; Potashkin, J.; Reed, R. A Potential Role for U2AF-SAP 155 Interactions in Recruiting U2 snRNP to the Branch Site. *Mol. Cell. Biol.* **1998**, *18*, 4752–4760.
43. Cretu, C.; Schmitzová, J.; Ponce-Salvatierra, A.; et al. Molecular Architecture of SF3b and Structural Consequences of Its Cancer-Related Mutations. *Mol. Cell* **2016**, *64*, 307–319.
44. Yan, C.; Wan, R.; Bai, R.; et al. Structure of a Yeast Activated Spliceosome at 3.5 Å Resolution. *Science* **2016**, *353*, 904–911.
45. Finci, L. I.; Zhang, X.; Huang, X.; et al. The Cryo-EM Structure of the SF3b Spliceosome Complex Bound to a Splicing Modulator Reveals a Pre-mRNA Substrate Competitive Mechanism of Action. *Genes Dev.* **2018**, *32*, 309–320.
46. Dvinge, H.; Bradley, R. K. Widespread Intron Retention Diversifies Most Cancer Transcriptomes. *Genome Med.* **2015**, *7*, 45.
47. Danan-Gotthold, M.; Golan-Gerstl, R.; Eisenberg, E.; et al. Identification of Recurrent Regulated Alternative Splicing Events across Human Solid Tumors. *Nucleic Acids Res.* **2015**, *43*, 5130–5144.
48. Kim, Y. J.; Abdel-Wahab, O. Therapeutic Targeting of RNA Splicing in Myelodysplasia. *Semin. Hematol.* **2017**, *54*, 167–173.
49. Wang, L.; Lawrence, M. S.; Wan, Y.; et al. SF3B1 and Other Novel Cancer Genes in Chronic Lymphocytic Leukemia. *N. Engl. J. Med.* **2011**, *365*, 2497–2506.
50. Ciriello, G.; Gatza, M. L.; Beck, A. H.; et al. Comprehensive Molecular Portraits of Invasive Lobular Breast Cancer. *Cell* **2015**, *163*, 506–519.
51. Imielinski, M.; Berger, A. H.; Hammerman, P. S.; et al. Mapping the Hallmarks of Lung Adenocarcinoma with Massively Parallel Sequencing. *Cell* **2012**, *150*, 1107–1120.
52. Harbour, J. W.; Roberson, E. D. O.; Anbunathan, H.; et al. Recurrent Mutations at Codon 625 of the Splicing Factor SF3B1 in Uveal Melanoma. *Nat. Genet.* **2013**, *45*, 133–135.
53. Bailey, P.; Chang, D. K.; Nones, K.; et al. Genomic Analyses Identify Molecular Subtypes of Pancreatic Cancer. *Nature* **2016**, *531*, 47–52.
54. Obeng, E. A.; Chappell, R. J.; Seiler, M.; et al. Physiologic Expression of Sf3b1(K700E) Causes Impaired Erythropoiesis, Aberrant Splicing, and Sensitivity to Therapeutic Spliceosome Modulation. *Cancer Cell* **2016**, *30*, 404–417.
55. Shirai, C. L.; White, B. S.; Tripathi, M.; et al. Mutant U2AF1-Expressing Cells Are Sensitive to Pharmacological Modulation of the Spliceosome. *Nat. Commun.* **2017**, *8*, 14060.
56. Lee, S. C.-W.; Abdel-Wahab, O. Therapeutic Targeting of Splicing in Cancer. *Nat. Med.* **2016**, *22*, 976–986.
57. Nakajima, H.; Hori, Y.; Terano, H.; et al. New Antitumor Substances, FR901463, FR901464 and FR901465. II. Activities against Experimental Tumors in Mice and Mechanism of Action. *J. Antibiot. (Tokyo)* **1996**, *49*, 1204–1211.
58. Sakai, Y.; Yoshida, T.; Ochiai, K.; et al. GEX1 Compounds, Novel Antitumor Antibiotics Related to Herboxidiene, Produced by *Streptomyces* sp. I. Taxonomy, Production, Isolation, Physicochemical Properties and Biological Activities. *J. Antibiot. (Tokyo)* **2002**, *55*, 855–862.
59. Mizui, Y.; Sakai, T.; Iwata, M.; et al. Pladienolides, New Substances from Culture of *Streptomyces Platensis* Mer-11107. III. In Vitro and In Vivo Antitumor Activities. *J. Antibiot. (Tokyo)* **2004**, *57*, 188–196.
60. Kaida, D.; Motoyoshi, H.; Tashiro, E.; et al. Spliceostatin A Targets SF3b and Inhibits Both Splicing and Nuclear Retention of Pre-mRNA. *Nat. Chem. Biol.* **2007**, *3*, 576–583.
61. Kotake, Y.; Sagane, K.; Owa, T.; et al. Splicing Factor SF3b as a Target of the Antitumor Natural Product Pladienolide. *Nat. Chem. Biol.* **2007**, *3*, 570–575.
62. Lagisetti, C.; Yermolina, M. V.; Sharma, L. K.; et al. Pre-mRNA Splicing-Modulatory Pharmacophores: The Total Synthesis of Herboxidiene, a Pladienolide-Herboxidiene Hybrid Analog and Related Derivatives. *ACS Chem. Biol.* **2014**, *9*, 643–648.
63. Fan, L.; Lagisetti, C.; Edwards, C. C.; et al. Sudemycins, Novel Small Molecule Analogues of FR901464, Induce Alternative Gene Splicing. *ACS Chem. Biol.* **2011**, *6*, 582–589.
64. Lee, S. C.-W.; Dvinge, H.; Kim, E.; et al. Modulation of Splicing Catalysis for Therapeutic Targeting of Leukemia with Mutations in Genes Encoding Spliceosomal Proteins. *Nat. Med.* **2016**, *22*, 672–678.

65. Eskens, F. A. L. M.; Ramos, F. J.; Burger, H.; et al. Phase I Pharmacokinetic and Pharmacodynamic Study of the First-in-Class Spliceosome Inhibitor E7107 in Patients with Advanced Solid Tumors. *Clin. Cancer Res.* **2013**, *19*, 6296–6304.
66. Hong, D. S.; Kurzrock, R.; Naing, A.; et al. A Phase I, Open-Label, Single-Arm, Dose-Escalation Study of E7107, a Precursor Messenger Ribonucleic Acid (pre-mRNA) Spliceosome Inhibitor Administered Intravenously on Days 1 and 8 Every 21 Days to Patients with Solid Tumors. *Invest. New Drugs* **2014**, *32*, 436–444.
67. Seiler, M.; Yoshimi, A.; Darman, R.; et al. H3B-8800, an Orally Available Small-Molecule Splicing Modulator, Induces Lethality in Spliceosome-Mutant Cancers. *Nat. Med.* **2018**, *24*, 497–504.
68. Diouf, B.; Lin, W.; Goktug, A.; et al. Alteration of RNA Splicing by Small Molecule Inhibitors of the Interaction between NHP2L1 and U4. *SLAS Discov.* **2018**, *23*, 164–173.
69. Mukherjee, N.; Lager, P. J.; Friedersdorf, M. B.; et al. Coordinated Posttranscriptional mRNA Population Dynamics during T-Cell Activation. *Mol. Syst. Biol.* **2009**, *5*, 288.
70. Brennan, C. M.; Steitz, J. A. HuR and mRNA Stability. *Cell. Mol. Life Sci.* **2001**, *58*, 266–277.
71. Latorre, E.; Carelli, S.; Raimondi, I.; et al. The Ribonucleic Complex HuR-MALAT1 Represses CD133 Expression and Suppresses Epithelial-Mesenchymal Transition in Breast Cancer. *Cancer Res.* **2016**, *76*, 2626–2636.
72. Meisner, N.-C.; Hintersteiner, M.; Mueller, K.; et al. Identification and Mechanistic Characterization of Low-Molecular-Weight Inhibitors for HuR. *Nat. Chem. Biol.* **2007**, *3*, 508–515.
73. Hinman, M. N.; Lou, H. Diverse Molecular Functions of Hu Proteins. *Cell. Mol. Life Sci.* **2008**, *65*, 3168–3181.
74. Wang, H.; Zeng, F.; Liu, Q.; et al. The Structure of the ARE-Binding Domains of Hu Antigen R (HuR) Undergoes Conformational Changes during RNA Binding. *Acta Crystallogr. D Biol. Crystallogr.* **2013**, *69*, 373–380.
75. Abdelmohsen, K.; Kuwano, Y.; Kim, H. H.; et al. Posttranscriptional Gene Regulation by RNA-Binding Proteins during Oxidative Stress: Implications for Cellular Senescence. *Biol. Chem.* **2008**, *389*, 243–255.
76. Izquierdo, J. M. Hu Antigen R (HuR) Functions as an Alternative Pre-mRNA Splicing Regulator of Fas Apoptosis-Promoting Receptor on Exon Definition. *J. Biol. Chem.* **2008**, *283*, 19077–19084.
77. Mukherjee, N.; Corcoran, D. L.; Nusbaum, J. D.; et al. Integrative Regulatory Mapping Indicates That the RNA-Binding Protein HuR Couples Pre-mRNA Processing and mRNA Stability. *Mol. Cell* **2011**, *43*, 327–339.
78. Al-Ahmadi, W.; Al-Ghamdi, M.; Al-Haj, L.; et al. Alternative Polyadenylation Variants of the RNA Binding Protein, HuR: Abundance, Role of AU-Rich Elements and Auto-Regulation. *Nucleic Acids Res.* **2009**, *37*, 3612–3624.
79. Katsanou, V.; Milatos, S.; Yiakouvakis, A.; et al. The RNA-Binding Protein Elavl1/HuR Is Essential for Placental Branching Morphogenesis and Embryonic Development. *Mol. Cell. Biol.* **2009**, *29*, 2762–2776.
80. Liu, L.; Christodoulou-Vafeiadou, E.; Rao, J. N.; et al. RNA-Binding Protein HuR Promotes Growth of Small Intestinal Mucosa by Activating the Wnt Signaling Pathway. *Mol. Biol. Cell* **2014**, *25*, 3308–3318.
81. Gubin, M. M.; Techasintana, P.; Magee, J. D.; et al. Conditional Knockout of the RNA-Binding Protein HuR in CD4⁺ T Cells Reveals a Gene Dosage Effect on Cytokine Production. *Mol. Med.* **2014**, *20*, 93–108.
82. DeMicco, A.; Naradikian, M. S.; Sindhava, V. J.; et al. B Cell-Intrinsic Expression of the HuR RNA-Binding Protein Is Required for the T Cell-Dependent Immune Response In Vivo. *J. Immunol. (Baltimore, Md. 1950)* **2015**, *195*, 3449–3462.
83. Yiakouvakis, A.; Dimitriou, M.; Karakasiliotis, I.; et al. Myeloid Cell Expression of the RNA-Binding Protein HuR Protects Mice from Pathologic Inflammation and Colorectal Carcinogenesis. *J. Clin. Invest.* **2012**, *122*, 48–61.
84. Katsanou, V.; Papadaki, O.; Milatos, S.; et al. HuR as a Negative Posttranscriptional Modulator in Inflammation. *Mol. Cell* **2005**, *19*, 777–789.
85. Wang, W.; Caldwell, M. C.; Lin, S.; et al. HuR Regulates Cyclin A and Cyclin B1 mRNA Stability during Cell Proliferation. *EMBO J.* **2000**, *19*, 2340–2350.
86. Levy, N. S.; Chung, S.; Furneaux, H.; et al. Hypoxic Stabilization of Vascular Endothelial Growth Factor mRNA by the RNA-Binding Protein HuR. *J. Biol. Chem.* **1998**, *273*, 6417–6423.
87. Tang, K.; Breen, E. C.; Wagner, P. D. Hu Protein R-Mediated Posttranscriptional Regulation of VEGF Expression in Rat Gastrocnemius Muscle. *Am. J. Physiol. Heart Circ. Physiol.* **2002**, *283*, H1497–H1504.
88. Wang, W.; Yang, X.; Cristofalo, V. J.; et al. Loss of HuR Is Linked to Reduced Expression of Proliferative Genes during Replicative Senescence. *Mol. Cell. Biol.* **2001**, *21*, 5889–5898.
89. Abdelmohsen, K.; Lal, A.; Kim, H. H.; et al. Posttranscriptional Orchestration of an Anti-Apoptotic Program by HuR. *Cell Cycle* **2007**, *6*, 1288–1292.
90. Ishimaru, D.; Ramalingam, S.; Sengupta, T. K.; et al. Regulation of Bcl-2 Expression by HuR in HL60 Leukemia Cells and A431 Carcinoma Cells. *Mol. Cancer Res.* **2009**, *7*, 1354–1366.
91. Kafasla, P.; Skliris, A.; Kontoyiannis, D. L. Post-Transcriptional Coordination of Immunological Responses by RNA-Binding Proteins. *Nat. Immunol.* **2014**, *15*, 492–502.
92. Atasoy, U.; Watson, J.; Patel, D.; et al. ELAV Protein HuA (HuR) Can Redistribute between Nucleus and Cytoplasm and Is Upregulated during Serum Stimulation and T Cell Activation. *J. Cell Sci.* **1998**, *111*, 3145–3156.
93. Galbán, S.; Kuwano, Y.; Pullmann, R.; et al. RNA-Binding Proteins HuR and PTB Promote the Translation of Hypoxia-Inducible Factor 1alpha. *Mol. Cell. Biol.* **2008**, *28*, 93–107.
94. Srikantan, S.; Gorospe, M. HuR Function in Disease. *Front. Biosci.* **2012**, *17*, 189–205.
95. Abdelmohsen, K.; Gorospe, M. Posttranscriptional Regulation of Cancer Traits by HuR. *Wiley Interdiscip. Rev. RNA* **2010**, *1*, 214–229.
96. Heinonen, M.; Hemmes, A.; Salmenkivi, K.; et al. Role of RNA Binding Protein HuR in Ductal Carcinoma In Situ of the Breast. *J. Pathol.* **2011**, *224*, 529–539.

97. Wang, J.; Li, D.; Wang, B.; et al. Predictive and Prognostic Significance of Cytoplasmic Expression of ELAV-Like Protein HuR in Invasive Breast Cancer Treated with Neoadjuvant Chemotherapy. *Breast Cancer Res. Treat.* **2013**, *141*, 213–224.
98. López, de Silanes, I.; Zhan, M.; Lal, A.; et al. Identification of a Target RNA Motif for RNA-Binding Protein HuR. *Proc. Natl. Acad. Sci. U.S.A.* **2004**, *101*, 2987–2992.
99. Denkert, C.; Koch, I.; von Keyserlingk, N.; et al. Expression of the ELAV-Like Protein HuR in Human Colon Cancer: Association with Tumor Stage and Cyclooxygenase-2. *Mod. Pathol.* **2006**, *19*, 1261–1269.
100. Kotta-Loizou, I.; Giaginis, C.; Theocharis, S. Clinical Significance of HuR Expression in Human Malignancy. *Med. Oncol.* **2014**, *31*, 1–19.
101. Giammanco, A.; Blanc, V.; Montenegro, G.; et al. Intestinal Epithelial HuR Modulates Distinct Pathways of Proliferation and Apoptosis and Attenuates Small Intestinal and Colonic Tumor Development. *Cancer Res.* **2014**, *74*, 5322–5335.
102. Zucal, C.; D'Agostino, V.; Loffredo, R.; et al. Targeting the Multifaceted HuR Protein, Benefits and Caveats. *Curr. Drug Targets* **2015**, *16*, 499–515.
103. Chae, M. J.; Sung, H. Y.; Kim, E. H.; et al. Chemical Inhibitors Destabilize HuR Binding to the AU-Rich Element of TNF- α mRNA. *Exp. Mol. Med.* **2009**, *41*, 824–831.
104. D'Agostino, V. G.; Adami, V.; Provenzani, A. A Novel High Throughput Biochemical Assay to Evaluate the HuR Protein-RNA Complex Formation. *PLoS One* **2013**, *8*, 1–9.
105. D'Agostino, V. G.; Lal, P.; Mantelli, B.; et al. Dihydroxanthone-I Interferes with the RNA-Binding Activity of HuR Affecting Its Post-Transcriptional Function. *Sci. Rep.* **2015**, *5*, 1–15.
106. Lal, P.; Cerofolini, L.; D'Agostino, V. G.; et al. Regulation of HuR Structure and Function by Dihydroxanthone-I. *Nucleic Acids Res.* **2017**, *45*, 9514–9527.
107. Manzoni, L.; Zucal, C.; Maio, D. Di.; et al. Interfering with HuR-RNA Interaction: Design, Synthesis and Biological Characterization of Tanshinone Mimics as Novel, Effective HuR Inhibitors. *J. Med. Chem.* **2018**, *61*, 1483–1498.
108. Wang, Z.; Bhattacharya, A.; Ivanov, D. N. Identification of Small-Molecule Inhibitors of the HuR/RNA Interaction Using a Fluorescence Polarization Screening Assay Followed by NMR Validation. *PLoS One* **2015**, *10*, 1–13.
109. Wu, X.; Lan, L.; Wilson, D. M.; et al. Identification and Validation of Novel Small Molecule Disruptors of HuR-mRNA Interaction. *ACS Chem. Biol.* **2015**, *10*, 1476–1484.
110. Kaur, K.; Wu, X.; Fields, J. K.; et al. The Fungal Natural Product Azaphilone-9 Binds to HuR and Inhibits HuR-RNA Interaction In Vitro. *PLoS One* **2017**, *12*, 1–18.
111. Ambros, V.; Horvitz, H. R. Heterochronic Mutants of the Nematode *Caenorhabditis elegans*. *Science* **1984**, *226*, 409–416.
112. Moss, E. G.; Tang, L. Conservation of the Heterochronic Regulator Lin-28, Its Developmental Expression and MicroRNA Complementary Sites. *Dev. Biol.* **2003**, *258*, 432–442.
113. Shyh-Chang, N.; Daley, G. Q. Lin28: Primal Regulator of Growth and Metabolism in Stem Cells. *Cell Stem Cell* **2013**, *12*, 395–406.
114. Balzeau, J.; Menezes, M. R.; Cao, S.; et al. The LIN28/let-7 Pathway in Cancer. *Front. Genet.* **2017**, *8*, 31.
115. Guo, Y.; Chen, Y.; Ito, H.; et al. Identification and Characterization of Lin-28 Homolog B (LIN28B) in Human Hepatocellular Carcinoma. *Gene* **2006**, *384*, 51–61.
116. Longfei Wang, A.; Nam, Y.; Lee, A. K.; et al. LIN28 Zinc Knuckle Domain Is Required and Sufficient to Induce Let-7 Oligouridylation. *Cell Rep.* **2017**, *18*, 2664–2675.
117. Nam, Y.; Chen, C.; Gregory, R. I.; et al. Molecular Basis for Interaction of Let-7 microRNAs with Lin28. *Cell* **2011**, *147*, 1080–1091.
118. Mayr, F.; Schütz, A.; Döge, N.; et al. The Lin28 Cold-Shock Domain Remodels Pre-Let-7 microRNA. *Nucleic Acids Res.* **2012**, *40*, 7492–7506.
119. Hagan, J. P.; Piskounova, E.; Gregory, R. I. Lin28 Recruits the TUTase Zcchc11 to Inhibit Let-7 Maturation in Mouse Embryonic Stem Cells. *Nat. Struct. Mol. Biol.* **2009**, *16*, 1021–1025.
120. Heo, I.; Joo, C.; Cho, J.; et al. Lin28 Mediates the Terminal Uridylation of Let-7 Precursor MicroRNA. *Mol. Cell* **2008**, *32*, 276–284.
121. Thornton, J. E.; Chang, H.-M.; Piskounova, E.; et al. Lin28-Mediated Control of Let-7 microRNA Expression by Alternative TUTases Zcchc11 (TUT4) and Zcchc6 (TUT7). *RNA* **2012**, *18*, 1875–1885.
122. Newman, M. A.; Thomson, J. M.; Hammond, S. M. Lin-28 Interaction with the Let-7 Precursor Loop Mediates Regulated microRNA Processing. *RNA* **2008**, *14*, 1539–1549.
123. Viswanathan, S. R.; Daley, G. Q.; Gregory, R. I. Selective Blockade of MicroRNA Processing by Lin28. *Science* **2008**, *320*, 97–100.
124. Rybak, A.; Fuchs, H.; Smirnova, L.; et al. A Feedback Loop Comprising Lin-28 and Let-7 Controls Pre-Let-7 Maturation during Neural Stem-Cell Commitment. *Nat. Cell Biol.* **2008**, *10*, 987–993.
125. Wilbert, M. L.; Huelga, S. C.; Kapeli, K.; et al. LIN28 Binds Messenger RNAs at GGAGA Motifs and Regulates Splicing Factor Abundance. *Mol. Cell* **2012**, *48*, 195–206.
126. Viswanathan, S. R.; Powers, J. T.; Einhorn, W.; et al. Lin28 Promotes Transformation and Is Associated with Advanced Human Malignancies. *Nat. Genet.* **2009**, *41*, 843–848.
127. Urbach, A.; Yermalovich, A.; Zhang, J.; et al. Lin28 Sustains Early Renal Progenitors and Induces Wilms Tumor. *Genes Dev.* **2014**, *28*, 971–982.
128. Molenaar, J. J.; Domingo-Fernández, R.; Ebus, M. E.; et al. LIN28B Induces Neuroblastoma and Enhances MYCN Levels via Let-7 Suppression. *Nat. Genet.* **2012**, *44*, 1199–1206.
129. Nguyen, L. H.; Robinton, D. A.; Seligson, M. T.; et al. Lin28b Is Sufficient to Drive Liver Cancer and Necessary for Its Maintenance in Murine Models. *Cancer Cell* **2014**, *26*, 248–261.
130. Zhou, J.; Ng, S.-B.; Chng, W.-J. LIN28/LIN28B: An Emerging Oncogenic Driver in Cancer Stem Cells. *Int. J. Biochem. Cell Biol.* **2013**, *45*, 973–978.
131. Lim, D.; Byun, W. G.; Koo, J. Y.; et al. Discovery of a Small-Molecule Inhibitor of Protein-MicroRNA Interaction Using Binding Assay with a Site-Specifically Labeled Lin28. *J. Am. Chem. Soc.* **2016**, *138*, 13630–13638.
132. Wang, L.; Rowe, R. G.; Jaimes, A.; et al. Small-Molecule Inhibitors Disrupt Let-7 Oligouridylation and Release the Selective Blockade of Let-7 Processing by LIN28. *Cell Rep.* **2018**, *23*, 3091–3101.

133. Roos, M.; Pradère, U.; Ngondo, R. P.; et al. A Small-Molecule Inhibitor of Lin28. *ACS Chem. Biol.* **2016**, *11*, 2773–2781.
134. Lightfoot, H. L.; Miska, E. A.; Balasubramanian, S. Identification of Small Molecule Inhibitors of the Lin28-Mediated Blockage of Pre-Let-7g Processing. *Org. Biomol. Chem.* **2016**, *14*, 10208–10216.
135. Nakamura, M.; Okano, H.; Blendy, J. A.; et al. Musashi, a Neural RNA-Binding Protein Required for *Drosophila* Adult External Sensory Organ Development. *Neuron* **1994**, *13*, 67–81.
136. Yano, M.; Hayakawa-Yano, Y.; Okano, H. RNA Regulation Went Wrong in Neurodevelopmental Disorders: The Example of Msi/Elavl RNA Binding Proteins. *Int. J. Dev. Neurosci.* **2016**, *55*, 124–130.
137. Fox, R. G.; Park, F. D.; Koechlein, C. S.; et al. Musashi Signaling in Stem Cells and Cancer. *Annu. Rev. Cell Dev. Biol.* **2015**, *31*, 249–267.
138. Rentas, S.; Holzapfel, N. T.; Belew, M. S.; et al. Musashi-2 Attenuates AHR Signalling to Expand Human Haematopoietic Stem Cells. *Nature* **2016**, *532*, 508–511.
139. Ohyama, T.; Nagata, T.; Tsuda, K.; et al. Structure of Musashi1 in a Complex with Target RNA: The Role of Aromatic Stacking Interactions. *Nucleic Acids Res.* **2012**, *40*, 3218–3231.
140. Lan, L.; Xing, M.; Douglas, J. T.; et al. Human Oncoprotein Musashi-2 N-Terminal RNA Recognition Motif Backbone Assignment and Identification of RNA-Binding Pocket. *Oncotarget* **2017**, *8*, 106587–106597.
141. Zearfoss, N. R.; Deveau, L. M.; Clingman, C. C.; et al. A Conserved Three-Nucleotide Core Motif Defines Musashi RNA Binding Specificity. *J. Biol. Chem.* **2014**, *289*, 35530–35541.
142. Iwaoka, R.; Nagata, T.; Tsuda, K.; et al. Structural Insight into the Recognition of r(UAG) by Musashi-1 RBD2, and Construction of a Model of Musashi-1 RBD1-2 Bound to the Minimum Target RNA. *Molecules* **2017**, *22*, 1–16.
143. Ma, L.; Xu, Y. L.; Ding, W. J.; et al. Prognostic Value of Musashi-1 in Endometrioid Adenocarcinoma. *Int. J. Clin. Exp. Pathol.* **2015**, *8*, 4564–4572.
144. Kharas, M. G.; Lengner, C. J. Stem Cells, Cancer, and MUSASHI in Blood and Guts. *Trends Cancer* **2017**, *3*, 347–356.
145. Kudinov, A. E.; Karanicolas, J.; Golemis, E. A.; et al. Musashi RNA-Binding Proteins as Cancer Drivers and Novel Therapeutic Targets. *Clin. Cancer Res.* **2017**, *23*, 2143–2153.
146. Kudinov, A. E.; Deneka, A.; Nikonova, A. S.; et al. Musashi-2 (MSI2) Supports TGF- β Signaling and Inhibits Claudins to Promote Non-Small Cell Lung Cancer (NSCLC) Metastasis. *Proc. Natl. Acad. Sci. U.S.A.* **2016**, *113*, 6955–6960.
147. Byers, R. J.; Currie, T.; Tholouli, E.; et al. MSI2 Protein Expression Predicts Unfavorable Outcome in Acute Myeloid Leukemia. *Blood* **2011**, *118*, 2857–2867.
148. Kharas, M. G.; Lengner, C. J.; Al-Shahrour, F.; et al. Musashi-2 Regulates Normal Hematopoiesis and Promotes Aggressive Myeloid Leukemia. *Nat. Med.* **2010**, *16*, 903–908.
149. Shou, Z.; Jin, X.; He, X.; et al. Overexpression of Musashi-1 Protein Is Associated with Progression and Poor Prognosis of Gastric Cancer. *Oncol. Lett.* **2017**, *13*, 3556–3566.
150. Liu, Y.; Fan, Y.; Wang, X.; et al. Musashi-2 Is a Prognostic Marker for the Survival of Patients with Cervical Cancer. *Oncol. Lett.* **2018**, *15*, 5425–5432.
151. Wang, Y.; Jiang, C. Q.; Fan, L. F. Correlation of Musashi-1, Lgr5, and pEGFR Expressions in Human Small Intestinal Adenocarcinomas. *Tumor Biol.* **2015**, *36*, 6075–6082.
152. Kang, M.-H.; Jeong, K. J.; Kim, W. Y.; et al. Musashi RNA-Binding Protein 2 Regulates Estrogen Receptor 1 Function in Breast Cancer. *Oncogene* **2017**, *36*, 1745–1752.
153. Lee, J.; An, S.; Choi, Y. M.; et al. Musashi-2 Is a Novel Regulator of Paclitaxel Sensitivity in Ovarian Cancer Cells. *Int. J. Oncol.* **2016**, *49*, 1945–1952.
154. Han, Y.; Ye, A.; Zhang, Y.; et al. Musashi-2 Silencing Exerts Potent Activity against Acute Myeloid Leukemia and Enhances Chemosensitivity to Daunorubicin. *PLoS One* **2015**, *10*, e0136484.
155. Minuesa, G.; Antczak, C.; Shum, D.; et al. A 1536-Well Fluorescence Polarization Assay to Screen for Modulators of the MUSASHI Family of RNA-Binding Proteins. *Comb. Chem. High Throughput Screen.* **2014**, *17*, 596–609.
156. Minuesa, G.; Albanese, S. K.; Chow, A.; et al. Small-Molecule Targeting of MUSASHI RNA-Binding Activity in Acute Myeloid Leukemia. *bioRxiv* **2018**, 321174.
157. Lan, L.; Appelman, C.; Smith, A. R.; et al. ScienceDirect Natural Product (–)-Gossypol Inhibits Colon Cancer Cell Growth by Targeting RNA-Binding Protein Musashi-1. *Mol. Oncol.* **2015**, *9*, 1–15.
158. Gu, L.; Zhang, H.; Liu, T.; et al. Discovery of Dual Inhibitors of MDM2 and XIAP for Cancer Treatment. *Cancer Cell* **2016**, *30*, 623–636.
159. Xiong, J.; Li, J.; Yang, Q.; et al. Gossypol Has Anti-Cancer Effects by Dual-Targeting MDM2 and VEGF in Human Breast Cancer. *Breast Cancer Res.* **2017**, *19*, 1–10.
160. Zeng, Y.; Ma, J.; Xu, L.; et al. Natural Product Gossypol and Its Derivatives in Precision Cancer Medicine. *Curr. Med. Chem.* **2017**, *24*, 28545375.
161. Chen, C.-W.; Hu, S.; Tsui, K.-H.; et al. Anti-Inflammatory Effects of Gossypol on Human Lymphocytic Jurkat Cells via Regulation of MAPK Signaling and Cell Cycle. *Inflammation* **2018**, *41*, 2265–2274.
162. Wang, Y.; Lai, H.; Fan, X.; et al. Gossypol Inhibits Non-Small Cell Lung Cancer Cells Proliferation by Targeting EGFR L858R/T790M. *Front. Pharmacol.* **2018**, *9*, 728.
163. Li, X.; He, J.; Li, B.; et al. The PPAR γ Agonist Rosiglitazone Sensitizes the BH3 Mimetic (–)-Gossypol to Induce Apoptosis in Cancer Cells with High Level of Bcl-2. *Mol. Carcinog.* **2018**, *57*, 1213–1222.
164. Lu, M.-D.; Li, L.-Y.; Li, P.-H.; et al. Gossypol Induces Cell Death by Activating Apoptosis and Autophagy in HT-29 Cells. *Mol. Med. Rep.* **2017**, *16*, 2128–2132.
165. Tang, C.; Meng, Q.; Zhang, K.; et al. Multi-Omics Analyses of Red Blood Cell Reveal Antioxidation Mechanisms Associated with Hemolytic Toxicity of Gossypol. *Oncotarget* **2017**, *8*, 103693–103709.
166. Warraich, S. T.; Yang, S.; Nicholson, G. A.; et al. TDP-43: A DNA and RNA Binding Protein with Roles in Neurodegenerative Diseases. *Int. J. Biochem. Cell Biol.* **2010**, *42*, 1606–1609.
167. Buratti, E.; Baralle, F. E. Multiple Roles of TDP-43 in Gene Expression, Splicing Regulation, and Human Disease. *Front. Biosci.* **2008**, *13*, 867–878.

168. Mackenzie, I. R. A.; Rademakers, R. The Role of Transactive Response DNA-Binding Protein-43 in Amyotrophic Lateral Sclerosis and Frontotemporal Dementia. *Curr. Opin. Neurol.* **2008**, *21*, 693–700.
169. Vanden Broeck, L.; Callaerts, P.; Dermaut, B. TDP-43-Mediated Neurodegeneration: Towards a Loss-of-Function Hypothesis? *Trends Mol. Med.* **2014**, *20*, 66–71.
170. Cassel, J. A.; Blass, B. E.; Reitz, A. B.; et al. Development of a Novel Nonradiometric Assay for Nucleic Acid Binding to TDP-43 Suitable for High-Throughput Screening Using AlphaScreen Technology. *J. Biomol. Screen.* **2010**, *15*, 1099–1106.
171. Gao, J.; Wang, L.; Huntley, M. L.; et al. Pathomechanisms of TDP-43 in Neurodegeneration. *J. Neurochem.* **2018**, *146*, 7–20.
172. Carballo, E. Feedback Inhibition of Macrophage Tumor Necrosis Factor—Production by Tristetraprolin. *Science* **1998**, *281*, 1001–1005.
173. Taylor, G. A.; Carballo, E.; Lee, D. M.; et al. A Pathogenetic Role for TNF Alpha in the Syndrome of Cachexia, Arthritis, and Autoimmunity Resulting from Tristetraprolin (TTP) Deficiency. *Immunity* **1996**, *4*, 445–454.
174. Patial, S.; Blakeshear, P. J. Tristetraprolin as a Therapeutic Target in Inflammatory Disease. *Trends Pharmacol. Sci.* **2016**, *37*, 811–821.
175. Guo, J.; Qu, H.; Chen, Y.; et al. The Role of RNA-Binding Protein Tristetraprolin in Cancer and Immunity. *Med. Oncol.* **2017**, *34*, 196.
176. Abi Hussein, H.; Geneix, C.; Petitjean, M.; et al. Global Vision of Druggability Issues: Applications and Perspectives. *Drug Discov. Today* **2017**, *22*, 404–415.
177. Volkamer, A.; Kuhn, D.; Grombacher, T.; et al. Combining Global and Local Measures for Structure-Based Druggability Predictions. *J. Chem. Inf. Model.* **2012**, *52*, 360–372.
178. Kozakov, D.; Hall, D. R.; Napoleon, R. L.; et al. New Frontiers in Druggability. *J. Med. Chem.* **2015**, *58*, 9063–9088.
179. Pagano, J. M.; Clingman, C. C.; Ryder, S. P. Quantitative Approaches to Monitor Protein-Nucleic Acid Interactions Using Fluorescent Probes. *RNA* **2011**, *17*, 14–20.
180. Moerke, N. J. Fluorescence Polarization (FP) Assays for Monitoring Peptide-Protein or Nucleic Acid-Protein Binding. In *Current Protocols in Chemical Biology*; John Wiley & Sons: Hoboken, NJ, 2009, Vol. 1, pp 1–15.
181. Rupesh, K. R.; Smith, A.; Boehmer, P. E. Ligand Induced Stabilization of the Melting Temperature of the HSV-1 Single-Strand DNA Binding Protein Using the Thermal Shift Assay. *Biochem. Biophys. Res. Commun.* **2015**, *454*, 604–608.
182. Edwards, K. A.; Baemner, A. J. Aptamer Sandwich Assays: Label-Free and Fluorescence Investigations of Heterogeneous Binding Events. *Anal. Bioanal. Chem.* **2010**, *398*, 2635–2644.
183. He, G.; Sun, D.; Ou, Z.; et al. The Protein Zfand5 Binds and Stabilizes mRNAs with AU-Rich Elements in Their 3'-Untranslated Regions. *J. Biol. Chem.* **2012**, *287*, 24967–24977.
184. Maurer, C. K.; Fruth, M.; Empting, M.; et al. Discovery of the First Small-Molecule CsrA-RNA Interaction Inhibitors Using Biophysical Screening Technologies. *Future Med. Chem.* **2016**, *8*, 931–947.
185. Katsamba, P.; Park, S.; Laird-Offringa, I. A. Kinetic Studies of RNA-Protein Interactions Using Surface Plasmon Resonance. *Methods* **2002**, *26*, 95–104.
186. Rio, D. C. Electrophoretic Mobility Shift Assays for RNA-Protein Complexes. *Cold Spring Harb. Protoc.* **2014**, *2014*, pdb.prot080721–pdb.prot080721.
187. Moon, M. H.; Hilimire, T.; Sanders, A. M.; et al. Measuring RNA-Ligand Interactions with Microscale Thermophoresis. *Biochemistry* **2018**, *57*, 4638–4643.
188. Asmari, M.; Ratih, R.; Alhazmi, H. A.; et al. Thermophoresis for Characterizing Biomolecular Interaction. *Methods* **2018**, *146*, 107–119.
189. Liang, Y. Applications of Isothermal Titration Calorimetry in Protein Science. *Acta Biochim. Biophys. Sin. (Shanghai)* **2008**, *40*, 565–576.
190. Foot, J. N.; Feracci, M.; Dominguez, C. Screening Protein-Single Stranded RNA Complexes by NMR Spectroscopy for Structure Determination. *Methods* **2014**, *65*, 288–301.
191. Carlomagno, T. Present and Future of NMR for RNA-Protein Complexes: A Perspective of Integrated Structural Biology. *J. Magn. Reson.* **2014**, *241*, 126–136.
192. Perederina, A.; Krasilnikov, A. S. Crystallization of RNA-Protein Complexes: From Synthesis and Purification of Individual Components to Crystals. In *Bacterial Regulatory RNA*; Humana Press: Totowa, NJ, 2012, Vol. 905, pp 123–143.
193. Ke, A.; Doudna, J. A. Crystallization of RNA and RNA-Protein Complexes. *Methods* **2004**, *34*, 408–414.
194. Russo Krauss, I.; Merlino, A.; Vergara, A.; et al. An Overview of Biological Macromolecule Crystallization. *Int. J. Mol. Sci.* **2013**, *14*, 11643–11691.
195. Minuesa, G.; Albanese, S. K.; Chow, A.; et al. Small-Molecule Targeting of MUSASHI RNA-Binding Activity in Acute Myeloid Leukemia. *bioRxiv* **2018**. DOI: 10.1101/321174.
196. Galicia-Vázquez, G.; Lindqvist, L.; Wang, X.; et al. High-Throughput Assays Probing Protein-RNA Interactions of Eukaryotic Translation Initiation Factors. *Anal. Biochem.* **2009**, *384*, 180–188.
197. Sommer, G.; Fedarovich, A.; Kota, V.; et al. Applying a High-Throughput Fluorescence Polarization Assay for the Discovery of Chemical Probes Blocking La:RNA Interactions In Vitro and in Cells. *PLoS One* **2017**, *12*, e0173246.

Interfering with HuR–RNA Interaction: Design, Synthesis and Biological Characterization of Tanshinone Mimics as Novel, Effective HuR Inhibitors

Leonardo Manzoni,^{†,○} Chiara Zucal,^{‡,○} Danilo Di Maio,^{§,○} Vito G. D'Agostino,[‡] Natthakan Thongon,[‡] Isabelle Bonomo,[‡] Preet Lal,[‡] Marco Miceli,^{||} Vanessa Baj,^{||} Marta Brambilla,^{||} Linda Cerofolini,^{⊥,#} Saioa Elezgarai,^{||} Emiliano Biasini,^{‡,||} Claudio Luchinat,[#] Ettore Novellino,[◆] Marco Fragai,^{⊥,#} Luciana Marinelli,^{*,◆} Alessandro Provenzani,^{*,‡} and Pierfausto Seneci^{*,||}

[†]Institute of Molecular Science and Technology (ISTM), CNR, Via Golgi 19, 20133 Milan, Italy

[‡]Centre for Integrative Biology (CIBIO), University of Trento, Via Sommarive 9, 38123 Povo, Trento, Italy

[§]Scuola Normale Superiore, Piazza dei Cavalieri 7, I-56126 Pisa, Italy

^{||}Chemistry Department, University of Milan, Via Golgi 19, 20133 Milan, Italy

[⊥]Consorzio Interuniversitario di Risonanze Magnetiche di Metallo Proteine (CIRMMP), Via L. Sacconi 6, 50019 Sesto Fiorentino, Florence, Italy

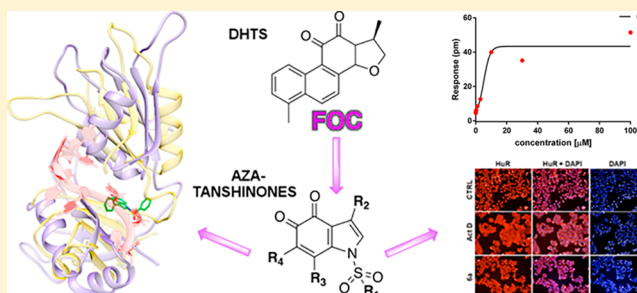
[#]CERM and Chemistry Department, University of Florence, Via della Lastruccia 3-13, 50019 Sesto Fiorentino, Florence, Italy

^{||}Istituto di Ricerche Farmacologiche Mario Negri, Milan, 20156, Italy

[◆]Pharmacy Department, University of Naples, Via Montesano 49, 80131 Naples, Italy

S Supporting Information

ABSTRACT: The human antigen R (HuR) is an RNA-binding protein known to modulate the expression of target mRNA coding for proteins involved in inflammation, tumorigenesis, and stress responses and is a valuable drug target. We previously found that dihydrotanshinone-I (DHTS, **1**) prevents the association of HuR with its RNA substrate, thus impairing its function. Herein, inspired by DHTS structure, we designed and synthesized an array of ortho-quinones (tanshinone mimics) using a function-oriented synthetic approach. Among others, compound **6a** and **6n** turned out to be more effective than **1**, showing a nanomolar K_i and disrupting HuR binding to RNA in cells. A combined approach of NMR titration and molecular dynamics (MD) simulations suggests that **6a** stabilizes HuR in a peculiar closed conformation, which is incompatible with RNA binding. Alpha screen and RNA-electrophoretic mobility shift assays (REMSA) data on newly synthesized compounds allowed, for the first time, the generation of structure activity relationships (SARs), thus providing a solid background for the generation of highly effective HuR disruptors.

**■ INTRODUCTION**

The human antigen R (HuR), also known as HuA or ELAVL1, is an ubiquitously expressed RNA binding protein that binds preferentially to adenine- and uridine-rich elements (ARE) of target coding and noncoding RNAs.^{1–3} HuR is primarily localized in the nucleus, where it exerts post-transcriptional functions such as splicing^{4,5} and alternative polyadenylation,⁶ although it shuttles to the cytoplasm carrying the targeted RNA to be spatiotemporally regulated in translation and stability.⁷ As a stress-response protein, HuR modulates the expression of target mRNA (containing AREs preferentially in their 3'UTR) coding for proteins involved in inflammation,⁸ cell division,⁹ tumorigenesis,^{10,11} angiogenesis,^{12,13} metastasis,¹⁴ senescence,¹⁵ apoptosis,^{16,17} immune,^{18,19} or stress responses.²⁰ The importance of HuR in inflammation and cancer has encouraged the research for

inhibitors/modulators to interfere with its biological activity.²¹ Several compounds have been named as HuR disruptors (i.e., molecules that can inhibit the HuR–RNA complex formation).^{22–30} For a detailed description of the known inhibitors and their properties, an exhaustive perspective has been recently published.³¹ However, neither systematic structure–activity relationships (SARs) studies, nor chemical synthesis of novel families of HuR inhibitors have been reported so far. From a structural point of view, rational design of HuR inhibitors is rather challenging due to the protein conformational plasticity.^{32–34} Moreover, HuR switches between at least two conformations upon binding/unbinding of its RNA substrate:

Received: August 12, 2017

Published: January 9, 2018

an “open” (apo) conformation, which is characterized by almost no contacts between its first two RNA recognition motif (RRM) domains, and a “closed” (holo) conformation, which is instead characterized by a few inter-residue contacts between the RRM domains.

Recently, as a result of a high throughput screening on a set of anti-inflammatory agents, we identified **1** (Dihydrotanshinone-I, DHTS, **Figure 1**), a low-molecular-weight natural

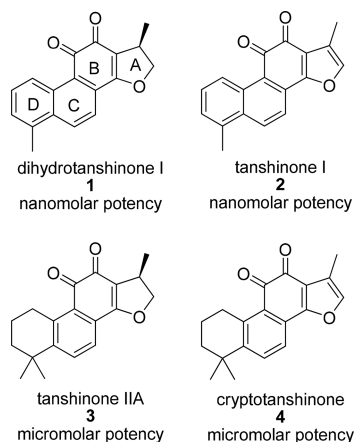


Figure 1. Naturally occurring tanshinones 1–4.

product able to interact with HuR, thus affecting its post-transcriptional functions.²⁷ Compound **1** is a major component of extracts from Danshen (*Salvia miltiorrhiza*) used in traditional Chinese medicine as a treatment for inflammation, cardiovascular, and cerebrovascular diseases.³⁵ Our detailed *in vitro* and *in vivo* characterization of **1** showed the HuR dependency of its mechanism of action²⁷ and its potency on cancer-linked HuR–mRNA interactions.¹¹ Naturally occurring tanshinones 2–4 (**Figure 1**) were tested as HuR inhibitors, observing a preference for an aryl condensed (compounds **1,2**) vs saturated D rings (compounds **3,4**).²⁷

Structural complexity has long hindered the synthetic exploitation of natural products as drug-oriented chemotypes. However, molecular editing through diverted total synthesis³⁶ and function-oriented synthesis (FOS)³⁷ are synthetic paths that help to transform a natural product to a simpler, equally active synthetic analogue.³⁸

We applied a FOS approach to **1**, starting from the bicyclic A–B scaffold **5** (**Figure 2**). It contains the *o*-quinone group

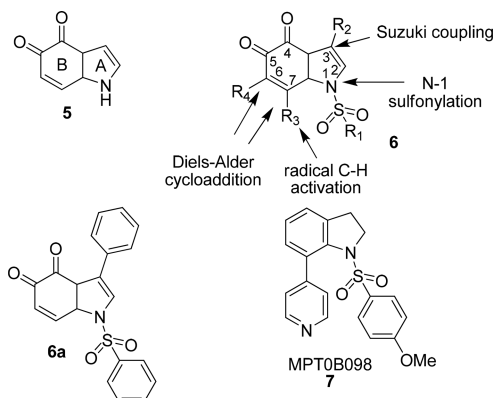


Figure 2. Tanshinone mimics as HuR inhibitors: core scaffold, function-oriented synthesis, active analogues.

and a pyrrole A ring, to provide novel, **1**-inspired, synthetic tanshinone mimics bearing R_1 – R_4 substitutions. Here the synthesis of a small library of tanshinone mimics **6a–t, w**, bearing substitutions in positions 1, 3, 6, and 7, is reported. Tanshinone mimics were tested for inhibition of HuR–RNA interactions and SARs were established. The most potent HuR inhibitor **6a** (**Figure 2**) was further characterized in a panel of *in vitro* and cellular assays and showed a direct K_D of 4.5 μ M to HuR. The molecular interaction of **6a** with HuR and with the HuR–mRNA complex was also elucidated via a combined approach of NMR and computational studies and grounded the path for the next generation of HuR inhibitors.

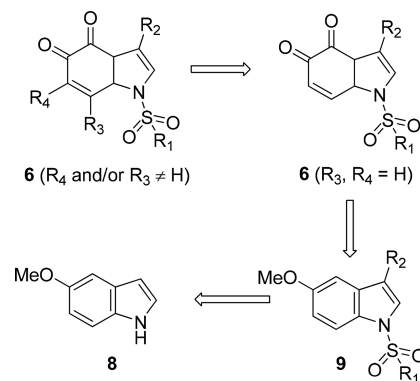
RESULTS AND DISCUSSION

Synthesis. Retrosynthesis. A FOS-based approach to natural products analogues entails the design of an uncomplicated synthetic strategy toward equally active, significantly simpler compounds. We built our strategy around a B ring-like ortho-quinone and we opted for a substituted, N-sulfonylated bicyclic A–B scaffold **6** as a function-oriented replacement for the tanshinone A–D ring system. The furan-pyrrole A ring switch was meant to provide HuR inhibition-inspired novelty, as the N-substituted indole MPT0B098 (**7**, **Figure 2**) is a negative modulator of HuR.³⁹ This compound bears a substituted sulfonamide in position 1, which was introduced on our A ring (scaffold **6**) to increase potency and further diversify our mimics from naturally occurring tanshinones.

We reasoned that a preliminary SAR around positions 1, 3, 6, and 7 on scaffold **6** could be established by exploiting N-sulfonylations (functionalization of N-1, $-\text{SO}_2\text{R}_1$), Suzuki couplings (functionalization of C-3, $-\text{R}_2$), radical CH functionalizations⁴⁰ and Michael additions (functionalization of C-7, $-\text{R}_3$) and Diels–Alder cycloadditions (functionalization of C-6 and C-7, $-\text{cycloR}_3\text{R}_4$, **Figure 2**).

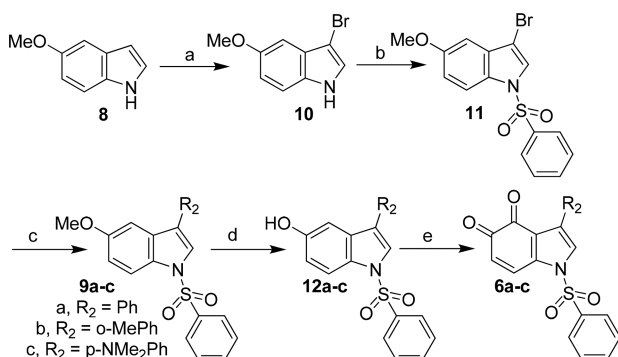
As to synthetic targets **6** ($R_1, R_2, R_4 \neq \text{H}$, or $R_1 - R_4 \neq \text{H}$, **Scheme 1**), we envisaged that functionalization of C-6 and/or

Scheme 1. Retrosynthetic Analysis to Tanshinone Mimics 6



C-7 could be carried out on 1,3-disubstituted indole-4,5-diones **6** ($R_3, R_4 = \text{H}$). Such compounds could be made by O-demethylation and oxidation of 1,3-disubstituted 5-methoxyindoles **9**. Compounds **9** could be prepared by 3-bromination of commercially available 5-methoxyindole **8**, followed by N-sulfonylation and Suzuki coupling (**Scheme 1**).

1-Alkyl/Arylsulfonyl-3-aryl Indole-4,5-Diones 6a–6j. The retrosynthetic scheme leading to 1,3-disubstituted indole-4,5-diones **6** ($R_1, R_2 \neq \text{H}$, $R_3 = R_4 = \text{H}$, **Figure 1**) was validated by synthesizing 1-phenylsulfonyl-3-phenyl indole-4,5-dione **6a** (**Scheme 2**). 5-Methoxyindole **8** was brominated in position

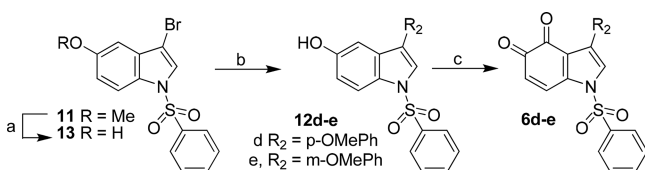
Scheme 2. Synthesis of 1-Phenylsulfonyl-3-aryl Indole-4,5-diones 6a–c^a

^aReagents and conditions: (a) Br₂, DMF, rt, 24 h, 74%; (b) PhSO₂Cl, *n*-Bu₄N⁺H₂SO₄⁻, aqueous 50% KOH, CH₂Cl₂, rt, 3 h, 90%; (c) arylboronic acid, Pd(PPh₃)₄, dry DME/EtOH 4/1, N₂ atmosphere, rt, reflux, 8 h, 83–92%; (d) 1 M BBr₃ in dry CH₂Cl₂, N₂ atmosphere, –78 to 5 °C, 87–99%; (e) IBX, EtOAc (40 °C) or DMF (rt), 2 to 24 h, 87–96%.

3 (step a, compound 10) and treated with phenylsulfonyl chloride (step b). 3-Bromo phenylsulfonamide 11 was reacted with phenyl boronic acid in a Suzuki coupling (step c) to provide, after careful optimization of the experimental protocol, 1-phenylsulfonyl-3-phenyl-5-methoxyindole 9a. Demethylation (step d, compound 12a) and oxidation with IBX⁴¹ (step e) led to 1-phenylsulfonyl-3-phenyl indole-4,5-dione 6a (Scheme 2) with an overall ≈35% yield.

3-Bromo phenylsulfonamide 11 was reacted with *o*- (R₂ = *o*-MePh, 9b) and *p*-substituted phenyl boronic acid (R₂ = *p*-NMe₂Ph, 9c) (step c), and respectively converted to 1-phenylsulfonyl-3-*o*-methylphenyl indole-4,5-dione 6b and 1-phenylsulfonyl-3-*p*-dimethylaminophenyl indole-4,5-dione 6c (steps d,e, Scheme 2) as reported for 6a.

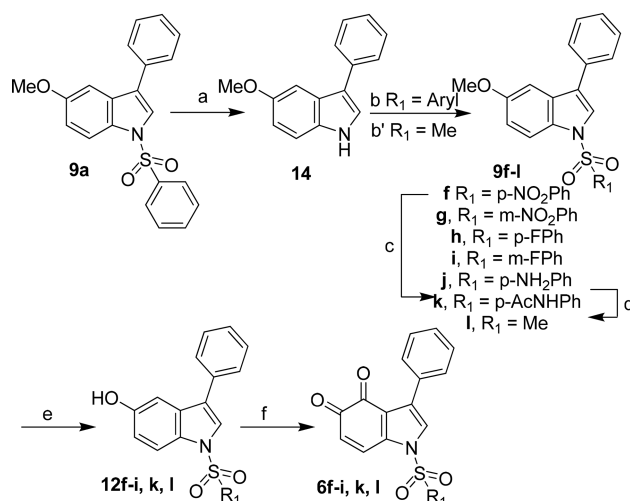
The synthesis of *p*-substituted (R₂ = *p*-OMe, 9d) and *m*-substituted (R₂ = *m*-OMe, 9e) aryl ethers (Scheme 3) required

Scheme 3. Synthesis of 1-Phenylsulfonyl-3-methoxyphenyl Indole-4,5-diones 6d,e^a

^aReagents and conditions: (a) 1 M BBr₃ in dry CH₂Cl₂, N₂ atmosphere, –78 to 5 °C, 86%; (b) methoxyphenylboronic acid, Pd(PPh₃)₄, dry DME/EtOH 4/1, N₂ atmosphere, rt, reflux, 8 h, 79–85%; (c) IBX, DMF, rt, 6 to 48 h, 67–87%.

demethylation of the 5-methoxy group on 3-bromo phenylsulfonamide 11 (step a) before Suzuki coupling (step b) and IBX oxidation (step c, Scheme 3) to avoid undesired demethylation of the 3-*m*- or *p*-methoxyphenyl group.

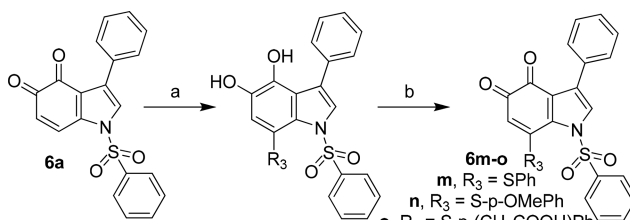
We attempted the synthesis of 1-alkylsulfonyl or 1-*m/p*-substituted arylsulfonyl-3-phenyl indole-4,5-diones 6f–l by replacing phenylsulfonyl chloride with alkyl- or *m/p*-arylsulfonyl chlorides (Scheme 2). Unfortunately, the Suzuki coupling protocol optimized for the synthesis of 9a was not applicable as such to other sulfonamides. Thus, we synthesized compounds 6f–i,k,l according to the longer, more efficient strategy depicted in Scheme 4.

Scheme 4. Synthesis of 1-Alkyl/Arylsulfonyl-3-phenyl Indole-4,5-diones 6f–i,k,l^a

^aReagents and conditions: (a) aqueous 3 M NaOH, 2/1 MeOH/THF, 80 °C, 2 h, 98%; (b) R₁SO₂Cl, *n*-Bu₄N⁺H₂SO₄⁻, 50% KOH, CH₂Cl₂, rt, 3 h, 87–92%; (b') NaH, mesyl chloride, dry DMF, N₂ atmosphere, 0 °C to rt, 3 h, 59%; (c) SnCl₂·2H₂O, 1/1 THF/MeOH, 80 °C, 2 h, 95%; (d) Ac₂O, pyridine, CH₂Cl₂, rt, 22 h, 82%; (e) 1 M BBr₃ in dry CH₂Cl₂, N₂ atmosphere, –78 to 5 °C, 73–99%; (f) IBX, EtOAc (40 °C) or DMF (rt), 2 to 24 h, 87–96%.

1-Phenylsulfonyl-3-phenyl-5-methoxyindole 9a was desulfonylated (step a, compound 14) and treated with aryl- (step b) or alkylsulfonamides (step b') to provide 1-*m/p*-substituted arylsulfonyl- and 1-methylsulfonyl-3-phenyl-5-methoxyindoles (respectively 9f–i and 9l) in good to excellent yields. 1-*p*-Nitrophenylsulfonyl-3-phenyl-5-methoxyindole 9f was reduced (step c, amine 9j) and acetylated to 1-*p*-acetamidophenylsulfonyl-3-phenyl-5-methoxyindole 9k (step d). Conversion of aryl ethers 9f–i,k,l into 1-*m/p*-substituted arylsulfonyl- or 1-alkylsulfonyl-3-phenyl indole-4,5-diones 6f–i,k,l (steps e and f, Scheme 4) was carried out as previously described for 6a.

1-Phenylsulfonyl-3-phenyl-7-thioaryl Indole-4,5-diones 6m–6o. The retrosynthetic scheme leading to 1,3,7-trisubstituted indole-4,5-diones 6 (R₁, R₂ ≠ H, R₃ = S–Ar, R₄ = H, Figure 2) was validated by synthesizing 1-phenylsulfonyl-3-phenyl-7-thiophenylindole-4,5-dione 6m (Scheme 5) via

Scheme 5. Synthesis of 1-Phenylsulfonyl-3-phenyl-7-thioaryl Indole-4,5-diones 6m–6o^a

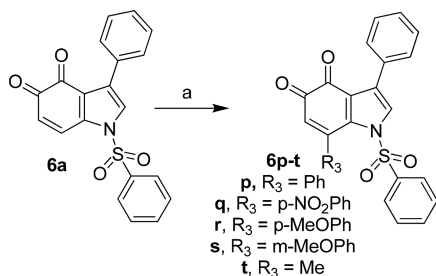
^aReagents and conditions: (a) aryl thiol, DMF, 2–3 h, rt, 62–88%; (b) IBX, DMF, 2 h, rt, 52–56%.

Michael addition of substituted benzenethiols on *o*-quinones.⁴¹ Namely, 1-phenylsulfonyl-3-phenyl indole-4,5-dione 6a was treated with thiophenol (step a), providing 1-phenylsulfonyl-3-phenyl-7-thiophenylindole-4,5-dione 6m after oxidation of the reduced form (step b, Scheme 5) in moderate yield after

extensive optimization. The optimized experimental protocol was used with *p*-methoxybenzenethiol (**6n**) and *p*-carboxymethylbenzenethiol (**6o**), observing moderate two step yields for both quinones.

1-Phenylsulfonyl-3-phenyl-7-aryl Indole-4,5-diones 6p–6t. The retrosynthetic scheme leading to 1,3,7-trisubstituted indole-4,5-diones **6** ($R_1, R_2, R_3 \neq H, R_4 = H$, Figure 1) was validated by synthesizing 1-phenylsulfonyl-3,7-diphenylindole-4,5-dione **6p** (Scheme 6) via Mn(III)-mediated radical addition of boronic

Scheme 6. Synthesis of 1-Phenylsulfonyl-3-phenyl-7-aryl Indole-4,5-diones 6p–6t^a

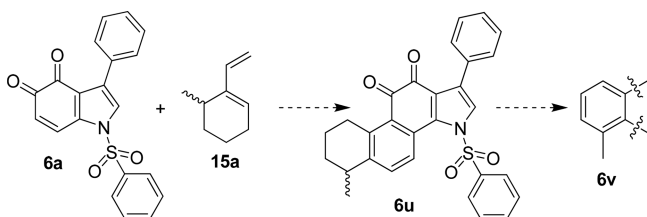


^aReagents and conditions: (a) boronic acid, Mn(OAc)₃, 1,2-dichloroethane, 80 °C, 30 to 150 min, 14–36%.

acids.^{40,42} 1-Phenylsulfonyl-3-phenyl indole-4,5-dione **6a** was treated with phenylboronic acid and Mn(OAc)₃ (step a), providing 1-phenylsulfonyl-3,7-diphenylindole-4,5-dione **6p** (Scheme 6). The experimental protocol required extensive optimization, and a moderate yield was finally obtained. The optimized experimental protocol was then used with aryl- (**6q–s**) and alkylboronic acids (**6t**), adapting the reaction time to each substrate (Scheme 5) and observing poor to moderate reaction yields.

Diels–Alder Cycloadducts 6u–6w. Validation of the retrosynthetic scheme to 1,3,6,7-tetrasubstituted indole-4,5-diones **6** ($R_1, R_2 \neq H, \text{cyclo } R_3, R_4$, Figure 1) targeted 1-phenyl-3-phenylsulfonyl-6-methylphenanthro[1,2-*b*]pyrrole-10,11-dione **6v**. We envisaged a Diels–Alder cycloaddition between 1-phenylsulfonyl-3-phenyl indole-4,5-dione **6a** and 6-methyl-1-vinylcyclohexene **15a**, followed by DDQ dehydrogenation/aromatization of tetrahydrocycloadduct **6u** to aromatic **6v** (Scheme 7).⁴³ Unfortunately, we could not obtain pure diene

Scheme 7. Attempted Synthesis of 6,7,8,9-Tetrahydro-1-phenyl-3-phenylsulfonyl-phenanthro[1,2-*b*]indole-10,11-dione 6v



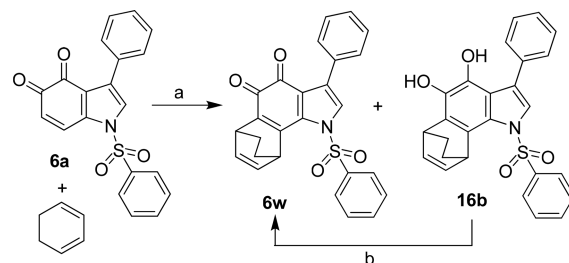
15a in reasonable amounts following the published synthetic procedure.⁴³

Due to the inhibitory activity observed with bicyclic indole-4,5-dione **6a** and some of its congeners, a tetracyclic, tanshinone-like core should not be necessarily needed to prevent HuR–mRNA interactions. Thus, cycloadditions on dienophile **6a** were targeted to introduce potency-oriented (additional interactions with the binding site on HuR) and/or

“druggability”-oriented substitutions on C-6 and C-7 (modulation of selectivity, solubility, and lipophilicity, etc.).

Diels–Alder cycloaddition between 1,3-cyclohexadiene **15b** and dienophile **6a** provided a mixture of desired *ortho*-quinone **6w** and diphenol **16b** (step a, Scheme 8). Oxidation (step b) converted the mixture to pure **6w**.

Scheme 8. Synthesis of Cycloadduct 6w^a



^aReagents and conditions: (a) cat. dry ZnCl₂, dry CH₂Cl₂, Ar atmosphere, 0 °C, 5 min, 88%; (b) CAN, 2/1 MeCN/H₂O, 0 °C, 10 min, quantitative.

A more systematic effort toward tanshinone-like 1,3,6,7-tetrasubstituted indole-4,5-diones **6** ($R_1, R_2 \neq H, \text{cyclo } R_3, R_4$, Figure 1) will be carried out, and reported in future.

Biochemical Characterization. Compounds 6a and 6n Are More Effective than 1 in Inhibiting the HuR–RNA Complex Formation. Tanshinone mimics **6a–i**, **6k–t**, and **6w** were evaluated using a previously developed biochemical tool based on Amplified Luminescent Proximity Homogenous Assay AlphaScreen technology.^{27,28} Recombinant His-tagged HuR (rHuR) bound to nickel chelate acceptor beads was incubated with a biotinylated single-strand AU-rich RNA probe (Bi–AU), recognized by streptavidin-coated donor beads. When rHuR binds to the Bi–AU, the beads are brought into proximity and a fluorescent signal can be detected. We evaluated the ability of tanshinone mimics to inhibit the rHuR–Bi–AU complex formation in saturation binding conditions. Knowing that the K_D value for the rHuR–Bi–AU interaction is 2.5 nM,²⁷ we fitted on AlphaScreen saturation curves the K_i values, quantifying the inhibitory efficiency of tested compounds from high to low nanomolar range (Table 1). Among tanshinone mimics showing K_i with a percentage of inhibition >50%, compounds **6a** ($K_i = 12.8$ nM) and **6n** ($K_i = 15$ nM) were more effective than **1**, whereas compounds **6h**, **6k**, **6l**, **6r**, and **6s** showed similar activity (Figure 3 and Table 1). Consistently with previous data,²⁷ K_i value of our compounds changes according to the host in which the recombinant protein is produced (Supporting Figure 1).

Tanshinone mimics **6b**, **6f**, **6m**, and **6o** resulted interfered with the emitted fluorescence in AlphaScreen;^{44,45} thus, we proceeded with a second independent, orthogonal assay protocol for these and a few other tanshinone mimics (Figure 4 and Supporting Figures 2 and 3). We evaluated their inhibitory activity via a non denaturing and non-cross-linked REMSA.^{27,28} After we mixed at least 10-fold excess of rHuR with 75 fmol of 5′-DY681-labeled AU-rich RNA probe (DY681-AU) or with 25 nM of FAM-RNA probe, we observed the formation of the higher, oligomeric molecular weight complex between protein and RNA. The concomitant addition of active tanshinone mimics (5 μM concentration) caused a reduction of the shifted RNA probe, allowing qualitative estimation of their inhibitory ability toward the Bi–AU ligand at equilibrium. We noticed a

Table 1. Abilities of Tanshinone Mimics To Inhibit the rHuR–Bi–AU Complex Formation^a

| Cpd | Structure | K _i ¹ , nM | Cpd | Structure | K _i ¹ , nM |
|-----|-----------|----------------------------------|-----|-----------|----------------------------------|
| 1 | | 50 | 6a | | 12.8 |
| 6b | | Interfering* | 6c | | >100 |
| 6d | | >200 | 6e | | >200 |
| 6f | | Interfering* | 6g | | >100 |
| 6h | | 48 | 6i | | >100 |
| 6k | | 81 | 6l | | 56 |
| 6m | | Interfering* | 6n | | 15 |
| 6o | | Interfering* | 6p | | >100 |
| 6q | | >100 | 6r | | 41 |
| 6s | | 55 | 6t | | >200 |
| 6w | | >300 | | | |

^aNotes: ¹Concentration (nM) leading to half-maximal inhibition of rHuR–Bi–AU complex. *Interfering with the fluorescence spectra of excitation–emission of donor and acceptor beads (histidine (nickel) chelate detection kit).

concordance between the two biochemical assays for compounds **6a**, **6c**, **6k**, **6n**, **6p–6t**, and **6w**. Tanshinone mimics **6b**,

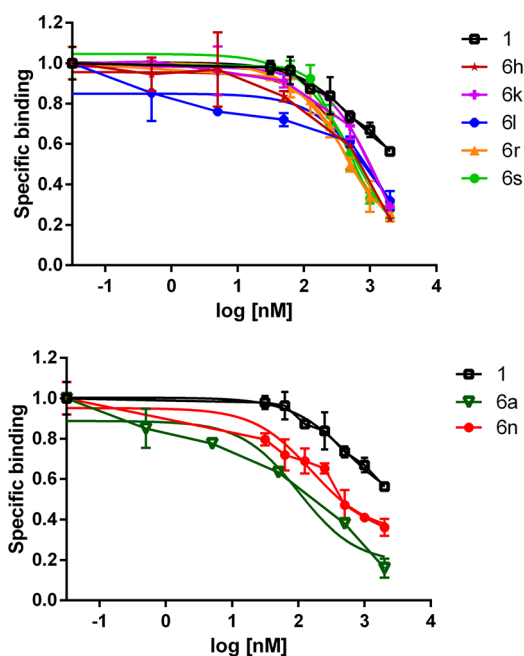


Figure 3. K_i calculation by Alpha screen assessing specific binding of His-tagged HuR and the AU-rich biotinylated RNA. K_i were calculated with respect to a K_D of 2.5 nM for the rHuR–Bi–AU interaction and normalized to control (DMSO). Fitting curves show nonlinear regression fits of the data according to a 1-site binding model in GraphPad Prism. Plotted bars are mean ± SD of two independent experiments.

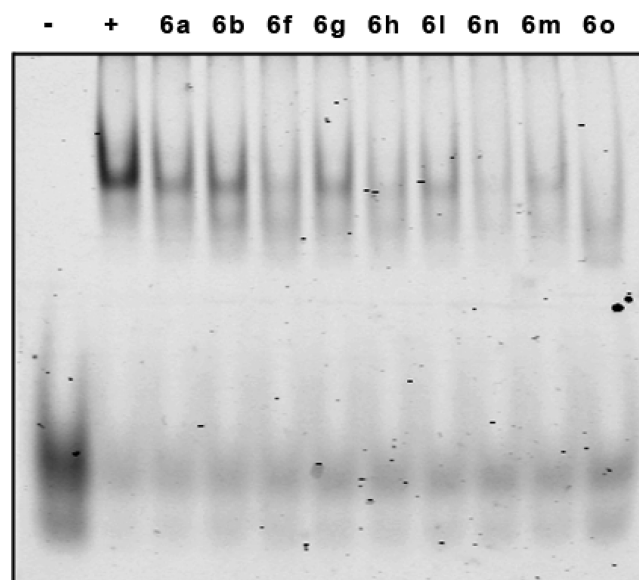


Figure 4. REMSA characterization of selected tanshinone mimics. REMSA assay performed with at least 10-fold excess of recombinant HuR incubated for 30 min with 75 fmol of 5'-DY681-labeled RNA probe. Incubation with RNA probe only (-), with rHuR, RNA probe and DMSO (+) used as positive control of the binding, and incubation with tanshinone mimics **6** (5 μM).

6f, **6m**, and **6o** were therefore classified as inhibitors endowed with intermediate potency (Figure 4). Compound **6a** was tested for binding to RNA probe via REMSA and circular dichroism (CD) (Supporting Figure 4A,B), showing no interference with the fluorescent probe and no change of the RNA conformation, thus suggesting the absence of an interaction with RNA.

Tanshinone Mimic 6a Directly Binds to HuR Protein and Modulates Its Binding with Intracellular Target mRNAs. Compound 6a was selected among the most potent tanshinone mimics for further evaluation. It showed a similar mechanism to 1 in interacting with the truncated form of HuR comprising the first two RRM domains (RRM1-RRM2) but not with the third domain (RRM3) and not with the RNA probe (Supporting Figure 4 and 5).

Dynamic mass redistribution (DMR) analysis⁴⁶ revealed, in a label-free format, a direct protein:6a interaction at the equilibrium (Figure 5). Full-length rHuR was immobilized onto the

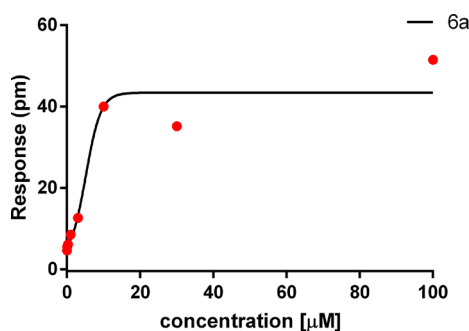


Figure 5. Compound 6a binds to recombinant HuR. Different concentrations of 6a were added to label-free microplate wells on which aliquots of full-length protein had previously been immobilized. Measurements were performed before (baseline, protein-coated wells) and after (final) adding the compound. The response (pm) was obtained subtracting the baseline output from the final output signals. The output signal for each well was obtained by subtracting the signal of the protein-coated reference area from the signal of uncoated area. The data (red dots) were fitted (black line) to a sigmoidal function using a 4-parameter logistic (4PL) nonlinear regression model: $R^2 = 0.944$; $p = 0.009$.

surface of label-free microplates by amine-coupling chemistry. Different amounts of 6a (0.03–100 μM) were added to the wells and the mass of molecular complexes was detected after 30 min incubation. Dose-dependent binding of 6a to rHuR was observed in the 0.3–10 μM range, sufficient to obtain saturation. The estimated affinity constant (K_D) was $\approx 4.5 \mu\text{M}$. The same experiment was performed with 1, but it was impossible to evaluate the K_D due to its poor solubility.²⁷

We then determined if 6a was interfering on HuR–RNA binding in MCF7 cells. We performed an RNA immunoprecipitation (RIP) assay⁴⁷ on MCF7 extracts testing three validated HuR transcripts. We clearly observed a subsequent decrease of the relative number of mRNA copies and a decreased expression level of such mRNAs (*ERBB2*, *CTNNB1*, *VEGF*) but not of non target genes (*RPLP0*, *HPRT1*) (Figure 6A,B). Therefore, compound 6a directly binds to HuR both *in vitro* and in cellular context, in a region contained between the first two RRM domains.

NMR and Molecular Modeling. *Tanshinone Mimic 6a Blocks HuR in a “Closed” Conformation.* The 2D ^1H – ^{15}N HSQC spectrum of RRM1-RRM2 domains showed well-dispersed signals in accordance with a folded protein structure, whose residues, including those of the linker region, have been previously assigned.²⁹ The resonances of residues forming the RRM1 domain are almost the same in the isolated domain⁴⁸ and in the RRM1-RRM2 construct. The large superimposition of the signals in the isolated RRM1 and in the tandem domains is in agreement with the relaxation data that show as the two domains move independently in solution in the absence of

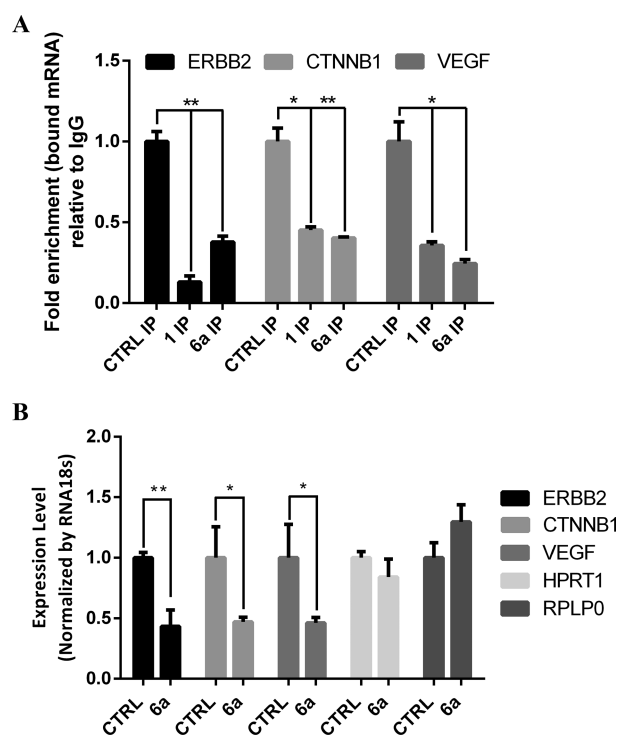


Figure 6. RIP and quantitative real-time PCR (qRT-PCR). (A) RIP was performed in MCF7 cells, lysed after 6 h treatment with DMSO (CTRL), 1 (1 μM) or 6a (5 μM). HuR antibody (IP) and an IgG isotype (IgG) were used for RNA precipitation. Changes in the mRNAs bound to HuR in the control or treatment condition were assessed by qRT-PCR and compared with the ones obtained with IgG precipitation, used as negative control. The relative values (Fold enrichment) were normalized to IgG, considering the value of the housekeeping gene *RPLP0*. (B) MCF7 were treated with 6a (5 μM) for 6 h to evaluate changes in total RNA levels. Expression level of *ERBB2*, *CTNNB1*, *VEGF*, *RPLP0*, and *HPRT1* were measured by qRT-PCR and normalized to *RNA18s*. Data are presented as mean \pm SD of a biological triplicate (* $p < 0.05$ and ** $p < 0.01$ versus CTRL).

RNA.²⁹ In line with the previously reported crystal structures of HuR, each domain in the RRM1-RRM2 construct is constituted by two α -helices and four β -strands.⁴⁹

The molecular interaction of 6a with RRM1-RRM2 tandem domains of HuR was evaluated through solution NMR.⁵⁰ Compound 6a shows improved solubility with respect to 1.²⁹ Its effects on the protein are appreciable in the 2D ^1H – ^{15}N HSQC in the presence of 0.6 equiv of the ligand, whereas with 1 comparable effects were observed after the addition of 4 equiv. As also reported for 1,²⁹ a generalized decrease in signal intensity was observed for the protein resonances, with few residues (Thr20, Leu22, Val66, Ser94, Tyr95, Ile103, Asn107, Leu108, Tyr109, Ile133, Val137, Leu138, Val139, Ser146) experiencing a stronger effect (Figure 7). Tanshinone mimic 6a and 1 interact with the protein in the same region, i.e. the β -platform of both domains. In particular, eight amino acids (Thr20, Ser94, Tyr95, Asn107, Leu108, Ile133, Val137, Leu138) experience a decrease in signal intensity with both ligands.

The generalized decrease of signal intensity, together with the distribution of affected residues over the large surfaces of the β -platform in each domain suggests an alteration of the equilibrium between “closed” and “open” conformations upon ligand binding. Specifically, the decrease of signal intensity was consistent with a mechanism where compound 6a stabilizes a “closed” conformation of HuR. Collectively, NMR analysis

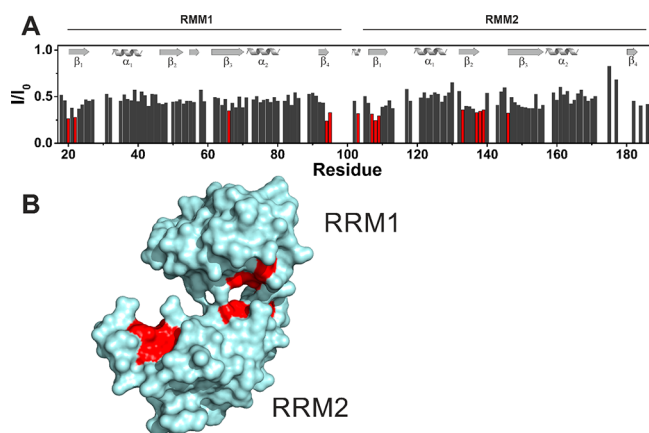


Figure 7. Compound **6a** stabilized recombinant HuR in a “closed” conformation. (A) Graphical representation of the intensity changes of RRM1-RRM2 HuR protein *per* residues in the presence of 0.6 equiv of **6a**. The residues exhibiting the highest decreases in signal intensities are colored in red. The secondary structures of the domains are reported on the graph. (B) Surface representation of the closed (PDB ID: 4ED5) conformation of HuR. The residues exhibiting the largest decrease in signal intensities in the presence of 0.6 equiv of **6a** are shown in red.

indicates that **1** and **6a** bind the HuR protein approximately in the same region, producing similar effects on protein dynamics. However, it is interesting to note that one residue (Ile103) of the interdomain linker (hereafter referred to as “hinge” loop) is

sensitive to **6a** and not to **1**. This experimental evidence would suggest for **6a** a binding site in a more close proximity of the hinge loop, with respect to **1**. To better explore this possibility, a molecular modeling study was performed.

To this purpose, a combined approach of docking calculations and extended molecular dynamics (MD) simulations was applied. Specifically, we first attempted a “blind” docking to the entire HuR surface, using two different docking software to better sample the binding space (AutoDock4.2 and Glide 6.5). Most of the highest-score poses of **6a** suggested by AutoDock were located within the RNA binding cleft (residues 18 to 95 of RRM1 and 107 to 185 of RRM2) and in proximity of the “hinge” loop. On the other hand, docking results with Glide converged toward one solution, which was different from those predicted by Autodock, though it was placed in proximity of the “hinge” loop as well. Therefore, albeit these results seem to indicate the region surrounding the “hinge” loop as the most likely binding region for **6a**, docking failed to unequivocally pinpoint one privileged binding mode, likely owing to omission of full receptor flexibility from the state-of-the-art docking software. To account for the missing receptor flexibility, we carried out multiple extended MD simulations on a reasonable number of **6a** binding modes, for a total simulation time of 6 μ s, and assessed their relative stability. Specifically, we opted for the binding pose predicted by Glide (Figure 8A) and the three best ranked and most diverse poses (in terms of root-mean-square deviation (RMSD) predicted by AutoDock) (Figure 8B,C,D). In all four cases, **6a** drifted away from its starting docking position and explored a significant portion of the HuR surface,

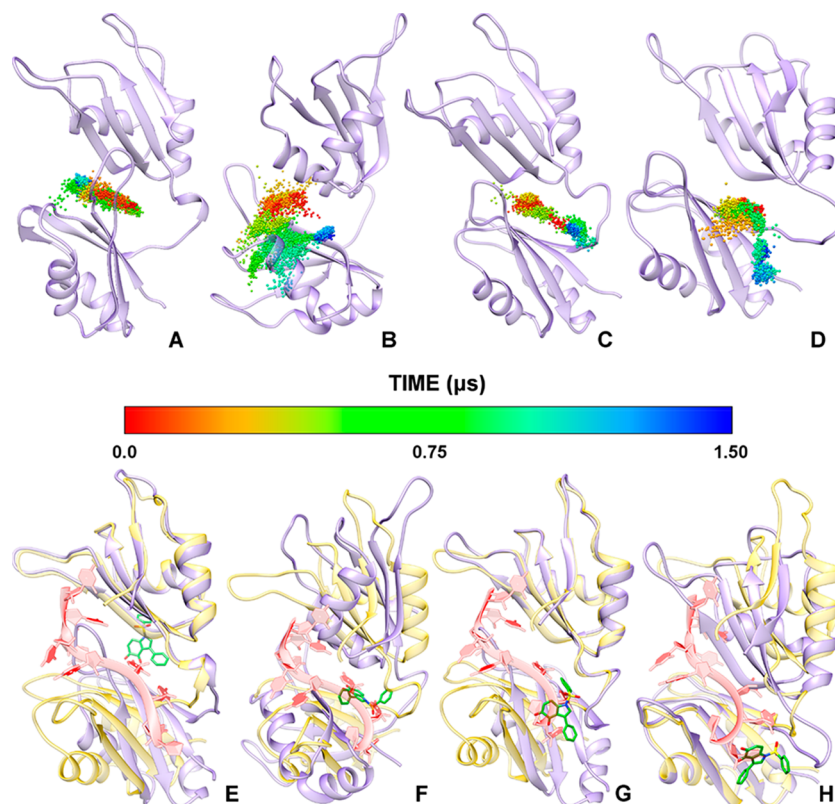


Figure 8. (A–D) **6a** exploration of the HuR RNA-binding pocket for each simulated pose. HuR is shown as purple cartoons, while the **6a** center of mass is shown as spheres colored according to the simulation time. (E,F) Global view of the HuR–**6a** complexes in each final MD simulation pose. Note how the binding of **6a** (green sticks) to HuR and the further closure of the mRNA binding cleft, as compared to the mRNA-bound conformation (yellow), prevent the accommodation of the mRNA strand (red ribbons). In both groups of pictures, panels related to the pose predicted by Glide and the three highest score poses predicted by Autodock are arranged from left to right, respectively.

as can be observed by following the movement of the center of mass of **6a** (Figure 8A–D), its RMSD vs time (Supporting Figure 6A) or its distance from the center of mass of the two RRM domains (Supporting Figure 6B). After about 1 μ s, each starting docking pose got stabilized and evolved to different final binding modes (Figure 8E–H) which remain individually stable for almost 500 ns. Specifically, out of the four final binding poses, one was located outside the RNA binding cleft (the Glide predicted binding pose, Figure 8E) while the other three were located within the latter pocket, in correspondence or in close proximity of the “hinge” loop. In these final poses **6a** stabilizes HuR in a conformational state that is structurally incompatible with RNA binding. In fact, in each case the two RRM domains were found to be more in contact with each other than in the HuR–RNA complex crystal structure (Figure 8E–H). Accordingly, we observed an increase in both the number of non-native interdomain contacts and the amount of surface area “buried” between the two RRM domains (see respectively Supporting Figure 7A and 7B). These results indicate that binding of **6a** to HuR is correlated with a closure of the RNA binding cleft and, consequently, with an overall decrease in the amount of interdomain space accessible for RNA binding.

Nevertheless, among the four poses issuing from our modeling approach, the one depicted in Figure 8F and more in detail in Figure 9 seems to be more in agreement with both the NMR

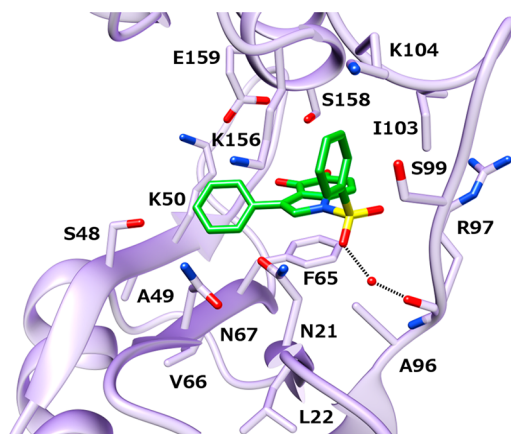


Figure 9. Most likely binding mode of **6a** (green sticks) to HuR (purple cartoons), as issuing from a representative structure of the last 500 ns of the MD simulation. HuR residues involved in binding interactions with **6a** are displayed as sticks.

data and the SARs reported here. Specifically, **6a** was found between the RRM1 beta sheets (β_1 , β_2 , β_3), the N-terminal part of the RRM2 α_2 helix and the “hinge” loop. In this binding arrangement (Figure 9), the phenyl ring in R_1 is accommodated in a narrow, laterally open, hydrophobic pocket, shaped by Ile103, Ser99, Lys104 and Lys156 residues, with which it establishes several CH- π interactions. Notably, one sulfonyloxygens establishes a water-bridged H-bond with the backbone C=O of Ala96, while the phenyl ring in R_2 , forms a cation- π interaction with Lys156 and several CH- π interactions with the CH₂ groups of Ser48, Lys50, Asn67 and Lys156. The indole-4, 5-dione moiety is inserted in a solvent exposed pocket, where it establishes CH- π interactions with Ala96, Lys156, Ser158 and, a π -stacking interaction with Phe65. In this regard, the quinone-oxygens, which point to the solvent exposed part of the pocket, likely play a crucial role in strengthening the π -stacking interaction with Phe65.

As compared to the other poses, in the above-described binding mode, **6a** is in close proximity with a larger number of HuR residues exhibiting the highest decreases in NMR signal intensity (Figure 7A). Precisely, these residues are Leu22, Val66, and Ile103. Notably, NMR pinpointed I103 in the “hinge” loop as a residue sensitive to binding of **6a** but not of **1**, which is known to stabilize HuR in a closed form without stably interacting with the “hinge” loop.²⁹ As compared to the other binding poses, which are located either outside the RNA binding cleft or in more solvent exposed regions, this binding mode (Figure 9) would be in line also with SARs studies. It would explain why substitutions on the phenyl ring in R_1 (**6f**, **6g**, **6h**, **6i**, **6k**, **6l**), though still causing a drop in the activity, are generally better tolerated than those on the phenyl ring in R_2 (**6b**, **6c**, **6d**, **6e**). In fact, thanks to the additional lateral space in the pocket hosting the phenyl ring in R_1 , this ring could slightly rotate around the S–N bond so as to allow the attachment of various substituents, even large ones as in the case of **6k**. This would not be possible at position R_2 , owing to potential steric clashes with residues shaping the pocket where it is hosted. This binding mode would also explain why the addition of electron-drawing substituents on the phenyl group in R_1 (**6f**, **6g**, **6h**, **6i**), particularly at the meta position (**6g**, **6i**), also causes a drop in the activity. In fact, these substitutions would likely weaken the aforementioned water-bridged H-bond with Arg97. Finally, SARs indicate that the addition of rigid and bulky substituents at position 6–7 (see **6w**) or 7 (**6p**, **6q**, **6r**, **6s**, **6t**) of the bicyclic scaffold (B ring) is also generally detrimental to binding. Steric clashes with the adjacent sulfonamidic group are very likely to arise as a result of their introduction, which would force a rotation around the S–N bond. That, according to our model, would in turn lead to a rupture of the water-bridged H-bond with Ala96 and of the hydrophobic interactions of the phenyl ring in R_1 . In the case of **6q**, but especially of **6r** and **6s**, the presence of a H-bond donor at position 7 may partially compensate for these detrimental effects through the potential formation of a H-bond with the near Arg97 side chain. The only exception to this trend is represented by **6n**, where the presence of a sulfur atom directly linked to the scaffold likely increases the rotational flexibility and makes the addition of a bulky group well tolerated.

In conclusion, our NMR and molecular modeling data provide useful insights into the binding mode and mechanism of action of this family of compounds, suggesting that they most likely bind HuR at the “hinge” region between the two RRM domains and stabilize HuR in a peculiar closed conformation, which is incompatible with RNA binding.

Biological Activity in Cancer Cell Lines. Selected Tanshinone Mimics Show Micromolar Cytotoxicity in Cancer Cells. We previously reported that the anticancer effects of **1** are influenced by HuR dosage, demonstrating that HuR is functionally connected with the intracellular effects of this pleiotropic natural product.²⁹ Similarly to **1**, the localization of HuR did not change during treatment with **6a** or other tanshinone mimics, suggesting that inhibition of HuR is connected with its binding performances and not with its subcellular localization (Figure 10).

We evaluated the cytotoxic effects of tanshinone mimics. Compounds **6a** and **6n** affected the viability of cells when treated for 72 h, together with **6b**, **6m**, **6k**, **6l** and **6t** at higher dosages (Figure 11). They were tested on breast cancer cell lines MCF7 and MDA-MB-231, and on pancreatic ductal adenocarcinoma cell line PANC-1. Tanshinone mimics were generally less effective

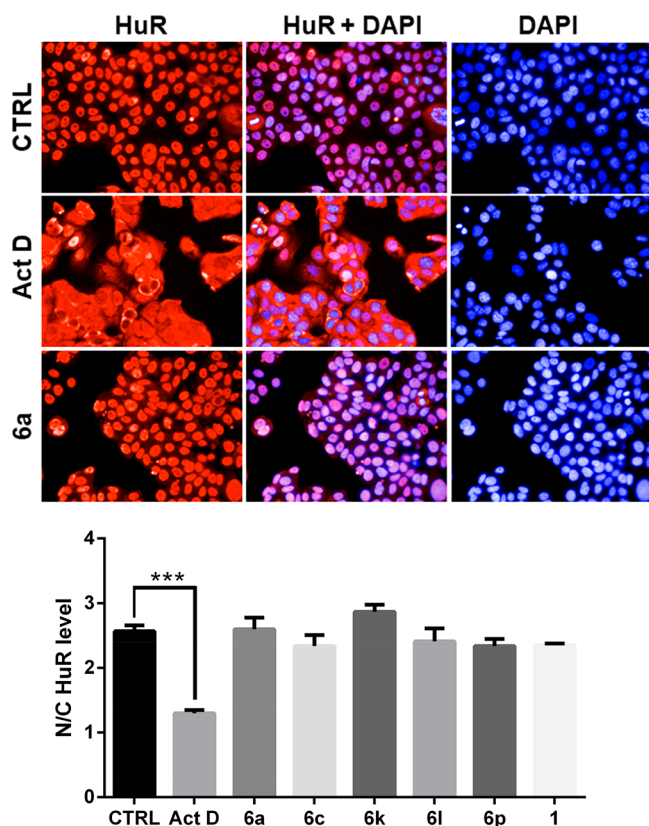


Figure 10. Representative immunofluorescence showing unchanged subcellular localization of HuR after **6a** treatment. HuR (red) or nuclei (blue, DAPI) after staining in MCF7 cells treated for 3 h with DMSO (CTRL) or 2.5 μM of actinomycin D (ActD)¹⁹ or 10 μM **6a**. Plotted in the graph are the ratio of HuR fluorescent signal between nucleus and cytoplasm (N/C). The image plate reader Operetta was used for image acquisition (40 \times high NA objective) and evaluation by selecting 13 fields/well. The ratio N/C represents the mean \pm SD of single cells for every well (***) $p < 0.001$.

tive than **1** on cell viability (Figure 11, Supporting Table S1), with an IC_{50} in the medium μM range (spanning from 20 to 50 μM for compounds **6a**, **6b**, **6n**, and **6m**, with PANC-1 being the most sensitive cell line to the tested compounds). An IC_{50} value was achieved for **6a**, **6b**, **6n**, **6m** compounds (Figure 11).

Additionally, tanshinone mimic **6a** could block the migration of PANC-1 and MDA-MB-231 cells (Figure 12 and Supporting Figure 8). Previously identified HuR disruptors show cytotoxic activity in cancer cell lines and in xenograft models. MS-444 induced cell death in colon cancer cells xenografted in nude mice,⁵¹ as did coumarin analogues in colon cancer cells *in vitro*.²³ Additionally, MS-444 chemo-prevented the development of intestinal tumors in APCmin mice, a model of familial adenomatous polyposis, but it was detrimental in the context of chemically induced inflammatory bowel disease (IBD). In this case, MS-444 favored azoxymethane/dextran sodium sulfate (AOM/DSS) tumorigenesis, size and invasiveness, therefore suggesting a careful evaluation of the utilization of HuR disruptors in the IBD settings.⁵² Tanshinone mimics **6a**, **6b**, **6m**, **6n**, **6k**, **6l**, and **6t** showed moderate IC_{50} in cancer cell lines, that was comparable to MS-444 (5 to 15 μM in colon cancer cell lines)⁵¹ and coumarin analogues (50 to 75 μM effective doses in colon cancer cell lines).²³ Therefore, tanshinone mimics do not affect HuR mobility directly and are endowed with interesting anti-tumor properties.

CONCLUSIONS

In our previous report, as a result of a high throughput screening on a set of anti-inflammatory agents, we identified **1**, a low-molecular-weight compound able to interact with HuR, thus affecting its post-transcriptional functions and contributing to its cytotoxic properties.²⁷ Very recently, we characterized its mechanism of action through a multidisciplinary strategy.²⁹ Here, inspired by **1** structure, we designed and synthesized an array of ortho-quinones (tanshinone mimics). They are the first family of HuR disruptors, through which the SARs reported here elucidate the steric/electrostatic requirements of a HuR binding site. In this regard, two complementary techniques, Alpha-Screen and REMSA, were used to quantify the inhibitory activity of tanshinone mimics **6a**–**t**. Among them, compounds **6a** and **6n** turned out to be more effective than **1** in HuR binding, showing a K_i of 12.8 and 15 nM respectively. In addition, **6a** is the only molecule, to our knowledge, for which a direct K_D against HuR can be measured through DMR ($K_D \approx 4.5 \mu\text{M}$). A combined approach of *in vitro* studies, NMR titration and MD simulations clarified the mechanism of action of compound **6a** that is to stabilize HuR in a peculiar closed conformation, which is incompatible with RNA binding.

From a biological point of view compound **1** inhibited viability and migration of breast cancer cell lines and induced cell death in colon cancer cells xenografted in nude mice in a HuR dependent manner,²⁹ although its pleiotropic effects contribute to its activity. The diminished cytotoxicity of tanshinone mimics compared to **1** could be ascribed to the reported multipharmacological effects of the latter,⁵³ or to limited bioavailability of tanshinone mimics. Nevertheless, our first generation tanshinone mimics are a valuable starting point to generate a more potent, *in vivo* active set of anticancer compounds. Our current efforts aim to further expanding our SARs, and to improve the efficacy of tanshinone mimics on HuR modulation in cells through the introduction of solubilizing moieties in position 1 and 7.

EXPERIMENTAL SECTION

Chemistry. Purity measurements were carried out by HPLC-MS, using NMR data to corroborate our findings. All our final compounds resulted to be $\geq 95\%$ pure.

General Procedures. ¹H NMR spectra were recorded on a Bruker Avance 400 MHz instrument in CDCl_3 , CD_3OD , or D_2O as solvent at 400 MHz. ¹³C NMR spectra were recorded in CDCl_3 , CD_3OD , or D_2O as solvent at 101 MHz. Coupling constants are given in Hertz and are rounded to the nearest 0.1 Hz. LC–MS data were collected with a Waters Acquity Ultra performance LC equipped with an Acquity UPLC HSS T3 column (2.1 mm \times 50 mm, 1.8 μm) and a SQD detector. Purifications were carried out either by flash chromatography on silica gel (particle size 60 μm , 230–400 mesh), on Kieselgel, or by Biotage flash chromatography [Biotage columns Si-25-M (150 \times 25 mm; silica gel (40–63 μm), flow rate 25 mL/min)], or by Biotage C_{18} reverse phase chromatography [Biotage column C_{18} HS (150 \times 25 mm; KP- C_{18} –HS (35–70 μm), flow rate 25 mL/min)]. Final compounds **6a**–**i**, **6k**–**p**, **6s** were purified by C_{18} reverse phase semipreparative HPLC using a Waters X-Bridge column (19 mm \times 15.0 cm, 5 μm). Melting points were determined with a Stuart Scientific SMP3 melting point apparatus. Solvents were distilled and dried according to standard procedures, and reactions requiring anhydrous conditions were performed under nitrogen or argon atmosphere.

1-Phenylsulfonyl-3-phenyl-4,5-dioxindole (6a). IBX⁴⁰ (548 mg, 1.96 mmol, 1.2 equiv) was added to a solution of 1-phenylsulfonyl-3-phenyl-5-hydroxy indole **12a** (570 mg, 1.63 mmol, 1 equiv) in EtOAc (8 mL, ≈ 0.17 M concentration), under vigorous stirring at room temperature. The reaction was monitored by TLC (eluants: *n*-Hexane/EtOAc 6/4). After 24 h, the reaction was filtered on Celite. After the

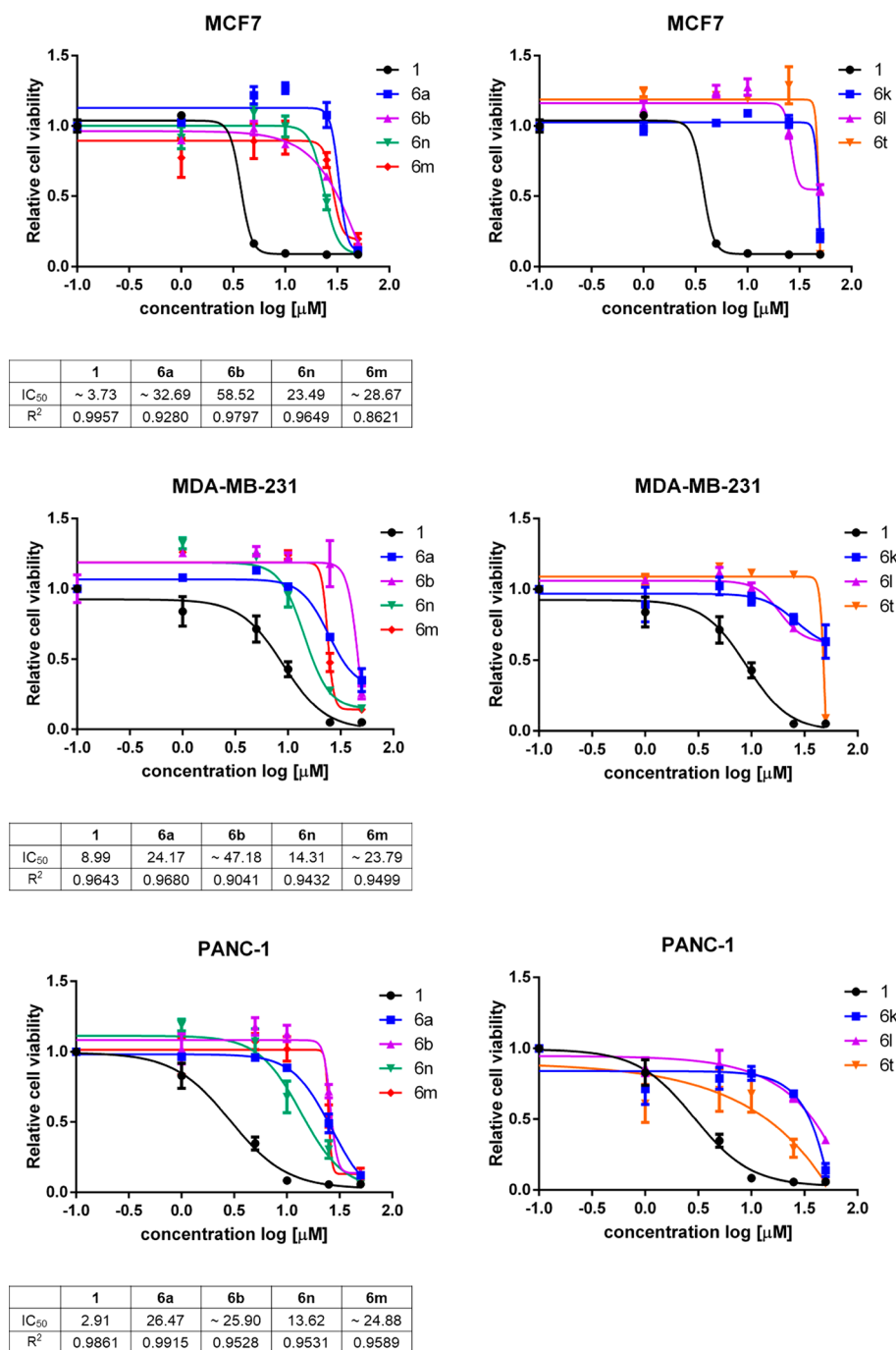


Figure 11. Cell viability of tanshinone mimics, assessed after 72 h of treatment with the indicated compounds (0–50 μM). Plotted bars are mean \pm SD of a biological duplicate, normalized to control (DMSO). Relative IC₅₀ and R² were calculated by nonlinear regression curve fitting.

solvent was concentrated, the crude (930 mg, purple solid) was purified by flash chromatography on silica gel (eluents: *n*-Hexane/EtOAc 6/4). Pure compound **6a** (515 mg, 1.42 mmol, 87% yield, \geq 95% purity) was obtained as a dark red solid, mp 140 °C (dec.). ¹H NMR (400 MHz, acetone d₆): δ (ppm) 8.25–8.23 (m, 2H, *o*-ArSO₂), 8.07 (d, 1H, *J* = 10.5 Hz, H7), 7.87 (tt, 1H, *J* = 7.5 Hz, *J* = 1.2 Hz, *p*-ArSO₂), 7.78–7.74 (m, 3H, H2, *m*-ArSO₂), 7.68–7.65 (m, 2H, *o*-Ar), 7.40–7.33 (m, 3H, *p*-Ar, *m*-Ar), 6.21 (d, 1H, *J* = 10.5 Hz, H6). ¹³C NMR (75.4 MHz, acetone d₆): δ (ppm) 182.3, 174.8, 138.5, 137.9, 136.5, 132.1, 131.5, 131.3, 130.5, 129.6, 129.1, 128.9, 128.5, 127.1. MS (ESI⁺): *m/z* 748.9 [2M+Na⁺]. Calculated MS, C₂₀H₁₃NO₄S: 363.06.

1-Alkyl/arylsulfonyl-3-phenyl-4,5-dioxoindoles, General Oxidation Procedure A (6a, 6f–h, 6l). IBX⁴⁰ (1.2 equiv) was added to a solution of 5-hydroxy indoles (1 equiv) in EtOAc (\approx 0.17 M concentration),

under vigorous stirring at room temperature. The reaction was monitored by TLC. When the reaction was completed (between 7 and 34 h), the mixture was filtered on Celite. After concentration of the solvent, the crude was purified by flash chromatography on silica gel, affording pure 1-arylsulfonyl-3-aryl-4,5-dioxo indoles as amorphous solids.

1-Arylsulfonyl-3-aryl-4,5-dioxoindoles, General Oxidation Procedure B (6b–e, 6i, 6k). IBX⁴⁰ (1.2 equiv) was added to a solution of 5-hydroxy indoles (1 equiv) in DMF (\approx 0.17 M concentration), at room temperature and under vigorous stirring. The reaction was monitored by TLC. When the reaction was completed (between 2 and 48 h), the mixture was diluted with water (20 volumes). The aqueous phase was extracted with EtOAc (10 volumes, until colorless). The collected organic layers were washed once with brine (20 volumes), dried with anhydrous Na₂SO₄, and filtered. The solvent was removed

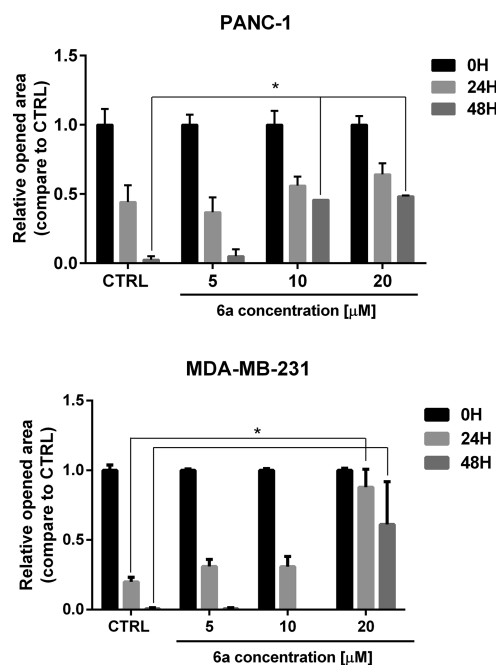


Figure 12. Scratch assay in PANC-1 and MDA-MB-231 cells. Images of invaded cells at 0, 24, and 48 h after scratching and treatment with DMSO (CTRL) or **6a** were taken from a time-lapse sequence of cell migration; wounds with consistent shape within each well were generated using a 200 μL tip. Residual open area at different time points is indicated as calculated by ImageJ software (* $p < 0.05$).

under reduced pressure, and the resulting crude was purified by flash chromatography on silica gel, affording pure 1-arylsulfonyl-3-aryl-4,5-dioxo indoles as amorphous solids.

1-Phenylsulfonyl-3-phenyl-7-thiophenyl-4,5-dioxoindole (6m). The title compound (30.2 mg, 45% yield over 2 steps, $\geq 95\%$ purity, mp 136 $^{\circ}\text{C}$ (dec.), purple solid) was prepared from 1-(phenylsulfonyl)-3-phenyl-4,5-dioxo indole **6a** (55 mg, 0.15 mmol, 1.0 equiv) and thiophenol (18.2 μL , 0.178 mmol, 1.18 equiv) in DMF (0.65 mL), following the general procedure for Michael reaction (2.5 h) and IBX oxidation. ^1H NMR (400 MHz, acetone- d_6): δ (ppm) 7.89–7.63 (m, 12H, Ar), 7.59 (s, 1H, H2), 7.42–7.31 (m, 3H, Ar), 6.91 (s, 1H, H6). ^{13}C NMR (100 MHz, acetone- d_6): δ (ppm) 177.2, 173.6, 140.3, 138.1, 137.2, 135.7, 135.6, 131.2, 130.5, 130.4, 129.1, 129.0, 128.5, 128.1, 128.0, 127.3, 122.3, 120.9, 119.5. MS (ESI $^+$): m/z 494.32 [$\text{M}+\text{Na}^+$]. Calculated MS, $\text{C}_{26}\text{H}_{17}\text{NO}_4\text{S}_2$: 471.06.

1-Phenylsulfonyl-3-phenyl-7-thioaryl-4,5-dioxoindoles, General Procedure for Michael Reaction (6m–o). A substituted thiophenol (1.18 equiv) was added to a solution of 1-(phenylsulfonyl)-3-phenyl-4,5-dioxo indole **6a** (1.0 equiv) in DMF (0.23M). The solution was stirred at room temperature for 2–3 h, then water (1 volume) was added. The mixture was extracted with EtOAc (four times, 4 volumes), and the collected organic phases were dried over sodium sulfate, filtered, and evaporated under reduced pressure. The crude was purified by reverse phase chromatography (eluent: A CH_3CN , B water, from 0% A to 100% A), affording the ortho-bisphenol (62%–88%). IBX (0.5–2 equiv) was then added to the ortho-bisphenol (1eq) in DMF (0.2 M) under stirring at rt. After reaction completion (2 h), water was added (1 volume), and the mixture was extracted with EtOAc (four times, 2 volumes). The collected organic phases were dried over sodium sulfate, filtered, and evaporated under reduced pressure. The crude residue was purified by reverse phase chromatography (eluent: A CH_3CN , B H_2O , from 0% A to 100% A) affording pure 1-(phenylsulfonyl)-3-phenyl-7-thioaryl-4,5-dioxo indoles as amorphous solids.

1-Phenylsulfonyl-3,7-diphenyl-4,5-dioxoindole (6p). The title compound (32 mg, 0.072 mmol, purple solid, 34% yield considering the recovery of 28 mg of unreacted **6a**) was obtained from 1-(phenylsulfonyl)-3-phenyl-4,5-dioxo indole **6a** (105 mg, 0.289 mmol,

1.0 equiv) and phenylboronic acid (55 mg, 0.452 mmol, 1.5 equiv) in dry DCE (3 mL, ≈ 0.09 M), following the general procedure for Mn(III)-mediated radical addition. ^1H NMR (400 MHz, DMSO d_6): δ (ppm) 8.27 (2H, d, $J = 7.7$ Hz, o-Hs of PhSO_2), 7.96 (1H, s, H2), 7.89–7.83 (2H, m, H6, p-H of PhSO_2), 7.76 (2H, t, $J = 7.7$ Hz, m-Hs of PhSO_2), 7.72–7.76 (2H, m, o-Hs of 3-Ph), 7.50–7.36 (8H, m, m- and p-Hs of 3-Ph, all Hs of 7-Ph). ^{13}C NMR (75.4 MHz, DMSO d_6): δ (ppm) 179.5, 173.4, 137.0, 136.8, 136.0, 134.9, 130.9, 130.6, 128.7, 128.3, 128.1, 127.6, 125.0, 123.8, 121.3. MS (ESI $^+$): m/z 440.21 [$\text{M}+\text{H}^+$]. Calculated MS, $\text{C}_{26}\text{H}_{17}\text{NO}_4\text{S}$: 439.09.

1-Phenylsulfonyl-3-phenyl-7-alkyl/aryl-4,5-dioxoindoles, General Procedure for Mn(III)-Mediated Radical Addition (6p–t).

1-(Phenylsulfonyl)-3-phenyl-4,5-dioxo indole **6a** (1.0 equiv) and a boronic acid (1.5 equiv) were dissolved in dry dichloroethane (DCE, ≈ 0.09 M in **6a**). The solution was stirred for 2 min and then Mn(OAc) $_3$ ·2H $_2$ O (3 equiv) was added. The mixture was kept under nitrogen atmosphere, stirred at 80 $^{\circ}\text{C}$ until reaction completion (monitoring by TLC, eluent: *n*-Hexane/EtOAc 7/3), and cooled at room temperature. Then, CH_2Cl_2 (2 volumes) and saturated aqueous NaHCO_3 (2 volumes) were added. The aqueous layer was extracted with CH_2Cl_2 (2 volumes, two times). The collected organic phases were washed with brine (8 volumes, two times), dried over sodium sulfate, filtered and evaporated under reduced pressure to give a crude solid. The crude was purified by flash chromatography (eluent: *n*-Hexane/EtOAc 7/3). Pure 1-(phenylsulfonyl)-3-phenyl-7-substituted-4,5-dioxo indoles were obtained as amorphous solids.

3-Bromo-5-methoxyindole (8). The synthesis of compound **8** was carried out as previously described,⁵⁴ and its analytical characterization confirmed its structure.

1-Phenylsulfonyl-3-phenyl-5-methoxyindole (9a). The synthesis of compound **9a** was carried out as previously described,⁵⁵ and its analytical characterization confirmed its structure.

1-Phenylsulfonyl-3-aryl-5-Substituted Indoles, General Suzuki Procedure (9b,c, 12d,e). 1-Phenylsulfonyl-3-bromo-5-methoxy- (**11**) or 5-hydroxy indole (**13**) (1 equiv) and an arylboronic acid (1.17 equiv) were placed in a two-necked round-bottom flask, equipped with a CaCl_2 valve. The flask was flushed with nitrogen to remove any trace of oxygen. The middle neck was closed by a rubber septum, then dry dimethoxyethane (DME, ≈ 0.07 M concentration in **11**) and previously deaerated aqueous 2 M K_2CO_3 (1.29 equiv) were added and the resulting mixture was stirred at room temperature under nitrogen atmosphere. Finally, PdTetrakis (0.05 equiv) and previously deaerated EtOH (final 4/1 DME/EtOH ratio) were added under nitrogen flushing. A pale yellow solution was formed. The rubber septum was removed, and then the main-middle neck was equipped with a condenser surmounted by a CaCl_2 valve. The pale yellow solution was stirred under nitrogen atmosphere, refluxed for 8 h, and left to stir at room temperature overnight. Then, the reaction mixture was diluted with a saturated solution of NH_4Cl (1 volume) and extracted with EtOAc (1.5 volumes, three times). The organic phase was washed with saturated aqueous NH_4Cl (3 volumes) and with brine (3 volumes), then dried over Na_2SO_4 and filtered. The crude was purified by flash chromatography on silica gel, affording pure 1-phenylsulfonyl-3-aryl-5-substituted indoles as amorphous solids.

1-Arylsulfonyl-3-phenyl-5-methoxyindoles, General N-Arylsulfonylation Procedure (9f–i). Aqueous 50% KOH (8 equiv) was added to a stirred mixture of 3-phenyl-5-methoxy indole **14** (1 equiv) and $n\text{-Bu}_4\text{N}^+\text{HSO}_4^-$ (0.1 equiv) in CH_2Cl_2 (≈ 0.2 M concentration in **14**). The reaction was stirred vigorously at room temperature for 10 min. An arylsulfonyl chloride (1.7 equiv) in CH_2Cl_2 (total ≈ 0.1 M concentration in **14**) was then added, and the mixture turned to orange-brown. The reaction was monitored by TLC (eluent: *n*-Hex/EtOAc 9/1). After 3 h, the reaction was stopped by diluting with water (1 volume) and extracting with CH_2Cl_2 (2 volumes, two times). The collected organic layers were washed with water (2 volumes) and brine (2 volumes), and dried over sodium sulfate. The solvent was evaporated under reduced pressure affording a crude. The crude was purified through flash chromatography on silica gel, affording pure 1-arylsulfonyl-3-phenyl-5-methoxy indoles as amorphous solids.

1-Phenylsulfonyl-3-bromo-5-methoxyindole (11). The synthesis of compound **11** was carried out as previously described,⁵⁶ and its analytical characterization confirmed its structure.

1-Phenylsulfonyl-3-phenyl-5-hydroxyindole (12a). Initially, 1 M BBr_3 in CH_2Cl_2 (26.4 mL, 6 equiv) was slowly added under nitrogen atmosphere and at -78°C to a stirred solution of 1-phenylsulfonyl-3-phenyl-5-methoxy indole **9a** (1.6 g, 4.41 mmol, 1 equiv) in dry CH_2Cl_2 (22 mL, ≈ 0.2 M concentration). The temperature was slowly increased to room temperature while monitoring by TLC (eluents: *n*-Hexane/EtOAc 8/2). The resulting dark green solution was immediately diluted with water (150 mL) and neutralized with saturated aqueous NaHCO_3 . The reaction mixture was extracted with CH_2Cl_2 (3×150 mL). The collected organic phases were then washed with brine (400 mL), dried over Na_2SO_4 , and filtered. The solvent was removed under reduced pressure. The crude (1.7 g) was purified by flash chromatography on silica gel, yielding pure compound **12a** (1.34 g, 3.84 mmol, 87% yield) as a white solid. ^1H NMR (400 MHz, acetone d_6): δ (ppm) 8.29 (s, 1H, OH), 8.05–8.03 (m, 2H, o-ArSO₂), 7.93 (d, 1H, *J* = 8.9 Hz, H7), 7.84 (s, 1H, H2), 7.69–7.65 (m, 3H, p-ArSO₂, o-Ar), 7.60–7.56 (m, 2H, m-ArSO₂), 7.50–7.46 (m, 2H, m-Ar), 7.38 (tt, 1H, *J* = 7.4 Hz, *J* = 1.2 Hz, p-Ar), 7.21 (d, 1H, *J* = 2.4 Hz, H4), 6.96 (dd, 1H, *J* = 8.9 Hz, *J* = 2.4 Hz, H6). ^{13}C NMR (75.4 MHz, acetone d_6): δ (ppm) 155.5, 138.9, 135.1, 134.0, 131.4, 130.4, 129.8, 128.6, 128.4, 127.8, 124.9, 115.6, 115.0, 106.0. MS (ESI⁺): *m/z* 721.0 [2M+Na⁺]. Calculated MS, $\text{C}_{20}\text{H}_{15}\text{NO}_3\text{S}$: 349.08.

1-Aryl/Alkylsulfonyl-3-Substituted-5-Hydroxyindoles, General Demethylation Procedure (12a–c, 12f–i, 12k, 12l, 13). First, 1 M BBr_3 in CH_2Cl_2 (6 equiv) was slowly added under nitrogen atmosphere and at -78°C to a stirred solution of 1-aryl/alkylsulfonyl-3-substituted-5-methoxy indoles (1 equiv) in dry CH_2Cl_2 (≈ 0.2 M concentration). The temperature was slowly increased to room temperature while monitoring by TLC, then it was immediately diluted with water (5 volumes) and neutralized with saturated aqueous NaHCO_3 . The reaction mixture was extracted with CH_2Cl_2 (5 volumes, three times). The collected organic phases were then washed with brine (15 volumes), dried over Na_2SO_4 , and filtered. The solvent was removed under reduced pressure. The crude hydroxyl indoles were purified by flash chromatography on silica gel, affording pure 1-aryl/alkylsulfonyl-3-substituted-5-hydroxy indoles as amorphous solids.

3-Phenyl-5-methoxyindole (14). Aqueous 3 M NaOH (21 mL, 63 mmol, 46 equiv) was added dropwise in 30 min to a solution of 1-phenylsulfonyl-3-phenyl-5-methoxy indole **9a** (500 mg, 1.38 mmol, 1 equiv) in 2/1 MeOH/THF (207 mL). The pale pink mixture was warmed up to 80°C . The reaction was monitored by TLC (eluant: *n*-Hex/EtOAc 8/2). After 2 h the reaction was stopped by acidifying with 3 N HCl (21 mL), and the organic solvents were evaporated under reduced pressure. The aqueous residue was extracted with EtOAc (3×100 mL). The collected organic layers were washed with brine (450 mL), and dried over sodium sulfate. The solvent was evaporated under reduced pressure affording a crude brown oil (365 mg), that was purified by flash chromatography on silica gel (eluant: *n*-Hex/EtOAc 85/15). Pure compound **14** (300 mg, 1.34 mmol, 97% yield) was obtained as a pale yellow solid. ^1H NMR (400 MHz, acetone d_6): δ (ppm) 10.33 (1H, bs, NH), 7.72–7.69 (2H, m, o-Ar), 7.58 (1H, d, *J* = 2.6 Hz, H2), 7.47–7.36 (4H, m, H4, H7, m-Ar), 7.26–7.21 (1H, m, p-Ar), 6.85 (1H, dd, *J* = 2.50 Hz, *J* = 8.80 Hz, H6), 3.84 (3H, s, OMe). MS (ESI⁺): *m/z* 748.9 [2M+Na⁺]. Calculated MS, $\text{C}_{15}\text{H}_{13}\text{NO}$: 223.27.

Biology. Amplified Luminescent Proximity Homogeneous Assay (ALPHA Screen). AlphaScreen assays have been performed using histidine (nickel) chelate detection kit (PerkinElmer, 6760619), based on the reaction of an His-tagged HuR protein and a biotinylated single strand RNA (BITEG-RNA), as previously described.²⁸ The full-length HuR recombinant protein has been expressed in *E. coli* Rosetta DH5a according to an already published protocol.²⁷ Hooking point curves, with 50 nM of BITEG-RNA probe, have been performed to test its activity after purification and dialysis. Dissociation equilibrium constants (K_d) were calculated with respect to a K_D of 2.5 nM for the Bi–AU ligand interaction, in the presence of as low as 0.5% DMSO (relative control) and of tanshinone mimics. Non specific interference with the assay has been evaluated by reacting the same amount of acceptor and donor

beads (20 $\mu\text{g}/\text{mL}/\text{well}$) with biotinylated-His₆ molecule in the same experimental conditions. GraphPad Prism software v5.1 has been used for fitting calculation and statistical significance. rHuR expressed in HEK293T has been purified according to a previously published protocol.²⁷

RNA-Electrophoretic Mobility Shift Assays (REMSAs). REMSAs were performed as previously indicated,²⁷ with minor modifications. Besides recombinant full-length HuR, HuR RRM1–2 and RRM3 constructs were used to express and purify proteins as previously described.^{27,29}

At least 10-fold excess of recombinant HuR and its RRMs were incubated for 30 min with either 75 fmol of 5'-DY681-labeled AU-rich RNA probe or with 25 nM of 5'-FAM-labeled RNA probe or with 500 nM of Cy-3-RNA probe and DMSO as control or tanshinone mimics at their reference doses. Then samples were loaded on 4% native polyacrylamide gel, image was developed with Odyssey infrared Imaging System (LI-COR Biosciences) for DY681-labeled RNA or in Typhoon Trio scanner (GE Healthcare) at high resolution for FAM and Cy-3 probe.

Dynamic Mass Redistribution (DMR). The EnSight Multimode Plate Reader (PerkinElmer) was used to perform DMR analyses. Full-length HuR protein (15 $\mu\text{L}/\text{well}$ of a 50 $\mu\text{g}/\text{mL}$ HuR solution in 20 mM sodium acetate buffer, pH 5.5) was immobilized on label-free microplate (EnSpire-LFB high sensitivity microplates) by amine-coupling chemistry, incubating the microplate o/n at 4°C . Importantly, each well contains a reactive area, containing chemical groups to allow amine coupling reaction, and empty area. After the initial step of immobilization, the unbound protein was washed away and the plate equilibrated using the assay buffer (HEPES 25 mM pH 8, 3 mM MgCl_2 , 100 mM NaCl, 8% Glycerol, 0.05% BSA, 0.005% Tween20). Next, the interaction between tanshinone mimics, diluted to different concentrations in the same buffer, and HuR protein was monitored during 30 min at room temperature. The EnSight software (Kaleido) acquires data by automatically subtracting the signal in the empty area from the one of the reactive area. Binding response is then calculated by subtracting the baseline read from the final read. This dual-control strategy guarantees that nonspecific signals arising from the potential interaction of the HuR protein with the surface of the plate are already subtracted in each well. All the steps were executed by employing a Zephyr Compact Liquid Handling Workstation. The Kaleido software was used to acquire and process the data.

Circular Dichroism Experiments. All experiments has been done by using a final 10 μM concentration of TNF-ARE and 10 μM **6a**, 10 mM in sodium phosphate buffer pH 7.3. CD spectra were measured in a JASCO-700 Spectrophotometer at 240–350 nm range (DMSO interfered below 240 nm), at 100 nm/min speed. Next 10 μM **6a** dissolved in sodium phosphate buffer pH 7.3 was also measured separately to exclude background from the **6a** (10 μM) + TNF ARE (10 μM) spectra. The analyzed spectra $\Delta\epsilon$ was then plotted using the Graphpad Prism 6 plotting tool.

Cell Culture. Human breast adenocarcinoma MCF7 (ICLC; HTL95021) and MDA-MB-231 (ICLC; HTL99004) and pancreatic carcinoma PANC-1 (kindly provided by G. Feldmann)⁵⁷ cell lines were cultured in high glucose Dulbecco's modified Eagle's medium (DMEM) supplemented with 10% fetal bovine serum (FBS, Lonza), 2 mM L-glutamine, 100 U/ml penicillin-streptomycin (Lonza) in standard growth conditions.

RIP and qRT-PCR. Five million MCF7 cells/sample were used for each RIP experiment, performed as previously described,⁵⁸ without cross-linking steps and using 1 $\mu\text{g}/\text{mL}$ of anti-HuR antibody (Santa Cruz, 71290) or of mouse IgG isotype (negative control, Santa Cruz 2025). TRIzol reagent was added directly to the beads for HuR-bound RNA isolation and processed for qRT-PCR analysis. Quantitative PCRs, after cDNA Synthesis (Thermo Scientific, K1612) were performed using Universal SYBR Master Mix (KAPA Biosystems, KR0389) on CFX-96/384 thermal cyclers (BIO-RAD), as previously described.²⁷ Fold enrichment was determined using the eq 2- $\Delta\Delta\text{Ct}$, where the Ct value for HuR and IgG IP was subtracted from the Ct value of the housekeeping gene RPLP0 to yield the ΔCt value. For each condition, ΔCt value for the HuR and IgG IP sample were calculated in triplicate. The delta Ct value for HuR in the IgG IP samples were calculated in the same way. Then delta–delta Ct values

were calculated from the difference between HuR IP samples and IgG IP samples. Total expression level of the different mRNAs was assessed by extracting total RNA from the control and treated samples and then qRT-PCRs have been performed as described previously. The sequence of the primer used for each PCR are the following:

| gene | primer sequence FW 5'-3' | primer sequence RV 5'-3' |
|--------|------------------------------|------------------------------|
| RPLP0 | CATTCTCGCTT- CCTGGAG | CTTGACCTTTTCAGC- AAGTGG |
| ERBB2 | GGTACTGAAAG- CCTTAGGGAAGC | ACACCATTGCTGTTC- CTTCCTC |
| VEGFA | CCGCAGACGTG- TAAATGTTCT | CGGCTTGTCACATCT- GCAAGTA |
| CTNBN1 | GACCTCATGGA- TGGGCTGCCT | GATTTACAAATAGCC- TAAACCAC |
| RNA18s | GCAGCTAGGAA- TAATGGAATAG | TGGCAAATGCTTTTCG- CTCTG |
| HPRT1 | TGACACTGGCA- AAACAATGCA | GGTCCTTTTCACCAG- CAAGCT |

Immunofluorescence Experiments. 8,000 MCF7 cells/well were seeded in a 96-well plate and treated with 1 μ M of **1**, or 10 μ M of tanshinone mimics, or 2.5 μ M of ActD (Sigma A1410) for 3 h and were fixed with 3.7% paraformaldehyde (PFA) for 15 min at RT. Cells were treated for 10 min with permeabilization buffer (200 mM sucrose, 0.2% Triton X-100) followed by blocking for 15 min with blocking buffer (2% Bovine Serum Albumin in PBS). Primary antibody anti-HuR 1:250 in 3% BSA and secondary fluorophore conjugated (Alexa 594 Red) antibody (1:500) were diluted in PBS + BSA 0.6%. DAPI Blue (1.5 μ g/mL) in PBS + BSA 0.6% was used to detect nuclei. PerkinElmer image plate reader Operetta was used for image acquisition and evaluation by selecting 13 fields/well. The ratio between nuclear and cytoplasmic signal represents the mean of single cells for every well.

Cell Viability Assay. To test cell viability, cells were grown and treated in 96 well-plate for 48 h. Cells were then assayed using OZBlue Cell Viability kit (Oz Biosciences, BL000). In brief, OZBlue was added at 10% volume of culture media to each well and cells were further incubated for 3 h at 37 °C. Fluorescence was then determined (excitation 560 and emission 590 nm) by a Tecan microplate reader. Cell survival was calculated with respect to control (DMSO), and IC₅₀ values were determined by fitting with GraphPad Prism software v5.1.

Cell Migration Assay. Cells were seeded for migration assay and treated with tanshinone mimics as previously described.⁵⁹ Images of the same field were acquired immediately ($t = 0$), after 24 and 48 h using a Leica DM IL Led microscope (5 \times magnification) and wounded-open areas were measured using ImageJ software.

Statistical Analysis. All data are expressed as means \pm SD from at least two independent experiments. Magnitude of significance was evaluated by student t test and probability (P) values <0.05, < 0.01, and <0.001 were indicated with *, **, *** symbols, respectively.

In Silico Pan Assay Interference, NMR, and Molecular Modeling studies. *In Silico Pan Assay Interference.* All compounds as reported in Table 1 were screened for Pan Assay Interference using the PAINS-Remover Web server (<http://www.cbligand.org>). All compounds passed this filtering.

NMR Measurements on Protein/Compound 6a Interaction. The assignment of RRM1-RRM2 tandem domains of HuR was previously reported (BMRB code: 27002).⁵⁰ The effect of the tanshinone mimic **6a** on the RRM1-RRM2 tandem domains of HuR (100 μ M) has been evaluated in the following experimental conditions: 20 mM Tris-Cl, pH 8, 10 mM Gly, 50 mM NaCl. 2D ¹H ¹⁵N HSQC spectra were acquired at 298 K on Bruker Avance 900 MHz NMR spectrometer to monitor the effect of increasing amounts of the ligand (HuR/compound **6a** molar ratio of 1:0.2, 1:0.4, 1:0.6, 1:0.8, 1:1, 1:2) added to the protein solution.

Docking Calculations. Molecular docking was carried out using the Glide 6.5⁶⁰ and the AutoDock 4.2⁶¹ software. **6a** three-dimensional structure was first generated and subsequently prepared through the LigPrep module, as implemented in the Maestro 10.0.013 graphical user interface.⁶² As experimental results suggest that (I) HuR cannot bind both

6a and RNA at the same time and that (II) **6a** stabilizes HuR in a "closed" conformation, we selected as receptor structure for docking calculations the structure of the HuR–mRNA complex (PDB ID: 4EDS),⁴⁹ and removed the RNA strand. Indeed this structure was not only the HuR highest resolution structure available but also the best representative structure of a HuR "closed" form available. Receptor structure was then prepared through the Protein Preparation Wizard, also implemented in Maestro, and the OPLS-2005 force field. Water molecules and residual crystallographic buffer components were removed, missing side chains were built using the Prime module, hydrogen atoms were added, side chains protonation states at pH 7.0 were assigned and, finally, minimization was performed until the RMSD of all the heavy atoms was within 0.3 Å of the crystallographically determined positions. In both cases, the binding pocket was identified by placing a cube centered in proximity of the "hinge" loop between the RRM1 and RRM2 domains. Docking calculations were performed as following. Docking with Glide was carried out in extra-precision (XP) mode, using GlideScore for ligand ranking. The inner box size was chosen to be 40 Å in all directions and the size of the outer box was set by choosing a threshold length for the ligand size to be docked of 30 Å. A maximum of 100 000 poses per ligand was set to pass to the grid refinement calculation, and the best 10 000 poses were kept for the energy minimization step. The maximum number of poses per ligand to be outputted was set to 10. In the case of docking with Autodock, the ligand and receptor structures were first converted to AD4 format files, adopting the Gasteiger-Marsili partial charges, via AutoDockTools.⁶¹ The box size was set to have 117 \times 125 \times 127 points in the three-dimensional space with a Grid spacing of 0.481 Å per point using AutoGrid 4.2. A hundred independent runs of the Lamarckian genetic algorithm local search (GALS) method per docking calculation were performed, by applying a threshold of maximum 10 million energy evaluations per run. The rest of the docking parameters was set as default. Docking conformations were clustered on the basis of their RMSD (tolerance = 2.0 Å) and were ranked according to the AutoDock scoring function. In both cases, the box size was chosen so as to encompass the whole RNA binding surface of HuR.

Molecular Dynamics Simulations and Analyses. The best ranked HuR–**6a** complexes, as issuing from the docking calculations, were submitted to MD simulations with NAMD,⁶³ using the ff99SBildn Amber force field parameters,^{64,65} for protein and the parameters recently developed by Allnér and co-workers for ions.⁶⁶ Parameters for **6a** were generated in two steps. Initially, charges were computed using the restrained electrostatic potential (RESP) fitting procedure.⁶⁷ The ESP was first calculated by means of the Gaussian09 package⁶⁸ using a 6-31G* basis set at Hartree–Fock level of theory, and then the RESP charges were obtained by a two-stages fitting procedure using the program RED.^{69,70} Missing bond, angle, torsion, and improper torsion angle parameters were then generated using Antechamber.⁷¹ The complex was then solvated in a 15 Å layer cubic water box using the TIP3P water model parameters. Neutrality was reached by adding five further Cl⁻ ions. The final system size was \sim 75 Å \times 74 Å \times 93 Å for a total number of atoms of \sim 48 000. A 10 Å cutoff (switched at 8.0 Å) was used for atom pair interactions. The long-range electrostatic interactions were computed by means of the particle mesh Ewald (PME) method using a 1.0 Å grid spacing in periodic boundary conditions. The RATTLE algorithm was applied to constrain bonds involving hydrogen atoms, and thus a 2 fs integration time step could be used. The system was minimized in two stages: first, a 20 000-step run was carried out with restraints on all the protein and ligand atoms (5 kcal/mol/Å²); then, a further 10 000-step minimization was carried out by applying restraints on the ligand and C α protein atoms only. A 2 ns NPT simulation at 200 K and 1 atm was performed with restraints on all the protein atoms (5 kcal/mol/Å²), to adjust the volume of the simulation box, while preserving the minimized protein structure obtained in the previous steps. Afterward, the system was slowly heated up to 300 K over a 3 ns period, gradually releasing the restraints (on the ligand and protein C α atoms only) to 1 kcal/mol/Å² along the thermalization process. Subsequently, the system was equilibrated for 2 ns, gradually reducing the restraints to zero. Production runs were then performed under NPT conditions at 1 atm and 300 K. Each

of the four simulations was extended up to 1.5 μ s. MD trajectory visualization and RMSD analysis were performed by means of the VMD software.⁷² All other analyses were performed using CPPTRAJ⁷³ or in-house scripts exploiting the MDAnalysis library.⁷⁴ For analysis purposes, trajectories were fitted onto the β -sheet backbone atoms, owing to the HuR high overall flexibility, using the first frame as reference and then one frame each 100 ps. In the specific case of contact analysis only, we employed a different reference structure. Indeed, as the aim of the analysis was also to discriminate between contacts established in the HuR mRNA-bound conformation and possible contacts characteristic of new **6a**-induced conformations, we made a distinction between native and non-native contacts. A non-native contact, contrarily to a native contact, is a contact between atoms within a convenient distance (here 4 Å) that is not present in a certain reference structure (here the structure used for the docking calculations). Figures were generated using the UCSF-Chimera software package⁷⁵ or in-house scripts with Matplotlib.⁷⁶

■ ASSOCIATED CONTENT

Supporting Information

The Supporting Information is available free of charge on the ACS Publications website at DOI: 10.1021/acs.jmedchem.7b01176.

Synthetic protocols and analytical characterization (NMR and HPLC-MS) for final compounds **6b–6k**, **6n–6o**, **6q–6w** and for synthetic intermediates. Availability of molecular formula strings. Supporting Figures S1–S8 are, respectively, related to the activity of compound **1** and **6a** with the rHuR produced in HEK293T, REMSA assays for tanshinone mimics, RMSD of MD simulations, and cell migration assays. Supporting Table 1, containing primary data from cell viability assays on tanshinone mimics (PDF) Structural animation (MPG) Compound data (CSV)

■ AUTHOR INFORMATION

Corresponding Authors

*E-mail for P.S.: pierfausto.seneci@unimi.it. Tel: +39 02-50314060. Fax: +39 02-50314074.

*E-mail for L.M.: lmarinel@unina.it. Tel: +39 081-679899. Fax: +39 081 676569.

*E-mail for A.P.: alessandro.provenzani@unitn.it. Tel: +390461283176. Fax: +390461283239.

ORCID

Leonardo Manzoni: 0000-0002-2056-8459

Ettore Novellino: 0000-0002-2181-2142

Luciana Marinelli: 0000-0002-4084-8044

Author Contributions

[○]L.M., C.Z., and D.D.M. contributed equally.

Notes

The authors declare the following competing financial interest(s): The molecules herein reported are present in patents: Italian Patent 151367 and PCT/IB2017/053519.

■ ACKNOWLEDGMENTS

Associazione Italiana per la Ricerca sul Cancro (AIRC) [17153 to A.P.]

■ ABBREVIATIONS USED

CAN, cerium ammonium nitrate; DDQ, 2,3-dichloro-5,6-dicyano-1,4-benzoquinone; DHTS, Dihydratanshinone I; DME, dimethoxyetane; DMF, dimethylformamide; EtOAc, ethyl acetate; FOS, function-oriented synthesis; HuR, human

antigene R; IBX, 2-iodoxybenzoic acid; MeCN, acetonitrile; NMR, nuclear magnetic resonance; THF, tetrahydrofuran

■ REFERENCES

- (1) Keene, J. D. RNA Regulons: Coordination of Post-Transcriptional Events. *Nat. Rev. Genet.* **2007**, *8* (7), 533–543.
- (2) Brennan, C. M.; Steitz, J. a. HuR and mRNA Stability. *Cell. Mol. Life Sci.* **2001**, *58* (2), 266–277.
- (3) Latorre, E.; Carelli, S.; Raimondi, I.; D'Agostino, V.; Castiglioni, I.; Zucal, C.; Moro, G.; Luciani, A.; Ghilardi, G.; Monti, E.; Inga, A.; Di Giulio, A. M.; Gorio, A.; Provenzani, A. The Ribonucleic Complex HuR-MALAT1 Represses CD133 Expression and Suppresses Epithelial-Mesenchymal Transition in Breast Cancer. *Cancer Res.* **2016**, *76* (9), 2626–2636.
- (4) Izquierdo, J. M. Hu Antigen R (HuR) Functions as an Alternative Pre-mRNA Splicing Regulator of Fas Apoptosis-Promoting Receptor on Exon Definition. *J. Biol. Chem.* **2008**, *283* (27), 19077–19084.
- (5) Mukherjee, N.; Corcoran, D. L.; Nusbaum, J. D.; Reid, D. W.; Georgiev, S.; Hafner, M.; Ascano, M.; Tuschl, T.; Ohler, U.; Keene, J. D. Integrative Regulatory Mapping Indicates That the RNA-Binding Protein HuR Couples Pre-mRNA Processing and mRNA Stability. *Mol. Cell* **2011**, *43* (3), 327–339.
- (6) Al-Ahmadi, W.; Al-Ghamdi, M.; Al-Haj, L.; Al-Saif, M.; Khabar, K. S. A. Alternative Polyadenylation Variants of the RNA Binding Protein, HuR: Abundance, Role of AU-Rich Elements and Auto-Regulation. *Nucleic Acids Res.* **2009**, *37* (11), 3612–3624.
- (7) Lebedeva, S.; Jens, M.; Theil, K.; Schwanhäusser, B.; Selbach, M.; Landthaler, M.; Rajewsky, N. Transcriptome-Wide Analysis of Regulatory Interactions of the RNA-Binding Protein HuR. *Mol. Cell* **2011**, *43* (3), 340–352.
- (8) Katsanou, V.; Papadaki, O.; Milatos, S.; Blackshear, P. J.; Anderson, P.; Kollias, G.; Kontoyiannis, D. L. HuR as a Negative Posttranscriptional Modulator in Inflammation. *Mol. Cell* **2005**, *19* (6), 777–789.
- (9) Wang, W.; Caldwell, M. C.; Lin, S.; Furneaux, H.; Gorospe, M. HuR Regulates Cyclin A and Cyclin B1 mRNA Stability during Cell Proliferation. *EMBO J.* **2000**, *19*, 2340–2350.
- (10) Abdelmohsen, K.; Pullmann, R.; Lal, A.; Kim, H. H.; Galban, S.; Yang, X.; Blethrow, J. D.; Walker, M.; Shubert, J.; Gillespie, D. a.; Furneaux, H.; Gorospe, M. Phosphorylation of HuR by Chk2 Regulates SIRT1 Expression. *Mol. Cell* **2007**, *25* (4), 543–557.
- (11) Abdelmohsen, K.; Gorospe, M. Posttranscriptional Regulation of Cancer Traits by HuR. *Wiley Interdiscip. Rev. RNA* **2010**, *1* (2), 214–229.
- (12) Levy, N. S.; Chung, S.; Furneaux, H.; Levy, A. P. Hypoxic Stabilization of Vascular Endothelial Growth Factor mRNA by the RNA-Binding Protein HuR. *J. Biol. Chem.* **1998**, *273* (11), 6417–6423.
- (13) Tang, K.; Breen, E. C.; Wagner, P. D. Hu Protein R-Mediated Posttranscriptional Regulation of VEGF Expression in Rat Gastrocnemius Muscle. *Am. J. Physiol. Heart Circ. Physiol.* **2002**, *283* (4), H1497–H1504.
- (14) Akool, E.-S.; Kleinert, H.; Hamada, F. M. A.; Abdelwahab, M. H.; Förstermann, U.; Pfeilschifter, J.; Eberhardt, W. Nitric Oxide Increases the Decay of Matrix Metalloproteinase 9 mRNA by Inhibiting the Expression of mRNA-Stabilizing Factor HuR. *Mol. Cell. Biol.* **2003**, *23* (14), 4901–4916.
- (15) Wang, W.; Yang, X.; Cristofalo, V. J.; Holbrook, N. J.; Gorospe, M. Loss of HuR Is Linked to Reduced Expression of Proliferative Genes during Replicative Senescence. *Mol. Cell. Biol.* **2001**, *21* (17), 5889–5898.
- (16) Ishimaru, D.; Ramalingam, S.; Sengupta, T. K.; Bandyopadhyay, S.; Dellis, S.; Tholanikunnel, B. G.; Fernandes, D. J.; Spicer, E. K. Regulation of Bcl-2 Expression by HuR in HL60 Leukemia Cells and A431 Carcinoma Cells. *Mol. Cancer Res.* **2009**, *7* (8), 1354–1366.
- (17) Abdelmohsen, K.; Lal, A.; Kim, H. H.; Gorospe, M. Posttranscriptional Orchestration of an Anti-Apoptotic Program by HuR. *Cell Cycle* **2007**, *6* (11), 1288–1292.

- (18) Kafasla, P.; Skliris, A.; Kontoyiannis, D. L. Post-Transcriptional Coordination of Immunological Responses by RNA-Binding Proteins. *Nat. Immunol.* **2014**, *15* (6), 492–502.
- (19) Atasoy, U.; Watson, J.; Patel, D.; Keene, J. D. ELAV Protein HuA (HuR) Can Redistribute between Nucleus and Cytoplasm and Is Upregulated during Serum Stimulation and T Cell Activation. *J. Cell Sci.* **1998**, *111*, 3145–3156.
- (20) Galbán, S.; Kuwano, Y.; Pullmann, R.; Martindale, J. L.; Kim, H. H.; Lal, A.; Abdelmohsen, K.; Yang, X.; Dang, Y.; Liu, J. O.; Lewis, S. M.; Holcik, M.; Gorospe, M. RNA-Binding Proteins HuR and PTB Promote the Translation of Hypoxia-Inducible Factor 1 α . *Mol. Cell Biol.* **2008**, *28* (1), 93–107.
- (21) Zucal, C.; D'Agostino, V.; Loffredo, R.; Mantelli, B.; Thongon, N.; Lal, P.; Latorre, E.; Provenzani, A. Targeting the Multifaceted HuR Protein, Benefits and Caveats. *Curr. Drug Targets* **2015**, *16* (5), 499–515.
- (22) Meisner, N.-C.; Hintersteiner, M.; Mueller, K.; Bauer, R.; Seifert, J.-M.; Naegeli, H.-U.; Ottl, J.; Oberer, L.; Guenat, C.; Moss, S.; Harrer, N.; Woisetschlaeger, M.; Buehler, C.; Uhl, V.; Auer, M. Identification and Mechanistic Characterization of Low-Molecular-Weight Inhibitors for HuR. *Nat. Chem. Biol.* **2007**, *3* (8), 508–515.
- (23) Wu, X.; Lan, L.; Wilson, D. M.; Marquez, R. T.; Tsao, W.-C.; Gao, P.; Roy, A.; Turner, B. A.; McDonald, P.; Tunge, J. A.; Rogers, S. A.; Dixon, D. A.; Aubé, J.; Xu, L. Identification and Validation of Novel Small Molecule Disruptors of HuR-mRNA Interaction. *ACS Chem. Biol.* **2015**, *10* (6), 1476–1484.
- (24) Wang, Z.; Bhattacharya, A.; Ivanov, D. N. Identification of Small-Molecule Inhibitors of the HuR/RNA Interaction Using a Fluorescence Polarization Screening Assay Followed by NMR Validation. *PLoS One* **2015**, *10* (9), e0138780.
- (25) Chae, M.-J.; Sung, H. Y.; Kim, E.-H.; Lee, M.; Kwak, H.; Chae, C. H.; Kim, S.; Park, W.-Y. Chemical Inhibitors Destabilize HuR Binding to the AU-Rich Element of TNF- α mRNA. *Exp. Mol. Med.* **2009**, *41* (11), 824–831.
- (26) Kwak, H.; Jeong, K.-C.; Chae, M.-J.; Kim, S.-Y.; Park, W.-Y. Flavonoids Inhibit the AU-Rich Element Binding of HuC. *BMB Rep.* **2009**, *42* (1), 41–46.
- (27) D'Agostino, V. G.; Lal, P.; Mantelli, B.; Tiedje, C.; Zucal, C.; Thongon, N.; Gaestel, M.; Latorre, E.; Marinelli, L.; Seneci, P.; Amadio, M.; Provenzani, A. Dihydrotanshinone-I Interferes with the RNA-Binding Activity of HuR Affecting Its Post-Transcriptional Function. *Sci. Rep.* **2015**, *5*, 16478.
- (28) D'Agostino, V. G.; Adami, V.; Provenzani, A. A Novel High Throughput Biochemical Assay to Evaluate the HuR Protein-RNA Complex Formation. *PLoS One* **2013**, *8* (8), e72426.
- (29) Lal, P.; Cerofolini, L.; D'Agostino, V. G.; Zucal, C.; Fuccio, C.; Bonomo, I.; Dassi, E.; Giuntini, S.; Di Maio, D.; Vishwakarma, V.; Preet, R.; Williams, S. N.; Fairlamb, M. S.; Munk, R.; Lehrmann, E.; Abdelmohsen, K.; Elezgarai, S. R.; Luchinat, C.; Novellino, E.; Quattrone, A.; Biasini, E.; Manzoni, L.; Gorospe, M.; Dixon, D. A.; Seneci, P.; Marinelli, L.; Fragai, M.; Provenzani, A. Regulation of HuR Structure and Function by Dihydrotanshinone-I. *Nucleic Acids Res.* **2017**, *45* (16), 9514–9527.
- (30) Kaur, K.; Wu, X.; Fields, J. K.; Johnson, D. K.; Lan, L.; Pratt, M.; Somoza, A. D.; Wang, C. C. C.; Karanicolos, J.; Oakley, B. R.; Xu, L.; De Guzman, R. N. The Fungal Natural Product Azaphilone-9 Binds to HuR and Inhibits HuR-RNA Interaction in Vitro. *PLoS One* **2017**, *12* (4), e0175471.
- (31) Nasti, R.; Rossi, D.; Amadio, M.; Pascale, A.; Unver, M. Y.; Hirsch, A. K. H.; Collina, S. Compounds Interfering with Embryonic Lethal Abnormal Vision (ELAV) Protein:RNA Complexes: An Avenue for Discovering New Drugs. *J. Med. Chem.* **2017**, *60* (20), 8257–8267.
- (32) Wang, H.; Zeng, F.; Liu, Q.; Liu, H.; Liu, Z.; Niu, L.; Teng, M.; Li, X. The Structure of the ARE-Binding Domains of Hu Antigen R (HuR) Undergoes Conformational Changes during RNA Binding. *Acta Crystallogr., Sect. D: Biol. Crystallogr.* **2013**, *69*, 373–380.
- (33) Scheiba, R. M.; de Opakua, A. I.; Díaz-Quintana, A.; Cruz-Gallardo, I.; Martínez-Cruz, L. A.; Martínez-Chantar, M. L.; Blanco, F. J.; Díaz-Moreno, I. The C-Terminal RNA Binding Motif of HuR Is a Multi-Functional Domain Leading to HuR Oligomerization and Binding to U-Rich RNA Targets. *RNA Biol.* **2014**, *11* (10), 1250–1261.
- (34) Díaz-Quintana, A.; García-Mauriño, S. M.; Díaz-Moreno, I. Dimerization Model of the C-Terminal RNA Recognition Motif of HuR. *FEBS Lett.* **2015**, *589* (10), 1059–1066.
- (35) Zhou, L.; Zuo, Z.; Chow, M. S. S. Danshen: An Overview of Its Chemistry, Pharmacology, Pharmacokinetics, and Clinical Use. *J. Clin. Pharmacol.* **2005**, *45* (12), 1345–1359.
- (36) Wilson, R. M.; Danishefsky, S. J. Small Molecule Natural Products in the Discovery of Therapeutic Agents: The Synthesis Connection. *J. Org. Chem.* **2006**, *71* (22), 8329–8351.
- (37) Wender, P. A.; Quiroz, R. V.; Stevens, M. C. Function through Synthesis-Informed Design. *Acc. Chem. Res.* **2015**, *48* (3), 752–760.
- (38) Crane, E. A.; Gademann, K. Capturing Biological Activity in Natural Product Fragments by Chemical Synthesis. *Angew. Chem., Int. Ed.* **2016**, *55* (12), 3882–3902.
- (39) Cheng, Y.-C.; Liou, J.-P.; Kuo, C.-C.; Lai, W.-Y.; Shih, K.-H.; Chang, C.-Y.; Pan, W.-Y.; Tseng, J. T.; Chang, J.-Y. MPT0B098, a Novel Microtubule Inhibitor That Destabilizes the Hypoxia-Inducible Factor-1 α mRNA through Decreasing Nuclear-Cytoplasmic Translocation of RNA-Binding Protein HuR. *Mol. Cancer Ther.* **2013**, *12* (7), 1202–1212.
- (40) Fujiwara, Y.; Domingo, V.; Seiple, I. B.; Gianatassio, R.; Del Bel, M.; Baran, P. S. Practical C-H Functionalization of Quinones with Boronic Acids. *J. Am. Chem. Soc.* **2011**, *133* (10), 3292–3295.
- (41) Frigerio, M.; Santagostino, M.; Sputore, S. A User-Friendly Entry to 2-Iodoxybenzoic Acid (IBX). *J. Org. Chem.* **1999**, *64* (12), 4537–4538.
- (42) Dickschat, A.; Studer, A. Radical Addition of Arylboronic Acids to Various Olefins under Oxidative Conditions. *Org. Lett.* **2010**, *12* (18), 3972–3974.
- (43) Lee, J.; Snyder, J. K. Ultrasound-Promoted Cycloadditions in the Synthesis of Salvia Miltiorrhiza Abietanoid O-Quinones. *J. Org. Chem.* **1990**, *55* (17), 4995–5008.
- (44) Eglén, R. M.; Reisine, T.; Roby, P.; Rouleau, N.; Illy, C.; Bossé, R.; Bielefeld, M. The Use of AlphaScreen Technology in HTS: Current Status. *Curr. Chem. Genomics* **2008**, *1*, 2–10.
- (45) Schorpp, K.; Rothenaigner, I.; Salmina, E.; Reinshagen, J.; Low, T.; Brenke, J. K.; Gopalakrishnan, J.; Tetko, I. V.; Gul, S.; Hadian, K. Identification of Small-Molecule Frequent Hitters from AlphaScreen High-Throughput Screens. *J. Biomol. Screening* **2014**, *19* (5), 715–726.
- (46) Massignan, T.; Cimini, S.; Stincardini, C.; Cerovic, M.; Vanni, I.; Elezgarai, S. R.; Moreno, J.; Stravalaci, M.; Negro, A.; Sangiovanni, V.; Restelli, E.; Riccardi, G.; Gobbi, M.; Castilla, J.; Borsello, T.; Nonno, R.; Biasini, E. A Cationic Tetrapyrrole Inhibits Toxic Activities of the Cellular Prion Protein. *Sci. Rep.* **2016**, *6* (1), 23180.
- (47) Latorre, E.; Castiglioni, I.; Gatto, P.; Carelli, S.; Quattrone, A.; Provenzani, A. Loss of Protein Kinase C δ /HuR Interaction Is Necessary to Doxorubicin Resistance in Breast Cancer Cell Lines. *J. Pharmacol. Exp. Ther.* **2014**, *349* (1), 99–106.
- (48) Mujo, A.; Lixa, C.; Carneiro, L. A. M.; Anobom, C. D.; Almeida, F. C.; Pinheiro, A. S. ¹H, ¹⁵N and ¹³C Resonance Assignments of the RRM1 Domain of the Key Post-Transcriptional Regulator HuR. *Biomol. NMR Assignments* **2015**, *9* (2), 281–284.
- (49) Benoit, R. M.; Meisner, N.-C.; Kallen, J.; Graff, P.; Hemmig, R.; Cèbe, R.; Ostermeier, C.; Widmer, H.; Auer, M. The X-Ray Crystal Structure of the First RNA Recognition Motif and Site-Directed Mutagenesis Suggest a Possible HuR Redox Sensing Mechanism. *J. Mol. Biol.* **2010**, *397* (5), 1231–1244.
- (50) Sigurdardottir, A. G.; Winter, A.; Sobkowitz, A.; Fragai, M.; Chirgadze, D.; Ascher, D. B.; Blundell, T. L.; Gherardi, E. Exploring the Chemical Space of the Lysine-Binding Pocket of the First Kringle Domain of Hepatocyte Growth Factor/scatter Factor (HGF/SF) Yields a New Class of Inhibitors of HGF/SF-MET Binding. *Chem. Sci.* **2015**, *6* (11), 6147–6157.
- (51) Blanco, F. F.; Preet, R.; Aguado, A.; Vishwakarma, V.; Stevens, L. E.; Vyas, A.; Padhye, S.; Xu, L.; Weir, S. J.; Anant, S.; Meisner-

Kober, N.; Brody, J. R.; Dixon, D. A. Impact of HuR Inhibition by the Small Molecule MS-444 on Colorectal Cancer Cell Tumorigenesis. *Oncotarget* **2016**, *7* (45), 74043–74058.

(52) Lang, M.; Berry, D.; Passecker, K.; Mesteri, I.; Bhujji, S.; Ebner, F.; Sedlyarov, V.; Evstatiev, R.; Dammann, K.; Loy, A.; Kuzyk, O.; Kovarik, P.; Khare, V.; Beibel, M.; Roma, G.; Meisner-kober, N.; Gasche, C. HuR Small-Molecule Inhibitor Elicits Differential Effects in Adenomatosis Polyposis and Colorectal Carcinogenesis. *Cancer Res.* **2017**, *77* (9), 2424–2438.

(53) Zhang, Y.; Jiang, P.; Ye, M.; Kim, S. H.; Jiang, C.; Lü, J. Tanshinones: Sources, Pharmacokinetics and Anti-Cancer Activities. *Int. J. Mol. Sci.* **2012**, *13* (10), 13621–13666.

(54) Bocchi, V.; Palla, G. High Yield Selective Bromination and Iodination of Indoles in N,N -Dimethylformamide. *Synthesis* **1982**, *1982* (12), 1096–1097.

(55) Leboho, T. C.; Michael, J. P.; van Otterlo, W. A. L.; van Vuuren, S. F.; de Koning, C. B. The Synthesis of 2- and 3-Aryl Indoles and 1,3,4,5-tetrahydropyrano[4,3-B]indoles and Their Antibacterial and Antifungal Activity. *Bioorg. Med. Chem. Lett.* **2009**, *19* (17), 4948–4951.

(56) Pathak, R.; Nhlapo, J. M.; Govender, S.; Michael, J. P.; van Otterlo, W. A. L.; de Koning, C. B. A Concise Synthesis of Novel Naphtho[a]carbazoles and Benzo[c]carbazoles. *Tetrahedron* **2006**, *62* (12), 2820–2830.

(57) Dong, J.; Feldmann, G.; Huang, J.; Wu, S.; Zhang, N.; Comerford, S. A.; Gayyed, M. F.; Anders, R. A.; Maitra, A.; Pan, D. Elucidation of a Universal Size-Control Mechanism in *Drosophila* and Mammals. *Cell* **2007**, *130* (6), 1120–1133.

(58) Keene, J. D.; Komisarow, J. M.; Friedersdorf, M. B. RIP-Chip: The Isolation and Identification of mRNAs, microRNAs and Protein Components of Ribonucleoprotein Complexes from Cell Extracts. *Nat. Protoc.* **2006**, *1* (1), 302–307.

(59) Thongon, N.; Castiglioni, I.; Zucal, C.; Latorre, E.; D'Agostino, V.; Bauer, I.; Pancher, M.; Ballestrero, A.; Feldmann, G.; Nencioni, A.; Provenzani, A. The GSK3 β Inhibitor BIS I Reverts YAP-Dependent EMT Signature in PDAC Cell Lines by Decreasing SMADs Expression Level. *Oncotarget* **2016**, *7* (18), 26551–26566.

(60) *Glide*, Schrödinger, LLC: New York, 2014.

(61) Morris, G. M.; Huey, R.; Lindstrom, W.; Sanner, M. F.; Belew, R. K.; Goodsell, D. S.; Olson, A. J. AutoDock4 and AutoDockTools4: Automated Docking with Selective Receptor Flexibility. *J. Comput. Chem.* **2009**, *30* (16), 2785–2791.

(62) *Maestro 10.0.013*; SQL Maestro Group: New York, 2014.

(63) Phillips, J. C.; Braun, R.; Wang, W.; Gumbart, J.; Tajkhorshid, E.; Villa, E.; Chipot, C.; Skeel, R. D.; Kalé, L.; Schulten, K. Scalable Molecular Dynamics with NAMD. *J. Comput. Chem.* **2005**, *26* (16), 1781–1802.

(64) Cornell, W. D.; Cieplak, P.; Bayly, C. I.; Gould, I. R.; Merz, K. M.; Ferguson, D. M.; Spellmeyer, D. C.; Fox, T.; Caldwell, J. W.; Kollman, P. A. A Second Generation Force Field for the Simulation of Proteins, Nucleic Acids, and Organic Molecules. *J. Am. Chem. Soc.* **1995**, *117* (19), 5179–5197.

(65) Lindorff-Larsen, K.; Piana, S.; Palmo, K.; Maragakis, P.; Klepeis, J. L.; Dror, R. O.; Shaw, D. E. Improved Side-Chain Torsion Potentials for the Amber ff99SB Protein Force Field. *Proteins: Struct., Funct., Genet.* **2010**, *78* (8), 1950–1958.

(66) Allnér, O.; Nilsson, L.; Villa, A. Magnesium Ion–Water Coordination and Exchange in Biomolecular Simulations. *J. Chem. Theory Comput.* **2012**, *8* (4), 1493–1502.

(67) Bayly, C. I.; Cieplak, P.; Cornell, W.; Kollman, P. A. A Well-Behaved Electrostatic Potential Based Method Using Charge Restraints for Deriving Atomic Charges: The RESP Model. *J. Phys. Chem.* **1993**, *97* (40), 10269–10280.

(68) Frisch, M. J.; Trucks, G. W.; Schlegel, H. B.; Scuseria, G. E.; Robb, M. A.; Cheeseman, J. R.; Scalmani, G.; Barone, V.; Mennucci, B.; Petersson, G. A.; Nakatsuji, H.; Caricato, M.; Li, X.; Hratchian, H. P.; Izmaylov, A. F.; Bloino, J.; Zheng, G.; Sonnenberg, J. L.; Hada, M.; Ehara, M.; Toyota, K.; Fukuda, R.; Hasegawa, J.; Ishida, M.; Nakajima, T.; Honda, Y.; Kitao, O.; Nakai, H.; Vreven, T.; Montgomery, J. A., Jr;

Peralta, J. E.; Ogliaro, F.; Bearpark, M.; Heyd, J. J.; Brothers, E.; Kudin, K. N.; Staroverov, V. N.; Kobayashi, R.; Normand, J.; Raghavachari, K.; Rendell, A.; Burant, J. C.; Iyengar, S. S.; Tomasi, J.; Cossi, M.; Rega, N.; Millam, J. M.; Klene, M.; Knox, J. E.; Cross, J. B.; Bakken, V.; Adamo, C.; Jaramillo, J.; Gomperts, R.; Stratmann, R. E.; Yazyev, O.; Austin, A. J.; Cammi, R.; Pomelli, C.; Ochterski, J. W.; Martin, R. L.; Morokuma, K.; Zakrzewski, V. G.; Voth, G. A.; Salvador, P.; Dannenberg, J. J.; Dapprich, S.; Daniels, A. D.; Farkas, O.; Foresman, J. B.; Ortiz, J. V.; Cioslowski, J.; Fox, D. J. *Gaussian 09*, Revision B.01; Gaussian, Inc.: Wallingford, CT, 2009.

(69) Dupradeau, F.-Y.; Pigache, A.; Zaffran, T.; Savineau, C.; Lelong, R.; Grivel, N.; Lelong, D.; Rosanski, W.; Cieplak, P. The R.E.D. Tools: Advances in RESP and ESP Charge Derivation and Force Field Library Building. *Phys. Chem. Chem. Phys.* **2010**, *12* (28), 7821–7839.

(70) Vanqualef, E.; Simon, S.; Marquant, G.; Garcia, E.; Klimerak, G.; Delepine, J. C.; Cieplak, P.; Dupradeau, F.-Y. R.E.D. Server: A Web Service for Deriving RESP and ESP Charges and Building Force Field Libraries for New Molecules and Molecular Fragments. *Nucleic Acids Res.* **2011**, *39* (Web Server issue), W511–W517.

(71) Wang, J.; Wang, W.; Kollman, P. A.; Case, D. A. Automatic Atom Type and Bond Type Perception in Molecular Mechanical Calculations. *J. Mol. Graphics Modell.* **2006**, *25* (2), 247–260.

(72) Humphrey, W.; Dalke, A.; Schulten, K. VMD: Visual Molecular Dynamics. *J. Mol. Graphics* **1996**, *14* (1), 33–38 pp 27–28.

(73) Roe, D. R.; Cheatham, T. E. PTRAJ and CPPTRAJ: Software for Processing and Analysis of Molecular Dynamics Trajectory Data. *J. Chem. Theory Comput.* **2013**, *9* (7), 3084–3095.

(74) Michaud-Agrawal, N.; Denning, E. J.; Woolf, T. B.; Beckstein, O. MDAnalysis: A Toolkit for the Analysis of Molecular Dynamics Simulations. *J. Comput. Chem.* **2011**, *32* (10), 2319–2327.

(75) Pettersen, E. F.; Goddard, T. D.; Huang, C. C.; Couch, G. S.; Greenblatt, D. M.; Meng, E. C.; Ferrin, T. E. UCSF Chimera—a Visualization System for Exploratory Research and Analysis. *J. Comput. Chem.* **2004**, *25* (13), 1605–1612.

(76) Hunter, J. D. et al. *Matplotlib v2.0.2*; Matplotlib Development Team, 2017.

Research Article

The Natural Carotenoid Crocetin and the Synthetic Tellurium Compound AS101 Protect the Ovary against Cyclophosphamide by Modulating SIRT1 and Mitochondrial Markers

Giovanna Di Emidio,¹ Giulia Rossi,¹ Isabelle Bonomo,² Gonzalo Luis Alonso,³ Roberta Sferra,⁴ Antonella Vetuschi,⁴ Paolo Giovanni Artini,⁵ Alessandro Provenzani,² Stefano Falone,¹ Gaspare Carta,¹ Anna Maria D'Alessandro,¹ Fernanda Amicarelli,^{1,6} and Carla Tatone¹

¹Department of Life, Health and Environmental Sciences, University of L'Aquila, L'Aquila, Italy

²Centre For Integrative Biology (CIBIO), Università degli Studi di Trento, Trento, Italy

³School of Agricultural Engineering, University of Castilla-La Mancha, Albacete, Spain

⁴Department of Biotechnological and Applied Clinical Sciences, University of L'Aquila, L'Aquila, Italy

⁵Department of Reproductive Medicine and Child Development, Division of Obstetrics and Gynaecology, University of Pisa, Pisa, Italy

⁶Institute of Translational Pharmacology (IFT), National Council of Research (CNR), L'Aquila, Italy

Correspondence should be addressed to Carla Tatone; carla.tatone@univaq.it

Received 28 July 2017; Accepted 1 October 2017; Published 15 November 2017

Academic Editor: Ryuichi Morishita

Copyright © 2017 Giovanna Di Emidio et al. This is an open access article distributed under the Creative Commons Attribution License, which permits unrestricted use, distribution, and reproduction in any medium, provided the original work is properly cited.

Cancer therapies are associated with increased infertility risk due to accelerated reproductive aging. Oxidative stress (OS) is a potential mechanism behind ovarian toxicity by cyclophosphamide (CPM), the most ovotoxic anticancer drug. An important sensor of OS is SIRT1, a NAD⁺-dependent deacetylase which regulates cellular defence and cell fate. This study investigated whether the natural carotenoid crocetin and the synthetic compound AS101 protect the ovary against CPM by modulating SIRT1 and mitochondrial markers. We found that the number of primordial follicles of female CD1 mice receiving crocetin plus CPM increased when compared with CPM alone and similar to AS101, whose protective effects are known. SIRT1 increased in CPM mouse ovaries revealing the occurrence of OS. Similarly, mitochondrial SIRT3 rose, whilst SOD2 and the mitochondrial biogenesis activator PGC1- α decreased, suggesting the occurrence of mitochondrial damage. Crocetin and AS101 administration prevented SIRT1 burst suggesting that preservation of redox balance can help the ovary to counteract ovarian damage by CPM. Decreased SIRT3 and increased SOD2 and PGC1- α in mice receiving crocetin or AS101 prior to CPM provide evidence for mitochondrial protection. Present results improve the knowledge of ovarian damage by CPM and may help to develop interventions for preserving fertility in cancer patients.

1. Introduction

Novel management strategies have led to increased rates of cancer survivors throughout the past three decades highlighting the need of posttreatment care to improve the patient's quality of life [1]. For females, a serious long-term side effect of cancer therapies is the increased infertility risk due to

accelerated reproductive aging leading to premature ovarian failure (POF) [2]. Hence, fertility preservation has been integrated into oncology practice giving rise to oncofertility, a new discipline that bridges oncology and reproductive research [3]. Current strategies are based mainly on assisted reproductive technologies (i.e., oocyte-embryo cryopreservation and ovarian tissue cryopreservation/transplantation)

that are suitable only for few categories of patients or are still experimental [1]. Suppression of the pituitary-gonadal axis via GnRH analogue administration has been so far the most feasible intervention although results of recent clinical trials are contradictory [4–6]. One of the possible reasons for limited progress in the field is the partial understanding of the mechanistic events that could be targeted to provide protection or repair from ovotoxicity (reviewed by [7, 8]). Similar to women, studies in rodents revealed that the predominant effect of anticancer cytotoxic treatments is the total or partial loss of the finite pool of dormant oocytes in the primordial follicles at concentrations relevant to human exposures [9–11].

Clinically, the most ovotoxic drugs are the alkylating agents including cyclophosphamide (CPM). This drug is widely used for the treatment of cancers affecting females in their childhood or reproductive age, including breast cancer [5, 12]. It is also used as an immunosuppressant for autoimmune diseases and multiple sclerosis and preventing organ transplant rejection [13–15]. CPM requires hepatic bioactivation to form the active metabolite phosphoramidate mustard (PM) that covalently binds to DNA, inducing DNA-DNA, DNA-protein crosslinks, and DNA double-strand breaks (DSB). Both oocytes and granulosa cells show these types of DNA damage following *in vitro* exposure of ovaries and cells [16, 17]. The activation of an ovarian DNA damage repair response has been reported in terms of early upregulation of specific genes including ATM (ataxia telangiectasia mutated) in neonatal rat ovaries exposed to PM. This response was associated with increased levels of proapoptotic genes and follicle loss by apoptosis [18, 19]. In addition to apoptosis, CPM-induced DNA damage may also cause activation of follicle dormancy by stimulating the PI3K/PTEN/AKT signalling pathway. The upregulation of AKT signalling would lead to phosphorylation/inhibition of FOXO3a transcription factor in primordial follicles and subsequent disruption of the regulatory mechanism underlying dormancy of primordial follicles [20, 21]. *In vivo* administration of AS101 (ammonium trichloro(dioxoethylene-o,o')tellurate), an immunomodulator with antitumor effects [22], inhibits AKT phosphorylation/activation induced by CPM and prevents the loss of primordial follicles. Beneficial effects on growing follicles were also observed [20].

A further potential mechanism behind CPM ovarian toxicity is oxidative stress (OS) (reviewed by [23, 24]). In a human granulosa cell line, exposure to a pre-activated CPM metabolite results in depletion of glutathione (GSH), a crucial cellular antioxidant, a rise in reactive oxygen species (ROS) and apoptosis. Consistently, GSH exposure reduces CPM-induced granulosa cell toxicity [25]. Moreover, *in vivo* administration of CPM has been associated with low GSH content, reduced SOD2 (Superoxide dismutase 2) activity, and increased lipid peroxidation in rat ovaries [26, 27]. Oxidative stress is thought to arise from biotransformation/detoxification of PM as described by Madden and Keating [28] in *in vitro* ovarian models.

An important sensor of cell redox state is SIRT1, one of the seven members of the mammalian sirtuin family, NAD⁺-dependent enzymes with deacetylase and/or mono-

ADP-ribosyl transferase activity [29–33]. By its numerous targets, SIRT1 orchestrates cellular defence and repair mechanisms and controls cell fate avoiding survival of damaged cells [34]. Mouse oocytes upregulate SIRT1 gene to cope with OS supporting a pivotal role for this protein in the early adaptive response to OS [35, 36]. In many tissues, SIRT1 abundance can be regulated by modulating the mRNA stability by the RNA-binding protein HuR (Hu antigen R). Indeed, HuR stabilises SIRT1 transcripts and promotes their polyribosome engagement for active translation [37]. An important SIRT1 substrate is PGC1- α (peroxisome proliferator-activated receptor gamma coactivator 1- α), an activator of mitochondrial biogenesis and a key regulator of mitochondrial gene expression required to meet energetic demands during cellular stresses [38]. These activities under stress conditions are also regulated by the mitochondrial sirtuin, SIRT3, throughout a complex network [39–41].

Although OS has been proposed as an important mechanism involved in CPM ovarian toxicity, the efficacy of *in vivo* antioxidant interventions has been poorly investigated [26, 27]. Systemic treatment with some carotenoids has been largely demonstrated to protect nonmalignant tissues against CPM toxicity by promoting antioxidant and anti-inflammatory effects [42–46]. Crocetin (8,8'-diapocartenedioic acid) belongs to the bioactive family of carotenoids derived from the stigmas of *Crocus sativus* (saffron spice) and well-known in traditional medicine [47, 48]. Crocetin is known to act as an effective free radical scavenger and lipid peroxidation inhibitor. Importantly, it effectively improved antioxidant biomarkers and attenuated inflammatory reaction [49–53]. Furthermore, crocetin is known to exert potent antitumour effects [54–56].

Based on the above observations, this work investigates whether (i) oral administration of the natural carotenoid crocetin prevents gonadotoxicity in female mice; (ii) SIRT1 is involved in the molecular pathways activated in the early ovarian response to CPM; and (iii) the protective effects of crocetin influence SIRT1 expression and mitochondrial toxicity induced by CPM. To address the first point, we tested the ability of crocetin to mitigate CPM-induced follicle loss, primordial follicle activation, and subfertility. To clarify SIRT1 involvement, we relied on a human granulosa cell line previously used to test CPM toxicity [25, 57], prior to investigation on the animal model. To gain knowledge about crocetin efficacy and mechanism of action, the fertoprotective agent AS101, known to protect the mouse ovary against CPM, was also tested [20].

2. Materials and Methods

2.1. Cyclophosphamide, Crocetin, and AS101 Preparation. Cyclophosphamide (CPM) was obtained from Baxter, Rome, Italy. A solution of CPM at a concentration of 25 mg/mL in PBS (pH 7.4) was freshly prepared.

Crocetin isolation was performed by crocetin esters [56] and purified by an internal method of the Verdù Cantó Saffron Spain Company (Novelda, Alicante, Spain). Crocetin quantification was analysed by the reverse-phase HPLC technique. Twenty μ L of crocetin aqueous solution (252 mg/L)

was filtered through a 0.45 μm PTFE filter and injected into an Agilent 1200 chromatograph (Palo Alto, CA) operating with a 150 mm \times 4.6 mm i.d. and 5 μm Phenomenex (Le Pecq Cedex, France) Luna C18 chromatographic column, at 30°C. Eluents were water (A) and acetonitrile (B) with the following elution gradient: 20% B, 0–5 min; 20–80% B, 5–15 min; 80% B, 15–18 min; and 20%B, 18–30 min. The flow rate was 0.8 mL·min⁻¹, and the DAD detector (Hewlett Packard, Waldbronn, Germany) was set at 440 nm for the detection of *cis/trans* crocetin. Crocetin quantification was estimated using the method based on the extinction coefficient and the related area calculated according to [58, 59].

AS101 was obtained from Tocris Biosciences, Bristol, UK. A solution of AS101 at a concentration of 150 mg/mL in PBS (pH 7.4) was freshly prepared.

2.2. Mice and Study Design. A total of 69 young CD-1 female mice aged 4 to 8 weeks (Charles River Italia s.r.l., Calco, Italy) were used in the present study. All the experiments were carried out in accordance with the guidelines for the care and use of laboratory animals approved by the Animal Care Committee of the University of L'Aquila. Mice were randomly divided into four groups:

- (i) CTRL: normal control mice were maintained on a standard laboratory pellet diet and water ad libitum, without administering medicine for 15 consecutive days. On the 15th day, they received a single intraperitoneal injection of 100 μL of PBS.
- (ii) CPM: mice were maintained on a standard laboratory pellet diet and water ad libitum, without administering medicine for 15 consecutive days. On the 15th day, they received a single intraperitoneal injection of CPM (100 mg/kg).
- (iii) CRO + CPM: mice received crocetin extract (100 mg/kg, [56]) by using a gastric gavage and were allowed free access to a standard laboratory pellet diet and water for 15 consecutive days. On the 15th day, they received a single intraperitoneal injection of 100 μL of CPM (100 mg/kg).
- (iv) AS101 + CPM: mice received AS101 (10 μg per mouse, [20]) by intraperitoneal injections on alternate days and were allowed free access to a standard laboratory pellet diet and water for 15 consecutive days. On the 15th day, they received a single intraperitoneal injection of 100 μL of CPM (100 mg/kg).

At 12 h and 24 h after the administration of CPM, three mice of each group were sacrificed by cervical dislocation (in accordance with the provisions of the EEC regulation 86/609), and ovaries were immediately placed into liquid nitrogen and then stored at -80°C for further analysis. The remaining animals were sacrificed 7 days post CPM, and ovaries were fixed in 4% paraformaldehyde (PFA) at 4°C overnight and paraffin-embedded. Ovarian sections of 5 μm were prepared for further analysis.

2.3. Haematoxylin and Eosin Staining and Follicular Classification. Ovarian sections were stained with haematoxylin and eosin (H&E) and analysed under a light microscope for differential follicle counts. Briefly, blind follicle counts were conducted on every fifth section of entire ovaries by two independent researchers. Follicle stage was classified according to [60]. The classification is based on (i) the size of the oocyte in follicles of different stages of development; (ii) the size of the follicle defined by the number of cells constituting the follicular envelope, and (iii) the morphology of the follicle. Primordial follicles are quiescent follicles characterized by a small oocyte, with a diameter of less than 20 μm , with up to 20 follicle cells attached to its surface on the largest cross-section. Growing follicles include primary follicles, characterized by one complete ring of follicle cells (21 to 60 cells on the largest cross-section) that surround a growing oocyte (diameter between 20 and 70 μm); secondary follicles, with two or three layers of follicle cells (61 to 200 cells on the largest cross section) surrounding a growing oocyte (diameter between 20 and 70 μm); and antral follicles, a fully grown oocyte (diameter 70 μm) surrounded by many layers of follicle cells separated by scattered areas or a cavity containing follicle fluid. Only those follicles in which the nucleus of the oocyte was clearly visible were considered and taken into account. The numbers were then multiplied by 5 in order to obtain an estimate of total follicle numbers per ovary [61].

2.4. Mating Protocol. The mating protocol proposed by Meirow et al. [10] in order to avoid the risk of CPM-related foetal malformations was selected. Briefly, twelve weeks after CPM, female mice from each experimental group were mated with untreated proven fertile males (two females to one male) for 1 week. Then, the females were separated for the duration of pregnancy (21 days) until 3 weeks after the birth of the litter. Females were remated every 8 weeks for a total of three successive mating rounds. The mean number of pups per mouse was counted after each mating round in all experimental groups.

2.5. In Vitro Culture of Granulosa Cells and Proliferation Analysis by BrdU Incorporation. COV434 cells are mitotic human granulosa cells used for *in vitro* studies of cytotoxic actions of chemotherapy drugs [25, 57, 62]. COV434 cells (Sigma-Aldrich, St. Louis, MO) were cultured in Dulbecco's modified Eagle's medium (DMEM), supplemented with 10% foetal bovine serum (FBS) and 1% penicillin/streptomycin and 2 mM L-glutamine. Cultures were maintained at 37°C in a CO₂ incubator with a controlled humidified atmosphere composed of 95% air and 5% CO₂. FBS, DMEM, penicillin/streptomycin, and all other reagents used for cell culture studies were purchased from Euroclone (Pero, Italy). Cells were seeded at a density of 2.5 \times 10⁴ cells per well in 96-well plates and exposed to the active CPM metabolite phosphoramidate mustard (PM, Niotech, Bielefeld, Germany) at concentrations ranging from 10 to 100 μM . The effects of PM on cell proliferation were assessed using the Cell Proliferation BrdU ELISA (Roche Applied Science, Mannheim, Germany) according to the manufacturer's instructions. Briefly, after 60 h, 10 μL of BrdU reagent was

added to each well and the cells were cultured for 12 h at 37°C. After 72 h of culture, cells were fixed with Carnoy's fixative (3:1 methanol: glacial acetic acid) for 20 minutes at -20°C. DNA was partially digested with nucleases to allow the antibody to access BrdU; then cells were incubated with a monoclonal antibody to BrdU, followed by incubation with the anti-BrdU antibody labelled with peroxidase. Finally, the peroxidase substrate ABTS was added, in order to obtain a coloured reaction product. The absorbance of the samples was measured at approximately 405 nm with a standard microplate reader (Sunrise, Tecan, Männedorf, Switzerland).

2.6. Quantitative Real-Time PCR. Granulosa cells were exposed to 50 μ M PM for 3 h, 6 h, and 12 h, and total RNA was extracted using TRIZOL reagent (Life Technologies-Thermo Fisher Scientific, Waltham, MA, USA) following the manufacturer's instructions. 1 μ g of total RNA was retro-transcribed in a final volume of 20 μ L using a cDNA Reverse Transcription kit (Life Technologies-Thermo Fisher Scientific). 2 μ L of cDNA was used for q-RT-PCRs using aCFX96 Touch™ Real-Time PCR Detection System (Bio-Rad Laboratories, Milan, Italy). Primer sequences were the following: *SIRT1*: FW 5'-CAGTGTCATGGTTCCTTGC-3' and REV 5'-AGGACATCGAGGAACCTACCTG-3'; *HuR*: FW 5'-GCTATGGCTTTGTGAACCTACGTG-3' and REV 5'-TGATGTA CAAGTTGGCGTCTTTG-3'; and *RNA18S*: FW 5'-GCAGC TAGGAATAATGGAATAG-3' and REV 5'-TGGCAAAT GCTTTCGCTCTG-3'. mRNA levels were detected using a KAPA SYBR® FAST qPCR Master Mix (2X) Kit (KAPA Biosystems, Wilmington, MA, USA) according to the manufacturer's protocol. Gene expression was normalized to the housekeeping gene RNA 18S. Comparisons in gene expression were calculated using the $2^{-\Delta\Delta C_t}$ method. Two biological replicates were performed, each in technical triplicates.

2.7. Sample Preparation and Western Blot Analysis. Ovarian tissues were homogenized in RIPA buffer by repeated freeze/thaw cycles in liquid nitrogen. After centrifugation (33,000 rpm for 1 h at 4°C), the supernatants were collected for protein analysis. Protein concentration was determined by a BCA protein assay kit (Pierce, Rockford, IL, USA). Protein samples were separated by SDS-PAGE and transferred to a polyvinylidene difluoride membrane (Sigma-Aldrich). Nonspecific binding sites were blocked overnight with 5% not-fat dry milk (Bio-Rad Laboratories) in Tris-buffered saline containing 0.05% Tween 20 (TBS-T). Membranes were incubated with rabbit polyclonal anti-pAKT1 (SC-135650, Santa Cruz Biotechnology Inc., Dallas, TX, USA, 1:250), rabbit polyclonal anti-pFOXO3a (Ab47285, Abcam, Cambridge, UK, 1:700), rabbit polyclonal anti-SIRT1 (Ab12193, Abcam, 1:700), mouse monoclonal anti-HuR (SC-71290, Santa Cruz Biotechnology Inc., 1:250), rabbit polyclonal anti-SIRT3 (Ab86871, Abcam, Cambridge, UK, 1:700), rabbit polyclonal anti-SOD2 (Ab86087, Abcam, 1:1000), rabbit polyclonal anti-PGC1- α (SC-13067, Santa Cruz Biotechnology Inc., 1:500), or mouse monoclonal anti- β actin antibody (Ab8226, Abcam; 1:3000) for 1 h at room temperature, followed by incubation with horseradish peroxidase- (HRP)-

conjugated anti-rabbit (Ab6721, Abcam, 1:3000) or anti mouse (Ab6728, Abcam, 1:2000) secondary antibody for 1 h at room temperature. After washing, specific immunoreactive complexes were detected by an ECL kit (Life Technologies-Thermo Scientific) and Uvitec Cambridge system (Alliance series, Cambridge, UK). When membrane reprobing was necessary, stripping was performed by incubation in Tris-buffered saline (pH 6.7) containing 100 mM beta-mercaptoethanol, 2% SDS, at 54°C for 30 min.

Immunoreactive bands were normalized to β -actin levels using ImageJ 1.44p software. Values were given as relative units (RU). Each experiment was performed in triplicate.

2.8. Statistical Analysis. All data are presented as mean \pm SEM. Statistical analysis was assessed by one-way ANOVA followed by Holm-Sidak multiple comparison. Analyses were performed using the Sigma Stat software (Jandel Scientific Corporation, San Rafael, CA, USA). *P* value < 0.05 was considered statistically significant.

3. Results

3.1. Pretreatment with Crocetin or AS101 Reduces CPM-Induced Follicle Loss. To assess the potential of crocetin as an attenuating agent against CPM toxicity, adult female mice were treated with a daily dose of 100 mg/kg crocetin for 15 days before administration of 100 mg/kg CPM. A group of adult female mice was treated with AS101 (10 μ g/mouse) on alternate days beginning 15 days before CPM treatment. Quantification of the different follicle populations was carried out in the ovaries 1 week after CPM administration. As shown in Figure 1(a), mice receiving crocetin prior to CPM retained a number of primordial follicles larger than CPM alone and not significantly different from untreated controls. Quantification of primordial follicles also revealed that the crocetin effect was similar to AS101. A number of growing follicles in mice receiving crocetin or AS101 prior to CPM was significantly larger than CPM alone reaching values similar to untreated controls.

3.2. Crocetin and AS101 Treatments Rescue Fertility in CPM-Treated Mice. To confirm that preservation of primordial follicles observed in CPM-treated mice receiving crocetin or AS101 was associated with increased fertility, mice from each experimental group were mated for three rounds. At the time of mating, all females had normal oestrous cycles, had similar weight, and appeared healthy. Our data show that a single dose of 100 mg/kg CPM did not affect the reproductive capability of mice until the third round of mating. At this time, we obtained no litter from the CPM mice since they were unable to get pregnant after one week of caging with males. By contrast, CPM-treated mice receiving crocetin or AS101 got pregnant after all mating rounds and presented a litter size not significantly different from the control group (Figure 2).

3.3. Effects of Crocetin and AS101 on PI3K/AKT/FOXO3A Pathway. To search for molecular mechanisms underlying protective effects of crocetin, we hypothesized a potential effect on the PI3K/AKT/FOXO3A pathway underlying

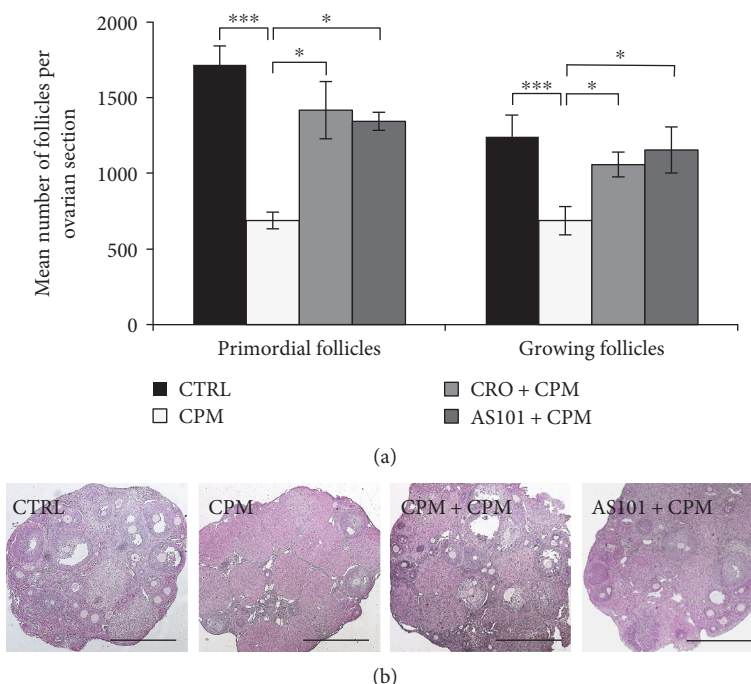


FIGURE 1: Crocetin reduces follicle loss after CPM treatment. (a) Differential follicle count was conducted on ovaries removed from adult (8 weeks old) female CD1 mice ($n=3$, per experimental group) 1 week after CPM treatment preceded or not by crocetin or AS101 pretreatment. Follicles were classified as quiescent primordial follicles or growing follicles. Data represent means \pm SEM. One-way ANOVA ($P < 0.001$), followed by multiple comparison by Holm-Sidak ($***P < 0.001$; $*P < 0.05$). (b) Representative histological sections of ovaries from the CTRL, CPM, CRO + CPM, and AS101 + CPM groups showing follicle reserve. Scale bars: 400 μ m.

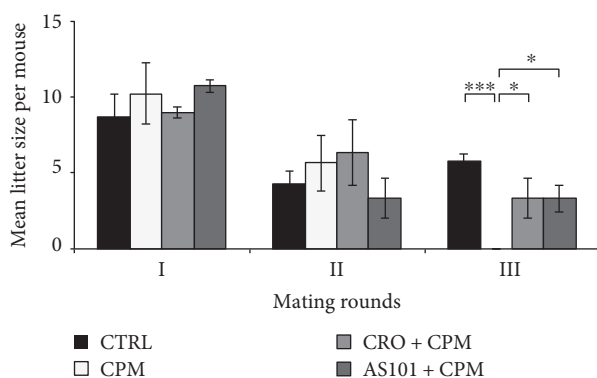


FIGURE 2: Crocetin and AS101 treatments rescue fertility in CPM-treated mice. Reproductive outcomes were assessed over three successive mating rounds in mice ($n=9$, per experimental group) that received CPM treatment preceded or not by crocetin or AS101 pretreatment. Litter size was counted after each mating round. Data represent means \pm SEM. One-way ANOVA ($P < 0.001$), followed by multiple comparison by Holm-Sidak ($***P < 0.001$; $*P < 0.05$).

primordial follicle activation. By looking at the effects at protein expression level, we found that CPM increased the activated form of AKT protein (pAKT) phosphorylated by PI3K and the inactive form of FOXO3a (pFOXO3a) phosphorylated by pAKT. By contrast, crocetin and AS101 treatment results in reduction of both pAKT and pFOXO3a

when compared with CPM alone (Figures 3(a) and 3(b)). However, crocetin effect was more pronounced than AS101 and similar to untreated control.

3.4. SIRT1 Protein and Its Regulator HuR Are Increased during the Early Response to CPM. To investigate the involvement of SIRT1 in the response to CPM, we conducted the first set of experiments in human granulosa cells aimed to analyse changes in mRNA levels of *SIRT1* and *HuR* after 3 h, 6 h, and 12 h of PM exposure. At first, we carried out experiments in order to identify the minimum effective dose of PM, the active metabolite of CPM. After 72 h of treatment, proliferation was significantly reduced in human granulosa cells cultured in the presence of 50 μ M PM. Since no further inhibition was observed at 100 μ M PM, ($P < 0.001$, Figure 4(a)), we employed the dose of 50 μ M PM in gene expression experiments. Then, we analysed the expression level of *SIRT1* and of *HuR* in COV434 cells exposed to 50 μ M PM for 3 h, 6 h, and 12 h. Both genes increased their expression level in a time-dependent manner, suggesting the activation of the OS response in this cell line (Figures 4(b) and 4(c)).

In the second set of experiment, mice received CPM and were sacrificed at 12 h and 24 h after CPM treatment. Our results show that SIRT1 protein level increased at 12 h and doubled its expression at 24 h after CPM treatment (Figure 5(a)). HuR protein increased at 12 h after CPM to decrease at 24 h (Figure 5(b)).

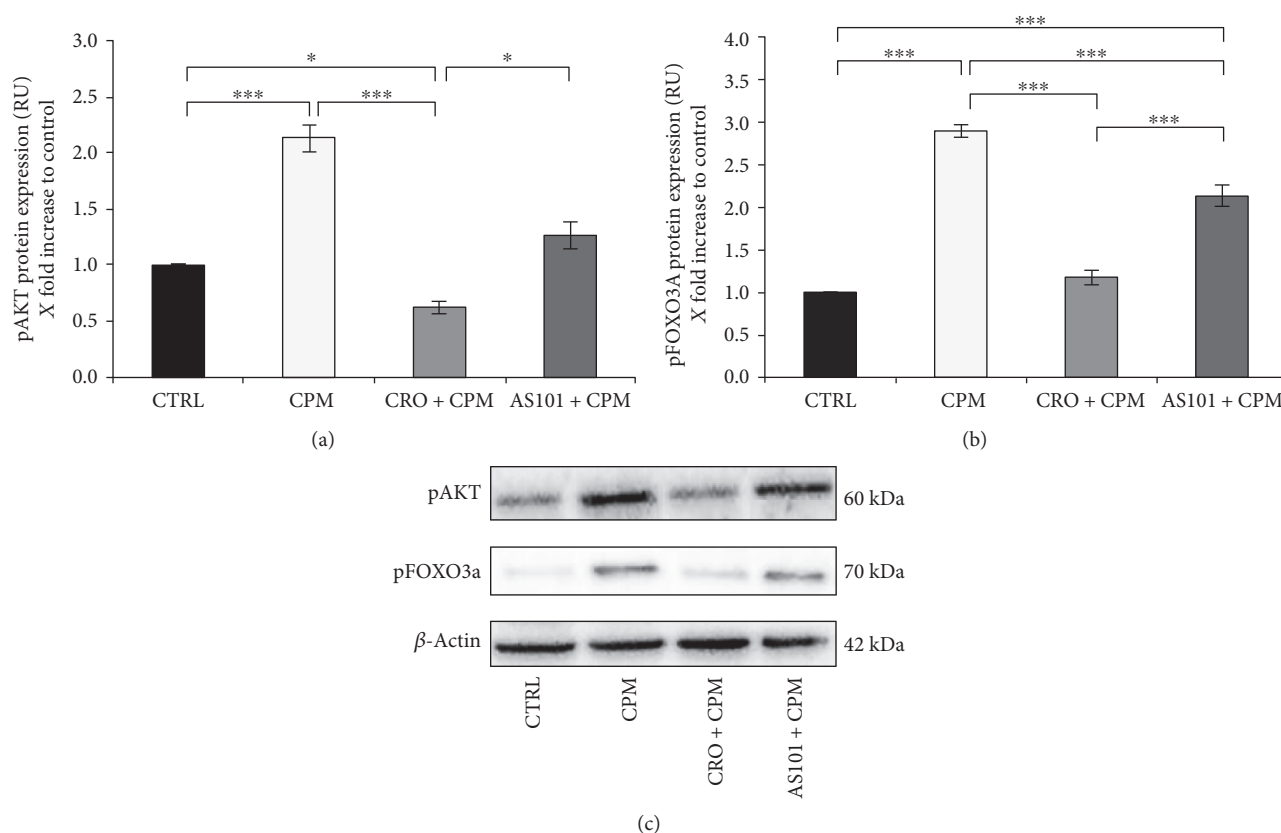


FIGURE 3: Crocetin reduces CPM-induced phosphorylation of key proteins in the PTEN/PI3K/Akt pathway. Protein analysis was conducted on ovaries from 8-week-old mice ($n = 3$, per experimental group) removed 24 hours after a single dose of CPM preceded or not by crocetin or AS101 pretreatment. Western blots of pAKT (a) and pFOXO3a (b) and representative images (c). Fold change is represented as a bar graph. Experiments were repeated three times with similar results. One-way ANOVA ($P < 0.001$), followed by multiple comparison by Holm-Sidak ($***P < 0.001$; $*P < 0.05$).

3.5. Crocetin and AS101 Prevent the SIRT1 Upregulation Induced by CPM. In the second set of experiments, we tested whether crocetin and AS101 act by modulating the early adaptive response regulated by SIRT1. Our data showed that crocetin treatment prevented the increased expression of SIRT1 induced by CPM treatment (Figure 6). Furthermore, mice receiving crocetin prior to CPM presented a SIRT1 expression level equivalent to untreated controls. AS101 induced a reduced activation of SIRT1 protein production in comparison to CPM treatment, but its levels were enhanced when compared to crocetin and untreated control mice.

3.6. Crocetin and AS101 Prevent CPM-Induced Changes in Mitochondrial Markers. To test whether the protective effect of crocetin was exerted throughout regulation of mitochondrial markers, we analysed the expression level of SIRT3, SOD2, and PGC1alpha. Similar to SIRT1, SIRT3 increased at 24 h following CPM (Figure 7(a)). Crocetin treatment prevented the SIRT3 increase induced by CPM although SIRT3 amount was lower than that observed in untreated controls. AS101 treatment promoted a similar effect. Moreover, CPM was found to significantly reduce SOD2 protein. Both crocetin and AS101 treatments attenuated this effect although

SOD2 level was lower than that observed in untreated controls (Figure 7(b)). Our results also showed that CPM mice presented lower levels of PGC1- α protein when compared with control whereas crocetin and AS101 induced a threefold increase of this protein in comparison to untreated controls (Figure 7(c)).

4. Discussion

Considering the increment in survival rates of cancer patients in their childhood or reproductive age, searching for fertoprotective agents is the main challenge in oncology practice. Here, we demonstrate for the first time that oral administration of crocetin, a natural carotenoid derivative and effective free radical scavenger, attenuates CPM-induced gonadotoxicity and modulates molecular pathways involved in the early ovarian response to this anticancer drug. These observations provide strong evidence that an imbalance of redox potential is the main factor underlying CPM-induced ovarian damage. Moreover, we outlined that crocetin effects at both molecular and biological levels resembled those by AS101, the most relevant candidate as a fertoprotective agent.

Crocetin, the main bioactive saffron compound [63, 64], is the hydrolysed active form of crocin, which is the most

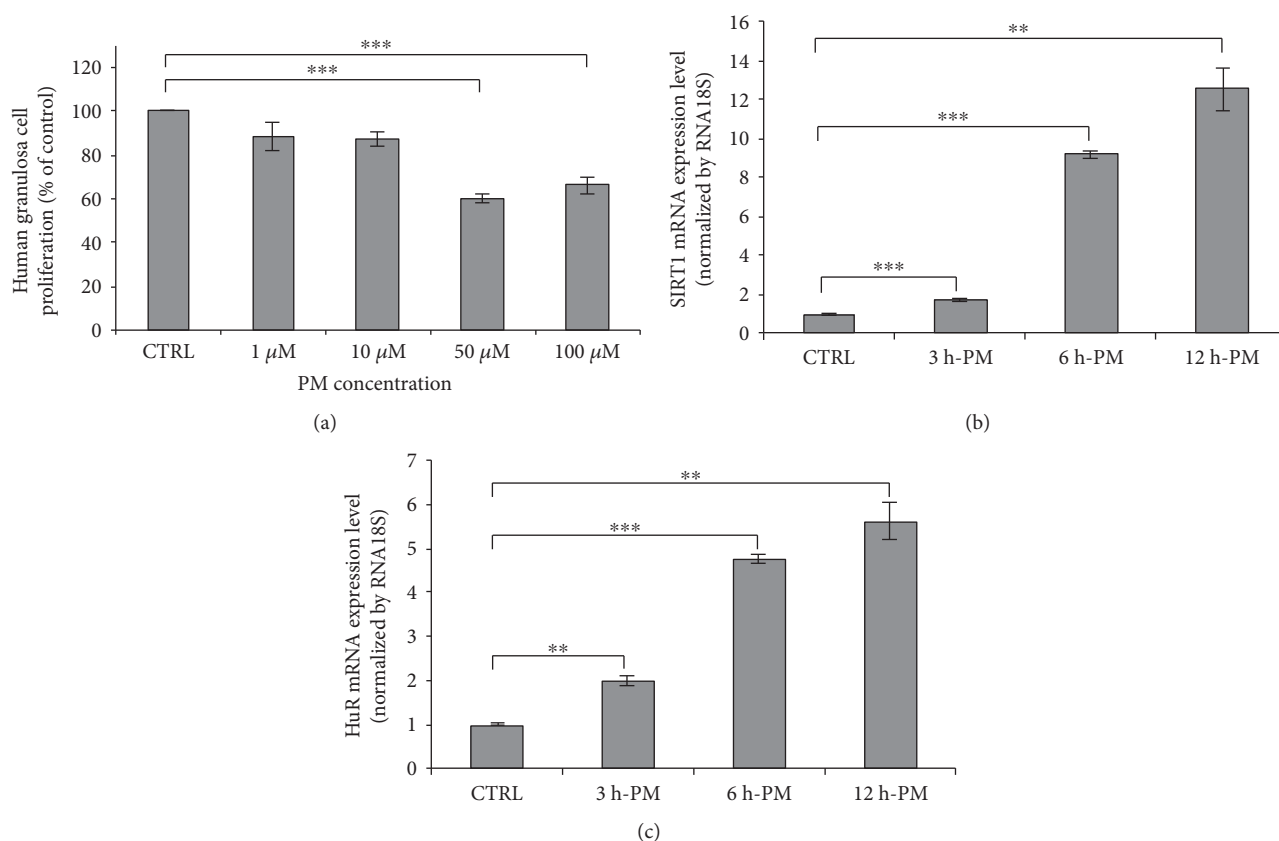


FIGURE 4: SIRT1 and HuR mRNA increase after a PM treatment in human granulosa cell. (a) After 72 h of treatment, human granulosa cells cultured in the presence of 50 μ M PM showed a significant reduction of proliferation. (b) SIRT1 and (c) HuR mRNA expression levels after 50 μ M PM treatment were evaluated by performing a q-RT PCR. RNA18S was used as an endogenous control. Data represent means \pm SEM. Experiments were done in triplicate ($n = 3$). ** $P < 0.01$, and *** $P < 0.001$.

investigated saffron carotenoid. In comparison with crocin, crocetin is more rapidly absorbed in the intestinal tract and exhibits greater efficacy [65]. It is well established that the therapeutic effects of crocetin against some types of cancers, including breast cancer, have been pointed out [47, 48, 54–56, 66–69]. Crocetin acts in a dose-dependent manner in *in vitro* models [47, 55, 67, 68]. Oral administration of crocetin has been employed in research on mice aimed to investigate its effects against retinal damage [70] and tumour growth [56, 69]. Crocetin has also been administrated to healthy adult human volunteers, demonstrating that it is beneficial also in humans [71, 72]. Although only one paper reported the prevention by crocetin of CPM side effects on the bladder and liver [73], a plethora of publications reveals that crocetin can provide protection against OS induced by toxicants or underlying disorders in numerous organs, tissues, and cells [49–52, 74–78].

Our data show that crocetin protects primordial and growing follicles from CPM injury and the mechanism underlying the protective action of crocetin is similar to that of AS101. Crocetin treatment results in the reduction of the phosphorylated/activated form of AKT protein (pAKT) and the phosphorylated/inactive form of FOXO3a (pFOXO3a) when compared with CPM. According to our results, crocetin treatment was more effective in reducing the activation

of the PI3K/AKT/FOXO3a pathway in response to CPM since pAKT and pFOXO3a levels were lower than that observed in AS101 although this difference did not result in higher efficacy in terms of follicle survival. Thus, it would be suggested that crocetin, similar to AS101, prevents dysregulation of follicle activation induced by CPM. Nevertheless, further investigation is needed to clarify whether crocetin, similar to AS101 [20], is able to reduce follicle apoptosis induced by CPM.

In addition to its role in follicle activation, FOXO3a is known to activate an antioxidant response when deacetylated by SIRT1. However, this function cannot be exerted when FOXO3a is phosphorylated by AKT. Thus, we can hypothesize that the increased levels of pFOXO3a in CPM ovaries may compromise the antioxidant response orchestrated by SIRT1.

SIRT1 plays a critical role in coordinating cellular response to stress, and SIRT1 levels are upregulated by cellular stressors, including metabolic, genotoxic, and oxidative stress [79]. Indeed, in our model of human granulosa cells sensitive to antiproliferative effects of CPM, Sirt1 and HuR transcription gradually increases with the same kinetics, demonstrating the involvement of SIRT1 in the early steps of cell response to CPM damage. This conclusion has been confirmed in the animal model where we observed that as

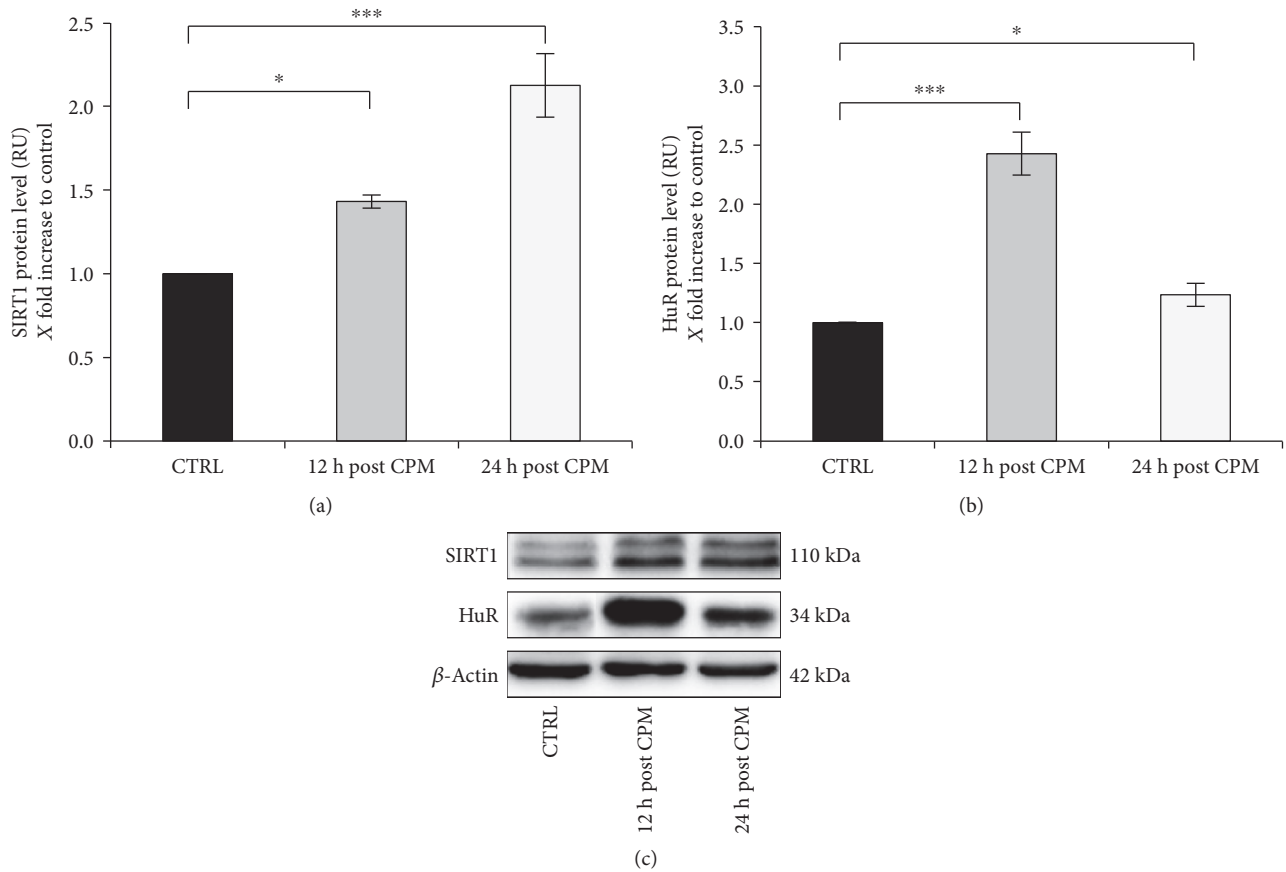


FIGURE 5: CPM treatment induces an increase of SIRT1 and HuR. Protein analysis was conducted on ovaries from 8-week-old mice ($n = 3$, per experimental group) removed 12 or 24 hours after a single dose of CPM. Western blots of SIRT1 (a) and HuR (b) and representative images (c). Fold change is represented as a bar graph. Experiments were repeated three times with similar results. One-way ANOVA ($P < 0.001$), followed by multiple comparison by Holm-Sidak ($***P < 0.001$; $*P < 0.05$).

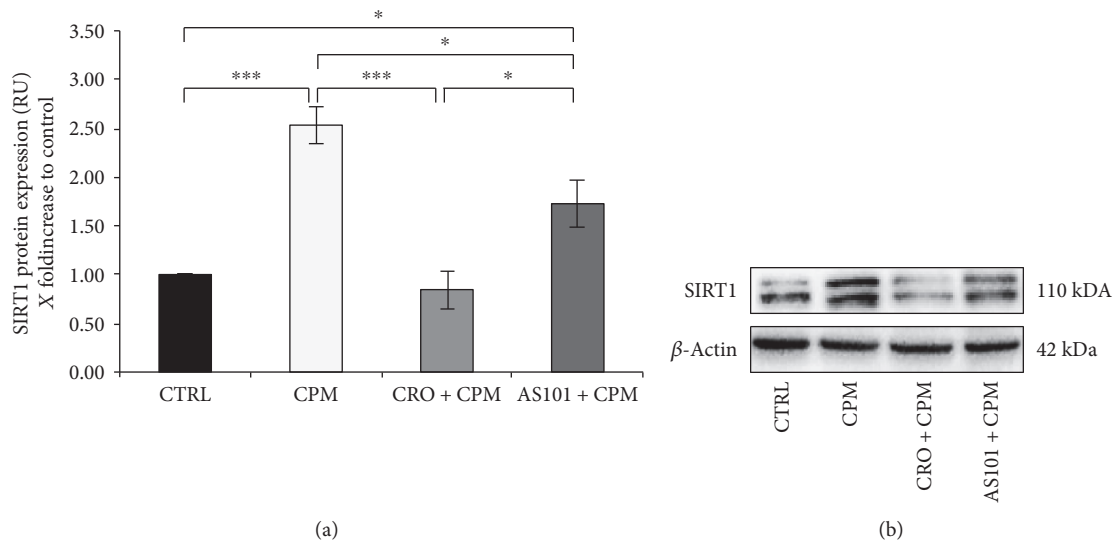


FIGURE 6: Crocetin and AS101 reduce CPM-induced activation of SIRT1 protein in the ovary. Protein analysis was conducted on ovaries from 8-week-old mice ($n = 3$, per experimental group) removed 24 hours after a single dose of CPM preceded or not by crocetin or AS101 pre-treatment. Western blots of SIRT1 (a) and representative images (b). Fold change is represented as a bar graph. Experiments were repeated three times with similar results. One Way ANOVA $P < 0.001$, followed by Multiple comparison by Holm-Sidak: $***P < 0.001$; $*P < 0.05$.

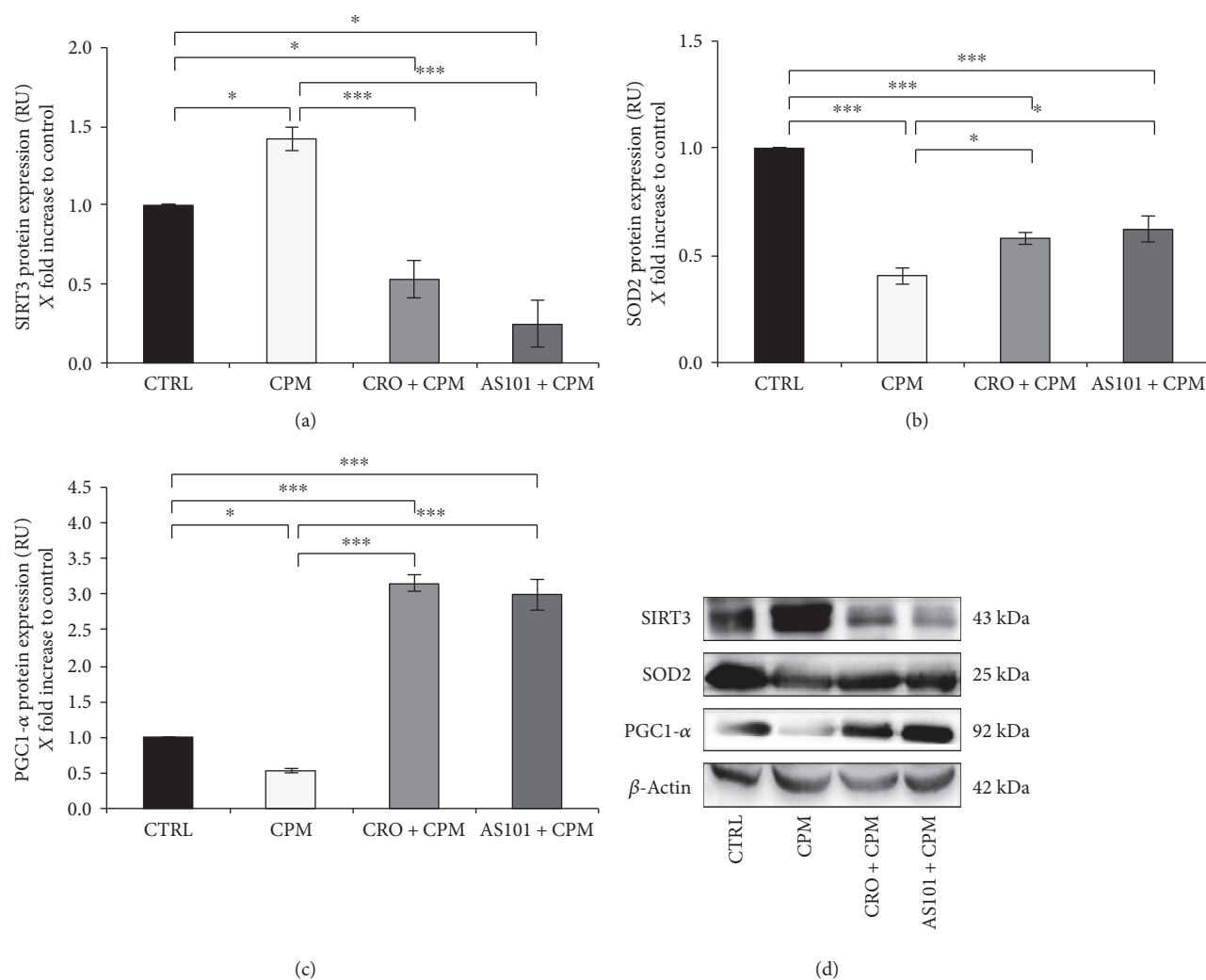


FIGURE 7: Crocetin and AS101 prevent CPM-induced mitochondrial damage assessed by SIRT3, SOD2, and PGC1- α protein levels in the ovary. Protein analysis was conducted on ovaries from 8-week-old mice ($n = 3$, per experimental group) removed 24 hours after a single dose of CPM preceded or not by crocetin or AS101 pretreatment. Western blots of SIRT3 (a), PGC1- α (b), and SOD2 (c) and representative images (d). Fold change is represented as a bar graph. Experiments were repeated three times with similar results. One-way ANOVA ($P < 0.001$), followed by multiple comparison by Holm-Sidak (** $P < 0.001$; * $P < 0.05$).

early as 12 h following CPM administration, the ovary activates an adaptive response based on upregulation of SIRT1 protein that peaks at 24 h. This pattern is preceded by upregulation of HuR which peaks at 12 h to decrease at 24 h indicating that in response to stress HuR may act transiently to stabilise SIRT1 transcripts prior to be degraded [80]. Nevertheless, other roles for HuR cannot be excluded. Posttranscriptional function of HuR has been described for a wide number of transcripts bearing AU-rich elements whose turnover is critical for cell fate [81–83].

Previous reports described a reduction of SIRT1 levels in rat ovaries in response to CPM and the protective role of caloric restriction associated with increased SIRT1 expression [84]. This is not in contrast with our results since we focused on the evaluation of the early response assessed before biological damage whereas the reduction of SIRT1 levels described elsewhere could be related to depletion of follicle population following CPM treatment.

Moreover, SIRT1 has been recently involved in the regulation of bioenergetics metabolism during folliculogenesis. In this regard, Cinco et al., [85] observed that oocyte expression of SIRT1 is increasing during primordial follicle awakening together with a significant increase of NAD^+ . This is related to the decreased $NADH/NAD^+$ levels resulting from the activation of oxidative phosphorylation for energy supply during growth. Thus, the increased levels of ovarian SIRT1 during the early phase of CPM damage may be the cause or the effect of primordial follicle activation leading to the burnout effect.

Our data showed that both crocetin and AS101 prevented the increased expression of SIRT1 induced by CPM. This could be ascribed to their ability to counteract CPM-induced changes in the redox potential leading to SIRT1 recruitment. However, the observation that levels of SIRT1 in the two groups are not the same would suggest that crocetin and AS101 have a different ability to modulate ovarian

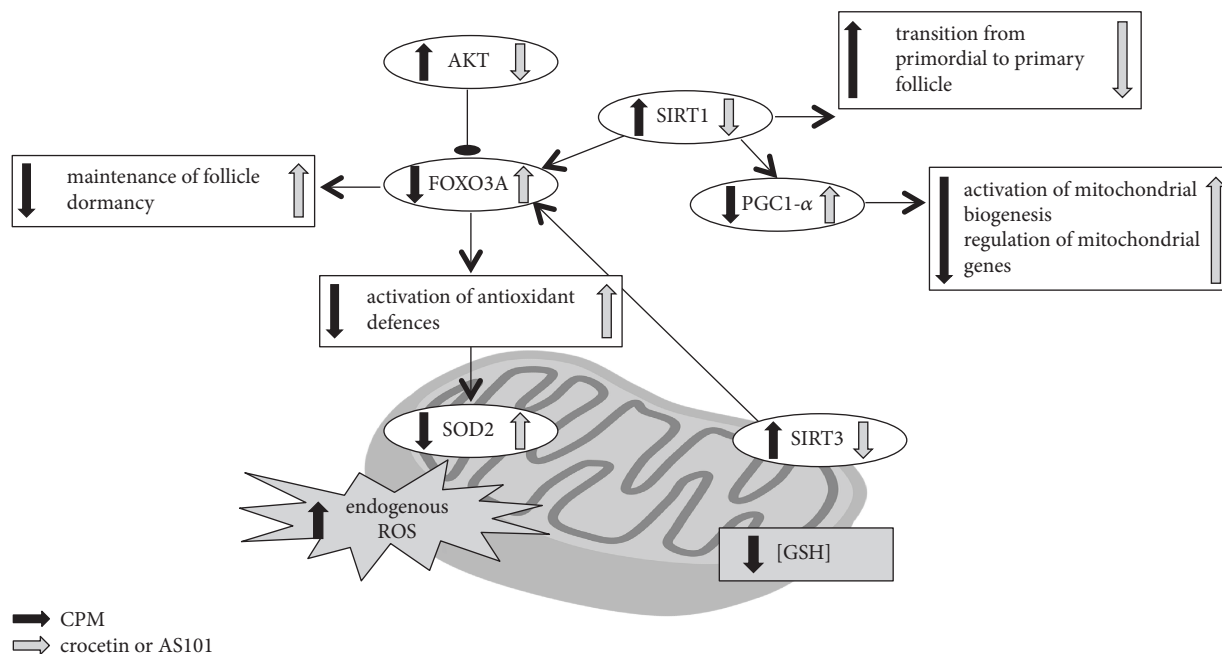


FIGURE 8: Possible mechanisms through which crocetin and AS101 reverse the early adaptive response of the ovary to CPM. Based on our results and current literature, CPM causes the activation of the PI3K/AKT/FOXO3A signalling pathway that ends with the activation of primordial follicles (“burnout” hypothesis). Increased oxidative stress, which probably arises from reduced GSH due to ovarian PM detoxification, is evidenced by reduced SOD2 levels and upregulation of the OS sensors SIRT1 and SIRT3. Upregulation of SIRT1 may contribute to CPM-induced follicle activation; upregulation of SIRT3 along with reduction of PGC1- α and SOD2 marks the CPM-induced mitochondrial damage. By contrast, the finding that crocetin and AS101 exert fertoprotective effects, prevent SIRT1 and SIRT3 rise, and maintain pFOXO3a, PGC1- α , and SOD2 levels provides evidence for a link between the burnout hypothesis, oxidative stress, and mitochondrial damage.

physiological environment, which influences SIRT1 expression. The hypothesis of the oxidative basis of CPM ovarian damage is supported by the finding that crocetin and AS101 prevented CPM-induced mitochondrial toxicity. In particular, crocetin and AS101 treatment counteracted the upregulation of the mitochondrial sirtuin SIRT3 induced by CPM. SIRT3 is considered a key coordinator of mitochondrial energy metabolism under stress conditions by directly targeting and modulating various processes [39–41] and downregulating mitochondrial protein synthesis [86]. Further evidence of OS and its mitochondrial basis are the downregulation of PGC1- α and SOD2 in CPM ovaries and the observation that these mitochondrial proteins severely increased their expression following crocetin and AS101 administration.

Therefore, it can be speculated that SIRT1 is recruited in order to regulate cell fate following CPM injury. In the experimental model proposed here, it seems to fail to orchestrate an efficient repair in concomitance with SIRT3, probably because its substrates, such as FOXO3a and PGC1- α , or downstream effectors, such as SOD2, are impaired. For these reasons, we propose that SIRT1 could be considered as a marker of CPM ovarian injury. Given its role as a sensor of damage and effector of cell fate, caution should be taken in proposing attenuating therapies based on SIRT1 targeting.

The inhibition of CPM-induced follicle loss by AS101 has been ascribed to its ability to inhibit AKT activation and reduce apoptosis in large growing follicles [20]. The finding

that a potent antioxidant such as crocetin exerts similar effects on the PI3K/AKT/FOXO3a pathway suggests that AS101 may also act upstream to this pathway by preventing the OS burst induced by CPM. This hypothesis is also supported by the observation that, similar to crocetin, AS101 prevents the activation of OS sensors and mitochondrial toxicity induced by CPM. It is also important to consider that beneficial effects by both crocetin and AS101 may be ascribed to their effects on the whole ovarian microenvironment. In this regard, crocetin’s ability to increase diffusion of oxygen through the plasma can contribute to counteract CPM-induced inhibition of follicular microvascularization [87]. Moreover, anti-inflammatory properties are known for both these agents [50, 53, 88, 89] although these effects in the ovary need to be investigated.

The present study represents a contribution to previous evidence in animal models about the use of saffron bioactive molecules in the fertility field. Recent investigations have revealed that crocetin and its derivative crocin have beneficial effects on *in vitro* oocyte maturation, sperm quality, and fertilization [90–94]. Moreover, crocin has been described to protect male gonad against CPM toxicity [46].

In conclusion, we speculate that the ovarian adaptive response to CPM consists in a complex network involving oxidative stress, SIRT1, and mitochondrial damage (Figure 8). Finally, due to its efficacy in the animal model and its anti-cancer properties and low toxicity in humans, this work demonstrates for the first time that crocetin presents all

the characteristics required for a natural fertoprotective agent to be included in future clinical studies.

Conflicts of Interest

The authors declare that they have no conflicts of interest.

Acknowledgments

The funds for this work were provided by the Department of Life, Health and Environmental Sciences, University of L'Aquila (RIA 2013-2016).

References

- [1] J. M. Levine, J. F. Kelvin, G. P. Quinn, and C. R. Gracia, "Infertility in reproductive-age female cancer survivors," *Cancer*, vol. 121, no. 10, pp. 1532–1539, 2015.
- [2] A. W. Loren, P. B. Mangu, L. N. Beck et al., "Fertility preservation for patients with cancer: American society of clinical oncology clinical practice guideline update," *Journal of Clinical Oncology*, vol. 31, no. 19, pp. 2500–2510, 2013.
- [3] T. K. Woodruff, "Oncofertility: a grand collaboration between reproductive medicine and oncology," *Reproduction*, vol. 150, no. 3, pp. S1–S10, 2015.
- [4] H. A. Parlakgumus, E. B. Kilicdag, F. A. Bolat, B. Haydardedeoglu, and A. Parlakgumus, "GnRH agonists and antagonists in rescue for cyclophosphamide-induced ovarian damage: friend or foe?," *Archives of Gynecology and Obstetrics*, vol. 291, no. 6, pp. 1403–1410, 2015.
- [5] M. Lambertini, F. Poggio, A. Levaggi, and L. Del Mastro, "Protecting ovaries during chemotherapy through gonad suppression: a systematic review and meta-analysis," *Obstetrics and Gynecology*, vol. 126, no. 4, p. 901, 2015.
- [6] R. Leonard, D. Adamson, G. Bertelli et al., "GnRH agonist for protection against ovarian toxicity during chemotherapy for early breast cancer: the Anglo Celtic Group OPTION trial," *Annals of Oncology*, vol. 28, no. 8, pp. 1811–1816, 2017.
- [7] H. Roness, L. Kalich-Philosoph, and D. Meirou, "Prevention of chemotherapy-induced ovarian damage: possible roles for hormonal and non-hormonal attenuating agents," *Human Reproduction Update*, vol. 20, no. 5, pp. 759–774, 2014.
- [8] H. Roness, O. Kashi, and D. Meirou, "Prevention of chemotherapy-induced ovarian damage," *Fertility and Sterility*, vol. 105, no. 1, pp. 20–29, 2016.
- [9] D. Meirou, H. Lewis, D. Nugent, and M. Epstein, "Subclinical depletion of primordial follicular reserve in mice treated with cyclophosphamide: clinical importance and proposed accurate investigative tool," *Human Reproduction*, vol. 14, no. 7, pp. 1903–1907, 1999.
- [10] D. Meirou, M. Epstein, H. Lewis, D. Nugent, and R. G. Gosden, "Administration of cyclophosphamide at different stages of follicular maturation in mice: effects on reproductive performance and fetal malformations," *Human Reproduction*, vol. 16, no. 4, pp. 632–637, 2001.
- [11] O. Oktem and K. Oktay, "A novel ovarian xenografting model to characterize the impact of chemotherapy agents on human primordial follicle reserve," *Cancer Research*, vol. 67, no. 21, pp. 10159–10162, 2007.
- [12] I. Ben-Aharon and R. Shalgi, "What lies behind chemotherapy-induced ovarian toxicity?," *Reproduction*, vol. 144, no. 2, pp. 153–163, 2012.
- [13] O. M. Colvin, "An overview of cyclophosphamide development and clinical applications," *Current Pharmaceutical Design*, vol. 5, no. 8, pp. 555–560, 1999.
- [14] G. E. Katsifis and A. G. Tzioufas, "Ovarian failure in systemic lupus erythematosus patients treated with pulsed intravenous cyclophosphamide," *Lupus*, vol. 13, no. 9, pp. 673–678, 2004.
- [15] M. A. Dooley and R. Nair, "Therapy insight: preserving fertility in cyclophosphamide-treated patients with rheumatic disease," *Nature Clinical Practice. Rheumatology*, vol. 4, no. 5, pp. 250–257, 2008.
- [16] S. K. Petrillo, P. Desmeules, T. Q. Truong, and P. J. Devine, "Detection of DNA damage in oocytes of small ovarian follicles following phosphoramidate mustard exposures of cultured rodent ovaries *in vitro*," *Toxicology and Applied Pharmacology*, vol. 253, no. 2, pp. 94–102, 2011.
- [17] S. Ganesan and A. F. Keating, "Phosphoramidate mustard exposure induces DNA adduct formation and the DNA damage repair response in rat ovarian granulosa cells," *Toxicology and Applied Pharmacology*, vol. 282, no. 3, pp. 252–258, 2015.
- [18] S. Ganesan and A. F. Keating, "The ovarian DNA damage repair response is induced prior to phosphoramidate mustard-induced follicle depletion, and ataxia telangiectasia mutated inhibition prevents PM-induced follicle depletion," *Toxicology and Applied Pharmacology*, vol. 292, pp. 65–74, 2016.
- [19] G. Bedoschi, P. A. Navarro, and K. Oktay, "Chemotherapy-induced damage to ovary: mechanisms and clinical impact," *Future Oncology*, vol. 12, no. 19, pp. 2333–2344, 2016.
- [20] L. Kalich-Philosoph, H. Roness, A. Carmely et al., "Cyclophosphamide triggers follicle activation and "burnout"; AS101 prevents follicle loss and preserves fertility," *Science Translational Medicine*, vol. 5, no. 185, article 185ra62, 2013.
- [21] A. Makker, M. M. Goel, and A. A. Mahdi, "PI3K/PTEN/Akt and TSC/mTOR signaling pathways, ovarian dysfunction, and infertility: an update," *Journal of Molecular Endocrinology*, vol. 53, no. 3, pp. R103–R118, 2014.
- [22] M. Hayun, Y. Naor, M. Weil et al., "The immunomodulator AS101 induces growth arrest and apoptosis in multiple myeloma: association with the Akt/survivin pathway," *Biochemical Pharmacology*, vol. 72, no. 11, pp. 1423–1431, 2006.
- [23] P. J. Devine, S. D. Perreault, and U. Luderer, "Roles of reactive oxygen species and antioxidants in ovarian toxicity," *Biology of Reproduction*, vol. 86, no. 2, p. 27, 2012.
- [24] U. Luderer, "Ovarian toxicity from reactive oxygen species," *Vitamins and Hormones*, vol. 94, pp. 99–127, 2014.
- [25] M. Tsai-Turton, B. T. Luong, Y. Tan, and U. Luderer, "Cyclophosphamide-induced apoptosis in COV434 human granulosa cells involves oxidative stress and glutathione depletion," *Toxicological Sciences*, vol. 98, no. 1, pp. 216–230, 2007.
- [26] D. O. Saleh and D. F. Mansour, "Ovario-protective effects of genistein against cyclophosphamide toxicity in rats: role of anti-müllerian hormone and oestradiol," *European Journal of Pharmacology*, vol. 789, pp. 163–171, 2016.
- [27] N. A. Yener, O. Sinanoglu, E. Ilter et al., "Effects of spirulina on cyclophosphamide-induced ovarian toxicity in rats: biochemical and histomorphometric evaluation of the ovary,"

- Biochemistry Research International*, vol. 2013, Article ID 764262, 6 pages, 2013.
- [28] J. A. Madden and A. F. Keating, "Ovarian xenobiotic biotransformation enzymes are altered during phosphoramidate mustard-induced ovotoxicity," *Toxicological Sciences*, vol. 141, no. 2, pp. 441–452, 2014.
- [29] S. Michan and D. Sinclair, "Sirtuins in mammals: insights into their biological function," *The Biochemical Journal*, vol. 404, no. 1, pp. 1–13, 2007.
- [30] B. J. Morris, "Seven sirtuins for seven deadly diseases of aging," *Free Radical Biology & Medicine*, vol. 56, pp. 133–171, 2013.
- [31] Y. S. Hori, A. Kuno, R. Hosoda, and Y. Horio, "Regulation of FOXOs and p53 by SIRT1 modulators under oxidative stress," *PLoS One*, vol. 8, no. 9, article e73875, 2013.
- [32] J. W. Hwang, H. Yao, S. Caito, I. K. Sundar, and I. Rahman, "Redox regulation of SIRT1 in inflammation and cellular senescence," *Free Radical Biology & Medicine*, vol. 61, pp. 95–110, 2013.
- [33] A. Salminen, K. Kaarniranta, and A. Kauppinen, "Crosstalk between oxidative stress and SIRT1: impact on the aging process," *International Journal of Molecular Sciences*, vol. 14, no. 2, pp. 3834–3859, 2013.
- [34] L. R. Saunders and E. Verdin, "Sirtuins: critical regulators at the crossroads between cancer and aging," *Oncogene*, vol. 26, no. 37, pp. 5489–5504, 2007.
- [35] G. Di Emidio, S. Falone, M. Vitti et al., "SIRT1 signalling protects mouse oocytes against oxidative stress and is deregulated during aging," *Human Reproduction*, vol. 29, no. 9, pp. 2006–2017, 2014.
- [36] C. Tatone, G. Di Emidio, M. Vitti et al., "Sirtuin functions in female fertility: possible role in oxidative stress and aging," *Oxidative Medicine and Cellular Longevity*, vol. 2015, Article ID 659687, 11 pages, 2015.
- [37] J. R. Revollo and X. Li, "The ways and means that fine tune Sirt1 activity," *Trends in Biochemical Sciences*, vol. 38, no. 3, pp. 160–167, 2013.
- [38] M. B. Hock and A. Kralli, "Transcriptional control of mitochondrial biogenesis and function," *Annual Review of Physiology*, vol. 71, pp. 177–203, 2009.
- [39] E. Michishita, J. Y. Park, J. M. Burneskis, J. C. Barrett, and I. Horikawa, "Evolutionarily conserved and nonconserved cellular localizations and functions of human SIRT proteins," *Molecular Biology of the Cell*, vol. 16, no. 10, pp. 4623–4635, 2005.
- [40] J. Brenmoehl and A. Hoeflich, "Dual control of mitochondrial biogenesis by sirtuin 1 and sirtuin 3," *Mitochondrion*, vol. 13, no. 6, pp. 755–761, 2013.
- [41] P. Parihar, I. Solanki, M. L. Mansuri, and M. S. Parihar, "Mitochondrial sirtuins: emerging roles in metabolic regulations, energy homeostasis and diseases," *Experimental Gerontology*, vol. 61, pp. 130–141, 2015.
- [42] D. M. Salvadori, L. R. Ribeiro, M. D. Oliveira, C. A. Pereira, and W. Beçak, "The protective effect of β -carotene on genotoxicity induced by cyclophosphamide," *Mutation Research/Fundamental and Molecular Mechanisms of Mutagenesis*, vol. 265, no. 2, pp. 237–244, 1992.
- [43] D. N. Tripathi and G. B. Jena, "Astaxanthin inhibits cytotoxic and genotoxic effects of cyclophosphamide in mice germ cells," *Toxicology*, vol. 248, no. 2, pp. 96–103, 2008.
- [44] S. Sadir, S. Deveci, A. Korkmaz, and S. Oter, "Alpha-tocopherol, beta-carotene and melatonin administration protects cyclophosphamide-induced oxidative damage to bladder tissue in rats," *Cell Biochemistry and Function*, vol. 25, no. 5, pp. 521–526, 2007.
- [45] S. Jnaneshwari, M. Hemshekhar, M. S. Santhosh et al., "Crocin, a dietary colorant, mitigates cyclophosphamide-induced organ toxicity by modulating antioxidant status and inflammatory cytokines," *The Journal of Pharmacy and Pharmacology*, vol. 65, no. 4, pp. 604–614, 2013.
- [46] Z. Bakhtiary, R. Shahrooz, A. Ahmadi, and L. Zarei, "Evaluation of antioxidant effects of crocin on sperm quality in cyclophosphamide treated adult mice," *Veterinary Research Forum*, vol. 5, no. 3, pp. 213–218, 2014.
- [47] W. G. Gutheil, G. Reed, A. Ray, S. Anant, and A. Dhar, "Crocin: an agent derived from saffron for prevention and therapy for cancer," *Current Pharmaceutical Biotechnology*, vol. 13, no. 1, pp. 173–179, 2012.
- [48] S. Samarghandian and A. Borji, "Anticarcinogenic effect of saffron (*Crocus sativus* L.) and its ingredients," *Pharmacognosy Research*, vol. 6, no. 2, pp. 99–107, 2014.
- [49] M. Venkatraman, D. Konga, R. Peramaiyan, E. Ganapathy, and S. Dhanapal, "Reduction of mitochondrial oxidative damage and improved mitochondrial efficiency by administration of crocetin against benzo[a]pyrene induced experimental animals," *Biological & Pharmaceutical Bulletin*, vol. 31, no. 9, pp. 1639–1645, 2008.
- [50] K. N. Nam, Y. M. Park, H. J. Jung et al., "Anti-inflammatory effects of crocin and crocetin in rat brain microglial cells," *European Journal of Pharmacology*, vol. 648, no. 1–3, pp. 110–116, 2010.
- [51] F. Yoshino, A. Yoshida, N. Umigai, K. Kubo, and M. C. Lee, "Crocetin reduces the oxidative stress induced reactive oxygen species in the stroke-prone spontaneously hypertensive rats (SHRSPs) brain," *Journal of Clinical Biochemistry and Nutrition*, vol. 49, no. 3, pp. 182–187, 2011.
- [52] R. Yang, L. Yang, X. Shen et al., "Suppression of NF- κ B pathway by crocetin contributes to attenuation of lipopolysaccharide-induced acute lung injury in mice," *European Journal of Pharmacology*, vol. 674, no. 2–3, pp. 391–396, 2012.
- [53] M. H. Boskabady and T. Farkhondeh, "Antiinflammatory, antioxidant, and immunomodulatory effects of *Crocus sativus* L. and its main constituents," *Phytotherapy Research*, vol. 30, no. 7, pp. 1072–1094, 2016.
- [54] A. Bolhassani, A. Khavari, and S. Z. Bathaie, "Saffron and natural carotenoids: biochemical activities and anti-tumor effects," *Biochimica et Biophysica Acta (BBA)-Reviews on Cancer*, vol. 1845, no. 1, pp. 20–30, 2014.
- [55] S. H. Kim, J. M. Lee, S. C. Kim, C. B. Park, and P. C. Lee, "Proposed cytotoxic mechanisms of the saffron carotenoids crocin and crocetin on cancer cell lines," *Biochemistry and Cell Biology*, vol. 92, no. 2, pp. 105–111, 2014.
- [56] C. Festuccia, A. Mancini, G. L. Gravina et al., "Antitumor effects of saffron-derived carotenoids in prostate cancer cell models," *BioMed Research International*, vol. 2014, Article ID 135048, 12 pages, 2014.
- [57] A. Yuksel, G. Bildik, F. Senbabaoglu et al., "The magnitude of gonadotoxicity of chemotherapy drugs on ovarian follicles and granulosa cells varies depending upon the category of the drugs and the type of granulosa cells," *Human Reproduction*, vol. 30, no. 12, pp. 2926–2935, 2015.

- [58] A. M. Sánchez, M. Carmona, S. A. Ordoudi, M. Z. Tsimidou, and G. L. Alonso, "Kinetics of individual crocetin ester degradation in aqueous extracts of saffron (*Crocus sativus* L.) upon thermal treatment in the dark," *Journal of Agricultural and Food Chemistry*, vol. 56, no. 5, pp. 1627–1637, 2008.
- [59] A. M. Sánchez, M. Carmona, A. Zalacain, J. M. Carot, J. M. Jabaloyes, and G. L. Alonso, "Rapid determination of crocetin esters and picrocrocetin from saffron spice (*Crocus sativus* L.) using UV-visible spectrophotometry for quality control," *Journal of Agricultural and Food Chemistry*, vol. 56, no. 9, pp. 3167–3175, 2008.
- [60] T. Pedersen and H. Peters, "Proposal for a classification of oocytes and follicles in the mouse ovary," *Journal of Reproduction and Fertility*, vol. 17, no. 3, pp. 555–557, 1968.
- [61] J. L. Tilly, "Ovarian follicle counts—not as simple as 1, 2, 3," *Reproductive Biology and Endocrinology*, vol. 1, p. 11, 2003.
- [62] H. Zhang, M. Vollmer, M. De Geyter et al., "Characterization of an immortalized human granulosa cell line (COV434)," *Molecular Human Reproduction*, vol. 6, no. 2, pp. 146–153, 2000.
- [63] L. Xi, Z. Qian, P. Du, and J. Fu, "Pharmacokinetic properties of crocin (crocetin digentiobiose ester) following oral administration in rats," *Phytomedicine*, vol. 14, no. 9, pp. 633–636, 2007.
- [64] A. Asai, T. Nakano, M. Takahashi, and A. Nagao, "Orally administered crocetin and crocins are absorbed into blood plasma as crocetin and its glucuronide conjugates in mice," *Journal of Agricultural and Food Chemistry*, vol. 53, no. 18, pp. 7302–7306, 2005.
- [65] B. Amin, A. Nakhsaz, and H. Hosseinzadeh, "Evaluation of the antidepressant-like effects of acute and sub-acute administration of crocin and crocetin in mice," *Avicenna Journal of Phytomedicine*, vol. 5, no. 5, pp. 458–468, 2015.
- [66] A. M. D'Alessandro, A. Mancini, A. R. Lizzi et al., "*Crocus sativus* stigma extract and its major constituent crocin possess significant antiproliferative properties against human prostate cancer," *Nutrition and Cancer*, vol. 65, no. 6, pp. 930–942, 2013.
- [67] Y. J. Zhong, F. Shi, X. L. Zheng et al., "Crocetin induces cytotoxicity and enhances vincristine-induced cancer cell death via p53-dependent and -independent mechanisms," *Acta Pharmacologica Sinica*, vol. 32, no. 12, pp. 1529–1536, 2011.
- [68] A. Zhang and J. Li, "Crocetin shifts autophagic cell survival to death of breast cancer cells in chemotherapy," *Tumour Biology*, vol. 39, no. 3, article 1010428317694536, 2017.
- [69] M. Sajjadi and Z. Bathaie, "Comparative study on the preventive effect of saffron carotenoids, crocin and crocetin, in NMU-induced breast cancer in rats," *Cell Journal*, vol. 19, no. 1, pp. 94–101, 2017.
- [70] Y. Ohno, T. Nakanishi, N. Umigai, K. Tsuruma, M. Shimazawa, and H. Hara, "Oral administration of crocetin prevents inner retinal damage induced by N-methyl-D-aspartate in mice," *European Journal of Pharmacology*, vol. 690, no. 1–3, pp. 84–89, 2012.
- [71] H. Mizuma, M. Tanaka, S. Nozaki et al., "Daily oral administration of crocetin attenuates physical fatigue in human subjects," *Nutrition Research*, vol. 29, no. 3, pp. 145–150, 2009.
- [72] N. Umigai, K. Murakami, M. V. Ulit et al., "The pharmacokinetic profile of crocetin in healthy adult human volunteers after a single oral administration," *Phytomedicine*, vol. 18, no. 7, pp. 575–578, 2011.
- [73] S. C. Nair, K. R. Panikkar, and R. K. Parthod, "Protective effects of crocetin on the bladder toxicity induced by cyclophosphamide," *Cancer Biotherapy*, vol. 8, no. 4, pp. 339–343, 1993.
- [74] A. Mancini, J. Serrano-Díaz, E. Nava et al., "Crocetin, a carotenoid derived from saffron (*Crocus sativus* L.), improves acetylcholine-induced vascular relaxation in hypertension," *Journal of Vascular Research*, vol. 51, no. 5, pp. 393–404, 2014.
- [75] Y. Wang, J. Sun, C. Liu, and C. Fang, "Protective effects of crocetin pretreatment on myocardial injury in an ischemia/reperfusion rat model," *European Journal of Pharmacology*, vol. 741, pp. 290–296, 2014.
- [76] S. Higashino, Y. Sasaki, J. C. Giddings et al., "Crocetin, a carotenoid from *Gardenia jasminoides* Ellis, protects against hypertension and cerebral thrombogenesis in stroke-prone spontaneously hypertensive rats," *Phytotherapy Research*, vol. 28, no. 9, pp. 1315–1319, 2014.
- [77] C. Zhou, W. Bai, Q. Chen et al., "Protective effect of crocetin against burn-induced intestinal injury," *The Journal of Surgical Research*, vol. 198, no. 1, pp. 99–107, 2015.
- [78] K. Niska, M. J. Santos-Martinez, M. W. Radomski, and I. Inkielewicz-Stepniak, "CuO nanoparticles induce apoptosis by impairing the antioxidant defense and detoxification systems in the mouse hippocampal HT22 cell line: protective effect of crocetin," *Toxicology In Vitro*, vol. 29, no. 4, pp. 663–671, 2015.
- [79] M. Buler, U. Andersson, and J. Hakkola, "Who watches the watchmen? Regulation of the expression and activity of sirtuins," *The FASEB Journal*, vol. 30, no. 12, pp. 3942–3960, 2016.
- [80] R. Raynes, J. Brunquell, and S. D. Westerheide, "Stress inducibility of sirt1 and its role in cytoprotection and cancer," *Genes & Cancer*, vol. 4, no. 3–4, pp. 172–182, 2013.
- [81] N. S. Levy, S. Chung, H. Furneaux, and A. P. Levy, "Hypoxic stabilization of vascular endothelial growth factor mRNA by the RNA-binding protein HuR," *The Journal of Biological Chemistry*, vol. 273, no. 11, pp. 6417–6423, 1998.
- [82] K. Abdelmohsen, R. Pullmann Jr., A. Lal et al., "Phosphorylation of HuR by Chk2 regulates SIRT1 expression," *Molecular Cell*, vol. 25, no. 4, pp. 543–557, 2007.
- [83] C. Zucal, V. D'Agostino, R. Loffredo et al., "Targeting the multifaceted HuR protein, benefits and caveats," *Current Drug Targets*, vol. 16, no. 5, pp. 499–515, 2015.
- [84] Y. Xiang, J. Xu, L. Li et al., "Calorie restriction increases primordial follicle reserve in mature female chemotherapy-treated rats," *Gene*, vol. 493, no. 1, pp. 77–82, 2012.
- [85] R. Cinco, M. A. Digman, E. Gratton, and U. Luderer, "Spatial characterization of bioenergetics and metabolism of primordial to preovulatory follicles in whole ex vivo murine ovary," *Biology of Reproduction*, vol. 95, no. 6, pp. 1–12, 2016.
- [86] Y. Yang, H. Cimen, M. J. Han et al., "NAD⁺-dependent deacetylase SIRT3 regulates mitochondrial protein synthesis by deacetylation of the ribosomal protein MRPL10," *The Journal of Biological Chemistry*, vol. 285, no. 10, pp. 7417–7429, 2010.
- [87] K. Ezoe, N. Murata, A. Yabuuchi et al., "Long-term adverse effects of cyclophosphamide on follicular growth and angiogenesis in mouse ovaries," *Reproductive Biology*, vol. 14, no. 3, pp. 238–242, 2014.

- [88] M. Brodsky, G. Halpert, M. Albeck, and B. Sredni, "The anti-inflammatory effects of the tellurium redox modulating compound, AS101, are associated with regulation of NF κ B signaling pathway and nitric oxide induction in macrophages," *Journal of Inflammation*, vol. 7, no. 1, p. 3, 2010.
- [89] D. Ling, B. Liu, S. Jawad et al., "The tellurium redox immunomodulating compound AS101 inhibits IL-1 β -activated inflammation in the human retinal pigment epithelium," *The British Journal of Ophthalmology*, vol. 97, no. 7, pp. 934–938, 2013.
- [90] E. Mokhber Maleki, H. Eimani, M. R. Bigdeli et al., "A comparative study of saffron aqueous extract and its active ingredient, crocin on the in vitro maturation, in vitro fertilization, and in vitro culture of mouse oocytes," *Taiwanese Journal of Obstetrics & Gynecology*, vol. 53, no. 1, pp. 21–25, 2014.
- [91] E. Mokhber Maleki, H. Eimani, M. R. Bigdeli, A. Golkar Narenji, and R. Abedi, "Effects of crocin supplementation during in vitro maturation of mouse oocytes on glutathione synthesis and cytoplasmic maturation," *International Journal of Fertility & Sterility*, vol. 10, no. 1, pp. 53–61, 2016.
- [92] V. Sapanidou, I. Taitzoglou, I. Tsakmakidis et al., "Antioxidant effect of crocin on bovine sperm quality and in vitro fertilization," *Theriogenology*, vol. 84, no. 8, pp. 1273–1282, 2015.
- [93] V. Sapanidou, I. Taitzoglou, I. Tsakmakidis et al., "Protective effect of crocetin on bovine spermatozoa against oxidative stress during in vitro fertilization," *Andrology*, vol. 4, no. 6, pp. 1138–1149, 2016.
- [94] G. Zullo, C. De Canditiis, M. E. Pero et al., "Crocetin improves the quality of in vitro-produced bovine embryos: implications for blastocyst development, cryotolerance, and apoptosis," *Theriogenology*, vol. 86, no. 8, pp. 1879–1885, 2016.



Hindawi
Submit your manuscripts at
<https://www.hindawi.com>



Regulation of HuR structure and function by dihydrotanshinone-I

Preet Lal^{1,†}, Linda Cerofolini^{2,†}, Vito Giuseppe D'Agostino¹, Chiara Zucal¹, Carmelo Fuccio², Isabelle Bonomo¹, Erik Dassi¹, Stefano Giuntini², Danilo Di Maio^{3,4}, Vikalp Vishwakarma⁵, Ranjan Preet⁵, Sha Neisha Williams⁵, Max S. Fairlamb⁵, Rachel Munk⁶, Elin Lehrmann⁶, Kotb Abdelmohsen⁶, Saioa R. Elezgarai⁷, Claudio Luchinat², Ettore Novellino⁸, Alessandro Quattrone¹, Emiliano Biasini^{1,7}, Leonardo Manzoni⁹, Myriam Gorospe⁶, Dan A. Dixon⁵, Pierfausto Seneci¹⁰, Luciana Marinelli^{8,*}, Marco Fragai^{2,*} and Alessandro Provenzani^{1,*}

¹Centre for Integrative Biology, CIBIO, University of Trento, Trento 38122, Italy, ²Centre for Magnetic Resonance, CERM, University of Florence, Sesto Fiorentino 50019, Italy, ³Scuola Normale Superiore, Pisa 56126, Italy, ⁴Istituto Nazionale di Fisica Nucleare (INFN), Pisa 56127, Italy, ⁵Department of Cancer Biology and University of Kansas Cancer Center, University of Kansas Medical Center, Kansas City, KS 66160, USA, ⁶National Institute on Aging, National Institutes of Health, Baltimore, MD 21224, USA, ⁷Istituto di Ricerche Farmacologiche Mario Negri, Milan 20156, Italy, ⁸Department of Pharmacy, University of Naples Federico II, Naples 80138, Italy, ⁹Istituto di Scienze e Tecnologie Molecolari (ISTM), CNR, Milan 20133, Italy and ¹⁰Dipartimento di Chimica, Università degli Studi di Milano, Milan 20133, Italy

Received January 30, 2017; Revised July 04, 2017; Editorial Decision July 06, 2017; Accepted July 07, 2017

ABSTRACT

The Human antigen R protein (HuR) is an RNA-binding protein that recognizes U/AU-rich elements in diverse RNAs through two RNA-recognition motifs, RRM1 and RRM2, and post-transcriptionally regulates the fate of target RNAs. The natural product dihydrotanshinone-I (DHTS) prevents the association of HuR and target RNAs *in vitro* and in cultured cells by interfering with the binding of HuR to RNA. Here, we report the structural determinants of the interaction between DHTS and HuR and the impact of DHTS on HuR binding to target mRNAs transcriptome-wide. NMR titration and Molecular Dynamics simulation identified the residues within RRM1 and RRM2 responsible for the interaction between DHTS and HuR. RNA Electromobility Shifts and Alpha Screen Assays showed that DHTS interacts with HuR through the same binding regions as target RNAs, stabilizing HuR in a locked conformation that hampers RNA binding competitively. HuR ribonucleoprotein immunoprecipitation followed by microarray (RIP-chip) analysis showed that DHTS

treatment of HeLa cells paradoxically enriched HuR binding to mRNAs with longer 3'UTR and with higher density of U/AU-rich elements, suggesting that DHTS inhibits the association of HuR to weaker target mRNAs. *In vivo*, DHTS potently inhibited xenograft tumor growth in a HuR-dependent model without systemic toxicity.

INTRODUCTION

The Human antigen R (ELAVL1, HuR) is an ubiquitously expressed RNA-binding protein, belonging to the ELAVL (Embryonic Lethal Abnormal Vision)-like family, that preferentially binds U- and AU-rich elements (AREs) abundant in the 3' untranslated regions (3'UTRs) of certain mRNAs. It is mainly localized within the nucleus (90%), where it exerts post-transcriptional functions such as splicing (1–4) and alternative polyadenylation (5–7), and is able to shuttle to the cytoplasm, where it mainly regulates the fate of target RNAs (8). HuR regulates cellular responses to differentiation, senescence, inflammatory factors, and immune stimuli by tightly controlling the post-transcriptional fate of specific mRNAs (9–12). Notably, HuR binds to and regulates the half-life of mRNAs and/or the translation of

*To whom correspondence should be addressed. Tel: +39 046 1283094; Fax: +39 046 1283239; Email: alessandro.provenzani@unitn.it
Correspondence may also be addressed to Marco Fragai. Tel: +39 055 4574261; Fax: +39 055 4574923; Email: fragai@cerm.unifi.it
Correspondence may also be addressed to Luciana Marinelli. Tel: +39 081 679899; Fax: +39 081 676569; Email: lmarinel@unina.it

[†]These authors contributed equally to this work as first authors.

mRNAs encoding key inflammatory cytokines and interleukins, such as tumor necrosis factor- α (TNF α) (13) and interleukin IL-1 β , IL-3 (14), IL-6 (15), IL-8, IL-10, IL-4, CXCL1 (16–18), in turn governing the development and maturation of B and T lymphocytes (19,20). HuR is highly expressed in many cancer types, and is believed to promote tumorigenesis by interacting with mRNAs encoding proteins implicated in cell proliferation and survival, angiogenesis, invasion, pharmacoresistance and metastasis (21–27). The role of HuR in inflammation and cancer has prompted the search for inhibitors/modulators to interfere with its biological activity (28–32).

A number of natural and synthetic molecules have been found to interfere with the formation of HuR/mRNA complexes *in vitro* (29,32–35). The structural basis of the interaction of such molecules with HuR is still poorly characterized. HuR contains three highly conserved RNA recognition motifs (RRMs) among which the first two, RRM1 and RRM2, bind with high affinity to U/AU-rich RNA (36). By contrast, the third domain, RRM3, contributes to the interaction of HuR with poly(A) tails of target mRNA, and is believed to be involved in mRNA-induced cooperative assembly of HuR oligomers (37) (Figure 1A). Each RRM domain adopts a β_1 - α_1 - β_2 - β_3 - α_2 - β_4 topology with the two α -helices packed in an antiparallel four-stranded β -sheet. Residues at conserved positions located on β -strands 1 and 3 are essential for mRNA binding, and are either involved in stacking interactions with mRNA bases or inserted between two sugar rings (38). At present, two crystal structures of the isolated RRM1 domain (PDB codes 3HI9 and 4FXV (39)) and two of the RRM1–RRM2 domains (PDB codes 4ED5 (40) and 4EGL) are available in the Protein Data Bank (PDB). Conformational changes occurring on the tandem RRM1–RRM2 domains are crucial for mRNA binding (40). As suggested by the crystal structures, the tandem construct adopts an ‘open’ conformation in the free form and a ‘closed’ conformation when the RRM1 and RRM2 domains bind mRNA (Figure 1B and C). This hypothesis is supported by SAXS data that show an equilibrium among ‘closed’ and ‘open’ conformations for HuR in solution, in the absence of mRNA. When a target mRNA sequence is present, the two domains form a stable complex with mRNA and adopt a ‘closed’ globular conformation around the mRNA strand (41).

Dihydroanthranone-I (DHTS) is a natural compound present in *Salvia miltiorrhiza* that interferes with the formation of HuR/RNA complexes (31). However, there is currently no detailed information about the specific interaction of DHTS with HuR or about the perturbations of the RNA-binding abilities of HuR transcriptome-wide. Here, we report the analysis of the interaction between DHTS and HuR by NMR, Molecular Dynamics simulation, and mutagenesis experiments. We have characterized the internal dynamics of the HuR RRM1–RRM2 domains, and have used this information to analyze the role of the two domains in ligand binding. In this respect, the identification of the flexibility of the two domains, RRM1 and RRM2, was particularly interesting. Moreover, ribonucleoprotein immunoprecipitation followed by microarray analysis revealed that DHTS dysregulates HuR by enriching HuR binding towards longer mRNAs highly rich in U/AU-rich 3'UTRs,

including the mRNAs that encode apoptotic and cell-cycle regulatory proteins in cells, and inhibits cancer cell growth *in vivo*.

MATERIALS AND METHODS

Cell lines and reagents

Human cervical adenocarcinoma HeLa cells (ATCC[®] CCL2[™]), colon carcinoma cells HCT116 (ATCC; Manassas, VA) were cultured in standard Dulbecco's Modified Eagle Medium (DMEM) supplemented with 10% fetal bovine serum (Gibco/Invitrogen), 1% L-glutamine (Gibco/Invitrogen), 1% penicillin–streptomycin (Invitrogen), and growth conditions at 37°C in 5% humidified CO₂ incubators. Creation and characterization of CRISPR/Cas9-mediated knockout of the *ELAVL1* gene in HCT116 cells was accomplished as described (42). Dihydroanthranone I (D0947) was purchased from Sigma and dissolved in ultrapure dimethylsulfoxide (DMSO, Amresco, N182) to 10 mM final concentration. Antibodies used recognized HuR (sc-71290; from Santa Cruz Biotechnology), His tag (anti-6x His (ab1187; from Abcam)) and β -actin (Clone C4; MP Biomedicals).

Cell and tumor growth assays

Transient transfection of cells with a HuR expression construct (pcDNA3.1/Zeo/HuR-Flag) or empty vector was accomplished using Lipofectamine Plus (Gibco/Invitrogen) as described (43) for 48 h, following addition of 10 μ M DHTS or vehicle. Cell survival was assayed using the MTT-based cell growth determination kit (Sigma-Aldrich) as previously described (30).

Anchorage- and serum-independent growth assays were accomplished by plating cells (20 cells per well) on 96-well ultra-low attachment plates (Corning) in spheroid growth medium (DMEM supplemented with 10 mM HEPES, N2 supplement (1 \times ; Gibco), B-27 supplement (1 \times ; Gibco), Insulin Transferrin Selenium (1 \times ; Gibco), FGF (10 ng/ml; Gibco) and EGF (20 ng/ml; Gibco)). After 3 days of growth, spheroids were treated with 10 μ M DHTS or vehicle for 15 days changing medium every 3 days. Individual spheroids ($n = 5$ –10/time point) were imaged every 3 days and area was measured using ImageJ software.

Six week-old athymic nude (Nu/Nu) mice were purchased from Jackson Laboratories and maintained under sterile conditions in cage micro-isolators according to approved IACUC guidelines. Parental HCT116 and a representative HuR knockout clone (2×10^6 cells) used between passages 14 and 23 were resuspended in PBS containing 50% Matrigel (Corning) and injected into the dorsal subcutaneous tissue (three mice/group with two tumors/mouse). Mice (three per group) received intraperitoneal (IP) injections of DHTS (10 mg/kg) dissolved in PBS/5% *N*-methyl pyrrolidine (NMP) (Sigma-Aldrich) or vehicle control every 48 h. Tumor volumes and body weight were measured three times per week using a caliper, and tumor volumes were calculated using the formula: volume = length \times width²/2. Upon termination of the experiment, mice were euthanized and tumors were harvested.

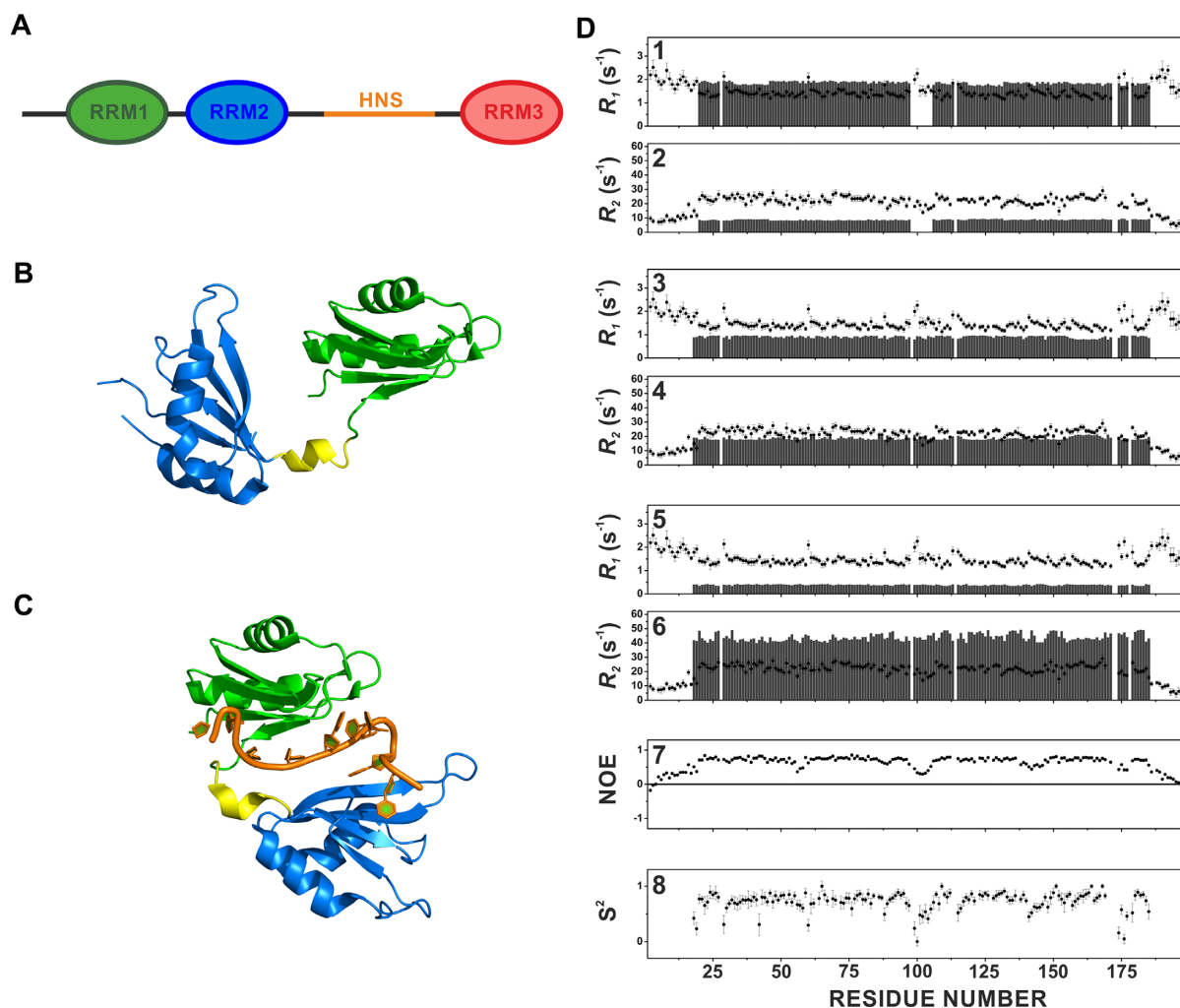


Figure 1. Multidomain organization of HuR (A). The RRM1–RRM2 tandem domains (RRM1 aminoacids (aa) Thr20–Pro98 and RRM2 aa Ala106–Asn186) are separated by a short linker of 7 residues (aa Ser99–Asp105), while RRM3 (aa Trp244–Asn322) is connected to the other two domains by a long hinge region of about 60 residues (aa Pro187–Gly243), which includes the HuR Nucleocytoplasmic Shuttling (HNS) sequence, responsible for nuclear/cytoplasmic shuttling of HuR. RRM1 is represented in green, RRM2 in blue and RRM3 in red. The HuR Nucleocytoplasmic Shuttling Sequence (HNS) is indicated in orange. Cartoon representation of the ‘open’ structure of the tandem RRM1–RRM2 domains crystallized in the absence of RNA (pdb code 4ED5) (B), and of the ‘closed’ structure of the tandem RRM1–RRM2 domains in complex with RNA (pdb code 4EGL) (C). The two domains and the linker are highlighted with different colors (RRM1 in green, linker in yellow and RRM2 in blue). (D) Comparison of experimental backbone ^{15}N R_1 values for RRM1–RRM2 (data collected at 298 K, black filled circles) with the calculated values (grey bars) for isolated RRM1 and RRM2 domains (1), for monomeric RRM1–RRM2 construct (3) and for rigid dimeric adduct (5). Comparison of experimental backbone ^{15}N R_2 values for RRM1–RRM2 (data collected at 298 K, black filled circles) with the calculated values (grey bars) for isolated RRM1 and RRM2 domains (2), for monomeric RRM1–RRM2 construct (4) and for rigid dimeric adduct (6). Experimental NOE values for RRM1–RRM2 (data collected at 298 K) (7) and S^2 order parameter calculated with the program TENSOR2 (8).

AlphaScreen and RNA electromobility shift (REMSA) assays

Amplified Luminescent Proximity Homogenous Assay (Alpha) with a 5'-Biotinylated RNA probe (Bi-TNF, 5'-AUUAUUUAUUUAUUUAUUUAUUUAUUUA) was used with FL-HuR and four studied mutants. 384-well optiplates (PerkinElmer; 6007299) were used with 20 μl final volume in each well. Hooking points of all the respective proteins were determined. Reagents were used in the nanomolar range using the AlphaScreen His detection kit (PerkinElmer) in alpha buffer (25 mM HEPES pH 7.4, 100 mM NaCl, 0.1% BSA). Donor and acceptor beads were used at 10 $\mu\text{g}/\text{ml}$ as their final concentration, proteins and constructs were ac-

ording to their hooking points and incubated for 1 hour at room temperature. Plates were read for fluorescence signals in an Enspire plate reader instrument (PerkinElmer; 2300-001A), and specific binding was calculated by subtracting the background, obtained in the absence of the protein. For REMSA experiments, equimolar concentrations of purified RRMs and FAM-TNF RNA probes were used (32) in REMSA buffer (20 mM HEPES pH 7.5, 50 mM KCl, 0.5 μg BSA, 0.25% glycerol) together with reference doses of DHTS were run on the native Polyacrylamide (6%) gel, in 0.5 \times TBE buffer at 55 V for 90 min. The gel was analysed by a Typhoon instrument (GE Healthcare; 00-4277-85 AC).

R_1 , R_2 and NOE measurements

The experiments for the determination of ^{15}N longitudinal and transverse relaxation rates and ^{15}N - ^1H NOE (44) were recorded at 298 K and 700 MHz on ^{15}N -enriched samples of the RRM1–RRM2 tandem domains of HuR. ^{15}N Longitudinal relaxation rates (R_1) were measured using a sequence modified to remove cross-correlation effects during the relaxation delay (45). Inversion recovery times ranging between 2.0 and 2500 ms, with a recycle delay of 3.5 s, were used for the experiments. ^{15}N transverse relaxation rates (R_2) were measured using a Carr-Purcell-Meiboom-Gill (CPMG) sequence (45,46), with delays ranging between 8.5 and 237.4 ms and a refocusing delay of 450 μs . Longitudinal and transverse relaxation rates were determined by fitting the cross-peak intensities as a function of the delay to a single-exponential decay using the Origin software. Heteronuclear NOE values were obtained from the ratio of the peak height for ^1H -saturated and unsaturated spectra. Theoretical predictions of NH R_1 and R_2 values for RRM1–RRM2 tandem domains were made using HYDRONMR (47) and the pdb structure 4ED5 (40), considering (i) the isolated domains, (ii) the monomeric and (iii) the dimeric constructs.

Molecular dynamics simulation and analysis

The HuR-DHTS complex, as issued from docking calculations (see SI for details), was submitted to MD simulation with NAMD (48) using the ff99SBildn Amber force field parameters (49,50) for proteins and the parameters recently developed by Allnér and co-workers for ions (51). Parameters for DHTS were generated in two steps. Initially, charges were computed using the restrained electrostatic potential (RESP) fitting procedure (52). The ESP was first calculated by means of the Gaussian09 package (53) using a 6–31G* basis set at Hartree-Fock level of theory, and then the RESP charges were obtained by a two-stages fitting procedure using the program RED (54,55). Missing bond, angle, torsion and improper torsion angle parameters were then generated using Antechamber (56). The complex was then solvated in a 15 Å layer cubic water box using the TIP3P water model parameters. Neutrality was ensured by adding five further Cl^- ions. The final system size was $\sim 74 \text{ \AA} \times 93 \text{ \AA} \times 74 \text{ \AA}$ for a total number of atoms of $\sim 48\,000$. A 10 Å cutoff (switched at 8.0 Å) was used for atom pair interactions. The long-range electrostatic interactions were computed by means of the particle mesh Ewald (PME) method using a 1.0 Å grid spacing in periodic boundary conditions. The RATTLE algorithm was applied to constrain bonds involving hydrogen atoms, and thus a 2 fs integration time step could be used. More details in the Supplementary Methods

RIP-chip protocol

To analyze the influence of DHTS on the interaction of HuR with endogenous mRNAs, immunoprecipitation (IP) of endogenous ribonucleoprotein complexes was performed as described previously (57). Briefly, HeLa cells were lysed in 20 mM Tris–HCl at pH 7.5, 100 mM KCl, 5 mM MgCl_2 , and 0.5% NP-40 for 10 min on ice and centrifuged at 15 000 $\times g$ for 10 min at 4°C. The supernatants were incubated for

2 h at 4°C with protein G Sepharose beads (GE Healthcare) coated either with anti-HuR or with control IgG antibodies (both from Santa Cruz Biotechnology). The beads were washed with NT2 buffer (50 mM Tris–HCl [pH 7.5], 150 mM NaCl, 1 mM MgCl_2 , 0.05% NP-40), followed by incubation with 20 units of RNase-free DNase I for 15 min at 37°C to remove the DNA. The samples were then incubated for 15 min at 55°C with 0.1% SDS–0.5 mg/ml proteinase K to digest proteins. Microarray analysis was performed in duplicate (GEO number GSE94360). The RNA from the IP samples was extracted using phenol–chloroform, precipitated, and used for cDNA microarray analysis or RT-qPCR validation.

Analysis of enriched mRNAs

GC content, length and secondary structure density (computed as the fraction of unpaired nucleotides) for the UTRs of DEC and INC genes were obtained from the AURA 2 database (58), and plotted with the R software. The enrichment of post-transcriptional regulatory elements was performed with the *Regulatory element enrichment* feature of AURA 2. Gene ontology and pathway enrichment analyses were performed with the Enrichr tool (59) on GO (Biological process, Molecular function and Cellular Component) and pathways (KEGG and Reactome) libraries, using a five genes overlap and minimum combined score of 2 as significance threshold. GO terms were clustered by semantic similarity with the GoSemSim R package (60), and the cluster score computed as the average combined score of composing terms.

RESULTS

NMR resonance assignment

The 2D ^1H - ^{15}N HSQC spectrum of tandem RRM1–RRM2 domains shows well-dispersed signals in agreement with a uniform and folded protein structure (Supplementary Figure S1). All the residues (but Pro172), including those forming the linker region that is crucial for the protein function, have been assigned (Supplementary Table S1, BMRB code: 27002). Our assignment of the tandem RRM1–RRM2 domains was also compared with the ones reported for the isolated RRM1 domain (61) as in the RRM1–RRM2 tandem domains (35). The resonances of residues forming the RRM1 domain are almost the same in the isolated domain (61), and in the RRM1–RRM2 construct. As reported by Wang and coworkers (35), this observation suggests that the RRM1 and RRM2 domains do not interact with each other when they form the tandem construct. Based on TALOS+ predictions, each domain in the RRM1–RRM2 construct is constituted by two α -helices and four β -strands, in agreement with the previously reported crystal structures of the RRM1 and RRM1–RRM2 domains of HuR (39,40,62) (Supplementary Figure S2).

Internal dynamics of RRM1–RRM2 tandem domains

To characterize protein dynamics, measurements of longitudinal (R_1) and transverse (R_2) relaxation rates of backbone amide nitrogens at 700 MHz, ^1H Larmor frequency,

and 298 K were performed on ^{15}N -enriched samples of the RRM1–RRM2 construct. Theoretical estimates of R_1 and R_2 values were calculated for the following model structures: (i) the isolated RRM1 (T20–P98) and RRM2 (A106–N186) domains (Figure 1D, panels 1, 2), (ii) the monomeric RRM1–RRM2 construct (Figure 1D, panels 3, 4) and, (iii) the dimeric adduct (Figure 1D, panels 5, 6) (PDB 4ED5). Figure 1D shows the experimental R_1 and R_2 values (black circles) as well as the theoretical ones (grey bars). The comparison of experimental R_1 and R_2 data with theoretical values calculated for the isolated RRM1 and RRM2 domains shows that experimental R_1 values were smaller and R_2 values are larger than their theoretical counterparts (Figure 1D, panels 1, 2). At the same time, experimental R_1 values were higher than theoretical estimates calculated for the monomeric construct in solution (Figure 1D, panel 3), indicating that the RRM1–RRM2 construct did not behave as a rigid body but instead displayed inter-domain flexibility, simulating a protein of lower molecular weight (63–65). Experimental R_2 values were instead slightly higher than their theoretical counterparts, indicating the occurrence of possible aggregation phenomena (Figure 1D, panel 4). On the other hand, experimental R_1 values were dramatically higher, and R_2 dramatically lower than theoretical values calculated for the rigid dimer (Figure 1D, panel 5, 6), suggesting that the RRM1–RRM2 dimer was not present in solution as a stable complex. Further indication of the presence of inter-domain flexibility was provided by the ^{15}N – ^1H NOE values for the linker residues Ser99 (0.46), Ser100 (0.34), Glu101 (0.31), Val102 (0.30), Ile103 (0.32) and Lys104 (0.40) (Figure 1D, panel 7). The small NOE values of the residues in the linker between the two domains are evidence of fast motions on ps–ns timescale (faster than the overall protein-tumbling rate). Very small NOE values are found also for the N- and C-terminal tails, and for some residues in the loops of RRM1 (Val56, Ala57, Gly58) and RRM2 (Gln141, Thr142, Leu145) domains. The order parameter S^2 calculated with the program TENSOR2 (66) starting from experimental R_1 , R_2 and NOE values is also reported in Figure 1D, panel 8. The S^2 values confirm the presence of high flexibility between the two domains, and for some loops within each domain.

DHTS stabilizes HuR in a closed conformation and competes with mRNA for binding

The interaction of HuR with DHTS was investigated through solution NMR. The significant precipitation of the ligand in the solution, occurring at the high concentrations required by the NMR analysis, prevented the estimation of the affinity constant. Nevertheless, after the addition of increasing amounts of DHTS to the protein, we observed a generalized decrease in signal intensity, with few residues (Thr20, Asn21, Ile52, Ser94, Tyr95, Ala106, Asn107, Leu108, Ile133, Asn134, Val137, Leu138, Arg147, Ile152, Phe154, Asp155, Lys182) experiencing a larger effect. These residues were located in the β -platform of both RRM domains (Figure 2A and B). The generalized decrease of signal intensity, and the distribution of affected residues over the large surfaces of the β -platform in each domain suggested an alteration of the equilibrium among ‘closed’

and ‘open’ conformations upon ligand binding. Specifically, the decrease of signal intensity was consistent with a mechanism where the small molecule stabilizes a ‘closed’ conformation of HuR. After the addition of DHTS to the protein, only negligible chemical shift changes occur. The residues experiencing the largest chemical shift perturbations are located close to the β -platforms (Supplementary Figure S3).

With the dual aim of bringing some insights into DHTS binding mode and mechanism of action, we carried out a molecular modeling study. We employed a ‘tandem’ approach of docking calculations and molecular dynamics (MD) simulations in the attempt to follow the protein/ligand reciprocal conformational mutations. We first performed a docking calculation to the whole mRNA binding surface of HuR by means of AutoDock 4.2, which converged to a single binding pose. As a result, DHTS was found at the center of the mRNA binding cleft, which is shaped by the RRM1 and RRM2 domains (residues 18–95 and 107–185, respectively), and in proximity of the inter-domain linker. To allow both the ligand and the protein to fully adapt to each other, we performed an extended (0.5- μs) MD simulation. During the first 100 ns of simulation, DHTS was displaced from its starting position laterally along the surface of the RRM domain β -sheets, though always remaining bound to the HuR surface (Supplementary Figure S4A and B). This displacement was accompanied by a HuR conformational shift towards a ‘closed’ form featuring the two RRM domains even closer to each other (Supplementary Figure S4C), and establishing further inter-residues contacts (Supplementary Figure S4D) lacking in the mRNA-bound conformation, e.g. a salt bridge between Asp-105 and Arg-153, a backbone hydrogen bond between Ile-133 and Asn-25 or a hydrophobic contact between Ile-133 and Ile-23. For the sake of comparison, a further 500 ns MD was performed, starting from the X-ray HuR–RNA complex. The simulation resulted in an overall greater structural stability as compared to the HuR–DHTS complex (Supplementary Figure S5A and B). Furthermore, we observed neither a decrease in the distance between the two RRM domains nor a significant increase in the number of inter-domain residue contacts (Supplementary Figure S5C and D).

In the final HuR–DHTS complex, which remained stable for the rest of the simulation, DHTS is accommodated in a narrow, elongated and mostly hydrophobic pocket (Figure 2C) shaped by residues of the two RRM domain β -sheets (RRM1: Ile-23, Asn-25, Tyr-26, Leu-61, Tyr-63, Phe-65; RRM2: Asp-105, Ile-133, Asn-134, Arg-153) and of inter-domain linker (Ile-103 side chain and Lys-104, Arg-97 and Ala-96). The aromatic rings of DHTS establish several π -interactions, among which a cation- π interaction with Arg-153 and a NH- π interaction with the Asn-134 side chain. However, although DHTS is gripped between the two domains, it does not bind HuR rigidly, but rather gently sways along the binding surface (Figure 2D). Taken together, our structural data indicate that DHTS competes with RNA for the binding to HuR, interacting with the β -platform of both RRM domains in the proximity of the interdomain linker, and thus stabilizing HuR in a closed conformation.

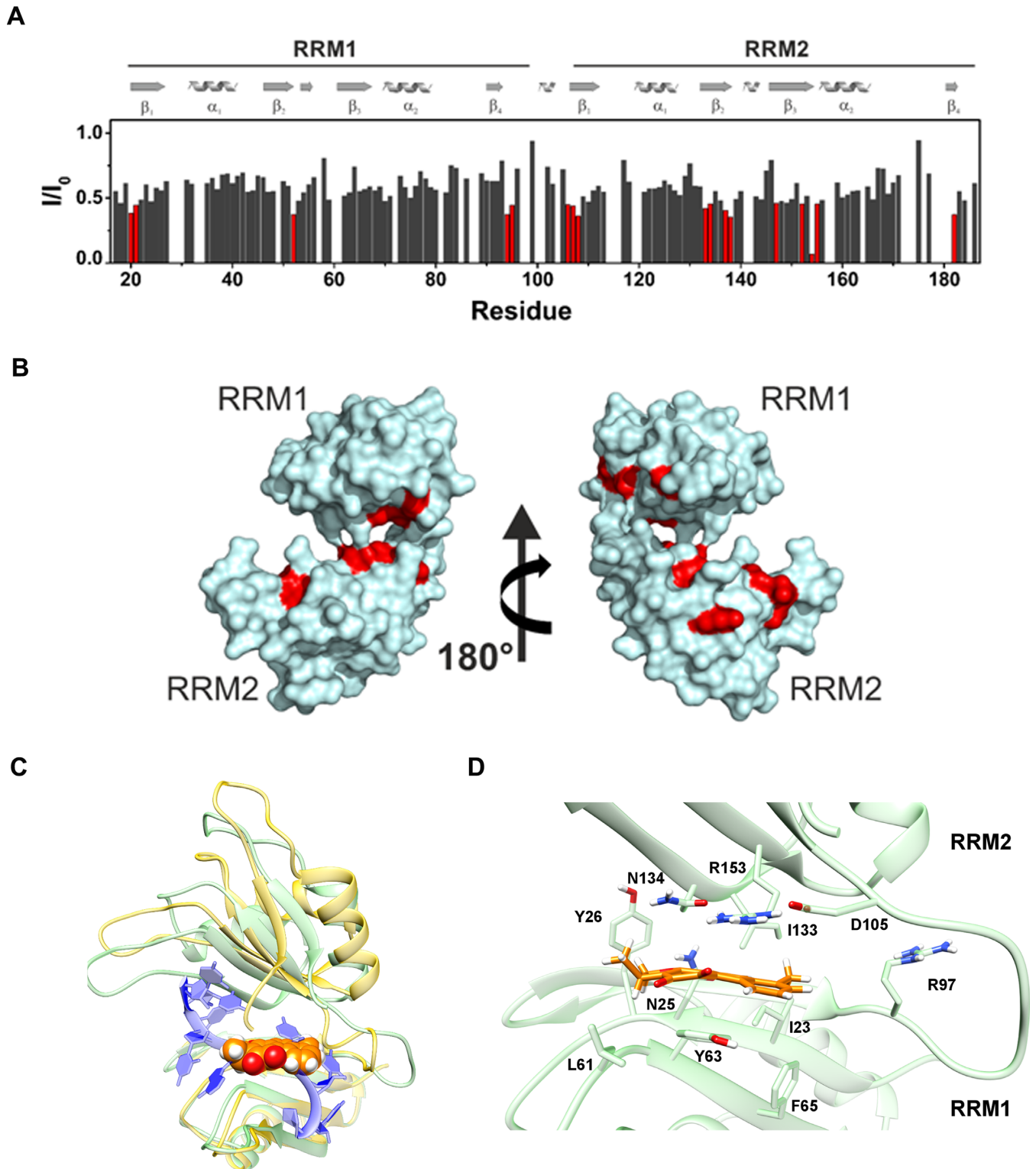


Figure 2. Graphical representation of the intensity changes per residues of RRM1–RRM2 HuR protein (50 μ M in solution) in the presence of DHTS (200 μ M) (A) and surface representation of the closed conformation of HuR (pdb: 4ED5) (B) with the residues exhibiting the highest decreases in signal intensities highlighted in red. (C) Global view of the HuR (green cartoons)-DHTS (orange spheres) complex. Note how the insertion of DHTS into the mRNA binding cleft and the further closure of the latter, as compared to the mRNA-bound conformation (yellow), prevents the accommodation of the mRNA strand (blue ribbons). (D) Theoretical DHTS binding mode, as suggested by our MD simulation. DHTS and HuR residues involved in binding interactions are displayed as sticks.

The β -platforms of RRM domains are involved in DHTS inhibitory activity

To support NMR and molecular modeling that addressed a specific interacting region on HuR, we produced HuR protein domains made of the first RRM domain (RRM1), of the second RRM domain (RRM2), of the RRM1–RRM2 wild-type RRM domains, and of RRM1 lacking 14 aminoacids at the C-terminus (Δ RRM1, missing residues from Ser94 to Asn107) and performed *in vitro* RNA binding experiments. Some of these residues belong to the inter-domain linker (Ser99–Asp105) and the others to the β -platform regions of the two domains, where some aminoacids experienced decreased intensity in the presence of DHTS (Ser94–Tyr95 in RRM1 and Ala106–Asn107 in RRM2). HuR domains were produced in *Escherichia coli* using the pET42 plasmid (31). We obtained the same purity for all the protein isoforms (Supplementary Figure S6). As single domains lose RNA-binding activity very quickly, the *in vitro* activity of the single protein domains and of their combination was evaluated by REMSA, mixing equimolar concentration of each, freshly prepared, with 0.2 μ M of the FAM-ARE ssRNA probe (Figure 3A). The RRM1–RRM2 isoform was used as positive control because it displayed a similar K_d (2.62 ± 0.6 nM (31)) to the FL HuR protein, and because it was used in the NMR experiments (35). RRM1 retained the capability to recognize mRNA substrates (40), however with a lower affinity compared to the RRM1–RRM2 construct, probably indicating a change in the stoichiometry of cooperative protein binding (Figure 3A, Supplementary Figure S7) (40,62).

Importantly, the RRM1–RNA complex was still sensitive to DHTS. After removing 14 aminoacids, the binding capacity of Δ RRM1 to RNA was slightly reduced ($\sim 20\%$) in comparison with the RRM1 domain (Figure 3A). Conversely, Δ RRM1 became resistant to DHTS, suggesting that this region is important for DHTS inhibitory activity (Figure 3A). REMSA performed with RRM2 and *in vitro* complementation of the two domains (RRM1 + M2 and Δ RRM1 + M2) did not provide information about the contact region of DHTS (Supplementary Figure S7B–D). By using fluorescence polarization, we analyzed the binding kinetics of proteins (200 nM) toward the FAM-ARE RNA probe (100 nM). We confirmed that full-length HuR and RRM1–RRM2 tandem domains behave almost similarly (average $K_{obs} \sim 4$ min), reaching equilibrium after 10 min. On the other hand, the RRM1 domain rapidly recognized the substrate ($K_{obs} \sim 1$ min), but this affinity was significantly impaired in the Δ RRM1 construct (K_{obs} of ~ 8 min) (Figure 3B). Circular dichroism (CD) experiments performed at 10 μ M concentration of both reagents, and NMR measurements ruled out a putative interaction between DHTS and RNA (Supplementary Figure S8A and B). Collectively, these findings show that the residues forming the β -platform and placed at the C-terminal in RRM1 domain are critical for RNA binding and the inhibitory activity of DHTS.

Single point mutations in the HuR–DHTS interacting region abolishes DHTS efficacy

Based on NMR data and an initial raw model of DHTS binding as derived by docking calculations, residues Ser94, Asn107, Ile133 and Asn134 of the RRM1–RRM2 inter-domain region were mutated to probe their relevance for DHTS binding. We produced residue-to-Alanine mutations in the full-length HuR sequence by site-directed mutagenesis (67) (Supplementary Figure S9). The preservation of the folding of the mutants was assessed by 1 H 1D NMR spectra (Supplementary Figure S10). By reacting equimolar amount of wild-type HuR or muteins with 0.2 μ M FAM-ssRNA, we observed an inhibitory effect of DHTS only with wild-type HuR, while any functional single point mutation led to resistance to DHTS (Figure 3C). Interestingly, we observed a qualitatively distinct binding profile among muteins: at least three discrete supershifts, numbered according to the molecular weight (1 being the lightest, 2, and 3), were detectable for wild-type HuR. Supershift 3 was markedly enriched in N134A and N107A, and to a lesser extent in I133A muteins (Figure 3C). This behavior could result from a higher efficiency in recognition and dimerization along the mRNA substrate, or alternatively from an aggregation-prone tendency of muteins that therefore aggregate on the same molecule of RNA probe. Indeed, mutants showed significantly lower K_d values, i.e. an increased affinity in saturation binding experiments with respect to wild-type HuR (Figure 3D, Supplementary Figures S11 and S12). Additionally, the raw signals at the hook point values for protein and RNA probes were significantly reduced in intensity compared to wild-type HuR, indicating a sub-optimal assay environment, compatible with ligand self-aggregation (68).

According to these data, when Ser94, Asn107, Ile133 and Asn134 are mutated into Alanine, DHTS does not bind to any mutein. The four residues are thus crucial in providing the required flexibility to HuR for its mRNA binding function.

DHTS prevents HuR binding to low AU-rich density mRNA, but enriches it to high AU-rich density species

We evaluated the ability of DHTS to disrupt the interaction of HuR with its target mRNAs by employing a transcriptome-wide approach. We performed a RIP-chip (ribonucleoprotein immunoprecipitation followed by microarray) experiment in HeLa cells, and observed that, out of the 2306 mRNAs bound to HuR, DHTS only reduced binding of 79 transcripts. Conversely, 558 mRNAs were enriched after treatment with DHTS. Therefore, contrary to our expectations, we observed an overall enrichment of mRNAs bound to HuR after treatment with DHTS. We reasoned that DHTS could displace mRNAs that had lower affinity to HuR than DHTS itself had, and, paradoxically, provide the opportunity for mRNAs with higher affinity for HuR than DHTS to bind in higher copy numbers to HuR. We observed that HuR-bound mRNAs had relatively higher frequency of U/AU-rich segments compared to the frequency transcriptome-wide, as expected (69). However, the U/AU density in UTRs in enriched mRNAs was significantly higher than that in downregulated mRNAs (Sup-

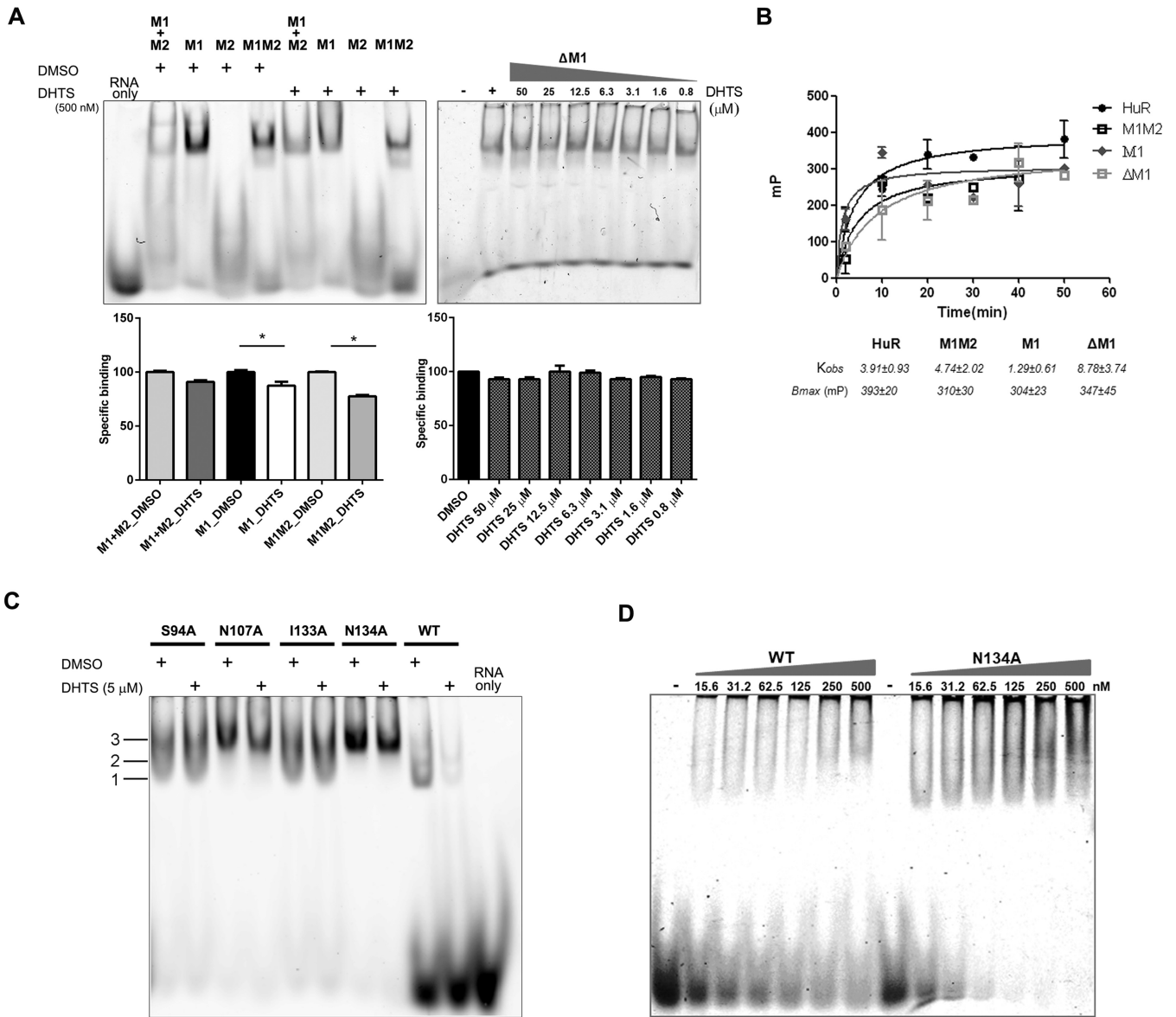


Figure 3. The inter-domain region between RRM1 and RRM2 is crucial for RNA and DHTS binding. (A) On left, representative REMSAs of at least three independent protein preparations of recombinant RRM1 + RRM2 (M1 + M2) domains, RRM1 (M1), RRM2 (M2), RRM1–RRM2 (M1M2) HuR proteins. REMSAs were performed with 0.2 μ M of protein, 0.2 μ M of Cy-3 RNA probe and DMSO or DHTS at indicated doses. On right, representative REMSA performed with 2.5 μ M of Δ RRM1 and 75 fM of probe RNA titrated with DHTS (concentration as shown in the legend). Densitometric quantification plotted below represents specific HuR–RNA binding challenged by DHTS. Mean \pm SD refers to three independent experiments ($n = 3$, * indicates t -test P -value < 0.05). (B) Kinetic saturation binding experiment by fluorescence polarization. 200 nM wild-type protein or mutants were incubated with FAM-ARE RNA probe (100 nM). Full-length HuR and RRM1–RRM2 tandem domains (M1M2) have similar K_{obs} . RRM1 (M1) is binding faster (K_{obs} of ~ 1 min), but deletion of the inter-domain region abolishes the binding properties of RRM1 (Δ M1) (K_{obs} of ~ 8 min). (C) RNA- and DHTS-interacting amino acids are crucial for DHTS and RNA binding, and for protein dimerization. Representative REMSAs of at least three independent protein preparations of recombinant full-length HuR and indicated mutants. REMSAs were performed with 0.2 μ M of protein, 0.2 μ M of Cy-3 RNA probe, and DMSO or 5 μ M DHTS. Mutants are insensitive to DHTS and show different binding patterns to the RNA probe. (D) Representative REMSAs of at least three independent protein purification performed with increasing concentration of WT and HuR single point mutant N134A with 75 fM of probe RNA.

plementary Table S2, median of 1.37 ARE nts/100 nts for enriched genes, 0.97 for depleted genes; mean of 2.24 ARE nts/100 nts for enriched genes, 1.49 for depleted genes; maximum of 81.97 ARE nts/100 nts for enriched genes, 7.92 for depleted ones). Moreover, the highest differences were observed in the 3'UTR (Figure 4A), where the percentage of AU bases increased from 58% (depleted) to 65% (enriched).

Additionally, 3'UTRs, but not 5'UTRs, were significantly longer for the enriched mRNAs (Figure 4B), while no differences in the density of secondary structure elements were observed (Figure 4C).

Functional analyses of depleted genes provided no considerable enrichment, due to the small size of the set and because it was partially composed of unannotated mRNAs.

UTR properties by response to DHTS

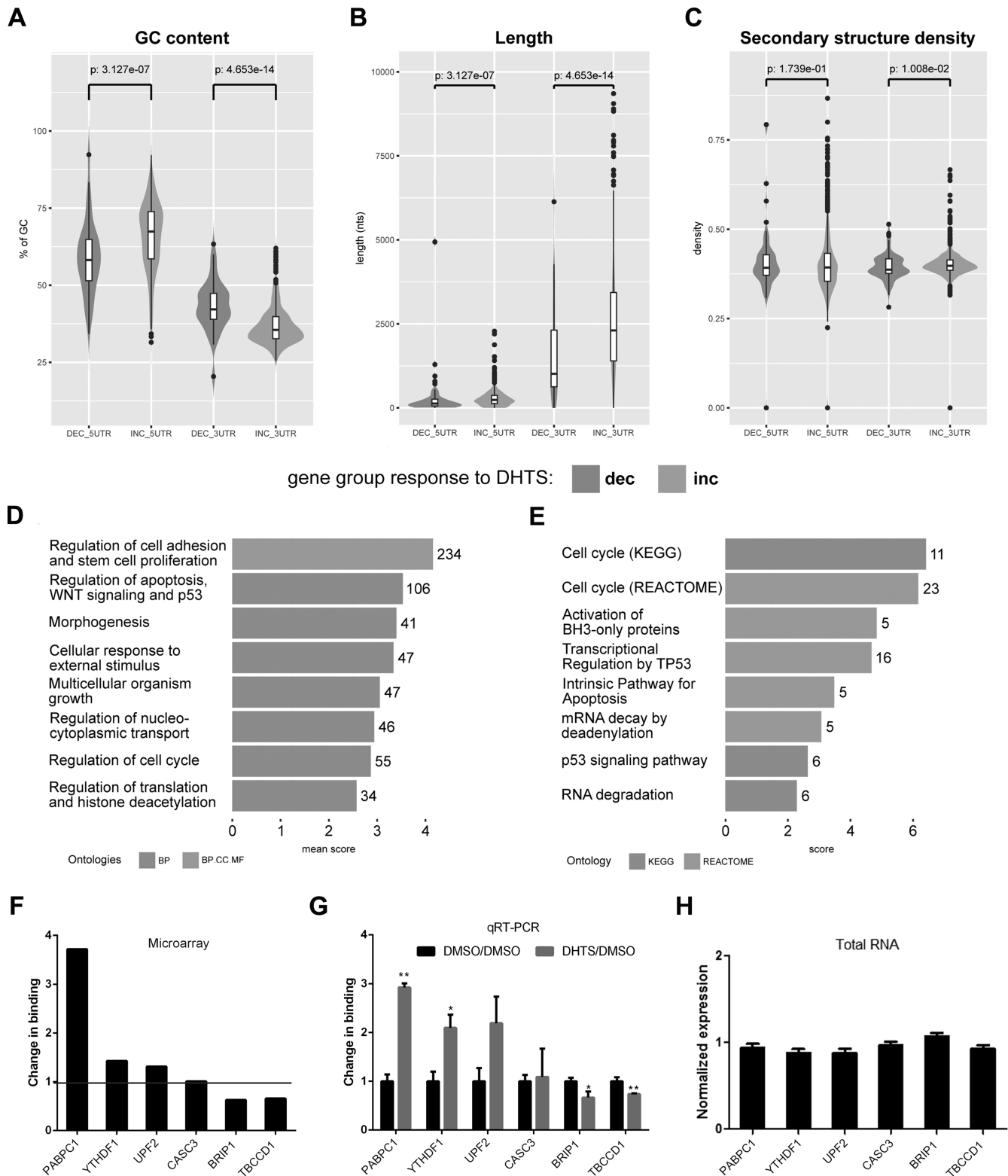


Figure 4. Enriched and depleted mRNAs and their UTRs have distinct properties. (A) Distribution of GC content for depleted (dec) and enriched (inc) UTRs, with Wilcoxon test-*P*-values of the differences. (B) Length distribution for depleted (dec) and enriched (inc) UTRs, with Wilcoxon test-*P*-values of the differences. (C) Secondary structure density (computed as the fraction of unpaired nucleotides) of depleted (dec) and enriched (inc) UTRs, with Wilcoxon test-*P*-values of the differences. (D) Gene Ontology enrichment analysis for the enriched gene set. Number of genes belonging to each terms cluster is shown at the end of the corresponding bar. Mean score represents the mean of the Enrichr combined score for all belonging terms. GO classes

Enriched mRNAs (Figure 4D and E, Supplementary Table S3) showed that, during DHTS treatment, HuR bound preferentially to mRNAs encoding proteins with functions in the regulation of gene expression, cell cycle progression, and apoptosis. Data validation also suggested that the changes in HuR binding were independent of changes in total mRNA levels, as mRNA abundance was generally unchanged (Figure 4F and G). In summary, the ability of DHTS to displace HuR-bound RNAs was specifically limited to mRNAs with a low affinity for HuR, which generally displayed lower AU content in their 3'UTRs.

DHTS is effective on HuR-positive models *in vitro* and *in vivo*

To evaluate this mechanism of action, in which a limited displacement of RNAs from HuR may be effective in HuR-dependent tumor growth, we studied tumor growth *in vitro* and *in vivo*. HCT116 colon cancer cells were used as a model, based on high endogenous levels of HuR and their sensitivity to HuR inhibition (30). Creation and characterization of CRISPR/Cas9-mediated knockout of the *ELAVL1* gene in HCT116 cells was accomplished as described (42). HCT116 and HuR-knockout cells (HCT116ΔHuR) were grown under anchorage- and serum-independent conditions to facilitate tumorspheroid growth, and HuR was observed to be needed for tumorsphere growth (Figure 5A and B). In the presence of DHTS, growth of HCT116 spheroids was attenuated 2-fold, whereas DHTS did not impact HCT116ΔHuR sphere growth (Figure 5A and B). To test the effects of DHTS on tumor growth *in vivo*, mice bearing HCT116 cell xenografts received IP injections of DHTS (10 mg/kg body weight) or vehicle every 48 h. Over the course of the experiment, DHTS was well tolerated and mice did not display any signs of acute toxicity and maintained similar weights. Significant anti-tumor effects of DHTS were observed, with approximately a 4-fold reduction in tumor size (Figure 5C and D). Additionally, the efficacy of DHTS was strictly dependent on the presence of HuR. HCT116ΔHuR cells grew significantly more slowly and formed smaller tumors, but were completely insensitive to DHTS. Furthermore, this decreased growth sensitivity of DHTS in HuR-deficient cells could be restored with expression of HuR in HCT116ΔHuR cells (Figure 5E and F). These results indicate that DHTS has significant antitumor activity *in vitro* and *in vivo* without major systemic toxicity, along with demonstrating specificity of HuR inhibition.

DISCUSSION

Previous efforts targeted towards HuR disruptors (28–30,32,70) identified small molecules that can inhibit the HuR–RNA interaction in the nanomolar range. Here, we have characterized from a structural and functional perspective the mechanism of action of DHTS, a disruptor of the HuR–RNA interaction, identifying the protein regions that promote the interaction, and providing hints for the rational design of more potent HuR inhibitors. Additionally, we showed the cellular effects of DHTS treatment on HuR ability to bind mRNAs, and we described a paradoxical enrichment of mRNAs containing longer 3'UTRs with increased AU content. Such effects result in dysregulation of HuR function, specific to cells that are strictly dependent on HuR function. Starting from the relaxation measurements of RNA-free protein in solution, we described the events preceding RNA binding. The analysis of NMR relaxation data indicates that the free RRM1–RRM2 construct is largely monomeric in solution. However, the observed R_2 values are slightly higher than those expected for a monomeric protein, suggesting the presence of an equilibrium with a fraction of protein experiencing a larger rotational correlation time. On the other hand, the discrepancy of observed R_1 data with respect to the theoretical values calculated for a rigid RRM1–RRM2 monomer are explained by the presence of inter-domain flexibility. The low NOE values suggest a significant conformational plasticity of the protein that is needed for mRNA binding. Therefore, even if it is reported that the RRM1–RRM2 tandem construct forms a separated functional unit from the RRM3 domain (71), RRM1 and RRM2 domains are not rigidly held together but undergo independent motions that can facilitate the recognition of the RNA partner. This confirms observations from the crystal structure of non-complexed HuR, where no contacts between the two domains were detected (40,62) and supports earlier results that phosphorylation at the linker (e.g. Ser100) had a profound impact on HuR binding to target mRNAs (72). Moreover, the large R_1 values and small NOE values seen for the linker indicate that this region highly influences the conformational change of the protein from an open/flexible free conformation towards a closed one bound to mRNA.

As previously reported (40), binding of mRNA to HuR can occur starting from the open/flexible state of the protein, where HuR first binds the mRNA strand via its RRM1 domain. As a result of the subsequent conformational change, the linker and the RRM2 domain bind the mRNA filament to form a stable complex (40). Therefore, the linker takes part in the binding allowing the reciprocal reorienta-

found in each cluster are represented by the bars color. (E) KEGG and REACTOME pathway enrichment analysis for the enriched gene set. Number of genes belonging to each pathway is shown at the end of the corresponding bar. The score is the Enrichr combined score for the pathway. Pathway database of each entry is represented by the bars color. RIP of HuR in DHTS-treated HeLa cells. (F) Microarray data for selected targets. Fold enrichment of each mRNA during DHTS treatment is reported, black bars represent microarray values obtained. (G) Validation of microarray data by RT-qPCR. Gray bars represent fold enrichment of each mRNA during DHTS treatment compared with the control condition (DMSO). Comparison between microarray (F) and RT-qPCR data (G) shows similar results for enriched transcripts (*PABPC1*, *YTHDF1* and *UPF2* mRNAs), unchanged transcripts (*CASC3* mRNA) and depleted transcripts (*BRIP1* and *TBCCD1* mRNAs). In RT-qPCR validation experiments, *RPLP0* mRNA was used as an endogenous control mRNA that did not bind to HuR. Error bars represent SD. P -value is * <0.05 . ** <0.001 . Microarray experiments were done in duplicate ($n = 2$), qRT-PCR in triplicate ($n = 3$). (H) RT-qPCR analysis of mRNAs bound to of HuR showing no changes in total expression levels after DHTS treatment. *RPLP0* mRNA was used as an endogenous control. Error bars represent SD. Experiments were done in triplicate ($n = 3$).

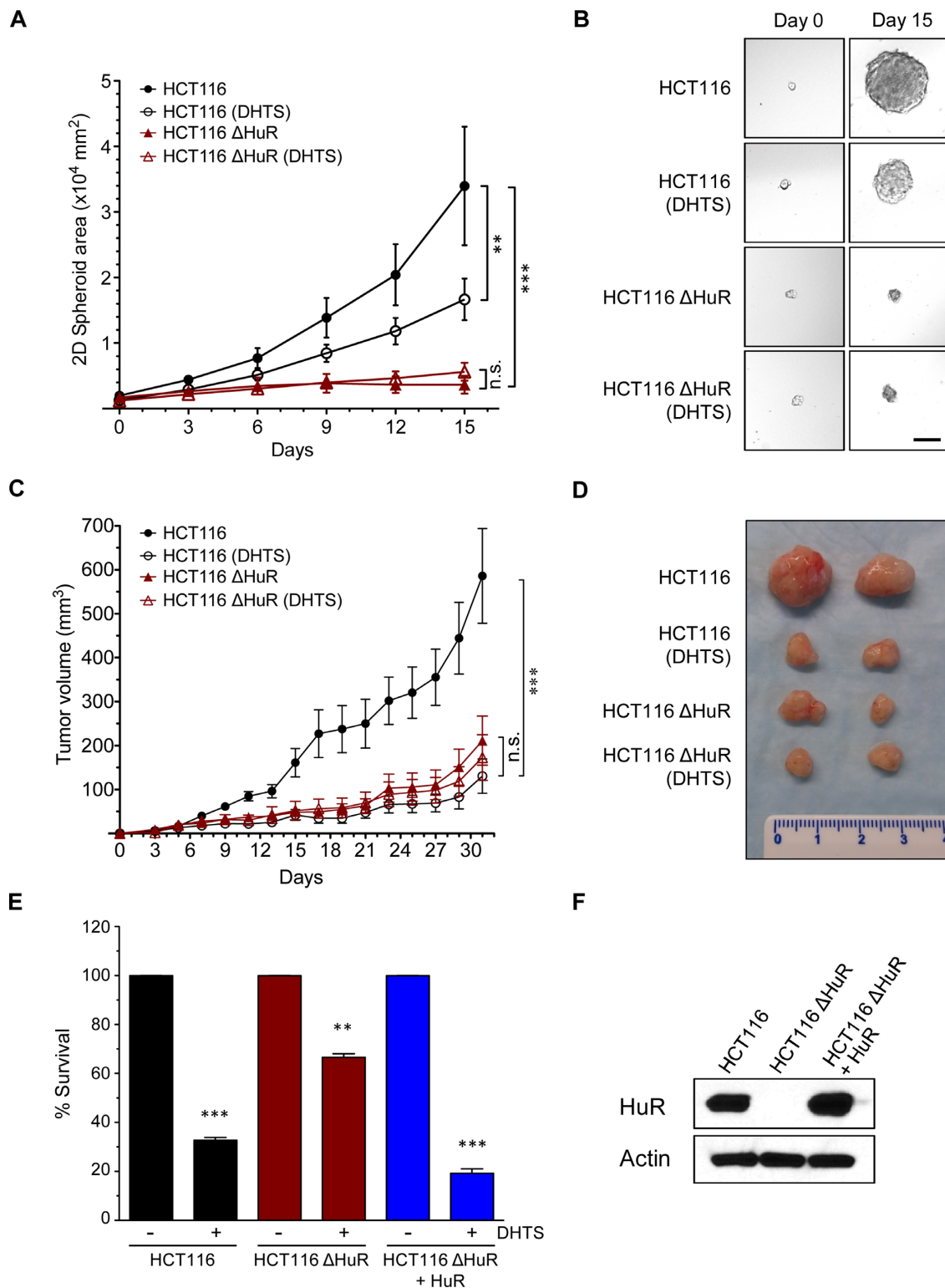


Figure 5. DHTS efficacy relies on HuR presence *in vivo*. (A) Spheroid growth of parental HCT116 (HCT116) and HuR-knockout cells (HCT116ΔHuR) treated with DHTS (10 μM) or vehicle. DHTS was added after 3 days of culture in spheroid growth medium on ultra-low adherence substrate and spheroid growth was tracked by imaging for 15 days. *P*-value is **<0.01, ***<0.001, n.s. = not significant. (B) Representative tumorsphere images from day 0 and day 15 of DHTS treatment. Scale bar = 100 μm. (C) Tumor growth of parental HCT116 and HuR-knockout cells (HCT116ΔHuR) xenografts in nude mice treated with 10 mg/kg DHTS or vehicle control every 48 h. *P*-value is ***<0.001, n.s. = not significant. (D) Representative tumors excised at day 31 are shown. (E) HuR-knockout cells (HCT116ΔHuR) were transfected a HuR-expression construct (+HuR), along with empty vector transfected parental HCT116 and HCT116ΔHuR cells. Cells were treated with DHTS (10 μM) or vehicle, and cell growth was assessed 6 days after the treatment using MTT assay. Cell survival was normalized to the respective control and are the average of three experiments. *P*-value is **<0.01, ***<0.001. (F) Western blot showing HuR complementation in HCT116ΔHuR+HuR cells and absence of HuR in HCT116ΔHuR cells. Actin was used as a loading control.

tion of the two domains and establishing interactions with the RNA strand. Addition of DHTS to unbound HuR results in a generalized decrease of the signal intensity of the NMR resonances, with some residues experiencing larger effects. It is likely that this behavior is due, at least in part, to a change in the conformational dynamics of the protein. Accordingly, upon complex formation with DHTS, in our MD simulation we observed a rather limited inter-domain flexibility, as a result of the shift in the conformational equilibrium between HuR forms in favor of a closed conformation. This result was not anticipated since, at least in principle, a change in the conformational dynamics of HuR could also have been achieved by stabilizing an open form of HuR. Indeed, residues located on the β -platforms of RRM1 and RRM2 domains, in the same regions involved in the binding with the mRNA strand, experience a deep quenching.

In our MD simulation, we observed a further closure of the RNA-binding groove, as compared to the RNA-bound conformation of HuR, and an ensuing increase in the number of inter-domain contacts, which could explain why the largest decreases in signal intensity were observed in residues belonging to these β -platforms. Deletion of the C-terminus region of RRM1 reduces the binding affinity of RRM1 to the mRNA probe but, importantly, abolishes the interaction between RRM1 and DHTS. This experimental validation of the NMR data and molecular modeling points to the residues next to the linker as being key structural elements responsible of the interaction between DHTS and HuR. Single aminoacid mutagenesis of Ser94, Asn107, Ile133, and Asn134 into alanine highlighted the importance of these residues in maintaining the equilibrium between the free protein in the monomer/dimer form and the closed-bound-to-RNA protein dimer, avoiding its aggregation on the RNA target. Interestingly, muteins are fully resistant to DHTS, further supporting that this small molecule competes for the same protein regions interacting with the target RNA. Collectively, these results suggest that DHTS stabilizes an unproductive 'closed' conformation of HuR and prevents the physiological re-orientation of the two domains needed to bind the target mRNA. Stabilization of such 'closed' conformation alters the protein dynamics, producing the observed generalized decrease of signal intensity of the resonances observed upon the addition of DHTS to the RRM1–RRM2 tandem domains. Unfortunately, the non-optimal solubility of DHTS hampered the quantitative assessment of its K_d .

In other experiments, we characterized the ability of DHTS to inhibit HuR activity *in vitro*, to modulate its post-transcriptional function in cell models, and its specificity towards other RNA-binding proteins. Additionally, we observed that DHTS inhibits the association step of HuR to its target RNAs, and that its cytotoxicity against cancer cells was HuR-dependent (31). The stable 'closed' form of the protein blocks the access to HuR for low affinity target RNAs. Indeed, paradoxically, the mRNAs with longer 3'UTR and higher U/AU content were more abundantly loaded on HuR after DHTS treatment, as they likely bind more avidly to HuR than DHTS itself. The levels of HuR-target RNAs were not changed during DHTS treatment, so a 'post-binding' mechanism of regulation can be inferred. Nevertheless, DHTS-dependent HuR dysreg-

ulation has a strong anti-cancer activity *in vivo*, as observed using a xenograft model of colon cancer (HCT116 cells). These findings are consistent with other results using colon, leukemia, cervical, and breast cancer cells, and indicate that DHTS can penetrate tumors effectively (73–76). The absence of systemic toxicity in treated animals supports the idea that general inhibition of HuR by small molecules can be a therapeutic avenue for future efforts, although the effects on the immune system should be evaluated in a non-immuno-compromised mouse model. Notably, HCT116 Δ HuR knockout cells *in vivo* showed a limited ability to develop tumors, but the extent of DHTS growth inhibition on these tumors did not match the effects on WT tumors. While we cannot discount that loss of HuR may impact cancer cell drug uptake, these results indicate *in vivo* specificity of DHTS and support the view that DHTS requires HuR for its antitumor influence. Finally, experimental and theoretical studies here reported suggest that the mechanism of action of DHTS is that of a competitive inhibitor of mRNA binding to HuR. These observations will be the ground for a rational design and synthesis of more potent small-molecule HuR disruptors.

SUPPLEMENTARY DATA

Supplementary Data are available at NAR Online.

FUNDING

Associazione Italiana per la Ricerca sul Cancro (AIRC) [17153 to A.P.]; University of Trento [Intramural funding 40201031 to A.P.]; Fondazione Cariplo [40102636 to A.P.]; AXonomIX research project (to A.Q.) financed by the Provincia Autonoma di Trento, Italy; National Institute of Aging Intramural Research Program of the National Institutes of Health [to M.G., K.A., R.M.]; National Institutes of Health [R01 CA134609 to D.D.]; NIH/NCI Cancer Center Support Grant [P30 CA168524 to D.D.]; Prevent Cancer Foundation and an Institutional Development Award (IDeA) from NIH/ NIGMS [P30 GM103495 to R.P.]. Funding for open access charge: Associazione Italiana per la Ricerca sul Cancro (AIRC).

Conflict of interest statement. None declared.

REFERENCES

1. Akaike, Y., Masuda, K., Kuwano, Y., Nishida, K., Kajita, K., Kurokawa, K., Satake, Y., Shoda, K., Imoto, I. and Rokutan, K. (2014) HuR regulates alternative splicing of the TRA2 β gene in human colon cancer cells under oxidative stress. *Mol. Cell. Biol.*, **34**, 2857–2873.
2. Izquierdo, J.M. (2008) Hu antigen R (HuR) functions as an alternative pre-mRNA splicing regulator of Fas apoptosis-promoting receptor on exon definition. *J. Biol. Chem.*, **283**, 19077–19084.
3. Mukherjee, N., Corcoran, D.L., Nusbaum, J.D., Reid, D.W., Georgiev, S., Hafner, M., Ascano, M., Tuschl, T., Ohler, U. and Keene, J.D. (2011) Integrative regulatory mapping indicates that the RNA-binding protein HuR couples pre-mRNA processing and mRNA stability. *Mol. Cell*, **43**, 327–339.
4. Lebedeva, S., Jens, M., Theil, K., Schwanhäusser, B., Selbach, M., Landthaler, M. and Rajewsky, N. (2011) Transcriptome-wide analysis of regulatory interactions of the RNA-binding protein HuR. *Mol. Cell*, **43**, 340–352.

5. Al-Ahmadi, W., Al-Ghamdi, M., Al-Haj, L., Al-Saif, M. and Khabar, K.S.A. (2009) Alternative polyadenylation variants of the RNA binding protein, HuR: abundance, role of AU-rich elements and auto-regulation. *Nucleic Acids Res.*, **37**, 3612–3624.
6. Dai, W., Zhang, G. and Makeyev, E. V. (2012) RNA-binding protein HuR autoregulates its expression by promoting alternative polyadenylation site usage. *Nucleic Acids Res.*, **40**, 787–800.
7. Dutertre, M., Chakrama, F.Z., Combe, E., Desmet, F.-O., Mortada, H., Polay Espinoza, M., Grataudou, L. and Auboeuf, D. (2014) A recently evolved class of alternative 3'-terminal exons involved in cell cycle regulation by topoisomerase inhibitors. *Nat. Commun.*, **5**, 3395.
8. Brennan, C.M. and Steitz, J.A. (2001) HuR and mRNA stability. *Cell. Mol. Life Sci.*, **58**, 266–277.
9. Srikantan, S. and Gorospe, M. (2012) HuR function in disease. *Front. Biosci.*, **17**, 189–205.
10. Papadaki, O., Milatos, S., Grammenoudi, S., Mukherjee, N., Keene, J.D. and Kontoyiannis, D.L. (2009) Control of thymic T cell maturation, deletion and egress by the RNA-binding protein HuR. *J. Immunol.*, **182**, 6779–6788.
11. Legnini, I., Morlando, M., Mangiacavalli, A., Fatica, A. and Bozzoni, I. (2014) A feedforward regulatory loop between HuR and the long noncoding RNA linc-MD1 controls early phases of myogenesis. *Mol. Cell*, **53**, 506–514.
12. Wang, W., Yang, X., Cristofalo, V.J., Holbrook, N.J. and Gorospe, M. (2001) Loss of HuR is linked to reduced expression of proliferative genes during replicative senescence. *Mol. Cell Biol.*, **21**, 5889–5898.
13. Sakai, K., Kitagawa, Y. and Hirose, G. (1999) Binding of neuronal ELAV-like proteins to the uridine-rich sequence in the 3'-untranslated region of tumor necrosis factor- α messenger RNA. *FEBS Lett.*, **446**, 157–162.
14. González-Feliciano, J.A., Hernández-Pérez, M., Estrella, L.A., Colón-López, D.D., López, A., Martínez, M., Maurás-Rivera, K.R., Lasalde, C., Martínez, D., Araujo-Pérez, F. *et al.* (2014) The role of HuR in the post-transcriptional regulation of interleukin-3 in T cells. *PLoS One*, **9**, e92457.
15. Zha, W., Wang, G., Pecora, B.S., Studer, E., Hylemon, P.B., Pandak, W.M. and Zhou, H. (2010) Role of RNA-binding protein HuR and CUGBP1 in LPS-induced interleukin-6 expression in macrophages. *FASEB J.*, **24**, 494.7–494.7.
16. Kim, Y., Noren Hooten, N., Dluzen, D.F., Martindale, J.L., Gorospe, M. and Evans, M.K. (2015) Posttranscriptional regulation of the inflammatory marker C-reactive protein by the RNA-binding protein HuR and MicroRNA 637. *Mol. Cell Biol.*, **35**, 4212–4221.
17. Gubin, M.M., Techasintana, P., Magee, J.D., Dahm, G.M., Calaluce, R., Martindale, J.L., Whitney, M.S., Franklin, C.L., Besch-Williford, C., Hollingsworth, J.W. *et al.* (2014) Conditional knockout of the RNA-binding protein HuR in CD4⁺ T cells reveals a gene dosage effect on cytokine production. *Mol. Med.*, **20**, 93–108.
18. Fan, J., Ishmael, F.T., Fang, X., Myers, A., Cheadle, C., Huang, S.-K., Atasoy, U., Gorospe, M. and Stellato, C. (2011) Chemokine transcripts as targets of the RNA-binding protein HuR in human airway epithelium. *J. Immunol.*, **186**, 2482–2494.
19. Diaz-Muñoz, M.D., Bell, S.E., Fairfax, K., Monzon-Casanova, E., Cunningham, A.F., Gonzalez-Porta, M., Andrews, S.R., Bunik, V.I., Zarnack, K., Curk, T. *et al.* (2015) The RNA-binding protein HuR is essential for the B cell antibody response. *Nat. Immunol.*, **16**, 415–425.
20. DeMicco, A., Naradikian, M.S., Sindhava, V.J., Yoon, J.-H., Gorospe, M., Wertheim, G.B., Cancro, M.P. and Bassing, C.H. (2015) B cell-intrinsic expression of the HuR RNA-binding protein is required for the T cell-dependent immune response in vivo. *J. Immunol.*, **195**, 3449–3462.
21. Mazan-Mamczarz, K., Hagner, P.R., Corl, S., Srikantan, S., Wood, W.H., Becker, K.G., Gorospe, M., Keene, J.D., Levenson, A.S. and Gartenhaus, R.B. (2008) Post-transcriptional gene regulation by HuR promotes a more tumorigenic phenotype. *Oncogene*, **27**, 6151–6163.
22. Wang, W., Furneaux, H., Cheng, H., Caldwell, M.C., Hutter, D., Liu, Y., Holbrook, N. and Gorospe, M. (2000) b. HuR regulates p21 mRNA stabilization by UV light. *Mol. Cell Biol.*, **20**, 760–769.
23. Latorre, E., Carelli, S., Raimondi, I., D'Agostino, V., Castiglioni, I., Zucal, C., Moro, G., Luciani, A., Ghilardi, G., Monti, E. *et al.* (2016) The ribonucleic complex HuR-MALAT1 represses CD133 expression and suppresses epithelial-mesenchymal transition in breast cancer. *Cancer Res.*, **76**, 2626–2636.
24. Latorre, E., Tebaldi, T., Viero, G., Sparta, A.M., Quattrone, A. and Provenzani, A. (2012) Downregulation of HuR as a new mechanism of doxorubicin resistance in breast cancer cells. *Mol. Cancer*, **11**, 13.
25. Latorre, E., Castiglioni, I., Gatto, P., Carelli, S., Quattrone, A. and Provenzani, A. (2014) Loss of protein kinase C δ /HuR interaction is necessary to doxorubicin resistance in breast cancer cell lines. *J. Pharmacol. Exp. Ther.*, **349**, 99–106.
26. Abdelmohsen, K. and Gorospe, M. (2010) Posttranscriptional regulation of cancer traits by HuR. *Wiley Interdiscip. Rev. RNA*, **1**, 214–229.
27. Levy, N.S., Chung, S., Furneaux, H. and Levy, A.P. (1998) Hypoxic stabilization of vascular endothelial growth factor mRNA by the RNA-binding protein HuR. *J. Biol. Chem.*, **273**, 6417–6423.
28. Meisner, N.-C., Hintersteiner, M., Mueller, K., Bauer, R., Seifert, J.-M., Naegeli, H.-U., Ottl, J., Oberer, L., Guenat, C., Moss, S. *et al.* (2007) Identification and mechanistic characterization of low-molecular-weight inhibitors for HuR. *Nat. Chem. Biol.*, **3**, 508–515.
29. Wu, X., Lan, L., Wilson, D.M., Marquez, R.T., Tsao, W., Gao, P., Roy, A., Turner, B.A., McDonald, P., Tunge, J. *et al.* (2015) Identification and validation of novel small molecule disruptors of HuR-mRNA interaction. *ACS Chem. Biol.*, doi:10.1021/cb500851u.
30. Blanco, F.F., Preet, R., Aguado, A., Vishwakarma, V., Stevens, L.E., Vyas, A., Padhye, S., Xu, L., Weir, S.J., Anant, S. *et al.* (2016) Impact of HuR inhibition by the small molecule MS-444 on colorectal cancer cell tumorigenesis. *Oncotarget*, doi:10.18632/oncotarget.12189.
31. D'Agostino, V.G., Lal, P., Mantelli, B., Tiedje, C., Zucal, C., Thongon, N., Gaestel, M., Latorre, E., Marinelli, L., Seneci, P. *et al.* (2015) Dihydroanthranone-I interferes with the RNA-binding activity of HuR affecting its post-transcriptional function. *Sci. Rep.*, **5**, 16478.
32. D'Agostino, V.G., Adami, V. and Provenzani, A. (2013) A novel high throughput biochemical assay to evaluate the HuR protein-RNA complex formation. *PLoS One*, **8**, e72426.
33. Chae, M.-J., Sung, H.Y., Kim, E.-H., Lee, M., Kwak, H., Chae, C.H., Kim, S. and Park, W.-Y. (2009) Chemical inhibitors destabilize HuR binding to the AU-rich element of TNF- α mRNA. *Exp. Mol. Med.*, **41**, 824–831.
34. Zucal, C., D'Agostino, V., Loffredo, R., Mantelli, B., Thongon, N., Lal, P., Latorre, E. and Provenzani, A. (2015) Targeting the multifaceted HuR protein, benefits and caveats. *Curr. Drug Targets*, **16**, 499–515.
35. Wang, Z., Bhattacharya, A. and Ivanov, D.N. (2015) Identification of small-molecule inhibitors of the HuR/RNA interaction using a fluorescence polarization screening assay followed by NMR validation. *PLoS One*, **10**, e0138780.
36. Fan, X.C. and Steitz, J.A. (1998) HNS, a nuclear-cytoplasmic shuttling sequence in HuR. *Proc. Natl. Acad. Sci. U.S.A.*, **95**, 15293–15298.
37. Scheiba, R.M., de Opakua, A.I., Diaz-Quintana, A., Cruz-Gallardo, I., Martínez-Cruz, L.A., Martínez-Chantar, M.L., Blanco, F.J. and Diaz-Moreno, I. (2014) The C-terminal RNA binding motif of HuR is a multi-functional domain leading to HuR oligomerization and binding to U-rich RNA targets. *RNA Biol.*, **11**, 1250–1261.
38. Maris, C., Dominguez, C. and Allain, F.H.-T. (2005) The RNA recognition motif, a plastic RNA-binding platform to regulate post-transcriptional gene expression. *FEBS J.*, **272**, 2118–2131.
39. Benoit, R.M., Meisner, N.-C., Kallen, J., Graff, P., Hemmig, R., Cèbe, R., Ostermeier, C., Widmer, H. and Auer, M. (2010) The x-ray crystal structure of the first RNA recognition motif and site-directed mutagenesis suggest a possible HuR redox sensing mechanism. *J. Mol. Biol.*, **397**, 1231–1244.
40. Wang, H., Zeng, F., Liu, Q., Liu, H., Liu, Z., Niu, L., Teng, M. and Li, X. (2013) The structure of the ARE-binding domains of Hu antigen R (HuR) undergoes conformational changes during RNA binding. *Acta Crystallogr. D. Biol. Crystallogr.*, **69**, 373–380.
41. Kim, H.S., Wilce, M.C.J., Yoga, Y.M.K., Pardini, N.R., Gunzburg, M.J., Cowieson, N.P., Wilson, G.M., Williams, B.R.G., Gorospe, M. and Wilce, J.A. (2011) Different modes of interaction by TIAR and HuR with target RNA and DNA. *Nucleic Acids Res.*, **39**, 1117–1130.
42. Lal, S., Cheung, E.C., Zarei, M., Preet, R., Chand, S.N., Mambelli-Lisboa, N.C., Romeo, C., Stout, M.C., Londin, E., Goetz, A. *et al.* (2017) CRISPR knockout of the HuR gene causes a xenograft lethal phenotype. *Mol. Cancer Res.*, doi:10.1158/1541-7786.MCR-16-0361.

43. Young, L.E., Moore, A.E., Sokol, L., Meisner-Kober, N. and Dixon, D.A. (2012) The mRNA stability factor HuR inhibits microRNA-16 targeting of COX-2. *Mol. Cancer Res.*, **10**, 167–180.
44. Barbato, G., Ikura, M., Kay, L.E., Pastor, R.W. and Bax, A. (1992) Backbone dynamics of calmodulin studied by ¹⁵N relaxation using inverse detected two-dimensional NMR spectroscopy: the central helix is flexible. *Biochemistry*, **31**, 5269–5278.
45. Kay, L.E., Nicholson, L.K., Delaglio, F., Bax, A. and Torchia, D. (1992) Pulse sequences for removal of the effects of cross correlation between dipolar and chemical-shift anisotropy relaxation mechanisms on the measurement of heteronuclear T1 and T2 values in proteins. *J. Magn. Reson.*, **97**, 359–375.
46. Peng, J.W. and Wagner, G. (1994) Investigation of protein motions via relaxation measurements. *Methods Enzymol.*, **239**, 563–596.
47. García de la Torre, J., Huertas, M.L. and Carrasco, B. (2000) HYDRONMR: prediction of NMR relaxation of globular proteins from atomic-level structures and hydrodynamic calculations. *J. Magn. Reson.*, **147**, 138–146.
48. Phillips, J.C., Braun, R., Wang, W., Gumbart, J., Tajkhorshid, E., Villa, E., Chipot, C., Skeel, R.D., Kalé, L. and Schulten, K. (2005) Scalable molecular dynamics with NAMD. *J. Comput. Chem.*, **26**, 1781–1802.
49. Cornell, W.D., Cieplak, P., Bayly, C.I., Gould, I.R., Merz, K.M., Ferguson, D.M., Spellmeyer, D.C., Fox, T., Caldwell, J.W. and Kollman, P.A. (1995) A second generation force field for the simulation of proteins, nucleic acids, and organic molecules. *J. Am. Chem. Soc.*, **117**, 5179–5197.
50. Lindorff-Larsen, K., Piana, S., Palmo, K., Maragakis, P., Klepeis, J.L., Dror, R.O. and Shaw, D.E. (2010) Improved side-chain torsion potentials for the Amber ff99SB protein force field. *Proteins*, **78**, 1950–1958.
51. Allnér, O., Nilsson, L. and Villa, A. (2012) Magnesium ion–water coordination and exchange in biomolecular simulations. *J. Chem. Theory Comput.*, **8**, 1493–1502.
52. Bayly, C.I., Cieplak, P., Cornell, W. and Kollman, P.A. (1993) A well-behaved electrostatic potential based method using charge restraints for deriving atomic charges: the RESP model. *J. Phys. Chem.*, **97**, 10269–10280.
53. Gaussian 09, Revision A.02 (2009) *Gaussian 09 Citation*. <http://gaussian.com/g09citation/>.
54. Dupradeau, F.-Y., Pigache, A., Zaffran, T., Savineau, C., Lelong, R., Grivel, N., Lelong, D., Rosanski, W. and Cieplak, P. (2010) The R.E.D. tools: advances in RESP and ESP charge derivation and force field library building. *Phys. Chem. Chem. Phys. PCCP*, **12**, 7821–7839.
55. Vanquelf, E., Simon, S., Marquant, G., Garcia, E., Klimerak, G., Delepine, J.C., Cieplak, P. and Dupradeau, F.-Y. (2011) R.E.D. Server: a web service for deriving RESP and ESP charges and building force field libraries for new molecules and molecular fragments. *Nucleic Acids Res.*, **39**, W511–W517.
56. Wang, J., Wang, W., Kollman, P.A. and Case, D.A. (2006) Automatic atom type and bond type perception in molecular mechanical calculations. *J. Mol. Graph. Model.*, **25**, 247–260.
57. Abdelmohsen, K., Srikantan, S., Yang, X., Lal, A., Kim, H.H., Kuwano, Y., Galban, S., Becker, K.G., Kamara, D., de Cabo, R. et al. (2009) Ubiquitin-mediated proteolysis of HuR by heat shock. *EMBO J.*, **28**, 1271–1282.
58. Dassi, E., Re, A., Leo, S., Tebaldi, T., Pasini, L., Peroni, D. and Quattrone, A. (2014) AURA 2: Empowering discovery of post-transcriptional networks. *Transl. (Austin, Tex.)*, **2**, e27738.
59. Chen, E.Y., Tan, C.M., Kou, Y., Duan, Q., Wang, Z., Meirelles, G.V., Clark, N.R. and Ma'ayan, A. (2013) Enrichr: interactive and collaborative HTML5 gene list enrichment analysis tool. *BMC Bioinformatics*, **14**, 128.
60. Yu, G., Li, F., Qin, Y., Bo, X., Wu, Y. and Wang, S. (2010) GOSemSim: an R package for measuring semantic similarity among GO terms and gene products. *Bioinformatics*, **26**, 976–978.
61. Mujo, A., Lixa, C., Carneiro, L.A.M., Anobom, C.D., Almeida, F.C. and Pinheiro, A.S. (2014) ¹H, ¹⁵N and ¹³C resonance assignments of the RRM1 domain of the key post-transcriptional regulator HuR. *Biomol. NMR Assign.*, doi:10.1007/s12104-014-9592-9.
62. Wang, H., Zeng, F., Liu, H., Teng, M. and Li, X. (2012) Crystal structure of two tandem RNA recognition motifs of Human antigen R. <https://www.ncbi.nlm.nih.gov/Structure/mmdb/mmdbsrv.cgi?uid=4EGL>.
63. Bertini, I., Fragai, M., Luchinat, C., Melikian, M., Mylonas, E., Sarti, N. and Svergun, D.I. (2009) Interdomain flexibility in full-length matrix metalloproteinase-1 (MMP-1). *J. Biol. Chem.*, **284**, 12821–12828.
64. Bertini, I., Calderone, V., Fragai, M., Jaiswal, R., Luchinat, C., Melikian, M., Mylonas, E. and Svergun, D.I. (2008) Evidence of reciprocal reorientation of the catalytic and hemopexin-like domains of full-length MMP-12. *J. Am. Chem. Soc.*, **130**, 7011–7021.
65. Cerofolini, L., Fields, G.B., Fragai, M., Galdes, C.F.G.C., Luchinat, C., Parigi, G., Ravera, E., Svergun, D.I. and Teixeira, J.M.C. (2013) Examination of matrix metalloproteinase-1 in solution: a preference for the pre-collagenolysis state. *J. Biol. Chem.*, **288**, 30659–30671.
66. Dosset, P., Hus, J.-C., Blackledge, M. and Marion, D. (2000) Efficient analysis of macromolecular rotational diffusion from heteronuclear relaxation data. *J. Biomol. NMR*, **16**, 23–28.
67. Morrison, K.L. and Weiss, G.A. (2001) Combinatorial alanine-scanning. *Curr. Opin. Chem. Biol.*, **5**, 302–307.
68. Arkin, M.R., Glicksman, M.A., Fu, H., Havel, J.J. and Du, Y. (2004) Inhibition of protein-protein interactions: non-cellular assay formats. In: Sittampalam, G.S., Coussens, N.P., Nelson, H., Arkin, M., Auld, D., Austin, C., Bejcek, B., Glicksman, M., Ingelse, J. and Iversen, P.W. (eds). *Assay Guidance Manual*. Eli Lilly & Company and the National Center for Advancing Translational Sciences, Bethesda.
69. de Silanes, I.L., Zhan, M., Lal, A., Yang, X. and Gorospe, M. (2004) Identification of a target RNA motif for RNA-binding protein HuR. *Proc. Natl. Acad. Sci. U.S.A.*, **101**, 2987–2992.
70. Wu, X., Lan, L., Smith, A., Marquez, R., Wilson, D., Rogers, S., Gao, P., Lovell, S., Karanicolas, J., Dixon, D. et al. (2015) Abstract 2449: Targeting an ‘undruggable’ RNA-binding protein: Discovery of small molecule inhibitors of HuR for novel breast cancer therapy. *Cancer Res.*, **75**, 2449–2449.
71. Scheiba, R.M., Aroca, Á. and Díaz-Moreno, I. (2012) HuR thermal stability is dependent on domain binding and upon phosphorylation. *Eur. Biophys. J.*, **41**, 597–605.
72. Abdelmohsen, K., Pullmann, R., Lal, A., Kim, H.H., Galban, S., Yang, X., Blethrow, J.D., Walker, M., Shubert, J., Gillespie, D. et al. (2007) Phosphorylation of HuR by Chk2 regulates SIRT1 expression. *Mol. Cell*, **25**, 543–557.
73. Wang, L., Hu, T., Shen, J., Zhang, L., Chan, R.L.-Y., Lu, L., Li, M., Cho, C.H. and Wu, W.K.K. (2015) Dihydrotanshinone I induced apoptosis and autophagy through caspase dependent pathway in colon cancer. *Phytomedicine*, **22**, 1079–1087.
74. Liu, J.-J., Wu, H.-H., Chen, T.-H., Leung, W. and Liang, Y.-C. (2015) 15,16-Dihydrotanshinone I from the functional food *Salvia miltiorrhiza* exhibits anticancer activity in human HL-60 leukemia cells: in vitro and in vivo studies. *Int. J. Mol. Sci.*, **16**, 19387–19400.
75. Ye, Y., Xu, W., Zhong, W., Li, Y. and Wang, C. (2012) Combination treatment with dihydrotanshinone I and irradiation enhances apoptotic effects in human cervical cancer by HPV E6 down-regulation and caspases activation. *Mol. Cell. Biochem.*, **363**, 191–202.
76. Tsai, S.-L., Suk, F.-M., Wang, C.-I., Liu, D.-Z., Hou, W.-C., Lin, P.-J., Hung, L.-F. and Liang, Y.-C. (2007) Anti-tumor potential of 15, 16-dihydrotanshinone I against breast adenocarcinoma through inducing G1 arrest and apoptosis. *Biochem. Pharmacol.*, **74**, 1575–1586.

ACKNOWLEDGEMENTS

During these 4 years, the work I have presented throughout this thesis has been possible thanks to all the people that contributed to it and all the ones that supported me.

I would like to begin expressing my gratitude to my tutor, Prof. Alessandro Provenzani, for making me part of this pivotal, widely and challenging project and giving me the opportunity to join his laboratory of Genomic Screening. Thanks to his support, I acquired a vast number of technical skills and met different collaborators, each of them turned out to be crucial for my personal and professional growth. During these years, Dr. Provenzani helped me in believing in my own capabilities providing me a daily stimulating and highly scientific environment, with his professional enthusiasm and spirit of discussion. On the other end, I would like to thank Dr. Vito D'Agostino that introduced me in the science world with his precious helps and teachings throughout these years.

My truly thankfulness is also extended to all the members of the lab that represented focal points during all these years. I would like to start thanking a past member, Rosa Loffredo, that since the beginning and until now taught me a lot with his patient, kind, near and far guidance and for her sincere friendship. Therefore, I would like to express my gratitude to present and past members involved in the project, starting from Chiara Zucal, that daily shared with me all the successes and helped me to face and resolve pitfalls with her experience and friendly attitude. I want to acknowledge the help, support and teachings given by two past members: Preet Lal, who opened the horizons concerning HuR project and helped me during these years with his professional and shine behavior and Natthakan Thongon that collaborated with us for the project development and taught me a lot with her great passion and hardworking approach.

I would like to thank the present members in the lab: Mariachiara Micaelli and Daniele Pollini for their great support and true friendship, along with Nausicaa Licata; Rosangela Digilio, that has collaborated as student in the HuR project, providing us an outstanding support and help. I thank the new members (Caterina and Agata), together with the students I trained during these years (Matteo, Gaia and Simone), they gave me the opportunity to challenge myself in teachings and gave me a huge help with my experiments.

I would like to express my gratitude and appreciation to all the collaborators I met during these years, starting from Dr. Alessio Nencioni and his lab, that taught me to handle human PBMCs during my visiting experience in Genova, but most of all, I am really thankful to Dr. Dimitris Kontoyiannis and his lab. He has been really inspiring researcher for me and with his cleverness and serious attitude really contributed to my personal and professional growth. During the period abroad I have spent in Vari (Greece) at the BRSC Alexander Fleming Institute, I have been trained to work with mice handling, primary culture and macrophages harvesting and for this, I have to thank all the members

of Kontoyiannis' lab, in particular: Marannia Saridaki, Margarita Chatzimike and Margarita Andreadou for the great hospitality they gave me and important teachings.

My gratitude goes to AIRC for the support and funding of the project and to Department of CIBIO, specially my colleagues and friends, such as all the members from the lab of Laboratory of Translational Genomics headed by Dr. Alessandro Quattrone, with whose I have shared the place, successes and pitfalls, receiving always true and big support.

Lastly, I would like to acknowledge the facilities in CIBIO, in particular HTS, Cell Analysis and Separation (e.g. Isabella Pesce), but mostly I would like to express all my sincere gratitude to the Animal facility, to Sergio Robbiati, but specially Marta Tarter really helped me to work with mice side by side and kindly and patiently supported me in acquiring all the skills I developed until now.